

Karlsruher Institut für Technologie

**Schriftenreihe
Kontinuumsmechanik im Maschinenbau**

23

Julian Karl Bauer

Fiber Orientation Tensors
and Mean Field Homogenization
Application to Sheet Molding Compound

Julian Karl Bauer

**Fiber Orientation Tensors and
Mean Field Homogenization**

Application to Sheet Molding Compound

Schriftenreihe
Kontinuumsmechanik im Maschinenbau
Band 23

Karlsruher Institut für Technologie (KIT)
Institut für Technische Mechanik
Bereich Kontinuumsmechanik

Hrsg. Prof. Dr.-Ing. habil. Thomas Böhlke

Eine Übersicht aller bisher in dieser Schriftenreihe erschienenen Bände
finden Sie am Ende des Buchs.

Fiber Orientation Tensors and Mean Field Homogenization

Application to Sheet Molding Compound

by
Julian Karl Bauer



Karlsruher Institut für Technologie
Institut für Technische Mechanik
Bereich Kontinuumsmechanik

Fiber Orientation Tensors and Mean Field Homogenization:
Application to Sheet Molding Compound

Zur Erlangung des akademischen Grades eines Doktor-Ingenieurs
von der KIT-Fakultät für Bauingenieur-, Geo- und Umweltwissen-
schaften des Karlsruher Instituts für Technologie (KIT) genehmigte
Dissertation

von Julian Karl Bauer, M.Sc.

Tag der mündlichen Prüfung: 29. Juli 2022

Hauptreferent: Prof. Dr.-Ing. habil. Thomas Seelig

Korreferent: Prof. Dr.-Ing. habil. Thomas Böhlke

Korreferent: Prof. Dr.-Ing. Andrew Hrymak

Impressum



Karlsruher Institut für Technologie (KIT)
KIT Scientific Publishing
Straße am Forum 2
D-76131 Karlsruhe

KIT Scientific Publishing is a registered trademark
of Karlsruhe Institute of Technology.
Reprint using the book cover is not allowed.

www.ksp.kit.edu



*This document – excluding parts marked otherwise, the cover, pictures and graphs –
is licensed under a Creative Commons Attribution-Share Alike 4.0 International License
(CC BY-SA 4.0): <https://creativecommons.org/licenses/by-sa/4.0/deed.en>*



*The cover page is licensed under a Creative Commons
Attribution-No Derivatives 4.0 International License (CC BY-ND 4.0):
<https://creativecommons.org/licenses/by-nd/4.0/deed.en>*

Print on Demand 2023 – Gedruckt auf FSC-zertifiziertem Papier

ISSN 2192-693X

ISBN 978-3-7315-1262-2

DOI 10.5445/KSP/1000152989

Zusammenfassung

Die effektiven mechanischen Eigenschaften von faserverstärkten Verbundwerkstoffen hängen stark von der Mikrostruktur, d. h. von der Ausrichtung der Fasern im Verbundwerkstoff, ab. In dieser Arbeit wird der Einfluss von Faserorientierungsverteilungen auf die effektiven Eigenschaften von langfaserverstärkten Verbundwerkstoffen untersucht. Die vorliegende Arbeit wird von der Deutschen Forschungsgemeinschaft (DFG) im Rahmen des interdisziplinären Graduiertenkollegs GRK 2078 finanziert. Daher liegt der Fokus auf sogenannten „Sheet Molding Compound“ (SMC) Materialien. SMC ist ein Verbundwerkstoff aus langen Glasfasern und duroplastischer Polymermatrix, für Leichtbauanwendungen mit flachen Bauteilformen, beispielsweise in der Automobilindustrie.

Gemittelte Information einer Faserorientierungsverteilung kann durch Faserorientierungstensoren quantifiziert werden. Ein vollständiges Bild des Einflusses dieses Richtungsmaßes auf die effektiven mechanischen Eigenschaften wird präsentiert, basierend auf einer neu abgeleiteten Vielfalt von Faserorientierungstensoren vierter Stufe. Diese Vielfalt wird identifiziert durch lineare invariante Zerlegung von Faserorientierungstensoren vierter Stufe, was zu einfachen und flexiblen Parametrisierungen führt. Beschränkungen durch materielle Symmetrie werden in diese Parametrisierungen einbezogen und zulässige Parameterbereiche werden bestimmt, indem positive Semi-Definitheit eingefordert wird. In dieser Arbeit werden Schließungsapproximationen durch die Vielfalt der Faserorientierungstensoren vierter Stufe kontrastiert. Mikrostrukturen von SMC werden durch planare Orientierungszustände

approximiert. Die Beziehung zwischen planaren Faserverteilungen und planaren Faserorientierungstensoren wird im Detail diskutiert. Dazu werden tensorielle Fourierreihen in 2D- und 3D-Darstellungen sowie die Maximum-Entropie-Rekonstruktion von Faserorientierungsverteilungen durch führende Faserorientierungstensoren untersucht. Eine detaillierte Analyse des Advani-Tucker-Orientierungsmittelwertes gibt Aufschluss über die Struktur verschiedener orientierungsgemittelter Meanfield-Homogenisierungen. Ein vollständiges Bild der Richtungsabhängigkeit der effektiven linear-elastischen Steifigkeiten, die durch diese Homogenisierungsverfahren vorhergesagt werden, wird beschrieben. Dazu wird eine innovative Visualisierungsmethode basierend auf Übersichtsplots und Polarplot-Ensembles entwickelt. Diese Methode ist anwendbar auf jede richtungsabhängige skalare Größe, die eine Funktion verschiedener planarer Faserorientierungstensoren ist.

Diese Arbeit motiviert die Verwendung von Faserorientierungsinformationen vierter Stufe und hat somit weitreichende Implikationen für virtuelle Prozessketten für planare langfaserverstärkte Bauteile.

Summary

Effective mechanical properties of fiber reinforced composites strongly depend on the microstructure, i.e., the fibers' alignment within the composite. In this work, the influence of fiber orientation distribution on the effective properties of long-fiber-reinforced composites is studied.

The present work is funded by the German Research Foundation (DFG) within the interdisciplinary research training group GRK 2078. Within this research group, the material class sheet molding compound (SMC) is of primary interest. SMC is a composite of long glass fibers and a thermoset polymer matrix, serving lightweight applications with flat component designs, for instance in the automotive industry.

Averaged information of a fiber orientation distribution can be quantified by fiber orientation tensors. This work gives a complete picture of the influence of fiber orientation tensors up to fourth order on effective mechanical properties, based on the newly derived variety of fourth-order fiber orientation tensors. This variety is identified by linear invariant decomposition of fourth-order fiber orientation tensors leading to simple and flexible parameterizations. Constraints of material symmetry are incorporated into these parameterizations and admissible parameter ranges are identified by demanding positive semi-definiteness. Throughout this work, closure approximations are contrasted by the variety of fourth-order fiber orientation tensors. Microstructures of SMC are approximated by planar orientation states. The correspondence of planar fiber distributions and planar fiber orientation tensors are presented in detail, deploying tensorial Fourier series in 2D- and 3D-frameworks as well as maximum entropy reconstruction of fiber orientation distri-

butions by leading fiber orientation tensors. Detailed analysis of the Advani-Tucker orientation average yields insights on the structure of several orientation-averaging mean field homogenization approximations. A complete picture of the directional dependence of effective linear elastic stiffnesses predicted by those mean field homogenizations is drawn. Therefore, an innovative visualization method based on overview plots and polar plot ensembles is derived. This method is applicable to any direction-dependent scalar quantity, which is a function of distinct planar fiber orientation tensors.

This work emphasizes the importance of fourth-order fiber orientation information and therefore has far-reaching implications for virtual process chains for planar long-fiber-reinforced components.

Acknowledgments

I would like to thank my supervisor Prof. Thomas Seelig for the many intense professional and scientific discussions we shared. Your continuous support and your commitment to education has broadened my view in many ways. You gave me the opportunity to develop my personality and I am very grateful that I could gain valuable knowledge. I would like to thank my co-supervisor Prof. Thomas Böhlke for his continued encouragement. Thank you for teaching me how to write scientific research papers, how to rethink communication and for your fruitful training in the area of accuracy and precision. I would like to express my special thanks to Prof. Andrew Hrymak for accepting the co-supervision of my thesis at short notice. Disregarding this inconvenience, he pursued this task full of enthusiasm. I thank Jun.-Prof. Matti Schneider for his inspiring lectures on microstructures and for introducing me to the topic of fiber orientation tensors. I thank Prof. Peter Betsch for his efforts to create a welcoming and inspiring scientific atmosphere at the Institute of Mechanics.

Special thanks go to all colleagues at the Institute of Mechanics (IFM) and the Institute of Engineering Mechanics (ITM). Thank you, Jonas Hund, for your friendship which is highly important to me. Our professional exchange and the learning experiences that I gained from following your studies for your doctorate helped me a lot in identifying new problems and solve them efficiently. You established for me the contact to Software Carpentry. I have fond memories of sharing fruits, vegetables and vegan delights with you during long working hours. Your support was outstanding. I would like to thank Paul Wasmer for his calmness,

his confidence and in particular for his critical comments whenever I came up with an idea that subsequently proved wrong. It was great sharing an office with you. I thank Philipp Kinon for inspiring professional discussions. I admire your sharp analytical skills and I definitely enjoyed our climbing adventures and vacations together. Thank you, Florian Schrammer, for your professionalism and our conversations about university and academic life. Furthermore, I would like to thank Moritz Hill for many in-depth discussions and his encouragement. I would like to thank Nils Meyer for creating a friendly and open-minded working atmosphere and for sharing thoughts on similar attitudes towards programming and coding tasks. Thanks, Juliane Lang, for our general exchange on Mechanics and for your hearty laugh. Thank you, Tarkes Dora Pallicity, for constantly spreading joy whenever we met and for your creative spirit. Thank you, Alexander Dyck, for being an inspiring role model. Thank you, Lordana Kehrer, for your seemingly endless patience and support in organizational matters. Thank you, Tom-Alexander Langhoff, for always having an open ear and your advice which always came at the right time. I would like to thank Johannes Görthofer for his great team spirit and his integrating nature. Whenever you are part of a group it is fun to join in its activities.

I thank Florian Kromm for instructing me in climbing, and for appreciating any kind of reality check. Thank you, Laura Thiemt, for your support and dedication. You taught me patience and confidence and you enabled me to work on this project successfully.

The research documented in this work has been funded by the German Research Foundation (DFG, Deutsche Forschungsgemeinschaft) - project number 255730231. The support by the German Research Foundation within the International Research Training Group “Integrated engineering of continuous-discontinuous long fiber reinforced polymer structures” (GRK 2078/2) is gratefully acknowledged.

Contents

Zusammenfassung	i
Summary	iii
Acknowledgments	v
1 Introduction	1
1.1 Motivation	1
1.2 Research objectives	3
1.3 Originality	4
1.4 State of the art	6
1.4.1 Fiber orientation tensors	6
1.4.2 Fiber orientation distribution reconstruction	7
1.4.3 Orientation-averaging mean field homogenization	8
1.5 Outline	9
1.6 Notation, frequently used acronyms, symbols, and operators	11
2 Continuum Mechanics	17
2.1 Motivation	17
2.2 Kinematics and deformation	18
2.3 Time derivatives	19
2.4 Stress	20
2.5 Balance equations	20
2.5.1 Divergence theorem	21
2.5.2 Transport theorem	21
2.5.3 General balance equation	22

2.5.4	Specific balance equations at regular points	23
2.6	Material modeling and closure of balance equations	26
2.7	Linear elasticity	28
3	Tensoralgebra	31
3.1	Motivation	31
3.2	Linear invariant decomposition	31
3.3	Irreducible tensors	34
3.4	Material symmetry	35
3.5	Irreducible tensors constrained by material symmetry	37
3.5.1	Second-order tensors	38
3.5.2	Fourth-order tensors	39
4	Variety of Fiber Orientation Tensors	45
4.1	Introduction	45
4.2	Fiber orientation	47
4.3	Orientation tensors of first kind	50
4.4	Orientation tensors of third kind	51
4.5	Variety of second-order orientation tensors	52
4.5.1	Parameterizations of the orientation triangle	56
4.6	Variety of fourth-order orientation tensors	59
4.6.1	Harmonic decomposition	62
4.6.2	Parameterizations and admissible parameter ranges	67
4.6.3	Transversely isotropic case	69
4.6.4	Orthotropic case	74
4.6.5	Planar case	82
4.7	A note on closure approximations	84
4.8	Summary and conclusions	86
5	Fiber Orientation Distributions Based on Planar Fiber Orientation Tensors of Fourth Order	91
5.1	Introduction	91

5.2	Directional measures as microstructure descriptors	93
5.2.1	Fiber orientation distribution function	93
5.2.2	Fiber orientation tensors	94
5.3	Admissible and distinct planar fiber orientation tensors . .	97
5.4	Reconstructed fiber orientation distribution functions . . .	104
5.4.1	Transition from 3D into 2D	106
5.4.2	Truncated fiber orientation distribution function in a 2D-framework	110
5.4.3	Maximum entropy reconstruction	112
5.4.4	Visualization of reconstructed planar fiber orientation distribution functions	117
5.4.5	Reconstruction solely based on second-order fiber orientation tensors	124
5.5	Summary and conclusion	126
6	On the Dependence of Orientation Averaging Mean Field Homogenization on Planar Fourth-Order Fiber Orientation Tensors	129
6.1	Introduction	129
6.2	Sheet molding compound and planar microstructures . .	132
6.3	Planar fourth-order fiber orientation tensors	137
6.4	Orientation averages	140
6.4.1	Reformulation of the explicit Advani-Tucker orientation average	141
6.4.2	Direct numerical integration and the adaptive scheme based on angular central Gaussian distributions	143
6.4.3	Orientation average by reconstructed planar FODF based on a maximum entropy method	144
6.5	Orientation-averaging mean field homogenization	146
6.5.1	Two-step Hashin-Shtrikman	148

6.5.2	Orientation-averaging Mori-Tanaka following Benveniste (1987)	153
6.5.3	Direct orientation average of a transversely isotropic stiffness	157
6.5.4	Direct orientation average of a transversely isotropic compliance	157
6.6	Graphical representation of elasticity tensors	157
6.7	Effective stiffnesses: Polar plots and the dependence on planar fourth-order fiber orientations	160
6.7.1	Visualization setup	160
6.7.2	Observations on bounds	167
6.7.3	Observations on the shape of the Young's modulus	168
6.7.4	Observations on the shape of the generalized bulk modulus	168
6.7.5	Implications of closure approximations based on second-order fiber orientation tensors	169
6.8	Summary and conclusions	170
7	Conclusions and Outlook	175
7.1	Conclusions	175
7.2	Outlook	179
A	Appendices to Chapter 4	181
A.1	Material symmetries of second-order tensors	181
A.2	Parameter sets of specific second-order orientation tensors	182
A.3	Coefficient-wise extrema of moment tensors	183
A.4	Parameterization of admissible $\mathbb{N}^{\text{ortho}}$ with Isotropic \mathbf{N}	186
B	Appendices to Chapter 5	187
B.1	Kelvin-Mandel notation and completely symmetric tensors of fourth order	187
B.2	Parameter sets in polar plots	189

C Appendices to Chapter 6	191
C.1 Kelvin-Mandel notation and completely symmetric tensors of fourth order	191
C.2 Harmonic decomposition of transversely isotropic elasticity tensors	191
C.3 Reformulation of the Advani-Tucker orientation average .	194
C.4 Advani-Tucker Orientation Average of Minor Symmetric Tensors	195
C.5 Connection to Notation in Kehrer et al. (2020)	199
C.6 Component representations of tensor inversions	199
C.7 Parameter sets in polar plots	202
C.8 Effective complementary elastic energy density	204
Bibliography	209

Chapter 1

Introduction

1.1 Motivation

Fiber-reinforced composites solve lightweight construction tasks in a wide variety of application areas. A major reason for the frequent use of these composites is their excellent mechanical performance at relatively low density. In the case of epoxy resins reinforced with glass fibers, competitive mechanical properties of the composite are achieved by the combination of the high strength and stiffness of the fibers with the flexibility of the matrix material. The microstructure of the composite, i.e., the amount, arrangement and orientation of the fibers, largely determines the effective properties. The realization of beneficial microstructures and, in particular, the suitable alignment of fibers in highly stressed areas of the component is therefore a crucial task in the design and manufacturing process. Optimal component design and optimized manufacturing requires a profound understanding of the relationship between fiber orientations and effective local mechanical material properties. The local mechanical properties can be determined by material models within the framework of continuum mechanics, on scales relevant to engineering. A practically relevant class of such material models are orientation-averaging linear elastic mean field homogenization methods, which are the focus of this work. These homogenization methods combine information on the microstructure

with mechanical properties of the constituents, fiber and matrix, to identify the effective material behavior. Fiber orientation tensors are well-established descriptors for the orientation of fibers on a selected discretization scale. They can be predicted numerically by process simulations as well as determined experimentally by computer tomography. The variety of second-order fiber orientation tensors is known and is represented graphically by the so-called fiber orientation triangle. Knowledge of the variety of all possible second-order fiber orientation tensors offers far-reaching simplification options for individual steps within a virtual process chain and facilitates the assessment and classification of microstructures. However, since the effective material behavior of solids depends on both second- and fourth-order fiber orientation tensors, the knowledge of the variety of fourth-order fiber orientation tensors is of great interest to obtain a complete picture of the realizable effective properties. The present work has been funded by the German Research Foundation (DFG) interdisciplinary research training group GRK 2078. This research training group focuses on the material class sheet molding compound (SMC), a composite of long glass fibers and thermoset polymer matrix, which is suitable for the mass production of flat components. In this work the variety of fourth-order fiber orientation tensors is studied and for the first time the complete picture of the realizable effective properties using microstructure properties in the form of planar fourth-order fiber orientation tensors is outlined. The subgroup of planar fourth-order fiber orientation tensors is of special interest, as the typical fiber lengths in SMC are in the range of two to ten times of the component thickness. Due to this length ratio and low tendency towards fiber bending, SMC microstructures may be described by a low-dimensional planar approximation.

1.2 Research objectives

The main objective of this thesis is the connection between local fiber orientation states in SMC components and effective mechanical properties. A compact and nevertheless complete representation of this connections is aimed at, which is in contrast to limited examinations of concrete examples, present in the literature. The identification of the variety of fiber orientation tensors of fourth-order represents the starting point for the investigations. This identification is done for general orientation states. In a subsequent step, subspaces of these general orientation states, which state reasonable approximations to SMC microstructures are of interest, possibly leading to compact representations. For the special case of planar orientation states, correlations between orientation tensors and orientation distributions are of concern. Therefore, methods reconstructing fiber orientation distributions by a set of leading fiber orientation tensors are given. These methods lead to a flexible numerical scheme for the calculation of orientation averages. Consequences of orientation states on effective mechanical properties are to be drawn for different orientation-averaging homogenizations. Visual representations for all realizable planar orientation states are of special value giving a simple picture of the dependencies between microstructure and effective mechanical properties. Emphasis is to be taken on linearity of effective stiffnesses in fiber orientation tensors within the Advani-Tucker orientation average.

The diversity of fiber orientation tensors is in direct contradiction to commonly used closure algorithms. Therefore, representations which contrast fourth-order information obtained by closure approximations and the variety of possible fourth-order information, are of interest.

1.3 Originality

The major novelties of this work, which is based on Bauer and Böhlke (2022c;a,b), are summarized.

- An invariant framework for parameterizations of fourth-order fiber orientation tensors based on deviators from the isotropic orientation state is developed. The most general case is obtained by an orthotropic deviator of second order and a triclinic deviator of fourth order. Within this framework, deviators of stronger material symmetries are obtained as special cases.
- Explicit parameterizations and admissible parameter ranges for orthotropic as well as planar fiber orientation tensors of fourth order are identified and visualized in Figures 4.5 to 4.8 and 5.1b.
- Boundaries of the set of admissible fiber orientation tensors of fourth order are identified to correspond to localized fiber orientation states which can be represented by empirical fiber orientation distribution functions with a limited number of Dirac-distributions.
- Redundancies and degeneration in the planar set of admissible fourth-order fiber orientation tensors are discussed in detail.
- A generic visual representation of the dependence of any scalar quantity on planar fourth-order fiber orientation tensors is derived and applied to fiber orientation distribution functions and effective mechanical properties.
- Drawbacks of fiber orientation distribution reconstruction based on truncated Fourier series expansion within two- and three-dimensional frameworks are demonstrated, highlighting the role of the isotropic reference states.
- For the planar case and within the two dimensional framework it is shown that interference of second- and fourth-order contributions leads to the variety of reconstructed FODF based on truncated Fourier series.

- The maximum entropy reconstruction of Müller and Böhlke (2016) is recast for the planar case in a two-dimensional framework, leading to a low-dimensional optimization problem.
- Fiber orientations of sheet molding compound are identified to be approximately planar, leading to a reduction of the independent components of fourth-order fiber orientation tensors from eleven to three in the orientation coordinate system.
- The orientation average of an elasticity tensor based on a fiber orientation tensor following Advani and Tucker III (1987) is linear in both the transversely isotropic elasticity tensor and the second- and fourth-order fiber orientation tensors.
- A new numerical formulation of the Advani-Tucker orientation average in fiber orientation tensors Advani and Tucker III (1987) for the special class of planar fiber orientations is proposed based on a maximum entropy reconstruction of fiber orientation distribution functions.
- Effective stiffnesses obtained by homogenizations which perform the orientation average in the stiffness domain and those which perform the average in the compliance domain are demonstrated to differ significantly with respect to the orientation dependence of the generalized bulk modulus.
- Possible directional dependence of the elastic response for Advani-Tucker averaged two-phase materials of isotropic constituents and planar orientation measures are comprehensively presented. This presentation is complete and can be used to express the orientation dependence of any quantity which is a function of planar fiber orientation tensors up to fourth order. The dependence is restricted by the limited averaged information given by fourth-order fiber orientation tensors and due to the constraints of linear elasticity.

1.4 State of the art¹

1.4.1 Fiber orientation tensors

Local fiber orientation distributions are completely defined by a fiber orientation distribution function (FODF). However, in applications the FODF is usually approximated by a limited number of fiber orientation tensors (FOT), as tensor representations fit into the continuum mechanics framework. Multiple kinds of orientation tensors exist, originating from Kanatani (1984). Applications related to fiber orientations include both identification of the fiber orientation information by experimental methods (Pinter et al., 2018) or process simulation (Meyer et al., 2020a) and usage of the orientation information in fullfield (Görthofer et al., 2020), mean field (Müller and Böhlke, 2016; Kehrer et al., 2020), or damage simulations (Schemmann et al., 2018b). Both groups of applications, identification and usage of orientation information, benefit from a well known variety of fiber orientation tensors. If the variety of fiber orientation tensors is well-defined, the identified orientation tensors can be assessed and the space of input parameters of methods predicting effective mechanical properties is set. The variety of second-order fiber orientation tensors is well known (Cintra Jr and Tucker III, 1995; Chung and Kwon, 2002; Cowin, 1985) and used, e.g., in Köbler et al. (2018); Görthofer et al. (2020); Köbler et al. (2021) to generate clear pictures of the dependence of mechanical properties on the second-order directional measures. However, concise descriptions and parameterizations of fourth-order fiber orientation tensors are rare. The variety of transversely isotropic fourth-order orientation tensors is identified by Nomura et al. (1970) and used in Müller and Böhlke (2016); Jack and Smith (2008). For a given second-order orientation tensor, closure approximations (Advani and Tucker III, 1990; Han and Im, 1999; Cintra Jr and Tucker III, 1995;

¹ Most of the content of this section is taken directly from Bauer and Böhlke (2022c;a;b).

Chung and Kwon, 2002; Montgomery-Smith et al., 2011a) identify a corresponding fourth-order orientation tensor based on assumptions. Although literature on closure approximations involves much information on fourth-order fiber orientation tensors, most closures state simplifying assumptions on the material symmetry of fourth-order FOT. In consequence, generic, i.e., triclinic FOT are not covered in the literature on closure approximations.

1.4.2 Fiber orientation distribution reconstruction

Fiber orientation distribution functions represent exact microstructure descriptors of the orientation of axisymmetric fibers within a specified volume of a fiber-reinforced composite (Kanatani, 1984; Advani and Tucker III, 1987). However, in practice (Böhlke et al., 2019; Görthofer et al., 2019) the exact distribution of fibers is commonly approximated by fiber orientation tensors which represent averaged directional measures and can be directly determined either by non-destructive analysis methods, such as computer tomography (Pinter et al., 2018; Schöttl et al., 2020) or by numerical flow simulations (Meyer et al., 2020a; Böhlke et al., 2019; Karl et al., 2021a). Some applications, e.g., damage modeling (Schemmann et al., 2018b) or averaging schemes (Hessman et al., 2021; Brylka, 2017), require FODF information and therefore motivate reconstruction of FODF from a given set of leading fiber orientation tensors. Due to the averaged character of fiber orientation tensors, no one-to-one correspondence between a set of leading FOT and a FODF exists. Truncated Fourier series are used by Schöttl et al. (2020); Jack and Smith (2004); Eik et al. (2016) to identify an FODF based on leading FOT. However, the identified functions do not meet the non-negativity requirement of a FODF. Non-negativity of the reconstructed FODF based on transversely isotropic leading FOT of order two and four, is enforced by Müller and Böhlke (2016) using a maximum entropy method. Maximum entropy methods are deployed, e.g., in Böhlke

(2005; 2006). Closure approximations (Advani and Tucker III, 1990; Chung and Kwon, 2001; 2002; Cintra Jr and Tucker III, 1995; Han and Im, 1999; Jack et al., 2010; Kuzmin, 2018; Montgomery-Smith et al., 2011a;b; Karl et al., 2021c; Dray et al., 2007) are commonly used to estimate fourth-order FOT based on second-order FOT and therefore have reconstruction character. The closures in Montgomery-Smith et al. (2011a;b) are based on assumptions on an FODF associated with the second- and fourth-order FOT of the closure and therefore state a FODF reconstruction scheme. Breuer et al. (2019) assess the reconstruction of FODFs based on closure approximations and minimum entropy method used by Böhlke (2005); Müller and Böhlke (2016).

1.4.3 Orientation-averaging mean field homogenization

Approximation of effective mechanical properties of heterogeneous materials by mean field homogenization dates back to Voigt (1889); Reuß (1929); Hill (1952) with major contributions by Hashin and Shtrikman (1962); Walpole (1966a;b); Willis (1977; 1981); Walpole (1969); Mori and Tanaka (1973) with a strong dependence on Eshelby (1957). The transformation of volume averages into averages over orientations (Böhlke, 2001) leads to orientation-averaging homogenizations (Benveniste, 1987; Duschlbauer et al., 2006; Hessman et al., 2021; Müller and Böhlke, 2016; Müller, 2016; Brylka, 2017; Schemmann et al., 2018b; Kehrer et al., 2020). Hessman et al. (2021) cast several popular orientation-averaging homogenizations (Hill, 1965b; Budiansky, 1965; Mori and Tanaka, 1973; Benveniste, 1987; Castañeda and Willis, 1995; Zheng and Du, 2001; Pierard et al., 2004) into a unified framework. Effective mechanical properties of SMC are identified by Trauth et al. (2021); Schemmann et al. (2018b); Kehrer (2019); Kehrer et al. (2020) using orientation-averaging mean field homogenization, whereas Görthofer et al. (2020) deploy a fast Fourier transform method (Schneider, 2021; Moulinec and Suquet, 1994; 1998). Most mean field homogenizations are based on the averaging

scheme of Advani and Tucker III (1987) which is directly formulated in FOT. However, some authors apply direct numerical integration based on FODF, e.g., Pettermann et al. (1997). Müller and Böhlke (2016) showed that the identification of effective mechanical properties based on second-order orientation tensors yields insufficient accuracy (Breuer et al., 2019). Closure approximations are used by, e.g., Jack and Smith (2007; 2008); Buck et al. (2015); Müller and Böhlke (2016); Goldberg et al. (2017) to model mechanical properties. However, as closure approximations are based upon assumptions and do not generate information, the assessment of Müller and Böhlke (2016) applies to those studies.

1.5 Outline

The present work starts with a compact introduction to selected topics of continuum mechanics, i.e., kinematics, stresses, balance equations and the role of material modeling, followed by tensor algebra with focus on linear invariant decompositions, irreducible tensors and material symmetry in Chapter 3.

The variety of fiber orientation tensors of order two and four is investigated in Chapter 4, which is based on Bauer and Böhlke (2022c). Positive semi-definiteness is discovered to define the set of admissible parameter ranges for parameterizations of fourth-order fiber orientation tensors. Constraints induced by material symmetry are utilized explicitly to derive admissible orientation tensors for the transversely isotropic and planar case. The orthotropic case is presented visually. Notes on closure approximations and their limitations close this chapter.

In Chapter 5, which is based on Bauer and Böhlke (2022a), the insights on admissible planar fiber orientation tensors are refined and the correspondence with fiber distributions is investigated. For the first time, a complete picture of planar fiber orientation distributions,

reconstructed from the planar subspace of fiber orientation tensors, is given. This picture is based on a visualization method which slices the space of admissible fiber orientation tensors. Reconstruction of fiber orientation distribution functions by truncated tensorial Fourier series demonstrates advantage of a two-dimensional framework for planar orientations. The variety of orientation distributions is explicitly explained by interference of second- and fourth-order contributions on fiber orientation distributions. A maximum entropy reconstruction method for planar fiber distributions is given in compact and explicit notation in a two-dimensional framework. An explicit representation of the exact closure for the planar case closes this chapter.

The transition from microstructure descriptors to mechanical properties is investigated in Chapter 6 based on Bauer and Böhlke (2022b). Local fiber orientation states of SMC components are identified as approximately planar. Based on this planarity assumption, the variety of associated fiber orientation tensors and distributions is known. In consequence, the complete picture of the effective mechanical properties obtained by orientation-averaging mean field homogenizations is presented. Characteristics of homogenization methods averaging in the stiffness or compliance domain are discussed. The orientation average of Advani-Tucker Advani and Tucker III (1987) is recast as linear invariant decomposition and a new numerical formulation based on reconstructed fiber distributions is given.

Finally, in Chapter 7 the results are summarized and an outlook on future research is given.

1.6 Notation, frequently used acronyms, symbols, and operators

Symbolic tensor notation is preferred in this work. Tensors of first order are denoted by bold lowercase letters such as \mathbf{q} , \mathbf{n} , \mathbf{v} , \mathbf{e} . Tensors of second-order are denoted by bold uppercase letters like \mathbf{N} or \mathbf{Q} and fourth-order tensors are denoted by, e.g., \mathbf{N} or \mathbf{D} . Tensors in representations for varying tensor order are represented by, e.g., $\mathbb{D}_{(k)}$, where k defines the tensor order. Tensorial quantities are defined in a three-dimensional space, unless underlined. If a tensor is underlined like, e.g., $\underline{\mathbf{q}}$ or $\underline{\mathbf{N}}$, it is defined in a two-dimensional space and follows this spaces algebra. A linear mapping of a second-order by a fourth-order tensor reads as $\mathbf{A} = \mathbb{C}[\mathbf{B}]$. The scalar product reads as $\mathbf{A} \cdot \mathbf{B}$. The tensor power, i.e., the k -th dyadic product of, e.g., a first order tensor \mathbf{a} is denoted by $\mathbf{a}^{\otimes k}$ yielding, e.g., $\mathbf{a}^{\otimes 3} = \mathbf{a} \otimes \mathbf{a} \otimes \mathbf{a}$. An orthonormal basis is denoted by $\{\mathbf{e}_i\}$ with $\mathbf{e}_i \cdot \mathbf{e}_j = \delta_{ij}$ and the Kronecker delta δ_{ij} . If a matrix of tensor coefficients is used in mixed notation, the coefficient matrix is directly followed by the tensor basis where the first index of the basis corresponds to the rows of the coefficients matrix, the second one to the columns. Summation convention applies, unless otherwise stated. Representations in index notation always refer to an orthonormal basis. The Rayleigh product is used to represent an active rotation of a physical quantity and for a first order tensor is defined by $\mathbf{Q} \star \mathbf{n} = n_i \mathbf{Q} \mathbf{e}_i$. Sets, i.e., collections of quantities, are denoted by calligraphic symbols, e.g., \mathcal{F} and are constructed by curly braces. Inside the curly braces, elements of the set are given explicitly, or by a generator expression following the pattern $\{\text{quantity} \mid \text{condition fulfilled inside set}\}$. Although this work and related code is based on Harris et al. (2020); Meurer et al. (2017), numbering and indices follow the continuum mechanics convention starting at one.

Acronyms

CODF	Crystal orientation distribution function
CT	Computer tomography
FODF	Fiber orientation distribution function
FOT	Fiber orientation tensor
IBOF	Invariant-based optimal fitting
iso	Isotropic
ORF	Orthotropic fitted
ortho	Orthotropic
perm	Permutation
plan	Planar
RV	Reference volume
RVE	Representative volume element
SMC	Sheet molding compound
sym	Symmetric
transv	Transversely isotropic
unidirect	Unidirectional

Latin letters

a, b, c, A, B, C	Scalar quantities
$\mathbf{a}, \mathbf{b}, \mathbf{c}$	Tensors of first order
$\mathbf{A}, \mathbf{B}, \mathbf{C}$	Tensors of second order
$\mathbb{A}, \mathbb{B}, \mathbb{C}$	Tensors of fourth order
$\mathbb{A}_{(k)}, \mathbb{B}_{(k)}, \mathbb{C}_{(k)}$	Tensors of k -th order
c_f	Fiber volume content
e	Mass specific internal energy
w^*	Complementary energy density

$E(\mathbf{n})$	Direction-dependent Young's modulus
G	Shear modulus
K	Compression modulus
$K(\mathbf{n})$	Direction-dependent generalized compression modulus
$\hat{\mathcal{S}}$	Singular surface
V_{RV}	Reference volume
\mathbf{n}	Normal vector, i.e., direction
\mathbf{q}	Heat flux
\mathbf{t}	Stress vector
\mathbf{u}	Displacement
\mathbf{x}	Position in current configuration
\mathbf{X}	Position in reference configuration
\mathbf{D}	Distortion rate tensor
\mathbf{F}	Structure tensor
$\hat{\mathbf{F}}$	Deformation gradient
\mathbf{H}	Displacement gradient
\mathbf{N}	Second-order fiber orientation tensor of Kanatani first kind
\mathbf{Q}	Rotation, i.e., element of $SO(3)$
\mathbb{A}_i^{SI}	Strain localization tensor of the i -th phase in the single inclusion problem
\mathbb{C}	Elastic stiffness
\mathbb{C}_0	Reference stiffness
$\bar{\mathbb{C}}^{\text{HSW2}}$	Effective stiffnessss of two-step Hashin Shtrikman homogenization scheme
$\bar{\mathbb{C}}^{\text{MTlinearStiffness}}$	Average of phase stiffnesses
$\bar{\mathbb{C}}^{\text{MTlinearCompliance}}$	Inverse of the average of phase compliances
$\bar{\mathbb{C}}^{\text{MTOAB}}$	Effective stiffnessss following Benveniste (1987)
\mathbb{F}	Structure tensor
\mathbb{I}	Identity on fourth-order tensors
\mathbb{I}^S	Identity on symmetric fourth-order tensors

\mathbb{N}	Fourth-order fiber orientation tensor of Kanatani first kind
$\mathbb{P}_1, \mathbb{P}_2$	Isotropic projectors
\mathbb{P}	Hill's polarization tensor
$\hat{\mathbb{D}}_{\langle k \rangle}$	Fiber orientation tensor of Kanatani third kind and k -th order

Greek letters

α_i	Weight of the i -th transversely isotropic structure tensor
η	Entropy
θ	Temperature
λ_i	i -th eigenvalue of \mathbb{N}
ρ	Density
ψ	Fiber orientation distribution function
χ	Movement
ε	Infinitesimal strain tensor
σ	Cauchy stress

Operators

$\det(\cdot)$	Determinant of a quantity
$\text{dev}(\cdot)$	Deviatoric part of a quantity
$\text{sym}(\cdot)$	Symmetric part of a quantity
(\cdot)	Material time derivative
$\mathcal{S}(\cdot)$	Symmetry group of a quantity
$[\cdot]$	Jump of a field quantity
$\underline{(\cdot)}$	Quantity in 2D framework

$(\cdot)^{\otimes k}$	k -th dyadic product of a quantity
$(\cdot)^T$	Transpose of a second-order tensor
$(\cdot)^T_R$	Right transpose of a fourth-order tensor
\star	Rayleigh product operator
$\{\mathbf{e}_i\}$	Orthonormal coordinate system
$\{\mathbf{v}_i\}$	Orthonormal eigensystem of \mathbb{N}
$(\cdot)^S$	Quantity at a singular surface
$(\cdot)_f$	Fiber quantity
$(\cdot)_m$	Matrix quantity
$\bar{(\cdot)}$	Effective quantity
$\langle \cdot \rangle$	Volume average over RVE
$\langle \langle \cdot \rangle \rangle$	Generalized average
$\langle \cdot \rangle_{AT}$	Advani-Tucker average
$\langle \cdot \rangle_{ATN}$	Advani-Tucker average explicitly formulated in fiber orientation tensor \mathbb{N}
$\langle \cdot \rangle_{ATGOS}$	Advani-Tucker average in formulation of Goldberg et al. (2017)
$\langle \cdot \rangle_{ME}$	Advani-Tucker average in numerical 2D maximum entropy formulation

Chapter 2

Continuum Mechanics

2.1 Motivation

Abstracted and restricted to a classical mechanical point of view, motion and deformation of physical bodies in an Euclidean space at different size-scales can be used to describe the environment we are living in. Continuum mechanics allows for a mathematically well-defined description of bodies, their motion and their deformation on a chosen size scale. The flexibility in choosing an appropriate size scale for engineering applications is a striking feature of continuum mechanics. For engineering tasks on macroscopic technical components, a consideration on the scale of molecules or atoms is not purposeful. For this reason, numerical implementations based on models, motivated by continuum mechanics, are ubiquitous in engineering. The best known application is structural analysis using the finite element method, to analyze stresses and deformations in technical components. The present work is focused on the analysis of microstructures, i.e., the structure of heterogeneous components, specifically fiber-reinforced polymers, and the effect of the microstructure on macroscopic material properties. Due to this focus, only a very small part of the continuum mechanics fundamentals is relevant for this work. In the following chapter, important basic terms are introduced and a classification in the broad context of continuum mechanics is given. This chapter in large parts follows Böhlke and

Frohnäpfel (2019); Böhlke (2014) and is influenced by Bertram and Glüge (2013); Bertram (2012).

2.2 Kinematics and deformation

We choose a closed region in a three-dimensional Euclidean space at a randomly chosen reference time and call this region material body. Points of a material body in the initial placement, called reference placement, can be identified by a position vector \mathbf{X} . The current placement of a material point is denoted by \mathbf{x} . The movement of a material point is described by a function

$$\mathbf{x}(\mathbf{X}, t) = \chi(\mathbf{X}, t), \quad (2.1)$$

taken to be invertible and twice continuously differentiable. Therefore, $\mathbf{x}(\mathbf{X}, t)$ at a given time t , defines a field specifying the current placement of a body composed of material points. The first partial derivative of the movement $\chi(\mathbf{X}, t)$ with respect to the reference placement

$$\hat{\mathbf{F}}(\mathbf{X}, t) = \frac{\partial \chi(\mathbf{X}, t)}{\partial \mathbf{X}} \quad (2.2)$$

is called deformation gradient and states the basis for several possible deformation measures capable of describing large deformations. However, in this work only small deformations are considered, which can be described by a linearized theory, developed hereafter. The displacement field is defined as

$$\mathbf{u}(\mathbf{X}, t) = \chi(\mathbf{X}, t) - \mathbf{X}. \quad (2.3)$$

Taking the first partial derivative of the displacement field $\mathbf{u}(\mathbf{X}, t)$ with respect to the reference placement \mathbf{X} , the displacement gradient is defined as

$$\mathbf{H}(\mathbf{X}, t) = \frac{\partial \mathbf{u}(\mathbf{X}, t)}{\partial \mathbf{X}}. \quad (2.4)$$

Based on the displacement gradient, a unique deformation measure for small deformations exists and is given by the infinitesimal strain tensor $\boldsymbol{\varepsilon}(\mathbf{x}, t)$, which can be calculated for a known field of displacement $\mathbf{u}(\mathbf{x}, t)$ by

$$\begin{aligned}\boldsymbol{\varepsilon}(\mathbf{x}, t) &= \frac{1}{2} \left(\frac{\partial \mathbf{u}(\mathbf{x}, t)}{\partial \mathbf{x}} + \left(\frac{\partial \mathbf{u}(\mathbf{x}, t)}{\partial \mathbf{x}} \right)^T \right) \\ &= \frac{1}{2} (\mathbf{H}(\mathbf{x}, t) + \mathbf{H}^T(\mathbf{x}, t)).\end{aligned}\quad (2.5)$$

The transposition \mathbf{A}^T of a second-order tensor \mathbf{A} is defined by

$$\mathbf{v} \cdot (\mathbf{A}^T \mathbf{w}) = \mathbf{w} \cdot (\mathbf{A} \mathbf{v}) \quad \forall \mathbf{v}, \mathbf{w} \quad (2.6)$$

with tensors of first order \mathbf{v} and \mathbf{w} . Theories, based on the infinitesimal strain tensor, which is linear in the deformation gradient, are called geometrically linear. Deformations are small, if $\|\mathbf{H}\| = \sqrt{\mathbf{H} \cdot \mathbf{H}} \ll 1$ holds and imply $\mathbf{x} \approx \mathbf{X}$.

2.3 Time derivatives

The material time derivative of a field quantity $\psi(\mathbf{X}, t)$ is given by

$$\dot{\psi}(\mathbf{X}, t) = \frac{\partial \psi(\mathbf{X}, t)}{\partial t}, \quad (2.7)$$

whereas the material time derivative of the same quantity parameterized as a function of the current placement $\psi(\mathbf{x}, t)$ is given by

$$\dot{\psi}(\mathbf{x}, t) = \frac{\partial \psi(\mathbf{x}, t)}{\partial t} + \frac{\partial \psi(\mathbf{x}, t)}{\partial \mathbf{x}} \cdot \mathbf{v}(\mathbf{x}, t) \quad (2.8)$$

following the chain rule with the velocity of a material point

$$\mathbf{v} = \dot{\mathbf{x}} = \frac{\partial \chi(\mathbf{X}, t)}{\partial t}. \quad (2.9)$$

2.4 Stress

Mechanical interaction between bodies can be described by the concept of forces. Similarly, mechanical interaction between material points located inside or at the boundary of a body can be described by force densities. The introduction of the principle of cuts (Bertram and Glüge, 2013) allows the definition of stress tensors. Let a body be mentally divided into two new bodies along a cut surface. The mechanical interaction that existed before the hypothetical separation process can be represented by a stress vector \mathbf{t} on each of the two, newly created cut surfaces. The stress vectors on both surfaces are of equal magnitude and oriented in opposite directions. According to Cauchy's theorem, a stress vector on the cut surface with normal \mathbf{n} is defined by

$$\mathbf{t} = \boldsymbol{\sigma} \mathbf{n} \quad (2.10)$$

and is associated with a symmetric second-order tensor, the Cauchy stress $\boldsymbol{\sigma}$. The Cauchy stress can be interpreted as a tensor-valued field $\boldsymbol{\sigma}(\mathbf{X})$ which assigns each point \mathbf{X} on a material body a local stress tensor.

2.5 Balance equations

The object of interest is an abstract material body which consists of material points. As this body might move in space, the volume occupied by the body $\mathcal{V}(t)$ might be a function of time. Points at which fields are smooth are called regular points. Smooth means continuous and

continuously differentiable. This smoothness of the fields is not given perpendicular to so-called singular surfaces $\hat{\mathcal{S}}(t)$. Singular surfaces (Bertram, 2012; Cermelli et al., 2005; Prahs, 2020) describe places where jumps of field quantities occur and separate areas of regular points. An example of singular surfaces are the interfaces of different phases in inhomogeneous materials, e.g., the interface between fibers and matrix in fiber reinforced composites.

2.5.1 Divergence theorem

For a given vector-valued field quantity \mathbf{b} and a domain $\mathcal{V}(t)$ with boundary $\partial\mathcal{V}(t)$ and singular surfaces $\hat{\mathcal{S}}(t)$, the surface integral over \mathbf{b} expressed by a volume integral is

$$\int_{\partial\mathcal{V}(t)} \mathbf{b} \cdot \mathbf{n} \, dA - \int_{\hat{\mathcal{S}}(t)} [\mathbf{b}] \cdot \mathbf{n} \, dA = \int_{\mathcal{V}(t)} \operatorname{div}(\mathbf{b}) \, dV \quad (2.11)$$

with the jump of \mathbf{b} at the singular surface $[\mathbf{b}] = \mathbf{b}^+ - \mathbf{b}^-$ and the normal \mathbf{n} at $\hat{\mathcal{S}}(t)$ pointing from the side where \mathbf{b} has the value \mathbf{b}^- towards the side where \mathbf{b} is equal to \mathbf{b}^+ . The divergence operator $\operatorname{div}(\cdot) = \operatorname{tr}(\operatorname{grad}(\cdot))$ is based on the trace operator $\operatorname{tr}(\cdot)$ and the gradient denoted by $\operatorname{grad}(\cdot)$. This relation is essential for transforming integral balances into local balances.

2.5.2 Transport theorem

Let $\mathcal{V}(t)$ be the volume of a certain domain, for example a body. This volume may change and therefore is a function of time. The time derivative of an integral over a domain depends both on the change of the integrated field quantity ψ and the change of the volume $\mathcal{V}(t)$ occupied by the domain. For a volume \mathcal{V} associated with a material, this

relation is described by

$$\frac{d}{dt} \int_{\mathcal{V}(t)} \psi dV = \int_{\mathcal{V}(t)} \frac{\partial \psi}{\partial t} dV + \int_{\partial \mathcal{V}(t)} \psi \mathbf{v} \cdot \mathbf{n} dA - \int_{\hat{\mathcal{S}}(t)} [\psi] v_{\perp}^S dA \quad (2.12)$$

with \mathbf{v} being the velocity field of the body, $[\psi]$ the jump of ψ at $\hat{\mathcal{S}}(t)$ and v_{\perp}^S the velocity of the singular surface normal to $\hat{\mathcal{S}}(t)$. In the absense of singular surfaces, combining Equation (2.12) with Equation (2.11) yields

$$\frac{d}{dt} \int_{\mathcal{V}(t)} \psi dV = \int_{\mathcal{V}(t)} \frac{\partial \psi}{\partial t} + \operatorname{div}(\psi \mathbf{v}) dV \quad (2.13)$$

being valid only at regular points.

2.5.3 General balance equation

We consider balancing a time-dependent field quantity $\psi(\mathbf{x}, t)$ over a material body. The volume occupied by the material body $\mathcal{V}(t)$ is a function of time t . The field quantity is said to be additive in nature and has an associated

- Production density $p_{\psi}(\mathbf{x}, t)$ representing the local production of ψ per unit volume
- Supply density $s_{\psi}(\mathbf{x}, t)$ representing the local supply of ψ per unit volume
- Non-convective flux $\mathbf{q}_{\psi}(\mathbf{x}, t)$ representing the local flux of ψ per unit area.

Fluxes caused by other physical processes than convection are called non-convective fluxes. Heat flux and Cauchy stress are examples of

non-convective fluxes. The balance of ψ over \mathcal{V} reads as

$$\frac{d}{dt} \int_{\mathcal{V}(t)} \psi dV = \int_{\mathcal{V}(t)} p_\psi + s_\psi dV + \int_{\partial\mathcal{V}(t)} \mathbf{q}_\psi \cdot \mathbf{n} dA. \quad (2.14)$$

The local form of this balance restricted to regular points is obtained using Equation (2.13) leading to

$$\frac{\partial \psi}{\partial t} + \operatorname{div}(\psi \mathbf{v}) = p_\psi + s_\psi + \operatorname{div}(\mathbf{q}_\psi) \quad (2.15)$$

with $\psi \mathbf{v}$ being the convective flux. If the volume in which Equation (2.14) is evaluated is completely shrunk to the singular surfaces, a jump condition for the field quantity at $\hat{S}(t)$ is obtained and reads

$$[\psi(\mathbf{v} \cdot \mathbf{n} - v_\perp^S)] - [\mathbf{q}_\psi] \cdot \mathbf{n} = 0. \quad (2.16)$$

In the case of a material singular surface, such as those present at phase boundaries in heterogeneous materials, $v^S = \mathbf{v}$ holds and the jump condition in Equation (2.16) reduces to a requirement on \mathbf{q}_ψ .

2.5.4 Specific balance equations at regular points

Balance equations for mass, linear momentum, angular momentum, energy, and entropy can be obtained from Equation (2.14) or Equation (2.15) using the quantities specified in Table 2.1. The remaining considerations within this chapter are restricted to regular points. Jump conditions at singular surfaces can be found in Böhlke (2014); Bertram (2012).

Mass

The balance of mass is given by

$$\dot{\rho} + \rho \operatorname{div}(\mathbf{v}) = 0 \quad (2.17)$$

Balance	Quantity: ψ	Produc.: p_ψ	Supply: s_ψ	Flux: \mathbf{q}_ψ
Mass	ρ	0	0	0
Lin. Momentum	$\rho\mathbf{v}$	0	$\rho\mathbf{b}$	σ
Ang. Momentum	$(\mathbf{x} - \mathbf{x}_0) \times \rho\mathbf{v}$	0	$(\mathbf{x} - \mathbf{x}_0) \times \rho\mathbf{b}$	$(\mathbf{x} - \mathbf{x}_0) \times \sigma$
Energy	$\rho e + \frac{\rho}{2}\mathbf{v} \cdot \mathbf{v}$	0	$\rho w + \rho\mathbf{b} \cdot \mathbf{v}$	$-\mathbf{q} + \sigma^\top \mathbf{v}$
Entropy	$\rho\eta$	ρp_η	$\frac{\rho}{\theta}w$	$-\frac{1}{\theta}\mathbf{q}$

Table 2.1: Building blocks to derive specific balance equations from the general balance equation. The ansatz for supply and flux of entropy are of constitute nature. The abbreviation produc. stands for production.

with the mass density ρ .

Linear momentum

The axiom of the balance of linear momentum fits experimental observations for non-relativistic cases and leads to

$$\rho\dot{\mathbf{v}} = \rho\mathbf{b} + \operatorname{div}(\boldsymbol{\sigma}). \quad (2.18)$$

with a mass force density \mathbf{b} .

Angular momentum

The balance of angular momentum, is an axiom, which for a Boltzmann continuum, i.e., a continuum without point-wise rotational degrees of freedom, results in a system of algebraic equations denoted by

$$\boldsymbol{\sigma} = \boldsymbol{\sigma}^\top. \quad (2.19)$$

Total energy

Total energy is the sum of kinetic and internal energy and its balance is

$$\rho \dot{e} + \frac{1}{2} \rho (\mathbf{v} \cdot \mathbf{v}) = \rho w - \operatorname{div}(\mathbf{q}) + \rho \mathbf{b} \cdot \mathbf{v} + \operatorname{div}(\boldsymbol{\sigma}^T \mathbf{v}) \quad (2.20)$$

with the heat source density w and the heat flux \mathbf{q} . The total energy is a conservation quantity because the production term vanishes. The local balances used in this section apply to material points. A material point can be considered as a thermodynamic system. The energy due to the motion of this system is its kinetic energy. The mass specific internal energy e contains the energy which is independent of the system's motion. The internal energy states a thermodynamic potential.

Kinetic energy

The balance of kinetic energy is obtained by scalar multiplication of Equation (2.18) with the velocity field \mathbf{v} leading to

$$\frac{1}{2} \rho (\mathbf{v} \cdot \mathbf{v}) = \rho \mathbf{b} \cdot \mathbf{v} + \operatorname{div}(\boldsymbol{\sigma}^T \mathbf{v}) - \boldsymbol{\sigma} \cdot \mathbf{D} \quad (2.21)$$

with the distortion rate tensor $\mathbf{D} = \operatorname{sym}(\operatorname{grad}(\mathbf{v}))$. This procedure implies that the balance of kinetic energy is another representation of information already included in the balance of linear momentum.

Internal energy

The balance of internal energy, given in Equation (2.22), is obtained by subtracting the balance of kinetic energy from the balance of total energy.

$$\rho\dot{e} + \frac{1}{2}\rho(\mathbf{v} \cdot \mathbf{v}) = \rho w - \operatorname{div}(\mathbf{q}) + \rho\mathbf{b} \cdot \mathbf{v} + \operatorname{div}(\boldsymbol{\sigma}^T \mathbf{v}) \quad \text{tot. (2.20)}$$

$$\frac{1}{2}\rho(\mathbf{v} \cdot \mathbf{v}) = \rho\mathbf{b} \cdot \mathbf{v} + \operatorname{div}(\boldsymbol{\sigma}^T \mathbf{v}) - \boldsymbol{\sigma} \cdot \mathbf{D} \quad \text{kin. (2.21)}$$

$$\rho\dot{e} = \rho w - \operatorname{div}(\mathbf{q}) + \boldsymbol{\sigma} \cdot \mathbf{D} \quad (2.22)$$

Entropy

The balance of entropy is given by

$$\rho\dot{\eta} = \frac{\rho w}{\theta} - \operatorname{div}\left(\frac{\mathbf{q}}{\theta}\right) + \rho p_\eta \quad (2.23)$$

with entropy η , temperature θ and the entropy production p_η , which has to be non-negative to satisfy the second law of thermodynamics.

2.6 Material modeling and closure of balance equations

The following considerations are limited to small deformations and in consequence, deformation is described by the infinitesimal strain tensor $\boldsymbol{\varepsilon}$. Further consequences are that the reference placement is approximately equal to the current placement ($\mathbf{X} \approx \mathbf{x}$), the density is approximately constant ($\rho \approx \rho_0$) and the symmetric part of the velocity gradient can be approximated by the rate of $\boldsymbol{\varepsilon}$, i.e., $\mathbf{D} \approx \dot{\boldsymbol{\varepsilon}}$ holds.

Applying the restrictions of small deformations and regular points, the

resulting balance equations

$$\rho \approx \rho_0 \quad (2.24)$$

$$\boldsymbol{\sigma} = \boldsymbol{\sigma}^\top \quad (2.25)$$

$$\rho \ddot{\mathbf{u}} = \rho \mathbf{b} + \operatorname{div}(\boldsymbol{\sigma}) \quad (2.26)$$

$$\rho \dot{e} = \rho w - \operatorname{div}(\mathbf{q}) + \boldsymbol{\sigma} \cdot \dot{\boldsymbol{\epsilon}} \quad (2.27)$$

$$\rho \dot{\eta} = \frac{\rho w}{\theta} - \operatorname{div}\left(\frac{\mathbf{q}}{\theta}\right) + \rho p_\eta \quad (2.28)$$

state the starting point to derive a closed system of field equations for initial boundary value problems. The quantities ρ , \mathbf{b} and w are known for a given initial boundary value problem. Displacement \mathbf{u} , temperature θ and a vector of internal variables $\underline{\alpha}$ are selected as base fields $\mathcal{B} = \{\mathbf{u}, \theta, \underline{\alpha}\}$. The base fields state the solution space of the initial boundary value problems.

From Equations (2.26) and (2.27) follows that the remaining set of quantities is $\mathcal{K} = \{\boldsymbol{\sigma}, e, \mathbf{q}, \eta\}$. These quantities are called constitutive quantities and are unknown and not yet linked to the base fields. From an engineering point of view, the entropy is usually not of practical interest. However, including entropy as an auxiliary quantity in the set of constitutive quantities permits to incorporate restrictions stated by the second law of thermodynamics. In order to generate a closed system of equations, a set of material functions \mathcal{M} has to be defined, expressing the constitutive quantities as functions of the base fields. As the constitutive quantities \mathcal{K} may also depend on gradients and time derivatives of the base fields, a set of input quantities \mathcal{E} is defined containing the base fields as well as their gradients and derivatives.

Material modeling is the process of defining the material functions \mathcal{M} such that $\mathcal{K} = \mathcal{M}(\mathcal{E})$ closes the system of Equations (2.24) to (2.28) while

- Fulfilling restrictions stated by material theory
- Not violating the second law of thermodynamics and

- Reproducing experimental observations.

Equations (2.24) and (2.25) state algebraic equations and can be fulfilled identically. Equations (2.26) and (2.27) state the primary partial differential equations and Equation (2.28) states the basis for restrictions caused by the second law of thermodynamics.

2.7 Linear elasticity

Within this work, only the simplest material model, linear elasticity for small deformations is considered. Linear elasticity implies, that there is no interaction between temperature and the displacement field. In addition, no state variables exist, as the current stress is solely determined by the current deformation. In consequence, the only non-trivial field equation is the balance of linear momentum in Equation (2.26) and material modeling is reduced to finding the relation between σ and ε .

Linear elasticity postulates this relation to be a linear mapping

$$\sigma = \mathbb{C} [\varepsilon] \quad (2.29)$$

defining the material stiffness \mathbb{C} . As the stiffness maps between symmetric tensors of second-order, without loss of generality, the stiffness can be assumed to have both minor symmetries. A fourth-order tensor \mathbb{C} is called minor symmetric, if

$$\mathbf{A} \cdot \mathbb{C} [\mathbf{B}] = \mathbf{A}^\top \cdot \mathbb{C} [\mathbf{B}] = \mathbf{A} \cdot \mathbb{C} [\mathbf{B}^\top] \quad \forall \mathbf{A}, \mathbf{B} \quad (2.30)$$

holds with \mathbf{A} and \mathbf{B} being tensors of second order and their transposition is defined in Equation (2.6). Hyperelasticity, i.e., postulating the existence of a strain energy density function, implies the main symmetry of the

stiffness \mathbb{C} . A fourth-order tensor \mathbb{C} is major symmetric, if

$$\mathbf{A} \cdot \mathbb{C} [\mathbf{B}] = \mathbf{B} \cdot \mathbb{C} [\mathbf{A}] \quad \forall \mathbf{A}, \mathbf{B} \quad (2.31)$$

holds. Based on the assumptions of linear elasticity and small deformations, the interaction between averaged microstructure descriptors and the linear elastic anisotropic effective material behavior is investigated within this work.

Chapter 3

Tensoralgebra

3.1 Motivation

Euclidean tensors, i.e., tensor components A_{ij} associated with a fixed orthonormal coordinate system $\{\mathbf{e}_i\}$, defining $\mathbf{A} = A_{ij}\mathbf{e}_i \otimes \mathbf{e}_j$, are established descriptors for physical quantities in continuum mechanics. Second- and fourth-order tensors have a special significance in continuum mechanics, since stress and strain are described by second-order tensors and linear constitutive laws can be represented as linear mappings between tensors of second order. Tensors of fourth order map second-order tensors linearly. A major contribution of this work is the identification of suitable parameterizations for special fourth-order tensors, namely fiber orientation tensors. The most important building blocks are linear invariant decompositions, irreducible tensors and material symmetry. Following Adams et al. (1992); Onat and Leckie (1988); Jerphagnon et al. (1978), material modeling can be reduced to the identification of irreducible tensors and definition of corresponding evolution equations.

3.2 Linear invariant decomposition

Linear invariant decomposition of symmetric second-order tensors is a common topic of continuum mechanics lessons. Applied to the stress

tensor, a linear invariant decomposition into the sum of a spherical and a deviatoric part reads as

$$\boldsymbol{\sigma} = \frac{1}{3} \text{tr}(\boldsymbol{\sigma}) \mathbf{I} + \text{dev}(\boldsymbol{\sigma}) \quad (3.1)$$

$$= -p \mathbf{I} + \text{dev}(\boldsymbol{\sigma}) \quad (3.2)$$

and can be motivated by the physical interpretation of the pressure p and remaining deviatoric stresses $\text{dev}(\boldsymbol{\sigma}) = \boldsymbol{\sigma} - \frac{1}{3} \text{tr}(\boldsymbol{\sigma}) \mathbf{I}$ with the identity on second-order tensors \mathbf{I} defined by $\mathbf{I}[\mathbf{v}] = \mathbf{v}$ for all first-order tensors \mathbf{v} . Both parts are orthogonal and transform differently with respect to rotations, i.e., actions of elements of the special orthogonal group $SO(3)$. The spherical part is isotropic by definition, i.e.,

$$\mathbf{Q} \star (-p \mathbf{I}) = -p \mathbf{I} \quad \forall \mathbf{Q} \in SO(3) \quad (3.3)$$

holds, whereas the deviatoric stress transforms with respect to $\mathbf{Q} \in SO(3)$ by

$$\mathbf{Q} \star \text{dev}(\boldsymbol{\sigma}) = \mathbf{Q} \text{dev}(\boldsymbol{\sigma}) \mathbf{Q}^{-1}. \quad (3.4)$$

The scalar pressure and the deviatoric stress do not interact with each other under the action of elements of $SO(3)$ and are called irreducible tensors, being of order zero and two. Linear invariant decompositions into irreducible tensors exist for tensors of arbitrary order and symmetry. However, in this work fourth-order tensors with at least minor and major symmetry are of special interest.

Different linear invariant decompositions are given in the literature, see Rychlewski (2000); Forte and Vianello (1996); Olive et al. (2017). A detailed discussion on specific decompositions defined by the selection of two pairs of symmetrization operators is given in Rychlewski (2000) and utilized in Section 4.6.1. However, the so-called harmonic decomposition is the most common decomposition (Forte and Vianello,

1996; Rychlewski, 2000; Böhlke and Brüggemann, 2001; Fernández and Böhlke, 2019; Lobos et al., 2017; Backus, 1970; Baerheim, 1993; Boehler et al., 1994; Mochizuki, 1988; Rychlewski, 2001; Lubarda and Chen, 2008) and decomposes a minor and major symmetric fourth-order tensor \mathbb{C} into

$$\begin{aligned} \mathbb{C}(h_1, h_2, \mathbf{H}_1, \mathbf{H}_2, \mathbb{H}) = \\ h_1 \mathbb{P}_1 + h_2 \mathbb{P}_2 + (\mathbf{I} \otimes \mathbf{H}_1 + \mathbf{H}_1 \otimes \mathbf{I}) + \mathbb{J}[\mathbf{H}_2] + \mathbb{H} \end{aligned} \quad (3.5)$$

with

$$h_1 = \mathbb{P}_1 \cdot \mathbb{C}, \quad h_2 = \frac{\mathbb{P}_2}{\|\mathbb{P}_2\|^2} \cdot \mathbb{C}, \quad \mathbb{H} = \text{dev}(\mathbb{C}) \quad (3.6)$$

and

$$\mathbf{H}_1 = \frac{1}{7} [5 \text{dev}(\mathbb{C}) - 4 \text{dev}(\mathbf{V})] \quad (3.7)$$

$$\mathbf{H}_2 = \frac{1}{7} [3 \text{dev}(\mathbb{C}) - 2 \text{dev}(\mathbf{V})] \quad (3.8)$$

based on the dilatational modulus \mathbb{C} and the Voigt tensor \mathbf{V} which are given by

$$(\mathbb{C})_{ij} = (\mathbb{C})_{ijkk} \quad (3.9)$$

$$(\mathbf{V})_{ij} = (\mathbb{C})_{ikjk}, \quad (3.10)$$

see Cowin (1989). The isotropic projectors \mathbb{P}_1 and \mathbb{P}_2 are given by

$$\mathbb{P}_1 = \frac{1}{3} \mathbf{I} \otimes \mathbf{I}, \quad \mathbb{P}_2 = \mathbb{I}^S - \mathbb{P}_1 \quad (3.11)$$

$$\text{with } \mathbb{I}^S = \frac{1}{2} (\mathbb{I} + \mathbb{I}^{T_R}), \quad \mathbb{I} = \mathbf{e}_i \otimes \mathbf{e}_j \otimes \mathbf{e}_i \otimes \mathbf{e}_j. \quad (3.12)$$

The right index transpose operator for fourth-order tensors $(\cdot)^{T_R}$ is defined by $(\mathbf{A} \otimes \mathbf{B})^{T_R} = \mathbf{A} \otimes \mathbf{B}^T$ for arbitrary second-order tensors \mathbf{A} ,

\mathbf{B} and the transpose of a second-order tensor $(\cdot)^T$. The deviatoric part of a fourth-order tensor is defined in Spencer (1970); Kanatani (1984); Böhlke (2001) and can be written as

$$\text{dev}(\mathbb{C}) = \mathbb{C} - \frac{6}{7}\text{sym}(\mathbb{C} \otimes \mathbf{I}) + \frac{3}{35}\mathbf{C} \cdot \mathbf{I} \text{ sym}(\mathbf{I} \otimes \mathbf{I}). \quad (3.13)$$

with the intermediate quantity $\mathbf{C} = \mathbb{C}[\mathbf{I}]$ and the operator $\text{sym}(\cdot)$ taking the completely symmetric part of a tensor (Spencer, 1970). The isotropic sixth-order tensor \mathbb{J} in Equation (3.5) is defined by

$$\begin{aligned} \mathbb{J} = & \frac{1}{2}(\mathbf{e}_i \otimes \mathbf{e}_j + \mathbf{e}_j \otimes \mathbf{e}_i) \\ & \otimes (\mathbf{e}_j \otimes \mathbf{e}_k + \mathbf{e}_k \otimes \mathbf{e}_j) \\ & \otimes (\mathbf{e}_k \otimes \mathbf{e}_i + \mathbf{e}_i \otimes \mathbf{e}_k), \end{aligned} \quad (3.14)$$

see Forte and Vianello (1996); Böhlke and Brüggemann (2001).

Consequently, any minor and major symmetric fourth-order tensor \mathbb{C} can be decomposed into a unique set of irreducible tensors h_1 , h_2 , \mathbf{H}_1 , \mathbf{H}_2 , \mathbb{H} of orders zero, zero, two, two and four. Following Forte and Vianello (1996, Equation (9)), the harmonic parts obtained from Equation (3.5) transform with respect to a rotation $\mathbf{Q} \in SO(3)$ with

$$\mathbf{Q} \star \mathbb{C} = (h_1, h_2, \mathbf{Q} \star \mathbf{H}_1, \mathbf{Q} \star \mathbf{H}_2, \mathbf{Q} \star \mathbb{H}). \quad (3.15)$$

3.3 Irreducible tensors

Irreducible tensors are completely (index) symmetric and traceless (Spencer, 1970; Forte and Vianello, 1996; Jerphagnon et al., 1978; Adams et al., 1992; Cowin, 1989; Rychlewski, 2000). Due to the complete symmetry and the condition of the vanishing trace, the number of independent components of the tensors obtained by the decomposition

in Equation (3.5) are

$$\dim(h_1) = 1, \quad \dim(h_2) = 1, \quad \dim(\mathbf{H}_1) = 5, \quad (3.16)$$

$$\dim(\mathbf{H}_2) = 5, \quad \dim(\mathbb{H}) = 9 \quad (3.17)$$

and reflect the dimension of the associated subspaces. In the absence of additional (material) symmetry a generic irreducible tensor of second order reads as

$$\mathbf{F}(\hat{q}_1, \hat{q}_2, \hat{q}_3, \hat{q}_4, \hat{q}_5) = \begin{bmatrix} \hat{q}_1 & \hat{q}_5 & \hat{q}_4 \\ & \hat{q}_2 & \hat{q}_3 \\ \text{sym} & & -(\hat{q}_1 + \hat{q}_2) \end{bmatrix} \mathbf{e}_i \otimes \mathbf{e}_j. \quad (3.18)$$

and an irreducible tensor of fourth order is given by

in Kelvin-Mandel notation and short hand notation for completely symmetric tensors defined in Appendix B.1 and derived in Section 4.6. Representations of irreducible tensors in Equations (3.18) and (3.19) combined with the harmonic decomposition in Equation (3.5) can be used to parameterize fourth-order tensors.

3.4 Material symmetry

The concept of material symmetries is an important tool for understanding consequences of the structured composition of matter (Jerrold N. Jephagnon)

et al., 1978). Even in the absence of such a structured composition, artificial assumption of material symmetry offers the possibility to reduce the dimensionality of a problem and to gain in this way simplified insights into underlying principles.

A quantity \mathbb{C} is symmetric with respect to a rotation, if the rotation does not affect the quantity, i.e.,

$$\mathbf{Q} \star \mathbb{C} = \mathbb{C} \quad (3.20)$$

holds. If Equation (3.20) is true for a specific \mathbf{Q} , this rotation is said to be part of the symmetry group of \mathbb{C} , denoted by $\mathcal{S}(\mathbb{C})$. Consequently, the symmetry group $\mathcal{S}(\mathbb{C})$ of a quantity \mathbb{C} is defined by

$$\mathbf{Q} \star \mathbb{C} = \mathbb{C} \quad \forall \mathbf{Q} \in \mathcal{S}(\mathbb{C}). \quad (3.21)$$

Forte and Vianello (1996) showed that eight material symmetries, i.e., eight distinct closed groups of elements of $SO(3)$, exist. These material symmetries are also referred to as material symmetry classes and their hierarchy is depicted in Fig. 3.1, following Bóna et al. (2007); Olive et al. (2022); Abramian et al. (2020); Weber et al. (2019). Zheng and Boehler (1994) discuss connections to the concept of point-groups. Visualizations of the material symmetry classes based on symmetry planes are given in Table 3.1 following Francois et al. (1998).

Material symmetry of a quantity simplifies its parameterization by reducing the number of independent components. Following Forte and Vianello (1996, Equation (10)), the symmetry group of a tensorial quantity \mathbb{C} is the intersection of the symmetry groups of its harmonic parts, i.e.,

$$\mathcal{S}(\mathbb{C}) = \mathcal{S}(\mathbf{H}_1) \cap \mathcal{S}(\mathbf{H}_2) \cap \mathcal{S}(\mathbb{H}). \quad (3.22)$$

Therefore, a physical quantity \mathbb{C} might be parameterized by the combina-

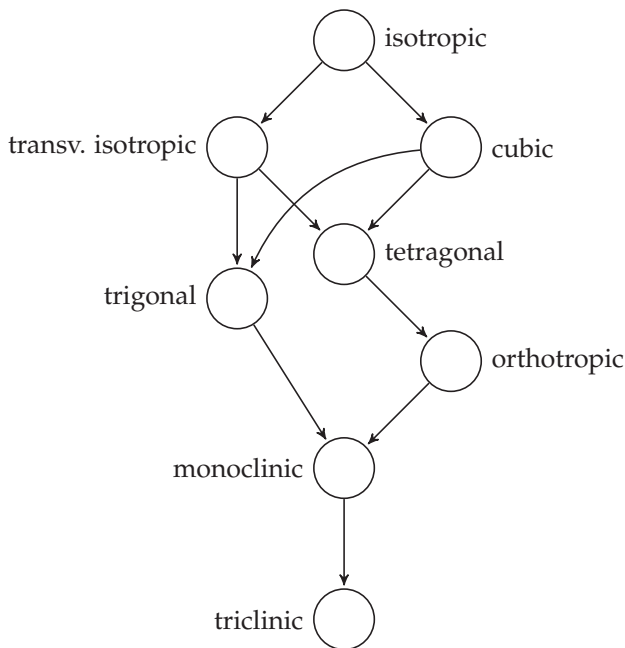


Figure 3.1: Hierarchy of material symmetries following Abramian et al. (2020); Francois et al. (1998). Arrows indicate inclusion, i.e., an arrow points from a symmetry classes with strong symmetry to a symmetry class which is included.

tion of a linear invariant decomposition and a set of irreducible tensors potentially constrained by material symmetry. Essential building blocks for such a parameterization are irreducible second- and fourth-order tensors constrained by material symmetry.

3.5 Irreducible tensors constrained by material symmetry

This section is based on personal communication with Prof. Dr.-Ing. habil. Thomas Böhlke, (Böhlke, 2021). Derived from the generic parame-

terizations of irreducible tensors in Equations (3.18) and (3.19), material symmetries lead to the tensors listed below.

3.5.1 Second-order tensors

Triclinic, monoclinic and orthotropic irreducible second-order tensors $\mathbf{F}^{\text{tricl}}$, \mathbf{F}^{mono} , $\mathbf{F}^{\text{ortho}}$ coincide and can not be distinguished, i.e., $\mathbf{F} = \mathbf{F}^{\text{tricl}} = \mathbf{F}^{\text{mono}} = \mathbf{F}^{\text{ortho}}$ holds. In other words, orthotropy is the weakest possible material symmetry an irreducible second-order tensor can have. This observation is directly related to the observation that any symmetric second-order tensor can be diagonalized. If an ordering convention for the eigenvectors based on eigenvalues applies, exactly four right-handed and four left-handed coordinate systems exist (Hasan et al., 2001; Bro et al., 2008). These are called eigensystems and lead to representations of Equation (3.18) with vanishing off-diagonal entries in the component matrix reading as

$$\mathbf{F}(q_1, q_2, \mathbf{Q}(q_3, q_4, q_5)) = \begin{bmatrix} q_1 & 0 & 0 \\ & q_2 & 0 \\ \text{sym} & & -(q_1 + q_2) \end{bmatrix} \hat{\mathbf{Q}} \mathbf{e}_i \otimes \hat{\mathbf{Q}} \mathbf{e}_j \quad (3.23)$$

with an orthogonal tensor

$$\hat{\mathbf{Q}}(q_3, q_4, q_5) = \hat{\mathbf{v}}_i \otimes \mathbf{e}_i \quad (3.24)$$

defined by three scalars and mapping the arbitrary but fixed basis $\{\mathbf{e}_i\}$ onto an eigensystem $\{\hat{\mathbf{v}}_i\}$. This observation highlights the relevance of Equation (3.22), since the symmetry group of one single harmonic part does not define the symmetry group of the decomposed quantity. However, eigensystems of a decomposed quantity, such as \mathbb{C} in Equation (3.5) are also eigensystems of the harmonic parts. Hereafter, the dependence

of the eigensystem on usually three scalar parameters is no longer stated explicitly and the representations are given directly in an eigensystem $\{\hat{\mathbf{v}}_i\}$.

A transversely isotropic irreducible tensor of second order in an eigen-system which first axis \mathbf{v}_1 is aligned with the transversely isotropic axis is given by

$$\mathbf{F}^{\text{transv}}(q_1) = q_1 \begin{bmatrix} 1 & 0 & 0 \\ & -1/2 & 0 \\ \text{sym} & & -1/2 \end{bmatrix} \hat{\mathbf{v}}_i \otimes \hat{\mathbf{v}}_j. \quad (3.25)$$

The definition of a valid eigensystem in the transversely isotropic case only requires two scalars, since any rotation about the transversely isotropic axis leads to an equally admissible eigensystem. The representation in Equation (3.25) coincides with those of trigonal and tetragonal irreducible tensors of second order, i.e., $\mathbf{F}^{\text{transv}} = \mathbf{F}^{\text{tetra}} = \mathbf{F}^{\text{trigo}}$ holds. Irreducible tensors of second order with isotropic or cubic material symmetry vanish, i.e., $\mathbf{F}^{\text{cubic}} = \mathbf{F}^{\text{iso}} = \mathbf{0}$.

3.5.2 Fourth-order tensors

Departing from the generic, i.e., triclinic, case in Equation (3.19) a monoclinic irreducible tensor of fourth-order is given by

$$\mathbf{F}^{\text{mono } z}(p_1, p_2, p_3, p_8, p_9) = \begin{array}{c|ccc} & -(p_1 + p_2) & p_1 & p_2 \\ & & -(p_1 + p_3) & p_3 \\ \hline & & & -(p_2 + p_3) \\ \text{completely} & & & \\ \hline & 0 & 0 & \sqrt{2} p_8 \\ & 0 & 0 & \sqrt{2} p_9 \\ & 0 & 0 & -\sqrt{2} (p_8 + p_9) \\ \text{symmetric} & & & \end{array} \quad (3.26)$$

$\mathbf{B}_{\xi}^{\hat{\mathbf{v}}} \otimes \mathbf{B}_{\zeta}^{\hat{\mathbf{v}}}$

in a coordinate system $\{\hat{v}_i\}$ with \hat{v}_3 aligned with the normal of the monoclinic symmetry plane, see Table 3.1. The constraints of material symmetry for weaker symmetries lead to the irreducible tensors

$$\mathbb{F}^{\text{ortho}}(p_1, p_2, p_3) = \quad (3.27)$$

$$\left[\begin{array}{ccc|ccc} -(p_1 + p_2) & p_1 & p_2 & 0 & 0 & 0 \\ & -(p_1 + p_3) & p_3 & 0 & 0 & 0 \\ & & -(p_2 + p_3) & 0 & 0 & 0 \\ \hline & \text{completely} & & & \text{symmetric} & \end{array} \right] \mathbf{B}_{\xi}^{\hat{v}} \otimes \mathbf{B}_{\zeta}^{\hat{v}},$$

$$\mathbb{F}^{\text{trigo xy}}(p_3, p_9) = \quad (3.28)$$

$$\left[\begin{array}{ccc|ccc} 8p_3 & -4p_3 & -4p_3 & 0 & 0 & 0 \\ 3p_3 & p_3 & p_3 & 0 & 0 & \sqrt{2}p_9 \\ 3p_3 & & 3p_3 & 0 & 0 & -\sqrt{2}p_9 \\ \hline & \text{completely} & & & \text{symmetric} & \end{array} \right] \mathbf{B}_{\xi}^{\hat{v}} \otimes \mathbf{B}_{\zeta}^{\hat{v}},$$

$$\mathbb{F}^{\text{tetra x}}(p_1, p_3) = \quad (3.29)$$

$$\left[\begin{array}{ccc|ccc} -2p_1 & p_1 & p_1 & 0 & 0 & 0 \\ & -(p_1 + p_3) & p_3 & 0 & 0 & 0 \\ & & -(p_1 + p_3) & 0 & 0 & 0 \\ \hline & \text{completely} & & & \text{symmetric} & \end{array} \right] \mathbf{B}_{\xi}^{\hat{v}} \otimes \mathbf{B}_{\zeta}^{\hat{v}},$$

$$\mathbb{F}^{\text{transv } x}(p_3) = p_3 \left[\begin{array}{ccc|ccc} 8 & -4 & -4 & 0 & 0 & 0 \\ & 3 & 1 & 0 & 0 & 0 \\ & & 3 & 0 & 0 & 0 \\ \hline & & & & & \\ \text{completely} & & & \text{symmetric} & & \end{array} \right] \mathbf{B}_\xi^{\hat{v}} \otimes \mathbf{B}_\zeta^{\hat{v}}, \quad (3.30)$$

and

$$\mathbb{F}^{\text{cubic}}(p_1) = p_1 \left[\begin{array}{ccc|ccc} -2 & 1 & 1 & 0 & 0 & 0 \\ & -2 & 1 & 0 & 0 & 0 \\ & & -2 & 0 & 0 & 0 \\ \hline & & & & & \\ \text{completely} & & & \text{symmetric} & & \end{array} \right] \mathbf{B}_\xi^{\hat{v}} \otimes \mathbf{B}_\zeta^{\hat{v}} \quad (3.31)$$

represented in coordinate systems aligned along characteristic axes of the material. Isotropic irreducible tensors vanish by definition. The superscripts of the irreducible tensors $\mathbb{F}^{\text{mono } z}$, $\mathbb{F}^{\text{trigo } xy}$, $\mathbb{F}^{\text{tetra } x}$ and $\mathbb{F}^{\text{transv } x}$ indicate, that for these material symmetry groups multiple minimal representations by tensor components exist. These representation are equivalent, but differ by the mapping of the axes of the coordinate system $\{\hat{v}_i\}$ and the characteristic axes of the material, see Table 3.1. The representations in Equations (3.26) to (3.31) fit the alignment of the visualizations in Table 3.1. The alignment of the dominant axes of the trigonal, tetragonal and transversely isotropic representations with \hat{v}_1 and the alignment of the symmetry plane normal of the monoclinic case with \hat{v}_3 proves to be practical later in this work. Representations of fiber orientation tensors of planar fiber-reinforced composites are directly connected to the selected representations if the out-of-plane normal of the plane of planarity is aligned with the local \hat{v}_3 axis and interpreted

as monoclinic symmetry plane. The fiber direction of unidirectional-reinforced composites is typically associated with either the \hat{v}_3 or \hat{v}_1 axis. In this work, the latter convention is followed.

Material Symmetry	Symmetry Planes	Generators
Triclinic		\mathbf{I}
Monoclinic		$\mathbf{Q}_{\mathbf{e}_3}^{\pi}$
Orthotropic		$\mathbf{Q}_{\mathbf{e}_1}^{\pi}, \mathbf{Q}_{\mathbf{e}_2}^{\pi}$
Trigonal		$\mathbf{Q}_{\mathbf{e}_3}^{\pi}, \mathbf{Q}_{\mathbf{e}_1}^{2\pi/3}$
Tetragonal		$\mathbf{Q}_{\mathbf{e}_1}^{\pi}, \mathbf{Q}_{\mathbf{e}_1}^{3\pi/2}$
Transversely isotropic		$\mathbf{Q}_{\mathbf{e}_2}^{\pi}, \mathbf{Q}_{\mathbf{e}_1}^{\varphi}$
Cubic		$\mathbf{Q}_{\mathbf{e}_1}^{3\pi/2}, \mathbf{Q}_{(\mathbf{e}_1+\mathbf{e}_2+\mathbf{e}_3)/\sqrt{3}}^{2\pi/3}$
Isotropic		$\mathbf{Q}_{\mathbf{v}}^{\varphi}$

Table 3.1: Visualization of symmetry planes of material symmetry classes. The specified non-unique generators are rotations, i.e., elements of $SO(3)$, which generate the complete symmetry group, if combined exhaustively (Weber et al., 2019). Two rotations \mathbf{Q}_1 and \mathbf{Q}_2 are combined to a third one \mathbf{Q}_3 by linear contraction, i.e., $\mathbf{Q}_3 = \mathbf{Q}_1 \mathbf{Q}_2$. The rotation $\mathbf{Q}_{\mathbf{e}_3}^{\pi}$ rotates about the axis \mathbf{e}_3 by the angle π and the rotation $\mathbf{Q}_{\mathbf{v}}^{\varphi}$ rotates about the arbitrary axis \mathbf{v} by the arbitrary but non-vanishing angle φ .

Chapter 4

Variety of Fiber Orientation Tensors¹

4.1 Introduction

The microstructure of fiber reinforced composites significantly affects the effective mechanical properties of the compound. Two local microstructure descriptors commonly used to predict the effective properties are the fiber volume fraction and the fiber orientation distribution. The local fiber orientation distribution is completely defined by a fiber orientation distribution function (FODF). However, in practical applications the FODF is usually approximated by a limited number of fiber orientation tensors, as tensor representations fit into the continuum mechanics framework. Multiple kinds of orientation tensors exist (Kanatani, 1984). Practical applications related to fiber orientations include both identification of the fiber orientation information by experimental methods (Pinter et al., 2018) or process simulation (Meyer et al., 2020a) and usage of the orientation information in full field (Görthofer et al., 2020), mean field (Müller and Böhlke, 2016; Kehrer et al., 2020) or damage simulations (Schemmann et al., 2018b). Both groups of applications, identification

¹ This chapter reproduces (Bauer and Böhlke, 2022c), i.e., Bauer, J. K., Böhlke, T., 2022. Variety of fiber orientation tensors. *Mathematics and Mechanics of Solids* 27 (7), 1185–1211, 10.1177/10812865211057602. Reproduced with permission. ©2021 The Authors. Published by SAGE Publications Ltd under CC BY-NC 4.0

and usage of orientation information, benefit from a well known variety of fiber orientation tensors. If the variety of fiber orientation tensors is well defined, the identified orientation tensors can be assessed and the space of input parameters of methods predicting effective mechanical properties is set. The variety of second-order fiber orientation tensors is well known (Cintra Jr and Tucker III, 1995; Chung and Kwon, 2002; Cowin, 1985) and used, e.g., in Köbler et al. (2018); Görthofer et al. (2020); Köbler et al. (2021) to generate clear pictures of the dependence of mechanical properties on the second-order directional measures. However, concise descriptions and parameterizations of fourth-order fiber orientation tensors are rare. The variety of transversely isotropic fourth-order orientation tensors is identified by Nomura et al. (1970) and used in Müller and Böhlke (2016); Jack and Smith (2008). Müller and Böhlke (2016) showed that the identification of effective mechanical properties based on second-order orientation tensors yields insufficient accuracy (Breuer et al., 2019). For a given second-order orientation tensor, closure approximations (Advani and Tucker III, 1990; Han and Im, 1999; Cintra Jr and Tucker III, 1995; Chung and Kwon, 2002; Montgomery-Smith et al., 2011a) identify a corresponding fourth-order orientation tensor based on assumptions. Closure approximations are used by, e.g., Jack and Smith (2007; 2008); Buck et al. (2015); Müller and Böhlke (2016); Goldberg et al. (2017) to model mechanical properties. Breuer et al. (2019) assess the reconstruction of FODFs based on closure approximations and minimum entropy method used by Böhlke (2005); Müller and Böhlke (2016). This paper addresses the research question on the variety of fiber orientation tensors of order two and four. The paper has review character and is structured as follows: The definition of FODF and fiber orientation tensors is followed by a review on the variety of second-order orientation tensors, leading to the orientation triangle. The classical parameterization of the orientation triangle is framed and parameterizations which highlight the isotropic state and material symmetry are motivated. Implications of index symmetry of fourth-order tensors

in Mandel (Mandel, 1965) notation are discussed, before fourth-order orientation tensors are treated as special Hooke tensors and harmonic decomposition is applied. This translates the reasoning of Kanatani (1984) into continuum mechanics notation, leading to simplified notation with focus on the isotropic state. A parameterization of a generic fourth-order orientation tensor is given based on a parameterization of the second-order orientation tensor in combination with a triclinic structure tensor. Admissible orientation states are identified by demanding positive semi-definiteness. Results of Nomura et al. (1970); Müller and Böhlke (2016) on admissible transversely isotropic orientation tensors are reproduced and framed by coefficient-wise constraints. Minimal sets of discrete fiber orientations leading to special transversely isotropic orientation states are presented and discussed. The variety of orthotropic fourth-order fiber orientation tensors is visualized. Transversely isotropic and planar orthotropic fourth-order orientation tensors are highlighted as limiting orthotropic cases and admissible parameter ranges are specified. A compact parameterization of planar orthotropic fourth-order orientation tensors is given. Minimal sets of discrete planar orthotropic fiber orientations visualize the character of fourth-order orientation information. The variety of planar fourth-order fiber orientation tensors including a parameterization and admissible ranges is given. This paper closes with notes on a small set of closure approximations which are contrasted by the variety of fourth-order orientation tensors.

4.2 Fiber orientation

Given a reference volume (RV) of arbitrary size and shape, which might be interpreted as the part of a body \mathcal{B} centered around position \mathbf{x} . The orientation of axisymmetric fibers inside this reference volume can be

described by the fiber orientation distribution function (FODF)

$$\psi : \mathcal{S}^2 \rightarrow \mathbb{R}, \text{ with } \mathcal{S}^2 = \{\mathbf{n} \in \mathbb{R}^3 \mid \|\mathbf{n}\| = 1\} \quad (4.1)$$

mapping any direction \mathbf{n} onto a scalar value $\psi(\mathbf{n})$. \mathcal{S}^2 is the two-dimensional surface of a unit sphere parameterized by, e.g., a unit vector \mathbf{n} . The function $\psi(\mathbf{n})$ is non-negative, i.e.

$$\psi(\mathbf{n}) \geq 0, \quad \forall \mathbf{n} \in \mathcal{S}^2 \quad (4.2)$$

holds and normalization of $\psi(\mathbf{n})$ implies

$$\int_{\mathcal{S}^2} \psi(\mathbf{n}) \, d\mathbf{n} = 1. \quad (4.3)$$

As fibers have a direction but no attitude, $\psi(\mathbf{n})$ is symmetric, i.e.

$$\psi(-\mathbf{n}) = \psi(\mathbf{n}), \quad \forall \mathbf{n} \in \mathcal{S}^2 \quad (4.4)$$

holds (see Görthofer et al. (2020); Advani and Tucker III (1987)). The fiber orientation distribution function solely describes the orientation of the fibers. Being a one-point statistic information, the FODF contains no additional information on, e.g., the spatial arrangement of the fibers inside the reference volume. In a heterogeneous material with spatially varying microstructure, the FODF usually is influenced by the size of the reference volume (see, e.g., size parameter in Görthofer et al. (2019, Figure 4)). If the fibers have identical volumes, e.g., because of identical length and constant cross section, the volume fraction $c_{\mathcal{F}}$ of those fibers pointing through $\mathcal{F} \subseteq \mathcal{S}^2$ on all fibers, is given by

$$c_{\mathcal{F}} = \frac{1}{V_f} \int_{V_{\mathcal{F}}} dV = \int_{\mathcal{F}} \psi(\mathbf{n}) \, d\mathbf{n} \quad (4.5)$$

with the volume of all fibers V_f and $V_{\mathcal{F}}$ being the volume of fibers pointing through \mathcal{F} (see Schemmann et al. (2015); Müller and Böhlke (2016)). Equation (4.5) demonstrates the transformation of a volume average, e.g., over $V_{\mathcal{F}}$, into an average over corresponding parts of the unit sphere. Volume averages on a reference volume V_{RV} of a field quantity $\mathbf{q}(\mathbf{x})$ which is axisymmetric about a spatially varying principle axis $\mathbf{n}(\mathbf{x})$ can be transformed into an average over S^2

$$\frac{1}{V_{RV}} \int_{V_{RV}} \mathbf{q}(\mathbf{x}) dV = \int_{S^2} \psi(\mathbf{n}) \mathbf{q}(\mathbf{n}) dn, \quad (4.6)$$

if \mathbf{q} can be parameterized solely in \mathbf{n} . Similar reasoning for volume averages over the special orthogonal group $SO(3)$ in context of crystal orientation distribution functions (CODF) are extensively used in literature, see, e.g., Böhlke (2005); Fernández and Böhlke (2019). ODF averages are limited to axisymmetric quantities since FODF is defined on directions. In contrast, CODF can be interpreted as rotations of coordinate systems and therefore induce no restriction on the quantity which is to be averaged. The FODF reflects the material symmetry of the microstructure. As a consequence,

$$\psi(\mathbf{S} \star \mathbf{n}) = \psi(\mathbf{n}) \quad \forall \mathbf{S} \in S_{RV} \subseteq SO(3) \quad (4.7)$$

holds. Equation (4.7) implies that $\psi(\mathbf{n})$ is symmetric with respect to all rotations \mathbf{S} which are contained in the symmetry group of the microstructure S_{RV} being a subset of $SO(3)$. Following Forte and Vianello (1996), eight different material symmetries exist and tensor representations of Hooke tensors following these symmetries are given in, e.g. Böhlke (2001). An inclusion scheme, depicting the hierarchy of the symmetry classes combined with illustrations of the symmetry planes, can be found in Francois et al. (1998, Fig. 4). Implications of material symmetries on second-order tensors are summarized in Appendix A.1.

4.3 Orientation tensors of first kind

In the standard framework of continuum mechanics, physical quantities are expressed as invariant tensors. This enables the use of known transformation rules and simplifies the storage in computer memory. Kanatani (1984) approximates experimentally obtained directional data by tensor series and Advani and Tucker III (1987) defines orientation tensors of Kanatani first kind (Kanatani, 1984) by

$$\mathbb{N}_{(k)} = \int_{S^2} \psi(\mathbf{n}) \mathbf{n}^{\otimes k} d\mathbf{n} \quad (4.8)$$

with $\mathbf{n}^{\otimes k}$ being the k -th moment of \mathbf{n} . For example, the resulting second- and fourth-order tensors are

$$\mathbf{N} = \mathbb{N}_{(2)} = \int_{S^2} \psi(\mathbf{n}) \mathbf{n} \otimes \mathbf{n} d\mathbf{n} \quad (4.9)$$

$$\mathbb{N} = \mathbb{N}_{(4)} = \int_{S^2} \psi(\mathbf{n}) \mathbf{n} \otimes \mathbf{n} \otimes \mathbf{n} \otimes \mathbf{n} d\mathbf{n}. \quad (4.10)$$

Equation (4.8) can be interpreted as a weighted summation of moment tensors. The moment tensor represents the tensorial character of a specific direction and weights are specified by the distribution information of the FODF. It follows from Equation (4.8) that \mathbf{N} and \mathbb{N} are completely symmetric with respect to index permutations. Odd orientation tensors vanish due to the symmetry of $\psi(\mathbf{n})$ and higher order tensors contain all tensors of lower order as

$$\mathbb{N}_{(k-2)} = \mathbb{N}_{(k)} [\mathbf{I}] \quad (4.11)$$

holds for $2 \leq k$ with the identity on second-order tensors \mathbf{I} . As a consequence of the normalization of both $\psi(\mathbf{n})$ and \mathbf{n} , the limiting case

of Equation (4.11) yields

$$\mathbf{N} \cdot \mathbf{I} = \text{tr}(\mathbf{N}) = 1. \quad (4.12)$$

Orientation tensors of Kanatani first kind (Kanatani, 1984) are commonly used to represent experimentally obtained directional data, e.g., from computer tomography scans or results of flow simulations (Görthofer et al., 2019).

4.4 Orientation tensors of third kind

The FODF can be expressed as a tensorial Fourier series

$$\psi(\mathbf{n}) = \frac{1}{4\pi} \sum_{k=0}^{\infty} \hat{\mathbb{D}}_{(k)} \cdot \mathbf{n}^{\otimes k} \quad (4.13)$$

which is called spherical harmonic expansion (Kanatani, 1984, page 154) and introduces orientation tensors of Kanatani third kind (Kanatani, 1984)

$$\hat{\mathbb{D}}_{(k)} = \frac{2k+1}{2^k} \binom{2k}{k} \text{dev}(\mathbb{N}_{(k)}). \quad (4.14)$$

Constructing $\hat{\mathbb{D}}_{(k)}$ in Equation (4.14) contains two steps, first taking the deviatoric part of $\mathbb{N}_{(k)}$ and second, scaling with factors for the series expansion given by $\frac{2k+1}{2^k} \binom{2k}{k}$. Skipping the second step, defines orientation tensors of third kind, as done by, e.g., Müller and Böhlke (2016), as

$$\mathbb{D}_{(k)} = \text{dev}(\mathbb{N}_{(k)}). \quad (4.15)$$

In combination with Equations (4.11) and (4.12) this leads for $k \in [2, 4]$ to

$$\mathbb{D}_{(2)} = \text{dev}(\mathbf{N}) = \mathbf{N} - \frac{1}{3}\mathbf{I}\text{tr}(\mathbf{N}) \quad (4.16)$$

$$= \mathbf{N} - \mathbf{N}^{\text{iso}} \quad (4.17)$$

$$\begin{aligned} \mathbb{D}_{(4)} = \text{dev}(\mathbb{N}) &= \mathbb{N} - \frac{6}{7}\text{sym}((\mathbb{N}[\mathbf{I}]) \otimes \mathbf{I}) \\ &\quad + \frac{3}{35}\text{sym}(\mathbf{I} \otimes \mathbf{I})\text{tr}(\mathbb{N}[\mathbf{I}]) \end{aligned} \quad (4.18)$$

$$= \mathbb{N} - \frac{6}{7}\text{sym}(\mathbf{N} \otimes \mathbf{I}) + \frac{3}{35}\text{sym}(\mathbf{I} \otimes \mathbf{I}) \quad (4.19)$$

with the isotropic orientation tensor of second order

$$\mathbf{N}^{\text{iso}} = \frac{1}{3}\mathbf{I}. \quad (4.20)$$

The operator $\text{dev}(\cdot)$ extracts the deviatoric part and the operator $\text{sym}(\cdot)$ extracts the totally symmetric part with respect to index symmetry. Definitions of the operators $\text{sym}(\cdot)$ and $\text{dev}(\cdot)$ for higher order tensors are given in Spencer (1970). In other communities, alternative representations of directional data are common. The connection to spherical harmonics in the context of quantitative texture analysis is discussed in Fernández and Böhlke (2019); Breuer et al. (2019); Kanatani (1984); Jack and Smith (2008).

4.5 Variety of second-order orientation tensors

Equations (4.2) and (4.8) imply that orientation tensors of Kanatani first kind (Kanatani, 1984) and second order \mathbf{N} are symmetric and positive semi-definite. As a consequence, \mathbf{N} can be diagonalized, i.e., pairs of eigenvalues λ_i with $\lambda_i \geq 0$ and orthonormal eigenvectors \mathbf{v}_i for

$i \in [1, 2, 3]$ exist, such that

$$\mathbf{N} = N_{ij}^{(2)} \mathbf{e}_i \otimes \mathbf{e}_j = \sum_{i=1}^3 \lambda_i \mathbf{v}_i \otimes \mathbf{v}_i = \begin{bmatrix} \lambda_1 & 0 & 0 \\ & \lambda_2 & 0 \\ \text{sym} & & \lambda_3 \end{bmatrix} \mathbf{v}_i \otimes \mathbf{v}_j \quad (4.21)$$

holds and there exists a rotation defined by an orthogonal tensor

$$\mathbf{Q} = \mathbf{v}_i \otimes \mathbf{e}_i \quad (4.22)$$

mapping the arbitrary but fixed basis $\{\mathbf{e}_i\}$ onto the basis $\{\mathbf{v}_i\}$. In the following, the orthonormal basis $\{\mathbf{v}_i\}$ spanned by the eigenvectors is called orientation coordinate system. The arbitrary ordering convention of the eigenvalues

$$\lambda_3 \leq \lambda_2 \leq \lambda_1 \quad (4.23)$$

is common in the literature (see Goldberg et al. (2017); Mentges et al. (2021)). The constraint in Equation (4.12) is equivalent to

$$\lambda_1 + \lambda_2 + \lambda_3 = 1 \quad (4.24)$$

and reduces the number of independent components of \mathbf{N} from six to five. The coordinate system $\{\mathbf{v}_i\}$ or equivalently the mapping \mathbf{Q} is defined by three scalars, leaving two scalars specifying structural information on fiber orientations inside the orientation coordinate system. As a consequence, the variety of \mathbf{N} can be expressed as a two dimensional space known as the orientation triangle, e.g., parameterized in pairs (λ_1, λ_2) , in combination with a mapping \mathbf{Q} which defines the orientation coordinate system. Information of \mathbf{N} is limited to the definition of a coordinate system and two half axes of an ellipsoid aligned with these coordinate axes, see Cowin (1985). The third half axis of the ellipsoid is defined by Equation (4.24). The weakest material symmetry which can

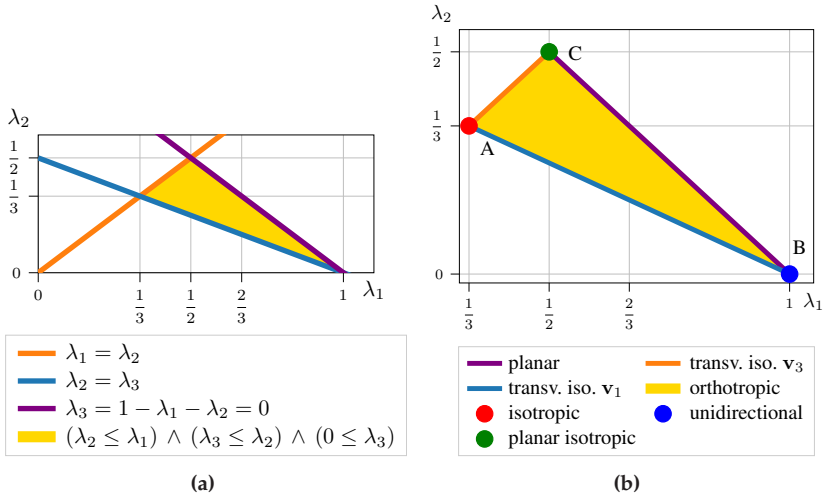


Figure 4.1: (a) Constraints defining the orientation triangle (b) Material symmetries in the orientation triangle (Cintra Jr and Tucker III, 1995)

be described by \mathbf{N} is orthotropy (see Cowin (1985) or Appendix A.1). Representations of orientation triangles are given, e.g., in Cintra Jr and Tucker III (1995); Chung and Kwon (2002); Goldberg et al. (2017); Köbler et al. (2018) as well as in Figure 4.1a. An alternative visualization is given by the orientation invariant map in Chung and Kwon (2002, Figure 1b). The triangle in Figure 4.1a is only one of possible orientation triangles and is called standard orientation triangle. The boundaries of the triangle are labeled in Figure 4.1a and follow directly from Equations (4.23) and (4.24) and $0 \leq \lambda_3$. Following Cintra Jr and Tucker III (1995), vertices and edges of the triangle are discussed, based on Figure 4.1b. The vertices A, B and C are given by the extremal orientation states, which are isotropic, unidirectional and planar isotropic. Starting from a planar isotropic state ($\lambda_1 = \lambda_2 = \frac{1}{2}$, $\lambda_3 = 0$) at vertex C, moving along the orange edge towards vertex A, λ_3 increases while λ_1 and λ_2 decrease uniformly until the isotropic state ($\lambda_1 = \lambda_2 = \lambda_3$) is reached. Continuing

from vertex A along the edge towards vertex B, the largest eigenvalue λ_1 increases while λ_2 and λ_3 decrease uniformly until the unidirectional state ($\lambda_1 = 1$, $\lambda_2 = \lambda_3 = 0$) is reached. All states along the edges CA and AB have at least two identical eigenvalues and therefore are transversely isotropic with principle axes being v_3 and v_1 respectively. The material symmetries of points of the orientation triangle are visualized in 4.1b and discussions can be found in Cowin (1985); Cintra Jr and Tucker III (1995). The states along the edge BC are planar as λ_3 vanishes. Starting from vertex B along the edge towards vertex C, λ_1 decreases and λ_2 increases until both are equal. All points inside the triangle including the edge between vertex B and C are orthotropic. In summary, two edges are transversely isotropic, one edge is planar and one point is isotropic. The triangles in Figures 4.1a and 4.1b are projections of one sixth of a orientation plane in the three-dimensional space spanned by $\{v_i\}$ given in Figure 4.2a. For each point in the orientation triangle, five corresponding points with identical structural properties and different ordering conventions of eigenvalues exist. To illustrate the redundancy which is inherent in the orientation plane, a randomly chosen orientation state with eigenvalues being any permutation of $(1/2, 1/3, 1/6)$ is marked in orange multiple times in Figures 4.2a and 4.2b. For each eigenvector in $\{v_i\}$, transversely isotropic orientation states with principle axis v_i are located along a straight line being the interSection of the orientation plane and a plane with $\lambda_m = \lambda_n$ for $i \neq m \neq n$. Planar states are found at the interSection of the orientation plane and planes of one vanishing eigenvalue. The central character of the isotropic state is reflected by Figure 4.2a. The three-dimensional representation in Figure 4.2a extends existing visualizations, e.g., in Goldberg et al. (2017, Figure 2), by adding material symmetries and motivates alternative parameterizations introduced in the next section.

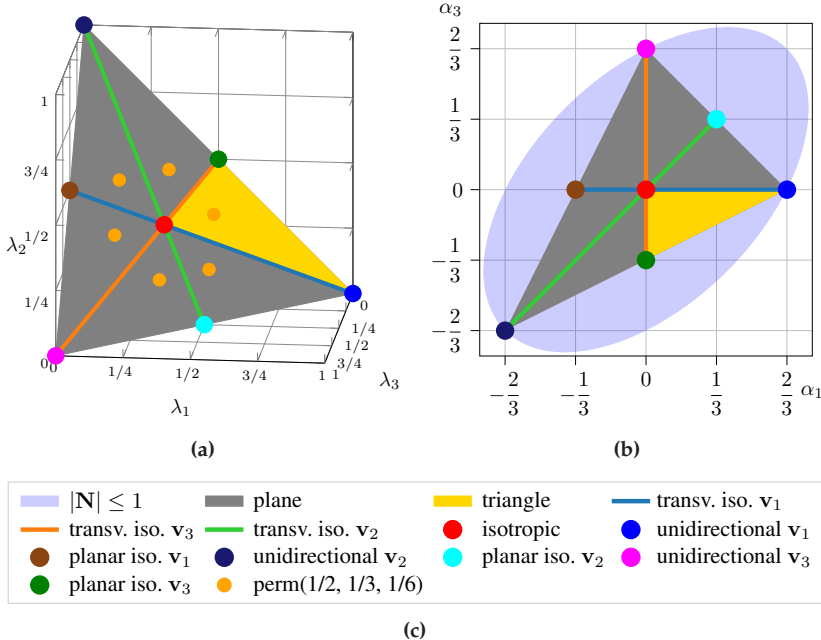


Figure 4.2: (a) Orientation plane, triangle and selected orientation states in the space spanned by the eigenvalues of \mathbf{N} (b) Plane, triangle, selected states and states constrained by the norm of \mathbf{N} in parameter space (α_1, α_3) (c) Shared legend of Figures 4.2a and 4.2b

4.5.1 Parameterizations of the orientation triangle

The classic parameterization of the orientation triangle in eigenvalues λ_1 and λ_2 is

$$\mathbf{N}(\lambda_1, \lambda_2) = \lambda_1 \mathbf{v}_1 \otimes \mathbf{v}_1 + \lambda_2 \mathbf{v}_2 \otimes \mathbf{v}_2 + (1 - \lambda_1 - \lambda_2) \mathbf{v}_3 \otimes \mathbf{v}_3 \quad (4.25)$$

with

$$\frac{1}{3} \leq \lambda_1 \leq 1 \quad \text{and} \quad \frac{1}{2}(1 - \lambda_1) \leq \lambda_2 \leq \min(\lambda_1, 1 - \lambda_1). \quad (4.26)$$

Introducing two transversely isotropic deviatoric structure tensors

$$\mathbf{F}^{\text{transv1}} = \begin{bmatrix} 1 & 0 & 0 \\ & -1/2 & 0 \\ \text{sym} & & -1/2 \end{bmatrix} \mathbf{v}_i \otimes \mathbf{v}_j \quad (4.27)$$

$$\mathbf{F}^{\text{transv3}} = \begin{bmatrix} -1/2 & 0 & 0 \\ & -1/2 & 0 \\ \text{sym} & & 1 \end{bmatrix} \mathbf{v}_i \otimes \mathbf{v}_j \quad (4.28)$$

enables an alternative parameterization of the orientation triangle by

$$\mathbf{N}(\alpha_1, \alpha_3) = \mathbf{N}^{\text{iso}} + \alpha_1 \mathbf{F}^{\text{transv1}} + \alpha_3 \mathbf{F}^{\text{transv3}} \quad (4.29)$$

with

$$0 \leq \alpha_1 \leq \frac{2}{3} \quad \text{and} \quad \frac{\alpha_1}{2} - \frac{1}{3} \leq \alpha_3 \leq 0. \quad (4.30)$$

The parameterization in Equation (4.29) highlights the central role of the isotropic state, which is reached for $\alpha_1 = \alpha_3 = 0$. Positive values of α_1 lead to a deviation from the isotropic state towards the unidirectional state in direction \mathbf{v}_1 . Deviation towards the planar isotropic state with principle axis \mathbf{v}_3 , i.e., away from the unidirectional state in direction \mathbf{v}_3 is described by α_3 . Figure 4.2b shows the orientation triangle as part of the orientation plane in the parameter space (α_1, α_3) . The orientation plane itself is part of those pairs of (α_1, α_3) which lead to orientations with norm less than one. If the separation into two transversely directions is not required, $\mathbf{F}^{\text{transv1}}$ and $\mathbf{F}^{\text{transv3}}$ can be combined to a generally orthotropic structure tensor of second order, leading to

$$\mathbf{N}(\hat{a}, \hat{c}) = \mathbf{N}^{\text{iso}} + \mathbf{F}^{\text{ortho}}(\hat{a}, \hat{c}). \quad (4.31)$$

with

$$\mathbf{F}^{\text{ortho}} (\hat{a}, \hat{c}) = \begin{bmatrix} \hat{a} & 0 & 0 \\ -(\hat{a} + \hat{c}) & 0 & 0 \\ \text{sym} & & \hat{c} \end{bmatrix} \mathbf{v}_i \otimes \mathbf{v}_j \quad (4.32)$$

A parameterization reflecting the arbitrariness of the ordering convention on λ_i and deploying barycentric coordinates is given as a function of three non-negative weights $0 \leq \hat{w}_i$ with $i \in [1, 2, 3]$ and $\hat{w}_\Sigma = \sum_{i=1}^3 \hat{w}_i$ by

$$\mathbf{N} (\hat{w}_1, \hat{w}_2, \hat{w}_3) = \mathbf{N} \left(\lambda_1 = \frac{\hat{w}_1}{\hat{w}_\Sigma}, \lambda_2 = \frac{\hat{w}_2}{\hat{w}_\Sigma} \right) \quad (4.33)$$

requiring $\hat{w}_\Sigma > 0$. See Goldberg et al. (2017, Figure 2) for a visualization of this parameterization. Each parameterization given in equations (4.25), (4.29), (4.31) and (4.33) in combination with a rotation, following Equation (4.22), can be used to represent all possible second-order orientation tensors. A table with parameters of special points in all parameterizations is given in Appendix A.2.

Parameterizations of all transversely isotropic \mathbf{N} , not being restricted to the standard orientation triangle, are given by

$$\mathbf{N}^{\text{transv}} (\lambda_1) = \mathbf{N} (\lambda_1, \lambda_2 = (1 - \lambda_1) / 2) \quad (4.34)$$

$$\mathbf{N}^{\text{transv}} (\alpha_1) = \mathbf{N} (\alpha_1, \alpha_3 = 0). \quad (4.35)$$

A parameterization of transversely isotropic \mathbf{N} inside the orientation triangle requires a piece-wise definition due to the kink at the isotropic

state leading to

$$\mathbf{N}^{\text{transv}}(\lambda_2) = \begin{cases} (1 - 2\lambda_2)\mathbf{v}_1 \otimes \mathbf{v}_1 + \lambda_2 \mathbf{v}_2 \otimes \mathbf{v}_2 + \lambda_2 \mathbf{v}_3 \otimes \mathbf{v}_3 & \text{if } 0 \leq \lambda_2 \leq \frac{1}{3}, \\ \lambda_2 \mathbf{v}_1 \otimes \mathbf{v}_1 + \lambda_2 \mathbf{v}_2 \otimes \mathbf{v}_2 + (1 - 2\lambda_2) \mathbf{v}_3 \otimes \mathbf{v}_3 & \text{if } \frac{1}{3} < \lambda_2 \leq \frac{1}{2}. \end{cases} \quad (4.36)$$

Planar second-order orientation tensors inside the orientation triangle can be parameterized by, e.g.

$$\begin{aligned} \mathbf{N}^{\text{planar}}(\alpha_1) &= \mathbf{N}\left(\alpha_1, \alpha_3 = \frac{\alpha_1}{2} - \frac{1}{3}\right) \\ &= \left(\frac{1}{2} + \frac{3}{4}\alpha_1\right) \mathbf{v}_1 \otimes \mathbf{v}_1 + \left(\frac{1}{2} - \frac{3}{4}\alpha_1\right) \mathbf{v}_2 \otimes \mathbf{v}_2 \end{aligned} \quad (4.37)$$

with $0 \leq \alpha_1 \leq 2/3$.

4.6 Variety of fourth-order orientation tensors

Equation (4.10) implies that \mathbb{N} is completely (or totally) symmetric, i.e., any permutation of the indices

$$N_{ijkl}^{(4)} = N_{\text{perm}(ijkl)}^{(4)} \quad (4.38)$$

holds for a representation with tensor coefficients $\mathbb{N} = N_{ijkl}^{(4)} \mathbf{e}_i \otimes \mathbf{e}_j \otimes \mathbf{e}_k \otimes \mathbf{e}_l$. Complete (index) symmetry reduces the number of independent components of a generic fourth-order tensor in three dimensions from $81 = 3^4$ to 15, as there are $15 = \binom{n+k-1}{k}$ unordered ways of choosing a combination of $k = 4$ elements from a set of $n = 3$ elements. Mandel notation, introduced in Mandel (1965) and also known as normalized Voigt notation (Mehrabadi and Cowin, 1990; Böhlke, 2001) enables compact two-dimensional representations of fourth-order tensors with at least minor symmetry. A fourth-order tensor $\mathbb{A} = A_{ijkl} \mathbf{e}_i \otimes \mathbf{e}_j \otimes \mathbf{e}_k \otimes \mathbf{e}_l$

is minor symmetric if it has both minor symmetries, i.e. $A_{ijkl} = A_{jikl} = A_{ijlk}$ holds. Introducing base tensors in an arbitrary Cartesian basis $\{\mathbf{e}_i\}$ by

$$\begin{aligned}\mathbf{B}_1 &= \mathbf{e}_1 \otimes \mathbf{e}_1, & \mathbf{B}_4 &= \frac{\sqrt{2}}{2} (\mathbf{e}_2 \otimes \mathbf{e}_3 + \mathbf{e}_3 \otimes \mathbf{e}_2), \\ \mathbf{B}_2 &= \mathbf{e}_2 \otimes \mathbf{e}_2, & \mathbf{B}_5 &= \frac{\sqrt{2}}{2} (\mathbf{e}_1 \otimes \mathbf{e}_3 + \mathbf{e}_3 \otimes \mathbf{e}_1), \\ \mathbf{B}_3 &= \mathbf{e}_3 \otimes \mathbf{e}_3, & \mathbf{B}_6 &= \frac{\sqrt{2}}{2} (\mathbf{e}_2 \otimes \mathbf{e}_1 + \mathbf{e}_1 \otimes \mathbf{e}_2),\end{aligned}\quad (4.39)$$

a minor symmetric tensor \mathbb{A} is represented by a six by six matrix of coefficients $A_{\xi\zeta}$

$$\begin{aligned}\mathbb{A} = A_{ijkl} \mathbf{e}_i \otimes \mathbf{e}_j \otimes \mathbf{e}_k \otimes \mathbf{e}_l &= A_{\xi\zeta} \mathbf{B}_\xi \otimes \mathbf{B}_\zeta = \\ \left[\begin{array}{cccccc} A_{1111} & A_{1122} & A_{1133} & \sqrt{2}A_{1123} & \sqrt{2}A_{1113} & \sqrt{2}A_{1112} \\ A_{2211} & A_{2222} & A_{2233} & \sqrt{2}A_{2223} & \sqrt{2}A_{2213} & \sqrt{2}A_{2212} \\ A_{3311} & A_{3322} & A_{3333} & \sqrt{2}A_{3323} & \sqrt{2}A_{3313} & \sqrt{2}A_{3312} \\ \sqrt{2}A_{2311} & \sqrt{2}A_{2322} & \sqrt{2}A_{2333} & 2A_{2323} & 2A_{2313} & 2A_{2312} \\ \sqrt{2}A_{1311} & \sqrt{2}A_{1322} & \sqrt{2}A_{1333} & 2A_{1323} & 2A_{1313} & 2A_{1312} \\ \sqrt{2}A_{1211} & \sqrt{2}A_{1222} & \sqrt{2}A_{1233} & 2A_{1223} & 2A_{1213} & 2A_{1212} \end{array} \right] \\ \mathbf{B}_\xi \otimes \mathbf{B}_\zeta\end{aligned}\quad (4.40)$$

with ξ and ζ summing from 1 to 6. A Hooke tensor \mathbb{B} is minor and major symmetric, i.e., in addition to the minor symmetry condition it holds

that $B_{ijkl} = B_{klji}$. The coefficient matrix of a Hooke tensor

$$\mathbb{B} = \begin{bmatrix} B_{11} & B_{12} & B_{13} & \sqrt{2}B_{14} & \sqrt{2}B_{15} & \sqrt{2}B_{16} \\ B_{12} & B_{22} & B_{23} & \sqrt{2}B_{24} & \sqrt{2}B_{25} & \sqrt{2}B_{26} \\ B_{13} & B_{23} & B_{33} & \sqrt{2}B_{34} & \sqrt{2}B_{35} & \sqrt{2}B_{36} \\ \sqrt{2}B_{14} & \sqrt{2}B_{24} & \sqrt{2}B_{34} & 2B_{44} & 2B_{45} & 2B_{46} \\ \sqrt{2}B_{15} & \sqrt{2}B_{25} & \sqrt{2}B_{35} & 2B_{45} & 2B_{55} & 2B_{56} \\ \sqrt{2}B_{16} & \sqrt{2}B_{26} & \sqrt{2}B_{36} & 2B_{46} & 2B_{56} & 2B_{66} \end{bmatrix} \mathbf{B}_\xi \otimes \mathbf{B}_\zeta \quad (4.41)$$

is symmetric and contains 21 independent parameters. Complete index symmetry of \mathbb{N} implies

$$\mathbb{N} = \left[\begin{array}{ccc|ccc} N_{11}^{(4)} & N_{12}^{(4)} & N_{13}^{(4)} & \sqrt{2}N_{14}^{(4)} & \sqrt{2}N_{15}^{(4)} & \sqrt{2}N_{16}^{(4)} \\ & N_{22}^{(4)} & N_{23}^{(4)} & \sqrt{2}N_{24}^{(4)} & \sqrt{2}N_{25}^{(4)} & \sqrt{2}N_{26}^{(4)} \\ & & N_{33}^{(4)} & \sqrt{2}N_{34}^{(4)} & \sqrt{2}N_{35}^{(4)} & \sqrt{2}N_{36}^{(4)} \\ \hline & \text{major symmetric} & & 2N_{23}^{(4)} & 2N_{36}^{(4)} & 2N_{25}^{(4)} \\ & & & & 2N_{13}^{(4)} & 2N_{14}^{(4)} \\ & & & & & 2N_{12}^{(4)} \end{array} \right] \mathbf{B}_\xi \otimes \mathbf{B}_\zeta. \quad (4.42)$$

In Equation (4.42) indices of redundant tensor coefficients are colored. The redundancy implies that six coefficients in the upper left quadrant and nine coefficients in the upper right quadrant of the coefficients in Mandel notation define a completely symmetric tensor. This motivates a short hand notation „completely symmetric“, which to the best of the authors' knowledge has not been used in the literature so far, see, e.g., Equation (4.55). As \mathbb{N} contains \mathbb{N} , the constraint on the trace of \mathbb{N} in Equation (4.12) reduces the number of independent components of \mathbb{N} by one to 14. In the literature erroneous implications of Equation (4.12) on the number of independent components of \mathbb{N} are found, see, e.g., Dray

et al. (2007). Expressing \mathbf{N} by contraction of \mathbb{N} , i.e.,

$$\mathbf{N} = \begin{bmatrix} N_{11}^{(4)} + N_{12}^{(4)} + N_{13}^{(4)} & N_{16}^{(4)} + N_{26}^{(4)} + N_{36}^{(4)} & N_{15}^{(4)} + N_{25}^{(4)} + N_{35}^{(4)} \\ N_{16}^{(4)} + N_{26}^{(4)} + N_{36}^{(4)} & N_{12}^{(4)} + N_{22}^{(4)} + N_{23}^{(4)} & N_{14}^{(4)} + N_{24}^{(4)} + N_{34}^{(4)} \\ N_{15}^{(4)} + N_{25}^{(4)} + N_{35}^{(4)} & N_{14}^{(4)} + N_{24}^{(4)} + N_{34}^{(4)} & N_{13}^{(4)} + N_{23}^{(4)} + N_{33}^{(4)} \end{bmatrix} e_i \otimes e_j \quad (4.43)$$

reveals the implication of Equation (4.12) on \mathbb{N} to be $N_{11}^{(4)} + N_{22}^{(4)} + N_{33}^{(4)} + 2N_{12}^{(4)} + 2N_{13}^{(4)} + 2N_{23}^{(4)} = 1$.

4.6.1 Harmonic decomposition

Linear invariant decompositions, including the classic harmonic decomposition, are frequently used on Hooke tensors. The fourth-order orientation tensor \mathbb{N} is a Hooke tensor and has additional index symmetry. Therefore, linear invariant decompositions can be applied to \mathbb{N} to study its structure. Literature on invariant decompositions of fourth-order tensors is extensive, see, e.g. Backus (1970); Mochizuki (1988); Baerheim (1993); Boehler et al. (1994); Forte and Vianello (1996); Olive et al. (2017) or those focusing on Hooke tensors and addressing an engineering audience Rychlewski (2000; 2001); Böhlke (2001).

Following Rychlewski (2000), a Hooke tensor \mathbb{H} with 21 independent components can be split into five parts ($K, G, \mathbf{H}_1, \mathbf{H}_2, \text{dev}(\mathbb{H})$) leading to

$$\begin{aligned} \mathbb{H} = 3K\mathbb{P}_1 + 2G\mathbb{P}_2 + \text{sym}_1(\mathbf{I} \otimes \mathbf{H}_1 + \mathbf{H}_1 \otimes \mathbf{I}) \\ + \text{sym}_2(\mathbf{I} \otimes \mathbf{H}_2 + \mathbf{H}_2 \otimes \mathbf{I}) + \text{dev}(\mathbb{H}) \end{aligned} \quad (4.44)$$

with isotropic projectors \mathbb{P}_1 and \mathbb{P}_2 , two symmetrization operators $\text{sym}_1(\cdot), \text{sym}_2(\cdot)$ and the deviatoric operator $\text{dev}(\cdot)$. The symmetrization

operators have to follow a special structure which is described in Rychlewski (2000). Two common choices of the symmetrization operators are used in the following. The numbers of independent parameters of the five parts ($K, G, \mathbf{H}_1, \mathbf{H}_2, \text{dev}(\mathbb{H})$) are (1, 1, 5, 5, 9) with the scalar compression modulus K and shear modulus G . The isotropic parts are obtained by projections, i.e.

$$3K = \mathbb{P}_1 \cdot \mathbb{H}, \quad 2G = \frac{1}{\|\mathbb{P}_2\|^2} \mathbb{P}_2 \cdot \mathbb{H} = \frac{1}{5} \mathbb{P}_2 \cdot \mathbb{H}. \quad (4.45)$$

The parts \mathbf{H}_1 and \mathbf{H}_2 depend on the choice of the operators $\text{sym}_1(\cdot)$ and $\text{sym}_2(\cdot)$ but for any choice are only functions of the dilatational modulus \mathbf{C} and the Voigt tensor \mathbf{V} which are given in index notation by

$$C_{ij} = H_{ijkk} \quad \text{and} \quad V_{ij} = H_{ikjk} \quad (4.46)$$

with $\mathbf{C} = C_{ij} \mathbf{e}_i \otimes \mathbf{e}_j$, $\mathbf{V} = V_{ij} \mathbf{e}_i \otimes \mathbf{e}_j$ and $\mathbb{H} = H_{ijkl} \mathbf{e}_i \otimes \mathbf{e}_j \otimes \mathbf{e}_k \otimes \mathbf{e}_l$. The classic harmonic decomposition, e.g., used in Böhlke (2001), is obtained for $\text{sym}_1(\cdot)$ being the identity and $\text{sym}_2(\cdot)$ symmetrizing the only remaining index asymmetry of Hooke tensors, leading to

$$\mathbf{H}_1^{\text{classic}} = \frac{1}{7} (5\text{dev}(\mathbf{C}) - 4 \text{ dev}(\mathbf{V})) \quad (4.47)$$

$$\mathbf{H}_2^{\text{classic}} = \frac{1}{7} (3\text{dev}(\mathbf{C}) - 2 \text{ dev}(\mathbf{V})). \quad (4.48)$$

Applying the classic harmonic decomposition to \mathbb{N} reveals that the dilatational modulus and the Voigt modulus of \mathbb{N} coincide and both are \mathbf{N} . Following Cowin (1989), a Hooke tensor whose dilatational modulus and Voigt tensor coincide, is said to fulfill the Cauchy relations. Any completely symmetric tensor and thus also any orientation tensor fulfills the Cauchy relations. Referencing Musgrave (1970), Cowin (1989) states about the Cauchy relations „ [...] the relations do not hold for most elastic materials, but only for materials which can be described as having

central-force laws operating between points of a simple lattice, [...] “. This observation fits the model of fibers pointing towards the origin of a unit sphere. A stiffness which is linear in the orientation tensors does not have to fulfill the Cauchy relations as its deviatoric parts (\mathbf{H}_1 and \mathbf{H}_2 in Equation (4.44)) might be multiples of \mathbb{N} and therefore do not coincide. Motivated by their orthogonality, Rychlewski (2000) proposes an alternative pair of symmetrization operators $\text{sym}_1(\cdot) = \text{sym}(\cdot)$ and $\text{sym}_2(\cdot) = \mathbb{I}^S - \text{sym}_1(\cdot)$ focusing on the index symmetry with the identity on symmetric fourth-order tensors \mathbb{I}^S . This choice leads to the corresponding parts

$$\mathbf{H}_1^{\text{index}} = \frac{1}{7} (\text{dev}(\mathbf{C}) + 2 \text{dev}(\mathbf{V})) \quad (4.49)$$

$$\mathbf{H}_2^{\text{index}} = \text{dev}(\mathbf{C}) - \text{dev}(\mathbf{V}). \quad (4.50)$$

As a consequence, \mathbb{N} can be decomposed into

$$\begin{aligned} \mathbb{N} &= 3\hat{K}\mathbb{P}_1 + 2\hat{G}\mathbb{P}_2 + \text{sym} \left(\mathbf{I} \otimes \frac{3}{7} \text{dev}(\mathbf{N}) + \frac{3}{7} \text{dev}(\mathbf{N}) \otimes \mathbf{I} \right) \\ &\quad + \text{dev}(\mathbb{N}) \end{aligned} \quad (4.51)$$

$$= 3\hat{K}\mathbb{P}_1 + 2\hat{G}\mathbb{P}_2 + 2 \text{sym} \left(\frac{3}{7} \text{dev}(\mathbf{N}) \otimes \mathbf{I} \right) + \text{dev}(\mathbb{N}) \quad (4.52)$$

$$= 3\hat{K}\mathbb{P}_1 + 2\hat{G}\mathbb{P}_2 + \frac{6}{7} \text{sym}(\text{dev}(\mathbf{N}) \otimes \mathbf{I}) + \text{dev}(\mathbb{N}). \quad (4.53)$$

Due to the isotropy of the isotropic projectors, the linearity of the scalar product and the normalization of $\psi(\mathbf{n})$, the projection of \mathbb{N} on either of the isotropic projectors is

$$\mathbb{P}_i \cdot \mathbb{N} = \mathbb{P}_i \cdot \int_{S^2} \psi(\mathbf{n}) \mathbf{n}^{\otimes 4} d\mathbf{n} = \mathbb{P}_i \cdot \mathbf{n}^{\otimes 4} \quad \text{with } i \in [1, 2]. \quad (4.54)$$

Consequently, the isotropic part of \mathbb{N} can be determined analyzing the

fourth-order moment $\mathbf{n}^{\otimes 4}$ which is given in Mandel notation by

$$\mathbf{n}^{\otimes 4} = \left[\begin{array}{ccc|ccc} n_1^4 & n_1^2 n_2^2 & n_1^2 n_3^2 & \sqrt{2} n_1^2 n_2 n_3 & \sqrt{2} n_1^3 n_3 & \sqrt{2} n_1^3 n_2 \\ n_2^4 & n_2^2 n_3^2 & n_3^4 & \sqrt{2} n_2^3 n_3 & \sqrt{2} n_1 n_2^2 n_3 & \sqrt{2} n_1 n_3^2 \\ & & & \sqrt{2} n_2 n_3^3 & \sqrt{2} n_1 n_3^3 & \sqrt{2} n_1 n_2 n_3^2 \end{array} \right] \begin{array}{c|c} \text{completely} & \text{symmetric} \end{array} \quad \mathbf{B}_\xi \otimes \mathbf{B}_\zeta \quad (4.55)$$

leading to

$$\begin{aligned} 3\hat{K} = \mathbb{P}_1 \cdot \mathbf{n}^{\otimes 4} &= \frac{1}{3} \begin{bmatrix} 1 & 1 & 1 & 0 & 0 & 0 \\ 1 & 1 & 1 & 0 & 0 & 0 \\ 1 & 1 & 1 & 0 & 0 & 0 \\ 0 & 0 & 0 & 0 & 0 & 0 \\ 0 & 0 & 0 & 0 & 0 & 0 \\ 0 & 0 & 0 & 0 & 0 & 0 \end{bmatrix} \mathbf{B}_\xi \otimes \mathbf{B}_\zeta \cdot (\mathbf{n}^{\otimes 4}) \\ &= \frac{1}{3} (n_1^4 + 2n_1^2 n_2^2 + 2n_1^2 n_3^2 + n_2^4 + 2n_2^2 n_3^2 + n_3^4) \\ &= \frac{1}{3} \end{aligned} \quad (4.56)$$

and

$$\begin{aligned} 2\hat{G} = \frac{\mathbb{P}_2}{\|\mathbb{P}_2\|^2} \cdot \mathbf{n}^{\otimes 4} &= \frac{1}{15} \begin{bmatrix} 2 & -1 & -1 & 0 & 0 & 0 \\ -1 & 2 & -1 & 0 & 0 & 0 \\ -1 & -1 & 2 & 0 & 0 & 0 \\ 0 & 0 & 0 & 3 & 0 & 0 \\ 0 & 0 & 0 & 0 & 3 & 0 \\ 0 & 0 & 0 & 0 & 0 & 3 \end{bmatrix} \mathbf{B}_\xi \otimes \mathbf{B}_\zeta \cdot (\mathbf{n}^{\otimes 4}) \\ &= \frac{2}{15}. \end{aligned} \quad (4.57)$$

Thus, the isotropic part of any fourth-order fiber orientation tensor is fixed due to the normalization of both $\psi(\mathbf{n})$ and \mathbf{n} and is given by

$$\begin{aligned} \mathbb{N}^{\text{iso}} &= 3\hat{K}\mathbb{P}_1 + 2\hat{G}\mathbb{P}_2 = \frac{1}{15} \begin{bmatrix} 3 & 1 & 1 & 0 & 0 & 0 \\ 1 & 3 & 1 & 0 & 0 & 0 \\ 1 & 1 & 3 & 0 & 0 & 0 \\ 0 & 0 & 0 & 2 & 0 & 0 \\ 0 & 0 & 0 & 0 & 2 & 0 \\ 0 & 0 & 0 & 0 & 0 & 2 \end{bmatrix} \mathbf{B}_\xi \otimes \mathbf{B}_\zeta \\ &= \frac{7}{35} \text{sym}(\mathbf{I} \otimes \mathbf{I}) \end{aligned} \quad (4.58)$$

leading to a compact representation of Equation (4.53) by

$$\mathbb{N} = \mathbb{N}^{\text{iso}} + \frac{6}{7} \text{sym}(\text{dev}(\mathbf{N}) \otimes \mathbf{I}) + \text{dev}(\mathbb{N}). \quad (4.59)$$

This representation emphasizes isotropy as the one element of directional measures. Equation (4.59) reveals that in contrast to the well known harmonic decomposition of Hooke tensors, the harmonic decomposition of fourth-order orientation tensors only contains one irreducible subspace of second order and the isotropic subspace degenerates from two scalars to a constant value. Coincidence of Equations (4.59) and (4.19) is given by

$$\text{sym}(\mathbf{I} \otimes \text{dev}(\mathbf{N})) = \text{sym}(\mathbf{I} \otimes \mathbb{N}) - \frac{1}{3} \text{sym}(\mathbf{I} \otimes \mathbf{I}). \quad (4.60)$$

Interpretation of \mathbb{N} as a Hooke tensor and applying the harmonic decomposition translates the reasoning of Kanatani (1984) into the language of continuum mechanics. \mathbb{N} can be parameterized by two deviators, one being of second and the other of fourth order. Both represent the deviation from the isotropic state. Five of the 14 independent parameters of \mathbb{N} define the second-order deviator and nine define the fourth-order deviator. Three independent parameters of the second-order deviator define an orientation coordinate system in which both deviators have

simplified representations (see the structure tensor in Equation (4.31) and the following section).

4.6.2 Parameterizations and admissible parameter ranges

The space of fourth-order orientation tensors \mathbb{N} , which fulfill the algebraic constraints imposed by Equation (4.8) and which can be derived from an FODF, remains to be identified. The variety of \mathbb{N} is known from Section 4.5. Therefore, Equation (4.59) reveals that the analysis of the variety of \mathbb{N} is reduced to the identification of a fourth-order deviator $\text{dev}(\mathbb{N})$. This fourth-order deviator reflects the material symmetry of the FODF and consequently also of \mathbb{N} and \mathbb{N} . As a consequence, special representations of the fourth-order deviator in the orientation coordinate system exist. Knowledge on material symmetries of Hooke tensors is applied to identify admissible ranges of the fourth-order deviator. The most general fourth-order orientation tensor has the structure

$$\mathbb{N}(\mathbb{N}, d_1, \dots, d_9) = \mathbb{N}^{\text{iso}} + \frac{6}{7} \text{sym}(\text{dev}(\mathbb{N}) \otimes \mathbf{I}) + \mathbb{F}^{\text{tricl}}(d_1, \dots, d_9) \quad (4.61)$$

with a triclinic deviatoric structure tensor

$$\begin{aligned} \mathbb{F}^{\text{tricl}}(d_1, \dots, d_9) &= \\ \left[\begin{array}{ccc|ccc} -(d_1 + d_2) & d_1 & d_2 & -\sqrt{2}(d_4 + d_5) & \sqrt{2}d_6 & \sqrt{2}d_8 \\ & -(d_1 + d_3) & d_3 & \sqrt{2}d_4 & -\sqrt{2}(d_6 + d_7) & \sqrt{2}d_9 \\ & & -(d_2 + d_3) & \sqrt{2}d_5 & \sqrt{2}d_7 & -\sqrt{2}(d_8 + d_9) \\ \hline & \text{completely} & & & & \text{symmetric} \end{array} \right] \\ & \mathbf{B}_\zeta^{\mathbf{v}} \otimes \mathbf{B}_\zeta^{\mathbf{v}} \end{aligned} \quad (4.62)$$

which is a function of nine scalar parameters. The Mandel basis $\mathbf{B}_\zeta^{\mathbf{v}} \otimes \mathbf{B}_\zeta^{\mathbf{v}}$ is spanned in the orientation coordinate system, i.e., for example the first definition in Equation (4.39) becomes $\mathcal{B}_1 = \mathbf{v}_1 \otimes \mathbf{v}_1$. Without loss of generality, any orthotropic parameterization of \mathbb{N} , e.g., Equation (4.35),

Symmetry class of ψ	Material symmetry reflected by	
	\mathbb{N}	\mathbb{N}
isotropic	isotropic	isotropic
cubic	cubic	isotropic
transv. iso.	transv. iso.	transv. iso.
tetragonal	tetragonal	transv. iso.
trigonal	trigonal	transv. iso.
orthotropic	orthotropic	orthotropic
monoclinic	monoclinic	orthotropic
triclinic	triclinic	orthotropic

Table 4.1: Implications of symmetry classes of the FODF ψ on the second- and fourth-order fiber orientation tensors

can be combined with Equation (4.62) yielding a set of parameters, e.g., $(\alpha_1, \alpha_3, d_1, \dots, d_9)$. If the FODF has a material symmetry, this symmetry also applies to the orientation tensors and reduces the number of independent parameters, see, e.g., the implications of transverse isotropy on the parameterization of \mathbb{N} in Equation (4.35). For a given material symmetry class, the number of independent parameters is fixed. All eight material symmetries imply different constraints on \mathbb{N} . However, e.g., triclinic, monoclinic and orthotropic symmetry of ψ lead to identical constraints on \mathbb{N} . In other words, triclinic, monoclinic and orthotropic symmetric second-order tensors coincide and are usually referred to as orthotropic (see Appendix A.1). Implications of the symmetry of the FODF on the symmetry of \mathbb{N} and \mathbb{N} are listed in Table 4.1. The hierarchy of material symmetries including visualizations of symmetry planes is given in Francois et al. (1998, figure. 4). As a consequence, index and material symmetry constrain the space of \mathbb{N} . The question on the variety of fiber orientation tensors is reduced to the determination of admissible parameter combinations. The flexible parameterization of fourth-order fiber orientation tensors in Equation (4.61) is new, highlights the isotropic state and can be easily adapted to stronger material symmetries. The remaining algebraic constraint on \mathbb{N} is positive semi-definiteness. Positive

semi-definiteness implies that

$$0 \leq \mathbb{N} \cdot (\mathbf{A} \otimes \mathbf{A}) \quad (4.63)$$

holds for any second-order tensor \mathbf{A} . Without loss of generality, \mathbf{A} can be restricted to symmetric second-order tensors as \mathbb{N} is symmetric and skew, and symmetric parts are orthogonal. As a consequence, Equation (4.63) can be written in Mandel notation stating a root finding problem of the characteristic polynomial of \mathbb{N} of degree six. \mathbb{N} is positive semi-definite if all of its eigenvalues Λ_i are non-negative, i.e.

$$0 \leq \Lambda_i \text{ for } i \in [1, \dots, 6] \quad (4.64)$$

holds. Explicit representations of the eigenvalues of \mathbb{N} are given for a limited number of material symmetries in Mehrabadi and Cowin (1990). Eigenvalues of fourth-order tensors can not be identified from coefficient matrices in Voigt notation. Mandel notation has to be used (Mehrabadi and Cowin, 1990; Böhlke, 2001; Mandel, 1965).

4.6.3 Transversely isotropic case

A transversely isotropic harmonic, i.e., completely symmetric and completely traceless, tensor of fourth order with principle axis in direction e_1 is a multiple of the structure tensor

$$\begin{aligned} \mathbb{F}^{\text{transv1}} &= \left[\begin{array}{ccc|ccc} 8 & -4 & -4 & 0 & 0 & 0 \\ & 3 & 1 & 0 & 0 & 0 \\ & & 3 & 0 & 0 & 0 \\ \hline & & & & & \\ \text{completely} & & & \text{symmetric} & & \end{array} \right] \mathbf{B}_\xi \otimes \mathbf{B}_\zeta \quad (4.65) \\ &= \mathbb{F}^{\text{tricl}}(-4, -4, 1, 0, 0, 0, 0, 0, 0), \end{aligned}$$

see, e.g., Fernández and Böhlke (2019, (75)), Lobos Fernández (2018, A.3) or Müller and Böhlke (2016, (11)) and can be expressed in terms of the triclinic structure tensor defined in Equation (4.62). In consequence, transversely isotropic fourth-order orientation tensors are parameterized in the orientation coordinate system by

$$\mathbb{N}^{\text{transv}}(\alpha, \rho) = \mathbb{N}^{\text{iso}} + \alpha \frac{6}{7} \text{sym}(\mathbf{F}^{\text{transv1}} \otimes \mathbf{I}) + \rho \mathbb{F}^{\text{transv1}} = \quad (4.66)$$

$$\mathbb{N}^{\text{iso}} + \left[\begin{array}{ccc|ccc} 6\alpha/7 + 8\rho & \alpha/14 - 4\rho & \alpha/14 - 4\rho & 0 & 0 & 0 \\ & -3\alpha/7 + 3\rho & -\alpha/7 + \rho & 0 & 0 & 0 \\ & & -3\alpha/7 + 3\rho & 0 & 0 & 0 \\ \hline & \text{completely} & & & \text{symmetric} & \end{array} \right] \mathbf{B}_\xi^{\mathbf{v}} \otimes \mathbf{B}_\zeta^{\mathbf{v}}.$$

The choice of the principle axis only effects the mapping \mathbf{Q} , defined in Equation (4.22), and parameterizations around \mathbf{v}_2 or \mathbf{v}_3 are equivalent, see, e.g., Müller and Böhlke (2016). Demanding positive eigenvalues leads to the set of admissible transversely isotropic fourth-order orientation tensors

$$\mathcal{N}^{\text{transv}} = \left\{ \mathbb{N}^{\text{transv}}(\alpha, \rho) \mid -\frac{1}{3} \leq \alpha \leq \frac{2}{3}, \right. \quad (4.67)$$

$$\left. \frac{1}{8}\alpha^2 - \frac{1}{42}\alpha - \frac{1}{90} \leq \rho \leq \frac{1}{56}\alpha + \frac{1}{60} \right\}$$

given, e.g., in Nomura et al. (1970); Müller and Böhlke (2016). The set $\mathcal{N}^{\text{transv}}$ combined with the parameterization in Equation (4.66) represents the variety of transversely isotropic fourth-order orientation tensors (Müller and Böhlke, 2016).

An alternative derivation of $\mathcal{N}^{\text{transv}}$ is given by Nomura et al. (1970, Equation (54)) deploying the Schwarz inequality on directional cosines to identify a relationship between \mathbf{N} and \mathbb{N} . This relationship implies constraints on the coefficients of \mathbb{N} which are reformulated in the notation

of this work as

$$\left(N_{kk}^{(2)} \mathbf{v}_k \otimes \mathbf{v}_k \right)^2 \leq N_{kk}^{(4)} \mathbf{B}_k^{\mathbf{v}} \otimes \mathbf{B}_k^{\mathbf{v}} \leq N_{kk}^{(2)} \mathbf{v}_k \otimes \mathbf{v}_k \quad (4.68)$$

for $k \in [1, 2, 3]$ without summation convention. To be precise, the set

$$\begin{aligned} \mathcal{N}_{\text{cosines}}^{\text{transv}} = & \left\{ \mathbb{N}^{\text{transv}} \mid \right. \\ & \left. \left(N_{kk}^{(2)} \mathbf{v}_k \otimes \mathbf{v}_k \right)^2 \leq N_{kk}^{(4)} \mathbf{B}_k^{\mathbf{v}} \otimes \mathbf{B}_k^{\mathbf{v}} \leq N_{kk}^{(2)} \mathbf{v}_k \otimes \mathbf{v}_k \right\} \end{aligned} \quad (4.69)$$

is identical to the set $\mathcal{N}^{\text{transv}}$. However, for weaker symmetries, positive definiteness is a stronger constraint than the conditions in Equation (4.68). Comparison of second- and fourth-order moment tensors (see, e.g., Equation (4.55)) motivates the reasoning behind Equation (4.68). In order to frame the implications of positive semi-definiteness, Figure 4.3 contains additional subsets, lines and special points discussed in the following. Interpretation of \mathbb{N} as weighted summation of moment tensors leads to coefficient-wise constraints on \mathbb{N} (see Appendix A.3). The set $\mathcal{N}_{\text{linear}}^{\text{transv}}$, defined in Equation (A.15), fulfills these coefficient-wise constraints. The set of transversely isotropic orientation states bounded by the norm of a singular orientation is denoted by

$$\mathcal{N}_{\text{norm}}^{\text{transv}} = \left\{ \mathbb{N}^{\text{transv}} \mid 0 \leq \|\mathbb{N}\|_{\text{Frobenius}} \leq 1 \right\}. \quad (4.70)$$

Figure 4.3 visualizes the relation $\mathcal{N}_{\text{norm}}^{\text{transv}} \subset \mathcal{N}_{\text{linear}}^{\text{transv}} \subset \mathcal{N}_{\text{norm}}^{\text{transv}}$. Special orientation states, such as the planar isotropic and unidirectional state are marked in Figure 4.3 for reference. The isotropic state \mathbb{N}^{iso} , defined in Equation (4.58), is located at $\alpha = \rho = 0$ and is part of a straight vertical line with $\alpha = 0$ which contains orientation states with isotropic second-order tensor. Therefore, the set of transversely isotropic orientation states with isotropic second-order orientation tensor is a one dimensional subspace of $\mathcal{N}^{\text{transv}}$ with limiting orientation states

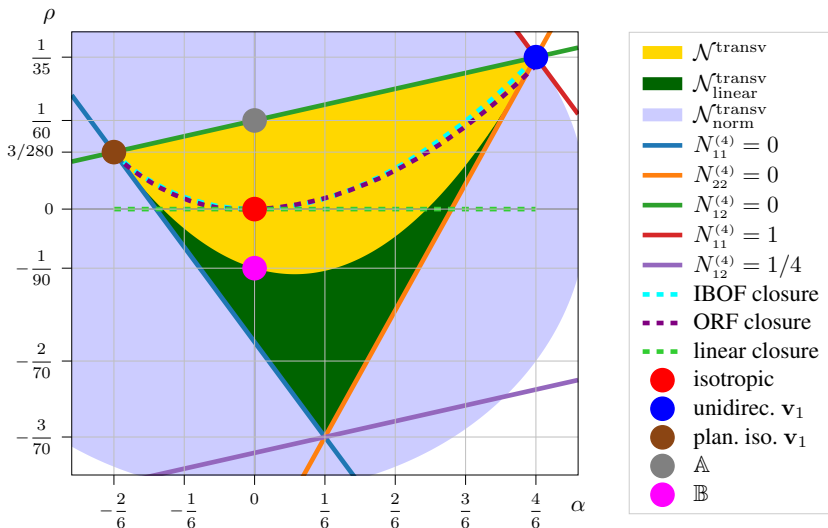


Figure 4.3: Transversely isotropic fourth-order orientation states following Nomura et al. (1970)

visualized in Figure 4.3 and given by

$$\begin{aligned} \mathbb{A} &= N^{\text{transv}} (\alpha = 0, \rho = 1/60) \\ &= \left[\begin{array}{ccc|ccc} 1/3 & 0 & 0 & 0 & 0 & 0 \\ & 1/4 & 1/12 & 0 & 0 & 0 \\ & & 1/4 & 0 & 0 & 0 \\ \hline & \text{completely} & & \text{symmetric} & & \end{array} \right] \mathbf{B}_{\xi}^{\mathbf{v}} \otimes \mathbf{B}_{\zeta}^{\mathbf{v}} \quad (4.71) \end{aligned}$$

and

$$\begin{aligned} \mathbb{B} &= \mathbb{N}^{\text{transv}} (\alpha = 0, \rho = -1/90) \\ &= \left[\begin{array}{ccc|ccc} 1/9 & 1/9 & 1/9 & 0 & 0 & 0 \\ & 1/6 & 1/18 & 0 & 0 & 0 \\ & & 1/6 & 0 & 0 & 0 \\ \hline & & & & & \\ \text{completely} & & & \text{symmetric} & & \end{array} \right] \mathbf{B}_\xi^v \otimes \mathbf{B}_\zeta^v. \end{aligned} \quad (4.72)$$

The states \mathbb{A} and \mathbb{B} can not be distinguished by means of second-order orientation tensors as

$$\mathbb{A}[\mathbf{I}] = \mathbb{B}[\mathbf{I}] = \mathbb{N}^{\text{iso}} \quad (4.73)$$

holds, but the states differ significantly. Figure 4.3 shows that for the special case of transversely isotropy, only two second-order fiber orientation tensors, namely those defined by $\alpha = -1/3$ and $\alpha = 2/3$, are connected to a corresponding fourth-order fiber orientation tensor by a one-to-one relation. The subsequent sections show that for weaker symmetries a one-to-one correspondence solely remains for the unidirectional case. Closure approximations, shortly discussed in Section 4.7, construct a one-to-one mapping between a given second-order fiber orientation tensor and an unknown fourth-order fiber orientation tensor. In Figure 4.3, three closures which are discussed in Section 4.7 are visualized and indicate that the variety of transversely isotropic fourth-order fiber orientation tensors is not fully reflected by the selected closures.

An intuitive interpretation of the orientation states described by \mathbb{A} and \mathbb{B} in Equations (4.71) and (4.72) is obtained by minimal sets of discrete fibers which are described by these fiber orientation tensors. The single fibers can be visualized and represent minimal realisations of states in $\mathbb{N}^{\text{transv}}$. To the best of the authors' knowledge, visualization of fiber orientation tensors by minimal discrete fiber arrangements is new. For

both the state \mathbb{A} and the state \mathbb{B} , an FODF can be build by a sum of delta functions with homogeneous weights

$$\psi(\mathbf{n}) = \frac{1}{N} \sum_i^N \frac{1}{2} (\delta(\mathbf{n} - \mathbf{n}_i) + \delta(\mathbf{n} + \mathbf{n}_i)) \quad (4.74)$$

based on a set of discrete fiber directions $\{\mathbf{n}_i \text{ with } i \in [1, \dots, N]\}$. Minimal sets of discrete fiber directions leading to orientation tensors \mathbb{A} and \mathbb{B} are

$$\mathcal{D}_{\mathbb{A}} = \left\{ \begin{bmatrix} 0 \\ \cos(\phi_i) \\ \sin(\phi_i) \end{bmatrix} \text{ with } \phi_i = \frac{2\pi(i-1)}{6} \text{ for } i \in [1, \dots, 6] \right\} \quad (4.75)$$

$$+ 3 \left\{ \begin{bmatrix} 1 \\ 0 \\ 0 \end{bmatrix} \right\} \text{ and}$$

$$\mathcal{D}_{\mathbb{B}} = \left\{ \begin{bmatrix} \cos(\pi/4) \\ \cos(\phi_i) \\ \sin(\phi_i) \end{bmatrix} \text{ with } \phi_i = \frac{2\pi(i-1)}{6} \text{ for } i \in [1, \dots, 6] \right\} \quad (4.76)$$

given in the orientation coordinate system $\{\mathbf{v}_i\}$. Visualizations of the sets of directions are given in Figures 4.4b and 4.4c. Comparison of the vector sets and inspection of Figures 4.4b, 4.4c and 4.3 allow for an interpretation of the parameter ρ in Equation (4.66). The lower the value of ρ , the more pronounced are directions towards diagonals between the principle axis of the orientation coordinate system.

4.6.4 Orthotropic case

An orthotropic harmonic tensor of fourth order is given by

$$\mathbb{F}^{\text{ortho}}(d_1, d_2, d_3) = \mathbb{F}^{\text{tricl}}(d_1, d_2, d_3, 0, 0, 0, 0, 0, 0) \quad (4.77)$$

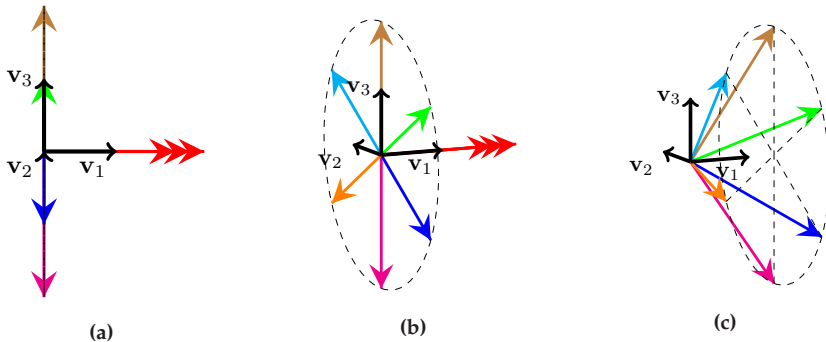


Figure 4.4: Visualization of minimal sets of discrete directions representing extremal transversely isotropic orientation states which are N -isotropic: (a), (b) Two views on \mathcal{D}_A leading to A , (b) \mathcal{D}_B leading to B

with $\mathbb{F}^{\text{trial}}$ defined in Equation (4.62). As the weakest material symmetry of second-order tensors is orthotropy, a parameterization of orthotropic fourth-order orientation tensors is given by

$$\begin{aligned} \mathbb{N}^{\text{ortho}}(\mathbf{N}, d_1, d_2, d_3) = \\ \mathbb{N}^{\text{iso}} + \frac{6}{7} \text{sym}(\text{dev}(\mathbf{N}) \otimes \mathbf{I}) + \mathbb{F}^{\text{ortho}}(d_1, d_2, d_3). \end{aligned} \quad (4.78)$$

The set of admissible orthotropic fourth-order orientation tensors is

$$\begin{aligned} \mathcal{N}^{\text{ortho}} = \left\{ \mathbb{N}^{\text{ortho}}(\mathbf{N}, d_1, d_2, d_3) \mid \right. \\ \left. 0 \leq \Lambda_i \forall \Lambda_i \text{ in eigenvalues of } \mathbb{N}^{\text{ortho}} \right\}, \end{aligned} \quad (4.79)$$

see Section 4.6.2.

Parameterization of \mathbf{N} following Equation (4.29) leads to

Three eigenvalues of $\mathbb{N}^{\text{ortho}}$ in the six dimensional space of the Mandel representation are directly given by

$$\frac{1}{2}\Lambda_1 = \frac{1}{14}(-2\alpha_1 + \alpha_3) + d_3 + \frac{1}{15}, \quad (4.81)$$

$$\frac{1}{2}\Lambda_2 = \frac{1}{14}(\alpha_1 + \alpha_3) + d_2 + \frac{1}{15}, \quad (4.82)$$

$$\frac{1}{2}\Lambda_3 = \frac{1}{14}(\alpha_1 - 2\alpha_3) + d_1 + \frac{1}{15}, \quad (4.83)$$

due to the diagonal form of the lower right quadrant of $\mathbf{N}^{\text{ortho}}$ in Equation (4.80). Following Mehrabadi and Cowin (1990, Equation (5.35)), the remaining eigenvalues ($\Lambda_4, \Lambda_5, \Lambda_6$) are the roots of the characteristic polynomial

$$\det(\mathbf{M} - \Omega \mathbf{I}) = 0 \quad (4.84)$$

being cubic in Ω , with the identity matrix of dimension three \mathbf{I} and the matrix

$$\mathbf{M} = \begin{bmatrix} \frac{3}{7}(2\alpha_1 - \alpha_3) - d_1 - d_2 + \frac{1}{5} & \frac{1}{14}(\alpha_1 - 2\alpha_3) + d_1 + \frac{1}{15} & \frac{1}{14}(\alpha_1 + \alpha_3) + d_2 + \frac{1}{15} \\ -\frac{3}{7}(\alpha_1 + \alpha_3) - d_1 - d_3 + \frac{1}{5} & \frac{1}{14}(-2\alpha_1 + \alpha_3) + d_3 + \frac{1}{15} & \frac{3}{7}(-\alpha_1 + 2\alpha_3) - d_2 - d_3 + \frac{1}{5} \\ \text{symmetric} & & \end{bmatrix}. \quad (4.85)$$

For transversely isotropic orientation tensors, a compact and explicit representation of the admissible parameters, is given by Equation (4.67). For the orthotropic case, explicit formulas specifying $\mathcal{N}^{\text{ortho}}$ by combinations of the parameters of $\mathbb{N}^{\text{ortho}}$, can be identified analytically, e.g., using complex or trigonometric expressions. As an alternative, non-negativity of eigenvalues can be demanded by alternating signs of monomials of the cubic characteristic following Vieta's formula preventing the need to explicitly calculate the eigenvalues. However, the resulting expressions are lengthy and therefore are not given here. For applications $\mathcal{N}^{\text{ortho}}$ can be calculated numerically.

However, for a given specific second-order orientation tensor \mathbf{N} , compact representations of sets of admissible tuples (d_1, d_2, d_3) , i.e., tuples leading to $\mathbb{N}^{\text{ortho}}(\mathbf{N}, d_1, d_2, d_3) \in \mathcal{N}^{\text{ortho}}$, exist. For reference, an explicit parameterization of admissible tuples for the special case of an isotropic second-order orientation tensor \mathbf{N}^{iso} is given in Appendix A.4. Admissible tuples for specific \mathbf{N} along three paths are visualized in Figures 4.6, 4.7 and 4.8. The paths are defined in Figure 4.5a. Figure 4.6 reveals that the admissible region of (d_1, d_2, d_3) for an isotropic second-order orientation tensor is symmetric and comparably large. Departing from the isotropic second-order orientation tensor along the blue path along \mathbf{v}_1 (see Figure 4.5a) towards the unidirectional state, the admissible region of (d_1, d_2, d_3) changes its shape and position in the space spanned by d_1 , d_2 and d_3 and finally degenerates to a single point representing the unidirectional state. As all points on the blue path are transversely isotropic with respect to the \mathbf{v}_1 -axis, the admissible ranges of the parameters d_1 and d_2 are identical along this path (see $\mathbb{F}^{\text{transv}1}$ in Equation (4.27)). Figure 4.7 contains views on the admissible tuples for specific second-order orientation tensors along the orange path, in 4.5a. Second-order orientation tensors along the orange path between the isotropic and the planar isotropic state are transversely isotropic with principle axis \mathbf{v}_3 . Therefore, admissible ranges of the

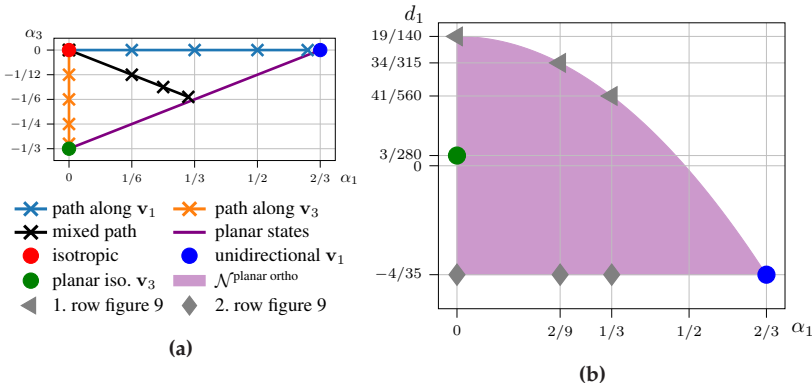


Figure 4.5: (a) Paths on the orientation triangle defining specific second-order orientation tensors used in Figures 4.6, 4.7 and 4.8 (b) Admissible ranges of d_1 for planar orthotropic orientation states and specific orientation states used in Figure 4.9. The legend is shared with Figure 4.5a.

parameters d_2 and d_3 change homogeneously and shrink along the path towards the planar isotropic second-order orientation tensor. For the planar isotropic second-order orientation tensor, the parameters d_2 and d_3 are fixed and equal $-3/70$. Therefore, at this second-order state the admissible region degenerates to a line and the remaining degree of freedom of an orthotropic fourth-order orientation tensor with planar isotropic $\mathbf{N}^{\text{planar iso}}$ is d_1 with admissible range $-4/35 \leq d_1 \leq 19/140$.

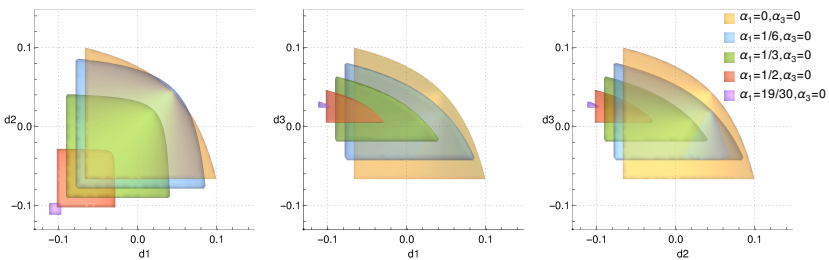


Figure 4.6: Three views on admissible ranges of (d_1, d_2, d_3) for specific second-order orientation tensors along the blue path (along \mathbf{v}_1) in Figure 4.5a

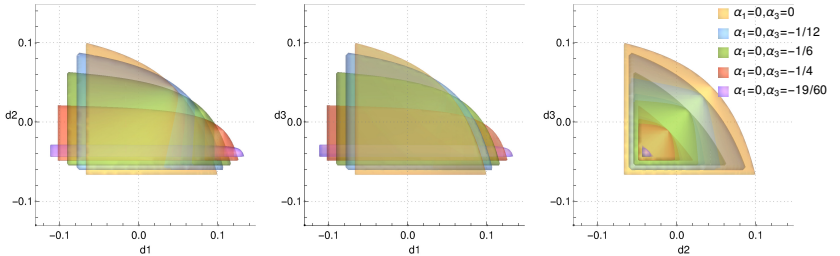


Figure 4.7: Three views on admissible ranges of (d_1, d_2, d_3) for specific second-order orientation tensors along the orange path (along \mathbf{v}_3) in Figure 4.5a

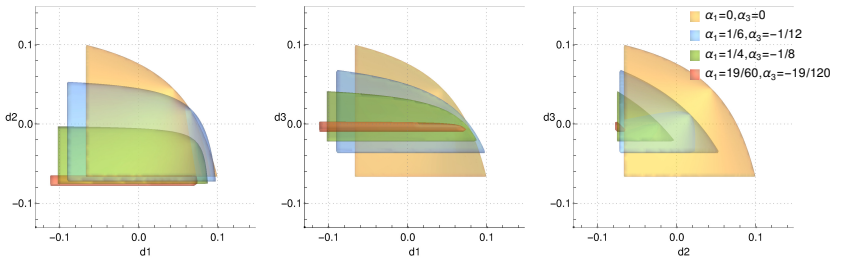


Figure 4.8: Three views on admissible ranges of (d_1, d_2, d_3) for specific second-order orientation tensors along the black path on orthotropic states in Figure 4.5a

The planar isotropic orientation state is located at $d_1 = 3/280$. Second-order orientation tensors of planar orientation states are located at the purple line in Figure 4.5a. This line connects the planar isotropic and the unidirectional states. Planar orthotropic fourth-order orientation tensors are degenerated in the sense that the parameters d_2 and d_3 are directly related to N , ensuring that the orientation state is planar. As a consequence, the remaining degree of freedom of planar orthotropic fourth-order orientation tensors is solely determined by the remaining parameter d_1 . In consequence, a parameterization of planar orthotropic

fourth-order orientation tensors is given by

$$\begin{aligned} \mathbb{N}^{\text{planar ortho}}(\alpha_1, d_1) &= \mathbb{N}^{\text{ortho}}\left(\mathbf{N} = \mathbf{N}^{\text{planar}}(\alpha_1), d_1, \right. \\ &\quad \left. d_2 = \frac{-15\alpha_1 - 6}{140}, d_3 = \frac{15\alpha_1 - 6}{140}\right) \end{aligned} \quad (4.86)$$

with $\mathbf{N}^{\text{planar}}(\alpha_1)$ following Equation (4.37). The set of admissible planar orthotropic orientation tensors

$$\begin{aligned} \mathcal{N}^{\text{planar ortho}} &= \left\{ \mathbb{N}^{\text{planar ortho}}(\alpha_1, d_1) \mid \right. \\ &\quad \left. 0 \leq \alpha_1 \leq \frac{2}{3}, -\frac{4}{35} \leq d_1 \leq \frac{19}{140} - \frac{9}{16}\alpha_1^2 \right\} \end{aligned} \quad (4.87)$$

is visualized in Figure 4.5b. For reference, the planar isotropic and unidirectional states are highlighted in Figure 4.5b. To the best of the authors' knowledge, the set of admissible orthotropic fiber orientation tensors of fourth order has not been presented in the literature before. Second-order orientation tensors which describe planar orientation states in a three-dimensional space have four variable parameters. Three of these four parameters define the mapping \mathbf{Q} (see Equation (4.22)) which defines the orientation coordinate system and the fourth parameter defines the orientation state. One possible choice for this fourth parameter is α_1 (see Equation (4.37)). Orthotropic fourth-order orientation tensors, which represent planar orientation states, add one additional independent parameter, e.g., d_1 . Figure 4.5b visualizes the admissible ranges of d_1 as a function of α_1 , assuming orthotropy. The admissible range of this fourth-order orientation tensor parameter d_1 degenerates to a single value in case of the unidirectional state. This degeneration reveals a valuable view on the information which is contained in \mathbb{N} but not in \mathbf{N} . The second-order orientation tensor \mathbf{N} contains directional measures in the directions defined by the axes of the orientation coordinate system.

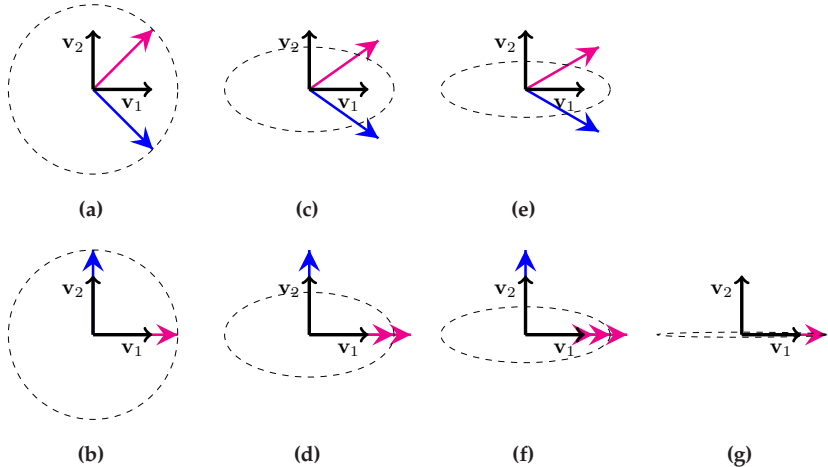


Figure 4.9: Visualizations of minimal discrete sets of directions in the orientation coordinate system $\{v_i\}$ for given planar orthotropic orientation tensors which are marked in Figure 4.9 and parameterized by α_1 and d_1 (see Equation (4.86)). (a) $\alpha_1 = 0, d_1 = 19/140$ with $\mathcal{D}^{(a)} = \{[1/\sqrt{2}, 1/\sqrt{2}-\varepsilon, 0], [1/\sqrt{2}, -(1/\sqrt{2}-\varepsilon), 0]\}$ with $\varepsilon \ll 1$ (b) $\alpha_1 = 0, d_1 = -4/35$ with $\mathcal{D}^{(b)} = \{[1, 0, 0], [0, 1, 0]\}$ (c) $\alpha_1 = 2/9, d_1 = 34/315$ with $\mathcal{D}^{(c)} = \{[\sqrt{2}/\sqrt{3}, 1/\sqrt{3}, 0], [\sqrt{2}/\sqrt{3}, -1/\sqrt{3}, 0]\}$ (d) $\alpha_1 = 2/9, d_1 = -4/35$ with $\mathcal{D}^{(d)} = \{2 \times [1, 0, 0], [0, 1, 0]\}$ (e) $\alpha_1 = 1/3, d_1 = 41/560$ with $\mathcal{D}^{(e)} = \{[\sqrt{3}/2, 1/2, 0], [\sqrt{3}/2, -1/2, 0]\}$ (f) $\alpha_1 = 1/3, d_1 = -4/35$ with $\mathcal{D}^{(f)} = \{3 \times [1, 0, 0], [0, 1, 0]\}$ (g) $\alpha_1 = 2/3, d_1 = -4/35$ with $\mathcal{D}^{(g)} = \{[1, 0, 0]\}$

An orthotropic fourth-order orientation tensor contains additional directional information representing the spread around the directions defined by the axes of the orientation coordinate system. For the unidirectional state, i.e., if all fibers are aligned in one direction, there is no spread. In the planar orthotropic case, there is only one spread. This mental model is a simplification of directional measures by spherical harmonics but suits engineering applications and can be used to interpret Figures 4.6 to 4.8. In the following, examples of planar orthotropic orientation states are discussed. Figures 4.9a to 4.9g visualize sets of discrete directions for planar orthotropic orientation states marked in figure 4.5b. The upper (lower) row of sub Figures in Figure 4.9 represents discrete sets of directions which lead to planar and orthotropic fourth-order orientation

tensors with maximum (minimum) admissible values d_1 (see Figure 4.5b for reference). A minimal set of discrete directions for each sub Figure in Figure 4.9 is given in the caption. The discrete sets of directions labeled $\mathcal{D}^{(i)}$ for $i \in [a, b, c, d, e, f, g]$ in the caption of Figure 4.9 can be combined with Equation (4.74) to identify the corresponding FODF and orientation tensors. For reference, limiting cases of orthotropic fourth order orientation tensors which contract to the planar isotropic second-order orientation tensor are given by

$$\mathbb{N}^{\text{planar ortho}} (\alpha_1 = 0, d_1 = 19/140) = \quad (4.88)$$

$$\left[\begin{array}{ccc|ccc} 1/4 & 1/4 & 0 & 0 & 0 & 0 \\ & 1/4 & 0 & 0 & 0 & 0 \\ & 0 & 0 & 0 & 0 & 0 \\ \hline & & & & & \\ \text{completely} & & \text{symmetric} & & & \end{array} \right] \mathbf{B}_\xi^v \otimes \mathbf{B}_\zeta^v$$

and

$$\mathbb{N}^{\text{planar ortho}} (\alpha_1 = 0, d_1 = -4/35) = \quad (4.89)$$

$$\left[\begin{array}{ccc|ccc} 1/2 & 0 & 0 & 0 & 0 & 0 \\ & 1/2 & 0 & 0 & 0 & 0 \\ & 0 & 0 & 0 & 0 & 0 \\ \hline & & & & & \\ \text{completely} & & \text{symmetric} & & & \end{array} \right] \mathbf{B}_\xi^v \otimes \mathbf{B}_\zeta^v.$$

4.6.5 Planar case

Without loss of generality, inspection of planar states is restricted to orientation states which are located inside the plane spanned by \mathbf{v}_1 and \mathbf{v}_2 . Following this convention, some coefficients of moment tensors

represented in the orientation coordinate system (see, e.g., equation (4.55) or (A.12)) vanish, because out of plane components of the unit vector, which builds the moment tensors, equal zero. Combining the knowledge of vanishing coefficients of $\mathbb{N}^{\text{planar}}$ with Equation (4.61) leads to the parameterization

$$\mathbb{N}^{\text{planar}}(\alpha_1, d_1, d_8) = \left[\begin{array}{ccc|ccc} \frac{3}{4}\alpha_1 - d_1 + \frac{27}{70} & d_1 + \frac{4}{35} & 0 & 0 & 0 & \sqrt{2}d_8 \\ & -\frac{3}{4}\alpha_1 - d_1 + \frac{27}{70} & 0 & 0 & 0 & -\sqrt{2}d_8 \\ & & 0 & 0 & 0 & 0 \\ \hline & & & & & \\ \text{completely} & & & & & \text{symmetric} \\ & & & & & \end{array} \right] \mathbf{B}_\xi^v \otimes \mathbf{B}_\zeta^v \quad (4.90)$$

which fits into the general triclinic framework given by equations (4.61) and (4.62) with

$$\begin{aligned} \mathbb{N}^{\text{planar}}(\alpha_1, d_1, d_8) &= \mathbb{N} \left(\mathbb{N}^{\text{planar}}(\alpha_1), d_1, \right. \\ &\quad d_2 = \frac{-15\alpha_1 - 6}{140}, d_3 = \frac{15\alpha_1 - 6}{140}, \\ &\quad \left. 0, 0, 0, 0, d_8, d_9 = -d_8 \right). \end{aligned} \quad (4.91)$$

Similar to the planar orthotropic case, the parameters d_2 and d_3 are directly related to \mathbb{N} , ensuring that out of plane coefficients in the upper left quadrant in Equation (4.90) vanish. Removing the orthotropic constraint adds degrees of freedom. However, the planar plane intrinsically acts as a symmetry plane and planar orientation states have at least monoclinic material symmetry. As a consequence of this material symmetry as well as due to the planarity itself, the parameters d_4 , d_5 , d_6 and d_7 in Equation (4.62), which is utilized in Equation (4.91), equal zero. Due to the planarity, $d_9 = -d_8$ holds in Equation (4.91) as

the coefficient $\sqrt{2} (d_8 + d_9)$ in Equation (4.62) has to vanish. This can be seen by comparison of Equation (4.62) and the moment tensor in Equation (A.12) where the planarity implies $\theta = \frac{\pi}{2}$. Demanding positive eigenvalues of $\mathbb{N}^{\text{planar}}$ in Equation (4.90) leads to the set of admissible planar fourth-order orientation tensors

$$\begin{aligned}\mathcal{N}^{\text{planar}} = & \left\{ \mathbb{N}^{\text{planar}}(\alpha_1, d_1, d_8) \mid 0 \leq \alpha_1 \leq \frac{2}{3}, \right. \\ & \left. -\frac{4}{35} \leq d_1 \leq \frac{19}{140} - \frac{9}{16}\alpha_1^2, -f(\alpha_1, d_1) \leq d_8 \leq f(\alpha_1, d_1) \right\}\end{aligned}\quad (4.92)$$

with

$$\begin{aligned}f(\alpha_1, d_1) = & \quad (4.93) \\ \frac{1}{140} \sqrt{304 - 1260 \alpha_1^2 + 420 d_1 - 11025 \alpha_1^2 d_1 - 19600 d_1^2}.\end{aligned}$$

To the best of the author's knowledge, this set is new in the literature and of great practical importance for shell-like components reinforced with long fibers. The set of admissible planar fourth-order orientation tensors is visualized in Figures 4.10a and 4.10b. The connection to the admissible ranges in the planar orthotropic case, which is illustrated in Figure 4.5b, is given by a projection of $\mathcal{N}^{\text{planar}}$ onto the plane $d_8 = 0$. In Figure 4.10c, the plotting range of the parameter α_1 is extended from one unidirectional state along a planar boundary of the orientation plane in Figure 4.2b towards a second unidirectional orientation state. This illustrates the continuity of the admissible ranges and the redundancy of the orientation plane.

4.7 A note on closure approximations

For a given second-order orientation tensor \mathbf{N} , closure approximations identify an unknown fourth-order orientation tensor $\mathbb{N}^{\text{unknown}}$ following

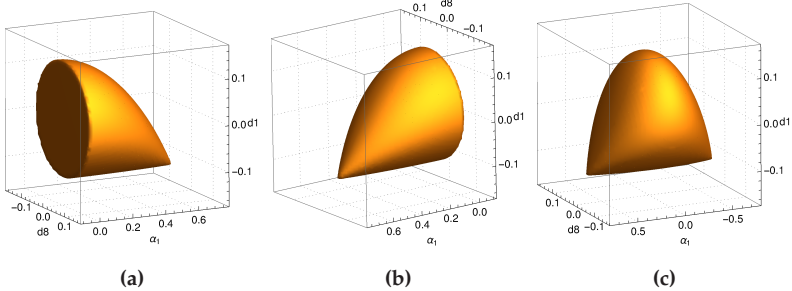


Figure 4.10: (a), (b) Views on $\mathcal{N}^{\text{planar}}$ (c) Transition of admissible parameters of planar states between two unidirectional orientation states visualized by varying the parameter α_1 in Equation (4.92) in the range $-2/3 \leq \alpha_1 \leq 2/3$.

a specific closure approach such that

$$\mathbb{N}^{\text{unknown}} [\mathbf{I}] = \mathbb{N} \quad (4.94)$$

holds. Based on the quantity which is directly affected by a closure's assumptions, closure approximations might be classified into three groups. The first group contains closures based on algebraic assumptions. Closures based on assumptions on the material symmetry of orientation tensors form the second group. The third group contains closures which state assumptions on the FODF. The linear closure is given by

$$\mathbb{N}^{\text{linear}} (\mathbb{N}) = \mathbb{N}^{\text{iso}} + \frac{6}{7} \text{sym} (\text{dev} (\mathbb{N}) \otimes \mathbf{I}), \quad (4.95)$$

belongs to the first group and is defined in Han and Im (1999, Equation (13)) or Advani and Tucker III (1990). The representation in (4.95) benefits from the notation introduced in Equations (4.58) and (4.59). The linear closure states that the unknown fourth-order orientation tensor is linear in the second-order orientation tensor. This implies vanishing fourth-order harmonic part, i.e., $\text{dev} (\mathbb{N}^{\text{unknown}}) = \mathbb{O}$. Figure 4.3 contains the linear closure as dashed light green line and clearly shows the limitations of this closure as the line is not completely within the admissible param-

eter space. The second group contains, e.g., orthotropic fitted closures which combine analytical insights on the material symmetry of fiber orientation tensors with fitting procedures reproducing selected flow simulation results. Examples are given in Cintra Jr and Tucker III (1995); Chung and Kwon (2001; 2002) and both the orthotropic fitted closure (ORF) (Cintra Jr and Tucker III, 1995) and the invariant-based optimal fitting closure (IBOF) (Chung and Kwon, 2002) are visualized in Figure 4.3 using nilsmeyerkit and JulianKarlBauer (2021). The third group contains closures, e.g., Montgomery-Smith et al. (2011a); Görthofer et al. (2020), which enable exact reconstructions of the unknown FODF, based on the assumption that the ODF belongs to a special class of FODFs. Therefore, assumptions are made on the FODF and tensors of any order can be constructed based on the reconstructed FODF. Although this short note on closures does not claim to be exhaustive, reference is made to additional closures, e.g., VerWeyst et al. (1999); Montgomery-Smith et al. (2011b); Jack et al. (2010). Reproduction of the FODF by maximization of the information entropy, e.g., Müller and Böhlke (2016) (see also Böhlke (2005)) states an alternative and its wording explicitly addresses the problem of gaining information by assumptions. Assessment of closure approximations is challenging since the definition of an application-independent metric for the quality of the closure is difficult. Nevertheless, assessments of closure approximations are given in Breuer et al. (2019); Jack and Smith (2007; 2008).

4.8 Summary and conclusions

Application of linear invariant decomposition with focus on index symmetry (Rychlewski, 2000) transfers the results of Kanatani (1984) into the continuum mechanics framework and leads to a compact representation of fourth-order fiber orientation tensors in Equations (4.58) and (4.59). A harmonic, i.e. completely symmetric and completely traceless, triclinic

fourth-order structure tensor is introduced in Equation (4.62). This structure tensor has a simplified structure in the coordinate system spanned by the eigenvectors of the second-order fiber orientation tensor and leads to a parameterization of generic fourth-order fiber orientation tensors in Equation (4.61). Material symmetries of the orientation distribution function reduce the number of independent parameters. In the triclinic case, the independent parameters are a second-order fiber orientation tensor plus nine scalars. Admissible ranges of the independent parameters are discussed in detail for orthotropy, transversely isotropy and planar cases. Insufficiency of coefficient-wise constraints are demonstrated for the transversely isotropic case. The variety of fourth-order fiber orientation tensors is given by the set of positive-definite tensors which can be expressed by Equation (4.61). Inspection of planar orthotropic states illustrates the character of fourth-order orientation information. Notes on closure approximations demonstrate their limitations on reflecting the variety of fourth-order fiber orientation tensors.

As a summary, the parameterizations of generic second-order orientation tensors \mathbf{N}

$$\mathbf{N}(\alpha_1, \alpha_3) = \mathbf{N}^{\text{iso}} + \alpha_1 \mathbf{F}^{\text{transv1}} + \alpha_3 \mathbf{F}^{\text{transv3}}, \quad \text{see (4.29)}$$

generic fourth-order orientation tensors \mathbb{N}

$$\begin{aligned} \mathbb{N}(\mathbf{N}, d_1, \dots, d_9) = & \\ \mathbb{N}^{\text{iso}} + \frac{6}{7} \text{sym}(\text{dev}(\mathbf{N}) \otimes \mathbf{I}) + \mathbb{F}^{\text{tric}}(d_1, \dots, d_9), & \end{aligned} \quad \text{see (4.61)}$$

orthotropic fourth-order orientation tensors $\mathbb{N}^{\text{ortho}}$

$$\begin{aligned} \mathbb{N}^{\text{ortho}}(\mathbf{N}, d_1, d_2, d_3) = & \\ \mathbb{N}^{\text{iso}} + \frac{6}{7} \text{sym}(\text{dev}(\mathbf{N}) \otimes \mathbf{I}) + \mathbb{F}^{\text{ortho}}(d_1, d_2, d_3) & \end{aligned} \quad \text{see (4.78)}$$

and planar fourth-order orientation tensors $\mathbb{N}^{\text{planar}}$

$$\begin{aligned}\mathbb{N}^{\text{planar}}(\alpha_1, d_1, d_8) = \mathbb{N} \left(\mathbb{N}^{\text{planar}}(\alpha_1), d_1, \right. & \quad \text{see (4.91)} \\ d_2 = \frac{-15\alpha_1 - 6}{140}, d_3 = \frac{15\alpha_1 - 6}{140}, \\ \left. 0, 0, 0, 0, d_8, d_9 = -d_8 \right)\end{aligned}$$

are repeated, including the structure tensors

$$\mathbf{F}^{\text{transv1}} = \begin{bmatrix} 1 & 0 & 0 \\ & -1/2 & 0 \\ \text{sym} & & -1/2 \end{bmatrix} \mathbf{v}_i \otimes \mathbf{v}_j, \quad \text{see (4.27)}$$

$$\mathbf{F}^{\text{transv3}} = \begin{bmatrix} -1/2 & 0 & 0 \\ & -1/2 & 0 \\ \text{sym} & & 1 \end{bmatrix} \mathbf{v}_i \otimes \mathbf{v}_j, \quad \text{see (4.28)}$$

$$\begin{aligned}\mathbb{F}^{\text{tricl}}(d_1, \dots, d_9) = & \quad \text{see (4.62)} \\ \left[\begin{array}{ccc|ccc} -(d_1 + d_2) & d_1 & d_2 & -\sqrt{2}(d_4 + d_5) & \sqrt{2}d_6 & \sqrt{2}d_8 \\ & -(d_1 + d_3) & d_3 & \sqrt{2}d_4 & -\sqrt{2}(d_6 + d_7) & \sqrt{2}d_9 \\ & & -(d_2 + d_3) & \sqrt{2}d_5 & \sqrt{2}d_7 & -\sqrt{2}(d_8 + d_9) \\ \hline & \text{completely} & & & \text{symmetric} & \end{array} \right] \\ \mathbf{B}_\xi^\nu \otimes \mathbf{B}_\zeta^\nu\end{aligned}$$

and

$$\mathbb{F}^{\text{ortho}}(d_1, d_2, d_3) = \mathbb{F}^{\text{tricl}}(d_1, d_2, d_3, 0, 0, 0, 0, 0, 0). \quad \text{see (4.77)}$$

Admissible parameter ranges follow from the requirement of positive semi-definiteness (see Equation (4.64)) and are explicitly given for special cases of material symmetry in Equations (4.67), (4.87), (4.92) and (A.16).

Beside the review contribution, novel technical and scientific contributions in this work are listed hereafter.

- An invariant framework for parameterizations of fourth-order fiber orientation tensors based on deviators from the isotropic orientation state is developed. The most general case is obtained by an orthotropic deviator of second order and an triclinic deviator of fourth order. Within this framework, deviators of stronger material symmetries are obtained as special cases with constrained parameters.
- Explicit parameterizations and admissible parameter ranges present in the literature are extended by orthotropic as well as planar fiber orientation tensors in a three-dimensional framework.
- Visualizations of admissible parameter sets are given for the first time for the orthotropic states in Figures 4.5 to 4.8 and for the planar states in Figures 4.10a.
- Positive semi-definiteness is identified to be a stronger constraint on admissible orientation tensors than linear constraints on tensor coefficients which themselves are identified to be stronger constraints than a bonded norm.
- A short hand notation for completely symmetric fourth-order tensors is introduced.
- Representations of discrete fiber sets (Figures 4.4 and 4.9) are identified to be an valuable visualization of orientation tensors.

These results enable engineers to parameterize the space of admissible fiber orientation tensors obtaining a valuable tool for engineering applications like model inspection or data validation.

Chapter 5

Fiber Orientation Distributions Based on Planar Fiber Orientation Tensors of Fourth Order¹

5.1 Introduction

Suitable microstructure descriptors are essential for the prediction of effective properties of fiber reinforced composites. Fiber orientation distribution functions (FODF) represent exact microstructure descriptors of the orientation of axisymmetric fibers within a specified volume of a fiber reinforced composite (Kanatani, 1984; Advani and Tucker III, 1987). However, in practice the exact distribution of fibers is commonly approximated by fiber orientation tensors (Böhlke et al., 2019; Görthofer et al., 2019) which represent averaged directional measures and can be directly determined by non-destructive analysis methods, such as computer tomography (Pinter et al., 2018; Schöttl et al., 2020). Furthermore, fiber orientation tensors fit into the tensor-based framework of continuum mechanics which is frequently used in material modeling

¹ This chapter reproduces (Bauer and Böhlke, 2022a), i.e., Bauer, J. K., Böhlke, T., 2022. Fiber orientation distributions based on planar fiber orientation tensors of fourth order. *Mathematics and Mechanics of Solids*, online first, 10.1177/10812865221093958. Reproduced with permission. ©2022 The Authors. Published by SAGE Publications Ltd under CC BY-NC 4.0

(Kehrer et al., 2020; Brylka, 2017; Hessman et al., 2021). The dependence of material models on the set of admissible second-order fiber orientation tensors is studied numerically in, e.g., Goldberg et al. (2017); Görthofer et al. (2020). However, the dependence of material models or other quantities of interest such as reconstructed FODF itself on fourth-order fiber orientation tensors is rarely studied analytically. In addition, for some applications, e.g., damage modeling (Schemmann et al., 2018b) or averaging schemes (Hessman et al., 2021; Brylka, 2017), the identification of a FODF based on given fiber orientation tensors is beneficial. Due to the averaged character of fiber orientation tensors, no one-to-one correspondence to an FODF exists. Nevertheless, for a given fiber orientation tensor, any associated FODF is of interest and eases the indirect visualization of fiber orientation tensors. Many fiber-reinforced composites are plate-like and if the mean fiber length is larger than the plate thickness the resulting fiber distribution is approximately planar. This holds, e.g., for sheet molding compound (Görthofer et al., 2019). For such planar fiber distributions, Bauer and Böhlke (2022c) identifies a set of all admissible fourth-order fiber orientation tensors. Based on this set and reconstruction methods following Kanatani (1984); Müller and Böhlke (2016), the variety of reconstructed FODF based on planar fiber orientation tensors of fourth order is studied in the current work.

This paper is structured as follows: Definitions of FODF and fiber orientation tensors are followed by a reformulation of planar fiber orientation tensors following Bauer and Böhlke (2022c). Within the admissible set of planar fourth-order fiber orientation tensors given by Bauer and Böhlke (2022c), a subset of distinct planar fourth-order fiber orientation tensors is identified. FODF approximations by truncated Fourier series with planar leading fiber orientation tensors in a three-dimensional framework are identified as non-planar and motivate a two-dimensional framework. The reconstruction of FODF based on the maximum entropy method following Müller and Böhlke (2016) is

recast into this two-dimensional framework. Discrete slices and points of the set of admissible and distinct planar fourth-order fiber orientation tensors are used to visualize reconstructed FODF based on fourth-order fiber orientation tensors. A note on FODF reconstruction solely based on second-order fiber orientation tensors including the exact closure (Montgomery-Smith et al., 2011a) closes this paper.

5.2 Directional measures as microstructure descriptors

Taking the average of a tensorial quantity over orientations requires a directional measure which quantifies the orientations. Established directional measures of axisymmetric fibers are the fiber orientation distribution function (FODF) and fiber orientation tensors of several kinds and orders. Both FODF and fiber orientation tensors quantify orientations inside a reference volume which might be interpreted as a section of specified size at a specific position \mathbf{x} inside a structural component. Consequently, the directional measurement depends on the size of this reference volume which usually represents a scaling parameter in measurement algorithms, see e.g., Görthofer et al. (2019, Figure 4) or Schöttl et al. (2020). This section introduces basic quantities and in large parts follows Bauer and Böhlke (2022c, sections 2.1 and 2.2).

5.2.1 Fiber orientation distribution function

The fiber orientation distribution function ψ at a given position inside a component

$$\psi : \mathcal{S}^2 \rightarrow \mathbb{R}, \text{ with } \mathcal{S}^2 = \{\mathbf{n} \in \mathbb{R}^3 \mid \|\mathbf{n}\| = 1\} \quad (5.1)$$

maps any direction \mathbf{n} onto a scalar value $\psi(\mathbf{n})$. \mathcal{S}^2 is the two-dimensional surface of a unit sphere in three dimensions parameterized by, e.g., a unit vector \mathbf{n} . The function $\psi(\mathbf{n})$ is non-negative, i.e.,

$$\psi(\mathbf{n}) \geq 0, \quad \forall \mathbf{n} \in \mathcal{S}^2 \quad (5.2)$$

holds and normalization of $\psi(\mathbf{n})$ implies

$$\int_{\mathcal{S}^2} \psi(\mathbf{n}) \, d\mathbf{n} = 1. \quad (5.3)$$

As fibers have a direction but no attitude, $\psi(\mathbf{n})$ is symmetric, i.e.,

$$\psi(-\mathbf{n}) = \psi(\mathbf{n}), \quad \forall \mathbf{n} \in \mathcal{S}^2 \quad (5.4)$$

holds (see Advani and Tucker III (1987); Görthofer et al. (2020)).

5.2.2 Fiber orientation tensors

Fiber orientation tensors of Kanatani first kind (Kanatani, 1984) are defined by

$$\mathbb{N}_{(k)} = \int_{\mathcal{S}^2} \psi(\mathbf{n}) \mathbf{n}^{\otimes k} \, d\mathbf{n} \quad (5.5)$$

with $\mathbf{n}^{\otimes k}$ being the k -th moment of \mathbf{n} . In this work, only the second- and fourth-order fiber orientation tensors

$$\mathbf{N} = \mathbb{N}_{(2)} = \int_{\mathcal{S}^2} \psi(\mathbf{n}) \mathbf{n} \otimes \mathbf{n} \, d\mathbf{n}, \quad (5.6)$$

$$\mathbb{N} = \mathbb{N}_{(4)} = \int_{\mathcal{S}^2} \psi(\mathbf{n}) \mathbf{n} \otimes \mathbf{n} \otimes \mathbf{n} \otimes \mathbf{n} \, d\mathbf{n} \quad (5.7)$$

are used. More details on the properties of $\mathbb{N}_{(k)}$ can be found, e.g., in Bauer and Böhlke (2022c). Higher order fiber orientation tensors of

Kanatani first kind contain all tensors of lower order as

$$\mathbb{N}_{\langle k-2 \rangle} = \mathbb{N}_{\langle k \rangle} [\mathbf{I}] \quad (5.8)$$

holds for $2 \leq k$ with the identity on second-order tensors $\mathbf{I} = \delta_{ij} \mathbf{e}_i \otimes \mathbf{e}_j$. In addition, for the second-order orientation tensor

$$\mathbf{N} \cdot \mathbf{I} = \text{tr}(\mathbf{N}) = 1 \quad (5.9)$$

holds due to normalization, see Bauer and Böhlke (2022c). Orientation tensors of Kanatani first kind are commonly used to represent directional data obtained by computer tomography scans or results of flow simulations (Görthofer et al., 2019). Basic properties of the second-order orientation tensor \mathbf{N} are briefly summarized following Bauer and Böhlke (2022c). \mathbf{N} is symmetric and positive semi-definite. In consequence, \mathbf{N} can be diagonalized, i.e., pairs of eigenvalues λ_i with $\lambda_i \geq 0$ and orthonormal eigenvectors \mathbf{v}_i for $i \in [1, 2, 3]$ exist, such that

$$\mathbf{N} = N_{ij}^{(2)} \mathbf{e}_i \otimes \mathbf{e}_j = \sum_{i=1}^3 \lambda_i \mathbf{v}_i \otimes \mathbf{v}_i = \begin{bmatrix} \lambda_1 & 0 & 0 \\ & \lambda_2 & 0 \\ \text{sym} & & \lambda_3 \end{bmatrix} \mathbf{v}_i \otimes \mathbf{v}_j \quad (5.10)$$

holds and there exists a rotation defined by an orthogonal tensor

$$\mathbf{Q} = \mathbf{v}_i \otimes \mathbf{e}_i \quad (5.11)$$

mapping the arbitrary but fixed basis $\{\mathbf{e}_i\}$ onto the basis $\{\mathbf{v}_i\}$. The orthonormal basis $\{\mathbf{v}_i\}$ spanned by the eigenvectors is, in the following, called orientation coordinate system. Based on the ordering convention

$$\lambda_3 \leq \lambda_2 \leq \lambda_1, \quad (5.12)$$

an established classification of structurally differing N exists (see Cintra Jr and Tucker III (1995); Chung and Kwon (2002); Goldberg et al. (2017); Köbler et al. (2018)). A visualization corresponding to this classification exists and is called orientation triangle. Any second-order orientation tensor can be represented by a pair (λ_1, λ_2) , which is connected to a point inside the orientation triangle and by a mapping Q which defines the orientation coordinate system. The FODF can be expressed in terms of fiber orientation tensors as a three-dimensional tensorial Fourier series

$$\psi(\mathbf{n}) = \frac{1}{4\pi} \sum_{k=0}^{\infty} \frac{2k+1}{2^k} \binom{2k}{k} \text{dev}(N_{(k)}) \cdot \mathbf{n}^{\otimes k} \quad (5.13)$$

which is called spherical harmonic expansion (Kanatani, 1984, page 154). The operator $\text{dev}(\cdot)$ extracts the deviatoric part and its definition for higher order tensors in a three-dimensional framework is given

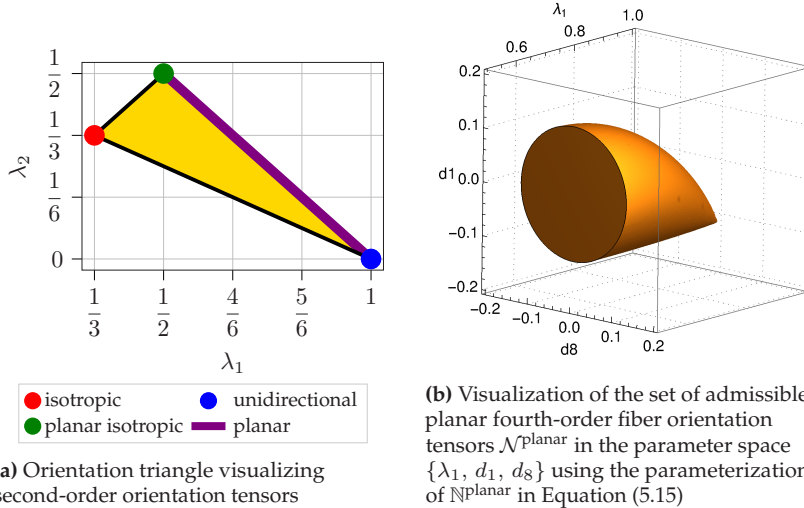


Figure 5.1

in Spencer (1970). Equation (5.13) implies, that in general an infinite number of orientation tensors of increasing order is required to express $\psi(\mathbf{n})$. However, for many practical applications only second and fourth-order orientation tensors are available at a specific location inside a component. Recent developments in computer tomography methods for fiber reinforced composites lead towards the identification of the FODF instead of fiber orientation tensors, see, e.g., Schöttl et al. (2021).

5.3 Admissible and distinct planar fiber orientation tensors

A parameterization of planar fiber orientation tensors of second order $\mathbf{N}^{\text{planar}}$ is given by

$$\begin{aligned}\mathbf{N}^{\text{planar}}(\lambda_1) &= \lambda_1 \mathbf{v}_1 \otimes \mathbf{v}_1 + (1 - \lambda_1) \mathbf{v}_2 \otimes \mathbf{v}_2 \\ &= \begin{bmatrix} \lambda_1 & 0 & 0 \\ & 1 - \lambda_1 & 0 \\ \text{sym} & & 0 \end{bmatrix} \mathbf{v}_i \otimes \mathbf{v}_j\end{aligned}\quad (5.14)$$

in the orientation coordinate system $\{\mathbf{v}_i\}$ defined in Equation (5.11) and with $1/2 \leq \lambda_1 \leq 1$. Bauer and Böhlke (2022c, Equation (87)) identify planar fiber orientation tensors of fourth order $\mathbf{N}^{\text{planar}}(\alpha_1, d_1, d_8)$ which can be reparameterized in λ_1 with $\alpha_1 = \frac{4}{3}(\lambda_1 - \frac{1}{2})$ leading to

$$\begin{aligned}\mathbf{N}^{\text{planar}}(\lambda_1, d_1, d_8) &= \\ \left[\begin{array}{ccc|ccc} \lambda_1 - d_1 - \frac{4}{35} & d_1 + \frac{4}{35} & 0 & 0 & 0 & \sqrt{2} d_8 \\ & (1 - \lambda_1) - d_1 - \frac{4}{35} & 0 & 0 & 0 & -\sqrt{2} d_8 \\ 0 & 0 & 0 & 0 & 0 & 0 \end{array} \right] \mathbf{B}_\xi^{\text{v}} \otimes \mathbf{B}_\zeta^{\text{v}} \\ \hline &\text{completely} && &\text{symmetric} &\end{aligned}\quad (5.15)$$

in Kelvin-Mandel (Thomson, 1856; Mandel, 1965; Mehrabadi and Cowin, 1990) notation, which is explained in detail in Appendix B.1. The Kelvin-Mandel basis $\mathbf{B}_\xi^Y \otimes \mathbf{B}_\zeta^Y$ is spanned in the orientation coordinate system $\{\mathbf{v}_i\}$, i.e., for example the fourth basis vector in Equation (B.1) becomes $\mathbf{B}_4^Y = \frac{\sqrt{2}}{2} (\mathbf{v}_2 \otimes \mathbf{v}_3 + \mathbf{v}_3 \otimes \mathbf{v}_2)$. In Equation (5.15), a short hand notation for completely symmetric fourth-order tensors following Bauer and Böhlke (2022c) is used, which is explained in Appendix B.1. Demanding positive eigenvalues of $\mathbb{N}^{\text{planar}}$ in Equation (5.15) leads to the set of admissible planar fourth-order orientation tensors

$$\mathcal{N}^{\text{planar}} = \left\{ \mathbb{N}^{\text{planar}}(\lambda_1, d_1, d_8) \mid \begin{array}{l} \frac{1}{2} \leq \lambda_1 \leq 1, \\ -\frac{4}{35} \leq d_1 \leq -\frac{4}{35} + \lambda_1 - \lambda_1^2, \\ -f(\lambda_1, d_1) \leq d_8 \leq f(\lambda_1, d_1) \end{array} \right\} \quad (5.16)$$

with

$$f(\lambda_1, d_1) = \frac{1}{35} \sqrt{-16 - 280 d_1 - 1225 d_1^2 + 140 \lambda_1 - 140 \lambda_1^2 + 1225 d_1 \lambda_1 - 1225 d_1 \lambda_1^2}, \quad (5.17)$$

see Bauer and Böhlke (2022c, Equation (89)). The set $\mathcal{N}^{\text{planar}}$ implicitly defines a body in the parameter space $\{\lambda_1, d_1, d_8\}$. This body is visualized in Figure 5.1b and contains all admissible planar fourth-order fiber orientation tensors. Any point inside this body represents a fourth-order orientation tensor.

As Bauer and Böhlke (2022c) derive $\mathcal{N}^{\text{planar}}$ solely from algebraic properties of $\mathbb{N}^{\text{planar}}$, no planar fourth-order fiber orientation tensor outside $\mathcal{N}^{\text{planar}}$ exists. Consequently, the parameterization $\mathbb{N}^{\text{planar}}(\lambda_1, d_1, d_8)$ combined with the parameter space $\mathcal{N}^{\text{planar}}$ allows for a complete study of the influence of fiber orientation on the mechanical response of

material models, which are based on fourth-order fiber orientation tensors of planar fiber architectures. However, not necessarily all points inside $\mathcal{N}^{\text{planar}}$ represent orientation states which differ structurally and therefore lead to different mechanical behavior. Two tensors \mathbb{A} and \mathbb{B} are called structurally identical if they differ solely by a rotation, i.e.,

$$\exists \mathbf{Q} \in \text{SO}(3) \text{ with } \mathbf{Q} \star \mathbb{A} = \mathbb{B} \quad (5.18)$$

holds with the special orthogonal group in three dimensions $\text{SO}(3)$. The parameterization of $\mathcal{N}^{\text{planar}}$ in Equation (5.15) and the corresponding set of admissible parameter combinations $\mathcal{N}^{\text{planar}}$ in Equation (5.16) is based on the orientation coordinate system which is introduced in Equations (5.10) to (5.12). However, for orientation states with planar isotropic second-order orientation tensor, i.e., $\lambda_1 = 1/2$, the eigenvalue problem identifying \mathbf{v}_1 and \mathbf{v}_2 is ill-posed. As the eigenvalues of \mathbf{N} ($\lambda_1 = 1/2$) are $1/2$, $1/2$ and 0 , any pair of two orthonormal vectors being pairwise perpendicular to \mathbf{v}_3 is a valid choice for the eigenvectors. The ambiguity of the orientation coordinate system introduces a redundancy in the set of admissible fourth-order orientation tensors given in Equation (5.16), i.e., multiple parameter combinations lead to structurally identical $\mathcal{N}^{\text{planar}}$. The shape of the body $\mathcal{N}^{\text{planar}}$ in Figure 5.1b motivates the reparameterization of $\mathcal{N}^{\text{planar}}(\lambda_1, d_1, d_8)$ as a function of $\lambda_1, \hat{r}, \hat{\beta}$ with

$$d_1 = \hat{d}_1 + \frac{1}{2} [\lambda_1 - \lambda_1^2] - \frac{4}{35}, \quad (5.19)$$

$$\hat{d}_1 = \hat{r} \sin(\hat{\beta}), \quad (5.20)$$

$$d_8 = \hat{r} \cos(\hat{\beta}). \quad (5.21)$$

The parameters \hat{r} and $\hat{\beta}$ are visualized in figure 5.2a and lead to a

reformulation of Equation (5.15) with

$$\mathbb{N}^{\text{planar}}(\lambda_1, \hat{r}, \hat{\beta}) = \left[\begin{array}{ccc|ccc} -\hat{r} \sin(\hat{\beta}) + \frac{\lambda_1^2}{2} + \frac{\lambda_1}{2} & \hat{r} \sin(\hat{\beta}) - \frac{\lambda_1^2}{2} + \frac{\lambda_1}{2} & 0 & 0 & 0 & \sqrt{2}\hat{r} \cos(\hat{\beta}) \\ -\hat{r} \sin(\hat{\beta}) + \frac{\lambda_1^2}{2} - \frac{3\lambda_1}{2} + 1 & 0 & 0 & 0 & 0 & -\sqrt{2}\hat{r} \cos(\hat{\beta}) \\ 0 & 0 & 0 & 0 & 0 & 0 \end{array} \right] \begin{array}{c|c} \text{completely} & \text{symmetric} \end{array} \quad (5.22)$$

$\mathbf{B}_\xi^v \otimes \mathbf{B}_\zeta^v$

and Equation (5.16) by

$$\mathcal{N}^{\text{planar}} = \left\{ \mathbb{N}^{\text{planar}}(\lambda_1, \hat{r}, \hat{\beta}) \mid \begin{array}{l} \frac{1}{2} \leq \lambda_1 \leq 1, \\ 0 \leq \hat{r} \leq \frac{1}{2} [\lambda_1 - \lambda_1^2], \\ 0 \leq \hat{\beta} < 2\pi \end{array} \right\}. \quad (5.23)$$

For the special case $\lambda_1 = 1/2$, the reparameterized fourth-order fiber orientation tensor reads as

$$\mathbb{N}^{\text{planar}}(\lambda_1 = 1/2, \hat{r}, \hat{\beta}) = \left[\begin{array}{ccc|ccc} -\hat{r} \sin(\hat{\beta}) + \frac{3}{8} & \hat{r} \sin(\hat{\beta}) + \frac{1}{8} & 0 & 0 & 0 & \sqrt{2}\hat{r} \cos(\hat{\beta}) \\ -\hat{r} \sin(\hat{\beta}) + \frac{3}{8} & 0 & 0 & 0 & 0 & -\sqrt{2}\hat{r} \cos(\hat{\beta}) \\ 0 & 0 & 0 & 0 & 0 & 0 \end{array} \right] \begin{array}{c|c} \text{completely} & \text{symmetric} \end{array} \quad (5.24)$$

$\mathbf{B}_\xi^v \otimes \mathbf{B}_\zeta^v$

and comparison with representations of rotations in Kelvin-Mandel

notation in Cowin and Mehrabadi (1995, section 3) and Mehrabadi and Cowin (1990, section 3) indicate a rotational redundancy. Active rotation of $\mathbb{N}^{\text{planar}}(\lambda_1 = 1/2, \hat{r}, \hat{\beta})$ by an angle of $-\hat{\beta}/4$ around the axis \mathbf{v}_3 leads to

$$\begin{aligned} & \mathbf{Q}^{\mathbf{v}_3} \left(\gamma = -\hat{\beta}/4 \right) \star \mathbb{N}^{\text{planar}} \left(\lambda_1 = 1/2, \hat{r}, \hat{\beta} \right) \\ &= \mathbb{N}^{\text{planar}} \left(\lambda_1 = 1/2, \hat{r}, \hat{\beta} = 0 \right) \\ &= \left[\begin{array}{ccc|cc} 3/8 & 1/8 & 0 & 0 & \sqrt{2}\hat{r} \\ & 3/8 & 0 & 0 & -\sqrt{2}\hat{r} \\ & & 0 & 0 & 0 \\ \hline & & & & \\ \text{completely} & & \text{symmetric} & & \end{array} \right] \mathbf{B}_{\xi}^{\mathbf{v}} \otimes \mathbf{B}_{\zeta}^{\mathbf{v}} \end{aligned} \quad (5.25)$$

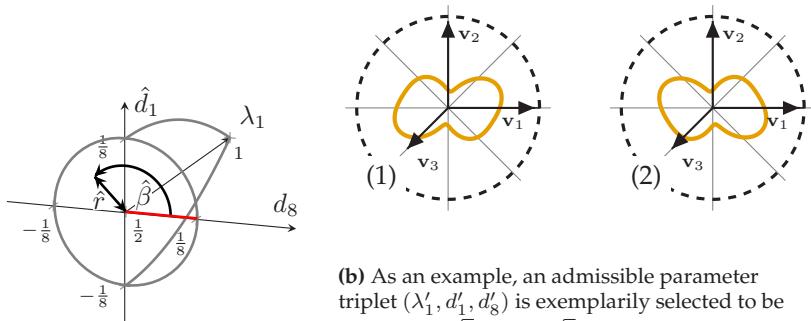
with a rotation around the axis \mathbf{v}_3 parameterized by the angle γ with

$$\mathbf{Q}^{\mathbf{v}_3} (\gamma) = \left[\begin{array}{ccc} \cos(\gamma) & -\sin(\gamma) & 0 \\ \sin(\gamma) & \cos(\gamma) & 0 \\ 0 & 0 & 1 \end{array} \right] \mathbf{v}_i \otimes \mathbf{v}_j. \quad (5.26)$$

As the angle $\hat{\beta}$ in Equation (5.25) is arbitrary and the right hand side of Equation (5.25) is independent of $\hat{\beta}$, any $\mathbb{N}^{\text{planar}}(\lambda_1 = 1/2, \hat{r}, \hat{\beta})$ can be expressed by a reference tensor $\mathbb{N}^{\text{planar}}(\lambda_1 = 1/2, \hat{r}, \hat{\beta} = 0)$ combined with a rotation by

$$\begin{aligned} & \mathbb{N}^{\text{planar}} \left(\lambda_1 = 1/2, \hat{r}, \hat{\beta} \right) = \\ & \mathbf{Q}^{\mathbf{v}_3} \left(\gamma = \hat{\beta}/4 \right) \star \mathbb{N}^{\text{planar}} \left(\lambda_1 = 1/2, \hat{r}, \hat{\beta} = 0 \right). \end{aligned} \quad (5.27)$$

In consequence, coincidence or symmetry of the eigenvalues λ_1 and λ_2 in the special case of $\lambda_1 = 1/2$, degenerates the space of structurally differing planar fiber orientation tensors of fourth order from a circle to



(a) The parameter space N^{planar} spanned by $(\lambda_1, \hat{d}_1, d_8)$ or equivalently $(\lambda_1, \hat{r}, \hat{\beta})$ following Equations (5.19) to (5.21). The line $(\lambda_1 = 1/2, \hat{r}, 0)$ with $0 \leq \hat{r} \leq 1/8$ is colored in red.

(b) As an example, an admissible parameter triplet (λ'_1, d'_1, d'_8) is exemplarily selected to be $(2/3, 1/[16\sqrt{2}], 1/[16\sqrt{2}])$. The polar plot (1) shows the projection of $N^{\text{planar}}(\lambda'_1, d'_1, d'_8)$ onto the v_1 - v_2 -plane, i.e., $N^{\text{planar}}(\lambda'_1, d'_1, d'_8) \cdot \mathbf{n}^{\otimes 4}(\varphi, \pi/2)$ with the fourth-order moment $\mathbf{n}^{\otimes 4}(\varphi, \theta)$ of a unit vector $\mathbf{n}(\varphi, \theta)$ in polar coordinates, e.g., defined in Equation (5.33). The polar plot (2) shows $N^{\text{planar}}(\lambda'_1, d''_1, -d'_8) \cdot \mathbf{n}^{\otimes 4}(\varphi, \pi/2)$.

Figure 5.2

a line. Fiber orientation tensors along this line act as reference tensors following Equation (5.27). The line is, e.g., parameterized by \hat{r} or equivalently by d_8 and one arbitrary choice is colored red in Figure 5.2a.

If N^{planar} serves as a directional measure, the full parameter range of d_8 , specified in Equation (5.16), is necessary to account for all admissible orientation states. If, in contrast, the influence of N^{planar} onto mechanical properties or reconstructed FODF is to be studied, a minimal parameter set of structurally differing planar fiber orientation tensors is of interest.

This set is given by

$$\begin{aligned}\hat{\mathcal{N}}^{\text{planar}} = & \left\{ \mathbb{N}^{\text{planar}}(\lambda_1, d_1, d_8) \mid \frac{1}{2} < \lambda_1 \leq 1, \right. \\ & -\frac{4}{35} \leq d_1 \leq -\frac{4}{35} + \lambda_1 - \lambda_1^2, \\ & \left. 0 \leq d_8 \leq f(\lambda_1, d_1) \right\} \\ \cup & \left\{ \mathbb{N}^{\text{planar}}(\lambda_1 = 1/2, d_1, d_8) \mid d_1 = 0, 0 \leq d_8 \leq 1/8 \right\} \quad (5.28)\end{aligned}$$

with $\mathbb{N}^{\text{planar}}$ and $f(\lambda_1, d_1)$ defined in Equations (5.15) and (5.17) and $f(\lambda_1 = 1/2, d_1 = 0) = 1/8$. Equation (5.28) accounts for the special case $\lambda_1 = 1/2$ and removes a second redundancy which is visualized in Figure 5.2b and derived by the following observation. Two fiber orientation tensors of fourth order $\mathbb{N}^{\text{planar}}(\lambda_1, d_1, d_8)$ which differ solely by the sign of the parameter d_8 are structurally identical and only differ by the rotation

$$\mathbf{Q}^{\text{mono } x} = \begin{bmatrix} 1 & 0 & 0 \\ 0 & -1 & 0 \\ 0 & 0 & -1 \end{bmatrix} \mathbf{v}_i \otimes \mathbf{v}_j \quad (5.29)$$

which rotates any physical quantity by 180° around the axis \mathbf{v}_1 . Due to its symmetries, for any planar fourth-order fiber orientation tensor

$$\mathbf{Q}^{\text{mono } x} \star \mathbb{N}^{\text{planar}}(\lambda_1, d_1, d_8) = \mathbb{N}^{\text{planar}}(\lambda_1, d_1, -d_8) \quad (5.30)$$

holds and motivates restriction to positive values of d_8 in the minimal set specified in Equation (5.28). This set can be used to study the influence of planar fourth-order orientation tensors on derived quantities.

5.4 Reconstructed fiber orientation distribution functions

In the previous section distinct and admissible planar fiber orientation tensors of fourth order are identified. The question of interest is, which fiber orientation distributions are associated to these tensors? It is evident from Equation (5.13) that for a given leading fiber orientation tensor there is non one-to-one correspondence to an FODF. However, identification of any FODF which is connected to the given leading fiber orientation tensor is of interest. An approximation of a FODF by leading fiber orientation tensors up to fourth order in a three-dimensional framework is given by

$$\hat{\psi}(\mathbf{n}, \mathbb{N}) = \frac{1}{4\pi} \left[1 + \frac{15}{2} \text{dev}(\mathbb{N}) \cdot \mathbf{n}^{\otimes 2} + \frac{315}{8} \text{dev}(\mathbb{N}) \cdot \mathbf{n}^{\otimes 4} \right], \quad (5.31)$$

following Equation (5.13), where \mathbb{N} can be expressed by \mathbb{N} based on Equation (5.8). Müller and Böhlke (2016) discuss that the approximation $\hat{\psi}(\mathbf{n}, \mathbb{N})$ is not necessarily non-negative, i.e., the condition stated on $\psi(\mathbf{n})$ in Equation (5.2) does not hold for the approximation $\hat{\psi}(\mathbf{n}, \mathbb{N})$, due to the truncation after the fourth-order term. For the special case of planar fiber orientation tensors $\mathbb{N}^{\text{planar}}$ the approximation in Equation (5.31) leads to

$$\begin{aligned} \hat{\psi}^{\mathbb{N}^{\text{planar}}}(\varphi, \theta, \lambda_1, d_1, d_8) &= \hat{\psi}\left(\mathbf{n}(\varphi, \theta), \mathbb{N}^{\text{planar}}(\lambda_1, d_1, d_8)\right) \quad (5.32) \\ &= \frac{1}{2048\pi} \left[20160d_8 \sin^4(\theta) \sin(4\varphi) \right. \\ &\quad + 3[72 - 6720d_1] \sin^4(\theta) \cos(4\varphi) \\ &\quad - 3[1120\lambda_1 - 560] [3 \cos(2\theta) + 1] \sin^2(\theta) \cos(2\varphi) \\ &\quad \left. - 420 \cos(2\theta) + 945 \cos(4\theta) + 435 \right] \end{aligned}$$

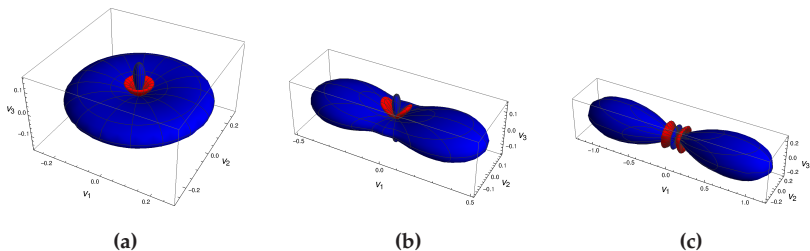


Figure 5.3: Approximation of the FODF by leading fiber orientation tensors up to fourth order following Equation (5.32), i.e., $\hat{y}^{\text{NPplanar}}(\varphi, \theta, \text{NPplanar}(\lambda_1, d_1, d_8))$ for three selected points in $\mathcal{N}^{\text{planar}}$. Positive values are plotted in blue and negative values are plotted in red. The parameters in the format (λ_1, d_1, d_8) are (a) $(1/2, 3/280, 0)$ (b) $(2/3, -1/315, 0)$ (c) $(1, -4/35, 0)$

with a parameterization of the unit vector \mathbf{n} in two spherical angles

$$\mathbf{n}(\varphi, \theta) = \sin(\theta) \cos(\varphi) \mathbf{v}_1 + \sin(\theta) \sin(\varphi) \mathbf{v}_2 + \cos(\theta) \mathbf{v}_3. \quad (5.33)$$

The approximation $\hat{\psi}^{\text{N}^{\text{planar}}}$ is not planar. Figures 5.3a to 5.3c show three-dimensional spherical plots of $\hat{\psi}^{\text{N}^{\text{planar}}}(\theta, \varphi, \lambda_1, d_1, d_8)$ for three selected combinations of the parameters λ_1 , d_1 and d_8 . Representation of non-smooth functions by Fourier series require an infinite number of non-vanishing Fourier coefficients. For any given planar FODF, the transition from non-vanishing values in the plane spanned by \mathbf{v}_1 and \mathbf{v}_2 , to vanishing values outside this plane is not smooth. In consequence, this transition is inadequately represented by the truncated spherical Fourier series $\hat{\psi}^{\text{N}^{\text{planar}}}$. As a result, planarity of a given fiber orientation tensor in a three-dimensional framework does not imply that derived quantities, such as reconstructed FODF, are planar as well. Following Bauer and Böhlke (2022c, Equation (59)), any fourth-order fiber orientation tensor in three dimensions can be expressed by two deviators $\text{dev}(\mathbf{N})$ and

$\text{dev}(\mathbb{N})$ fulfilling

$$\mathbb{N} = \mathbb{N}^{\text{iso}} + \frac{6}{7} \text{sym}(\text{dev}(\mathbb{N}[\mathbf{I}]) \otimes \mathbf{I}) + \text{dev}(\mathbb{N}). \quad (5.34)$$

Vanishing deviators, i.e., $\text{dev}(\mathbb{N}) = 0$ and $\text{dev}(\mathbb{N}) = 0$ describe the isotropic state $\mathbb{N}^{\text{iso}} = \frac{7}{35} \text{sym}(\mathbf{I} \otimes \mathbf{I})$ which corresponds to the FODF $\psi(\mathbf{n}, \mathbb{N}^{\text{iso}}) = \frac{1}{4\pi}$ and which is not planar. For $\mathbb{N}^{\text{planar}}$ the deviators from the isotropic state which are also utilized in Equation (5.31) read as

$$\text{dev}(\mathbb{N}^{\text{planar}}) = \begin{bmatrix} \lambda_1 - 1/3 & 0 & 0 \\ 0 & 2/3 - \lambda_1 & 0 \\ \text{sym} & 0 & -1/3 \end{bmatrix} \mathbf{v}_i \otimes \mathbf{v}_j, \quad (5.35)$$

$$\text{dev}(\mathbb{N}^{\text{planar}}) = \quad (5.36)$$

$$\left[\begin{array}{ccc|c} \lambda_1/7 - d_1 - \frac{1}{35} & d_1 & 1/35 - \lambda_1/7 & \begin{matrix} 0 & 0 & \sqrt{2} d_8 \\ 0 & 0 & -\sqrt{2} d_8 \\ 0 & 0 & 0 \end{matrix} \\ (1 - \lambda_1)/7 - d_1 - 1/35 & 1/35 - (1 - \lambda_1)/7 & 3/35 & \hline \text{completely} & \text{symmetric} & & \end{array} \right]$$

$$\mathbf{B}_{\xi}^{\mathbf{v}} \otimes \mathbf{B}_{\zeta}^{\mathbf{v}}$$

and demonstrate the drawbacks of expressing planar fiber orientation tensors in a three-dimensional framework since the planarity has to be enforced by deviation from the isotropic state. Note that the fourth-order deviator depends on the parameter λ_1 which defines the second-order fiber orientation tensor.

5.4.1 Transition from 3D into 2D

Motivated by the previous section and following Kanatani (1984); Blinowski et al. (1996); Vianello (1997); Desmorat and Desmorat (2015); Vannucci (2018), planar quantities are expressed in a two-dimensional

framework with representations

$$\underline{\underline{a}} = \sum_{i=1}^2 \underline{a}_i \underline{\mathbf{e}}_i = \underline{a}_1 \underline{\mathbf{e}}_1 + \underline{a}_2 \underline{\mathbf{e}}_2 + 0 \underline{\mathbf{e}}_3, \quad (5.37)$$

$$\begin{aligned} \underline{\underline{A}} &= \sum_{i=1}^2 \sum_{j=1}^2 \underline{A}_{ij} \underline{\mathbf{e}}_i \otimes \underline{\mathbf{e}}_j \\ &= \sum_{i=1}^2 \sum_{j=1}^2 \underline{A}_{ij} \underline{\mathbf{e}}_i \otimes \underline{\mathbf{e}}_j + \sum_{i=1}^3 0 \underline{\mathbf{e}}_i \otimes \underline{\mathbf{e}}_3 + \sum_{j=1}^3 0 \underline{\mathbf{e}}_3 \otimes \underline{\mathbf{e}}_j, \end{aligned} \quad (5.38)$$

$$\underline{\underline{\mathbb{A}}} = \sum_{\xi=1}^3 \sum_{\zeta=1}^3 \underline{A}_{\xi\zeta} \underline{\mathbf{B}}_\xi \otimes \underline{\mathbf{B}}_\zeta = \sum_{\xi \in [1, 2, 4]} \sum_{\zeta \in [1, 2, 4]} \underline{A}_{\xi\zeta} \underline{\mathbf{B}}_\xi \otimes \underline{\mathbf{B}}_\zeta \quad (5.39)$$

with generic tensors $\underline{\underline{a}}$, $\underline{\underline{A}}$, $\underline{\underline{\mathbb{A}}}$. This notation directly connects objects in \mathbb{R}^2 and \mathbb{R}^3 and requires the reader to select the appropriate two or three dimensional view onto the planar physical quantity of interest, which is part of the three-dimensional reality. For the two-dimensional Kelvin-Mandel bases $\underline{\mathbf{B}}_1 = \mathbf{B}_1$, $\underline{\mathbf{B}}_2 = \mathbf{B}_2$ and $\underline{\mathbf{B}}_3 = \mathbf{B}_4$ holds. To be explicit, for indices of tensor components in the 2D-framework $i, j \in [1, 2]$ and $\xi, \zeta \in [1, 2, 3]$ holds in contrast to $i, j \in [1, 2, 3]$ and $\xi, \zeta \in [1, 2, 3, 4, 5, 6]$ in the 3D-framework.

If planar orientation tensors are derived from a two-dimensional framework, naturally no out-of-plane tensor components exist. Basic planar isotropic tensors in the 2D framework are given by

$$\underline{\mathbf{I}} = \delta_{ij} \underline{\mathbf{e}}_i \otimes \underline{\mathbf{e}}_j = \begin{bmatrix} 1 & 0 \\ \text{sym} & 1 \end{bmatrix} \underline{\mathbf{e}}_i \otimes \underline{\mathbf{e}}_j, \quad (5.40)$$

$$\underline{\mathbf{I}}^S = \delta_{\xi\zeta} \underline{\mathbf{B}}_\xi \otimes \underline{\mathbf{B}}_\zeta = \begin{bmatrix} 1 & 0 & 0 \\ & 1 & 0 \\ \text{sym} & & 1 \end{bmatrix} \underline{\mathbf{B}}_\xi \otimes \underline{\mathbf{B}}_\zeta, \quad (5.41)$$

and

$$\underline{\mathbb{P}}_1 = \frac{1}{2} \underline{\mathbf{I}} \otimes \underline{\mathbf{I}}, \quad \underline{\mathbb{P}}_2 = \underline{\mathbb{I}}^S - \underline{\mathbb{P}}_1 \quad (5.42)$$

following Blinowski et al. (1996, Equation (2.3)), Aßmus et al. (2017, Equation (38)). Deviator operators are defined by

$$\text{dev}(\underline{\mathbf{A}}) = \underline{\mathbf{A}} - \frac{1}{2} (\underline{\mathbf{A}} \cdot \underline{\mathbf{I}}) \underline{\mathbf{I}}, \quad (5.43)$$

$$\begin{aligned} \text{dev}(\underline{\mathbb{A}}) &= \text{sym}(\underline{\mathbb{A}}) - \text{sym}(\text{sym}(\underline{\mathbb{A}}) [\underline{\mathbf{I}}] \otimes \underline{\mathbf{I}}) \\ &\quad + \frac{1}{8} \text{sym}(\underline{\mathbf{I}} \otimes \underline{\mathbf{I}}) (\underline{\mathbf{I}} \cdot \underline{\mathbb{A}} [\underline{\mathbf{I}}]) \end{aligned} \quad (5.44)$$

following Kanatani (1984, (7.13)) and Vianello (1997, section 3). The central fiber orientation tensor in the two-dimensional framework is identified as

$$\begin{aligned} \underline{\mathbb{N}}^{\text{piso}} &= \left(\frac{\underline{\mathbb{P}}_1}{\|\underline{\mathbb{P}}_1\|} \cdot \underline{\mathbf{n}}^{\otimes 4} \right) \underline{\mathbb{P}}_1 + \left(\frac{\underline{\mathbb{P}}_2}{\|\underline{\mathbb{P}}_2\|} \cdot \underline{\mathbf{n}}^{\otimes 4} \right) \underline{\mathbb{P}}_2 = \frac{1}{2} \underline{\mathbb{P}}_1 + \frac{1}{4} \underline{\mathbb{P}}_2 \quad (5.45) \\ &= \frac{1}{8} \begin{bmatrix} 3 & 1 & | & 0 \\ & 3 & | & 0 \\ \hline \text{compl.} & & | & \text{sym.} \end{bmatrix} \underline{\mathbf{B}}_\xi \otimes \underline{\mathbf{B}}_\zeta \\ &= \mathbb{N}^{\text{planar}}(\lambda_1 = 1/2, d_1 = 0, d_8 = 0) \end{aligned}$$

and is called planar isotropic fiber orientation tensor of fourth order. It should be noted that this is not the only fourth-order fiber orientation tensor which contracts to the planar isotropic second-order fiber orientation tensor. Deploying harmonic decomposition in the 2D-framework following Blinowski et al. (1996, Equation (2.25)) or Desmorat and

Desmorat (2015, Equation (18)) with

$$\begin{aligned} \underline{\mathbb{A}} = & \left(\frac{\underline{\mathbb{P}}_1}{\|\underline{\mathbb{P}}_1\|} \cdot \underline{\mathbb{A}} \right) \underline{\mathbb{P}}_1 + \left(\frac{\underline{\mathbb{P}}_2}{\|\underline{\mathbb{P}}_2\|} \cdot \underline{\mathbb{A}} \right) \underline{\mathbb{P}}_2 + \text{sym}(\text{dev}(\underline{\mathbb{A}}[\mathbf{I}]) \otimes \mathbf{I}) \\ & + \text{dev}(\underline{\mathbb{A}}) \end{aligned} \quad (5.46)$$

and knowledge on irreducible tensors, any fourth-order fiber orientation tensor is parameterized by

$$\underline{\mathbb{N}}(\lambda_1, p_1, p_2) = \underline{\mathbb{N}}^{\text{piso}} + \text{sym}(\underline{\mathbf{F}}(\lambda_1) \otimes \mathbf{I}) + \underline{\mathbb{F}}(p_1, p_2) \quad (5.47)$$

with

$$\underline{\mathbf{F}}(\lambda_1) = (\lambda_1 - 1/2) \begin{bmatrix} 1 & 0 \\ \text{sym} & -1 \end{bmatrix} \underline{\mathbf{v}}_i \otimes \underline{\mathbf{v}}_j, \quad (5.48)$$

$$\begin{aligned} \underline{\mathbb{F}}(p_1, p_2) = & p_1 \begin{array}{c|c} -1 & 1 \\ & -1 \\ \hline \text{compl.} & \text{sym.} \end{array} \underline{\mathbf{B}}_\xi^\mathbf{v} \otimes \underline{\mathbf{B}}_\zeta^\mathbf{v} \\ & + p_2 \begin{array}{c|c} 0 & 0 \\ 0 & -\sqrt{2} \\ \hline \text{compl.} & \text{sym.} \end{array} \underline{\mathbf{B}}_\xi^\mathbf{v} \otimes \underline{\mathbf{B}}_\zeta^\mathbf{v}. \end{aligned} \quad (5.49)$$

Coincidence with the parameterization in the 3D-framework is given by the prefactor in Equation (5.48) and the specific choice of the factors $p_1 = d_1 - 3/280$ and $p_2 = d_8$ leading to

$$\begin{aligned} \underline{\mathbb{N}}(\lambda_1, d_1, d_8) = & \\ & \begin{array}{c|c} \lambda_1 - d_1 - 4/35 & d_1 + 4/35 \\ (1 - \lambda_1) - d_1 - 4/35 & \\ \hline \text{compl.} & \end{array} \begin{array}{c} \sqrt{2}d_8 \\ -\sqrt{2}d_8 \\ \hline \text{sym.} \end{array} \underline{\mathbf{B}}_\xi^\mathbf{v} \otimes \underline{\mathbf{B}}_\zeta^\mathbf{v}. \end{aligned} \quad (5.50)$$

The shift by $3/280$ is required due to the different expansion points in 2D and 3D. As the point of expansion in Equation (5.47), i.e., $\underline{\mathbb{N}}^{\text{piso}}$, is planar itself, the deviators are compact and formatted into the 3D-framework read as

$$\text{dev}(\underline{\mathbb{N}}) = \begin{bmatrix} \lambda_1 - 1/2 & 0 & 0 \\ 0 & 1/2 - \lambda_1 & 0 \\ \text{sym} & 0 & 0 \end{bmatrix} \mathbf{v}_i \otimes \mathbf{v}_j, \quad (5.51)$$

$$\text{dev}(\underline{\mathbb{N}}) = \quad (5.52)$$

$$\left[\begin{array}{ccc|ccc} \frac{3}{280} - d_1 & -\left(\frac{3}{280} - d_1\right) & 0 & 0 & 0 & \sqrt{2}d_8 \\ \frac{3}{280} - d_1 & 0 & 0 & 0 & 0 & -\sqrt{2}d_8 \\ 0 & 0 & 0 & 0 & 0 & 0 \end{array} \right] \mathbf{B}_{\xi}^{\mathbf{v}} \otimes \mathbf{B}_{\zeta}^{\mathbf{v}}.$$

completely	symmetric
------------	-----------

The deviators specified in Equations (5.35), (5.36), (5.51) and (5.52) directly enter approximations of the FODF in terms of truncated Fourier series.

5.4.2 Truncated fiber orientation distribution function in a 2D-framework

In analogy to the three-dimensional case in Equation (5.13), FODF can be reconstructed in a two-dimensional framework. A FODF is given in terms of fiber orientation tensors by a tensorial Fourier series (Kanatani, 1984, page 158)

$$\underline{\psi}(\underline{\mathbf{n}}) = \frac{1}{2\pi} \sum_{k=0}^{\infty} 2^k \text{dev}(\underline{\mathbb{N}}_{(k)}) \cdot \underline{\mathbf{n}}^{\otimes k} \quad (5.53)$$

with a unit tensor of first order $\underline{\mathbf{n}}$ and fiber orientation tensors of k -th order in two dimensions $\underline{\mathbb{N}}_{(k)}$. An approximation of the FODF $\underline{\psi}(\underline{\mathbf{n}})$ by leading fiber orientation tensors up to fourth order is given by

$$\hat{\underline{\psi}}(\underline{\mathbf{n}}, \underline{\mathbb{N}}) = \frac{1}{2\pi} [1 + 4 \operatorname{dev}(\underline{\mathbb{N}}) \cdot \underline{\mathbf{n}}^{\otimes 2} + 16 \operatorname{dev}(\underline{\mathbb{N}}) \cdot \underline{\mathbf{n}}^{\otimes 4}], \quad (5.54)$$

and combined with $\underline{\mathbb{N}}(\lambda_1, p_1, p_2)$ and $\underline{\mathbf{n}}(\varphi) = \cos(\varphi) \underline{\mathbf{v}}_1 + \sin(\varphi) \underline{\mathbf{v}}_2$ leads to

$$\begin{aligned} \hat{\underline{\psi}}(\varphi, \lambda_1, p_1, p_2) = \frac{1}{2\pi} & \left[1 + (4\lambda_1 - 2) \cos(2\varphi) \right. \\ & \left. - 16p_1 \cos(4\varphi) + 16p_2 \sin(4\varphi) \right]. \end{aligned} \quad (5.55)$$

Introducing the coordinate transformation

$$p_1 = \hat{r} \sin(\hat{\beta}), \quad p_2 = \hat{r} \cos(\hat{\beta}) \quad (5.56)$$

yields the following formulation

$$\begin{aligned} \hat{\underline{\psi}}(\varphi, \lambda_1, \hat{r}, \hat{\beta}) = \frac{1}{2\pi} & \left[1 + 4 \left(\lambda_1 - \frac{1}{2} \right) \cos(2\varphi) \right. \\ & \left. - 16\hat{r} \sin(\hat{\beta} - 4\varphi) \right]. \end{aligned} \quad (5.57)$$

The parameterization of $\hat{\underline{\psi}}$ in Equation (5.57) separates second and fourth-order contributions into one trigonometric summand each. The cosinus-contribution of the second-order fiber orientation tensor is always aligned with the coordinate axes of the orientation coordinate system and its amplitude scales with λ_1 , being zero for the planar isotropic case, i.e., $\lambda_1 = 1/2$ and the frequency is two in the interval $\varphi \in [0, 2\pi]$. The fourth-order summand is a sinusoidal function of double the frequency of the second-order term, with phase shift $\hat{\beta}$ and an amplitude which scales with \hat{r} . The frequency implies that this fourth-order term has four maxima and four minima within the

parameter range of $\varphi \in [0, 2\pi)$. In consequence, in the planar isotropic case, Equation (5.57) degenerates to

$$\hat{\psi}\left(\varphi, \lambda_1 = \frac{1}{2}, \hat{r}, \hat{\beta}\right) = \frac{1}{2\pi} \left[1 - 16\hat{r} \sin(\hat{\beta} - 4\varphi) \right] \quad (5.58)$$

which directly indicates, that the parameter $\hat{\beta}$ implies a rotation of $\hat{\psi}$ by an angle of $\hat{\beta}/4$ around the axis v_3 of the 3D-framework pointing out of the 2D-plane. If $\lambda_1 \neq 1/2$, the interference of the second- and fourth-order summands, which have different frequencies, leads to the variety of $\hat{\psi}$. The structure of Equation (5.57) shows, that $\hat{\psi}$ may be represented by circular harmonics. Further details on harmonic representations of planar tensors of fourth order can be found, e.g., in Vannucci (2018, chapter 4) and Forte and Vianello (2014).

5.4.3 Maximum entropy reconstruction

Identification of a representative FODF based on a given leading fiber orientation tensor is of importance for several applications, e.g., numerical calculation of orientation averages of direction dependent mechanical properties (Hessman et al., 2021; Schemmann et al., 2018b; Brylka, 2017). Truncated Fourier series are used in the literature to identify an FODF based on fiber orientation tensors (Schöttl et al., 2020; Jack and Smith, 2004; Eik et al., 2016) although the identified functions do not meet the non-negativity requirement of a FODF. Naive averaging with partly negative FODF leads to non-physical results. Müller and Böhlke (2016) give a solution to the reconstruction problem and identify FODF based on leading fiber orientation tensors by maximizing the information-theoretic entropy fulfilling normalization and non-negativity constraints. For limited available information, the entropy principle yields the most likely FODF fulfilling specified constraints. In this context “most likely” corresponds to “maximizing entropy”. The procedure of Müller and

Böhlke (2016) is briefly repeated for the special case of fourth-order fiber orientation tensors and tailored to planar fiber orientation tensors. The maximum entropy approximation $\hat{\psi}^{\text{me}}(\mathbf{n})$ maximizes the information-theoretic entropy $E(\hat{\psi})$

$$E(\hat{\psi}) = - \int_{S^{n-1}} \hat{\psi}(\mathbf{n}) \ln \hat{\psi}(\mathbf{n}) \, dS \quad (5.59)$$

and fulfills the constraints

$$G = \mathbb{G}_{<0>} = \int_{S^{n-1}} \hat{\psi}(\mathbf{n}) \, dS - 1, \quad (5.60)$$

$$\mathbf{G} = \mathbb{G}_{<2>} = \int_{S^{n-1}} \hat{\psi}(\mathbf{n}) \operatorname{dev}(\mathbf{n}^{\otimes 2}) \, dS - \operatorname{dev}(\mathbf{N}), \quad (5.61)$$

$$\mathbb{G} = \mathbb{G}_{<4>} = \int_{S^{n-1}} \hat{\psi}(\mathbf{n}) \operatorname{dev}(\mathbf{n}^{\otimes 4}) \, dS - \operatorname{dev}(\mathbb{N}) \quad (5.62)$$

where the constraint G ensures the normalization and \mathbf{G} and \mathbb{G} ensure that the solution $\hat{\psi}^{\text{me}}(\mathbf{n})$ meets the given orientation tensors. The domain of the integral depends on the dimensionality of the given orientation tensor and is either the surface of the unit sphere S^2 for planar 3D tensors or the circumference of the unit circle S^1 for 2D tensors. The problem

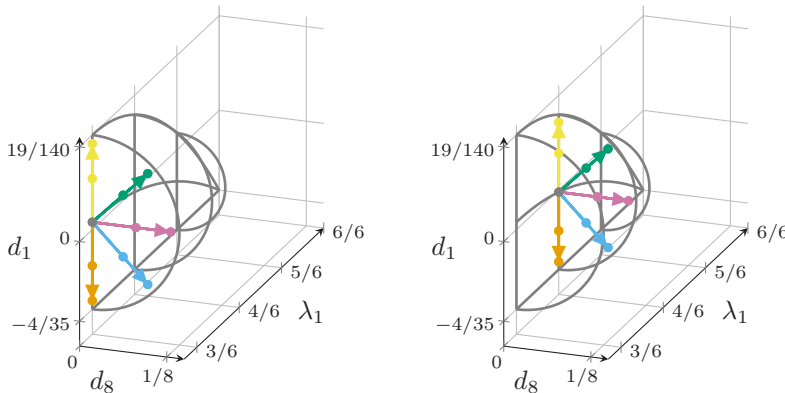
$$\max_{\hat{\psi}} E(\hat{\psi}) \quad \text{with} \quad \mathbb{G}_{<\alpha>} = 0_{<\alpha>} \quad \text{for } \alpha \in [0, 2, 4] \quad (5.63)$$

corresponds to the Lagrange functional

$$\mathcal{L}(\hat{\psi}) = E(\hat{\psi}) - \sum_{\alpha \in [0, 2, 4]} \mathbb{L}_{<\alpha>} \cdot \mathbb{G}_{<\alpha>} \quad (5.64)$$

with Lagrange multipliers $L = \mathbb{L}_{<0>}$, $\mathbf{L} = \mathbb{L}_{<2>}$ and $\mathbb{L} = \mathbb{L}_{<4>}$. The solution is given by the root of the first variation of \mathcal{L} , i.e., $\delta \mathcal{L}(\hat{\psi}) = 0$ and is formulated in the Lagrange multipliers by

$$\hat{\psi}^{\text{me}}(\mathbf{n}, L, \mathbf{L}, \mathbb{L}) = \exp(-1 - L - \mathbf{L} \cdot \operatorname{dev}(\mathbf{n}^{\otimes 2}) - \mathbb{L} \cdot \operatorname{dev}(\mathbf{n}^{\otimes 4})) \quad (5.65)$$



(a) Paths and points in the plane $\lambda_1 = 3/6$ (b) Points in the plane $\lambda_1 = 4/6$ used in figure 5.9

Figure 5.4: Definition of representative points in the parameter space $\hat{\mathcal{N}}^{\text{planar}}$ of planar fourth-order fiber orientation tensors. The outer points in radial directions do not lie on the boundary of the admissible region. Parameters of each point are listed in Table B.1.

which fulfills the non-negativity condition identically. The Lagrange multipliers are obtained by solving the system of equations stated by the constraints in Equations (5.60) to (5.62) with $\hat{\psi}(\mathbf{n})$ being replaced by $\hat{\psi}^{\text{me}}(\mathbf{n}, L, \mathbf{L}, \mathbf{L})$ from Equation (5.65). Due to the projection of the Lagrange multipliers onto deviators of the moment tensors in Equation (5.65), the Lagrange multipliers are without loss of generality irreducible, i.e., completely symmetric and traceless (Rychlewski, 2000; Spencer, 1970). Table 5.1 lists the number of independent components of irreducible tensors which depend on the tensor order and the dimensionality of the vector space. The number of independent components of

Tensor order	2D	3D
2	2	5
4	2	9

Table 5.1: Number of independent component of irreducible tensors depending on order and dimensionality of the vector space

the Lagrange multipliers L , \mathbf{L} and \mathbb{L} sum up to $1 + 5 + 9 = 15$ and $1 + 2 + 2 = 5$ in three and two dimensions respectively and correspond to the fourteen independent components of \mathbb{N} and four independent components of $\underline{\mathbb{N}}$ plus one normalization constraint each. In tensor notation, Equations (5.60) to (5.62) read as $1+9+81 = 91$ scalar equations, whereas in symmetric Kelvin-Mandel notation the identical equations yield $1 + 6 + 36$ scalar equations. These naive views on the set of equations illustrate that a minimal and redundancy-free parameterization deploying index symmetry of the Lagrange multipliers is required. Such a parameterization is necessary to reduce the dimensionality of the system of equations to at most 15 or 5 depending on the dimensionality of used tensor framework. Three out of five independent components of \mathbf{N} in 3D and one out of two independent components of $\underline{\mathbf{N}}$ in 2D define the orientation coordinate system. In the orientation coordinate system, the second-order orientation tensor has diagonal structure. Off-diagonal components of the second order Lagrange multiplier ensure that the orientation coordinate systems of the reconstructed FODF and the original fiber orientation tensors coincide. Based on the orientation coordinate system, a generic representation of the Lagrange multipliers of order two and four in three dimensions is given by

$$\mathbf{L}(b_1, \dots, b_5) = \begin{bmatrix} b_1 & b_5 & b_4 \\ & b_2 & b_3 \\ \text{sym} & & -(b_1 + b_2) \end{bmatrix} \mathbf{v}_i \otimes \mathbf{v}_j, \quad (5.66)$$

$$\begin{aligned} \mathbb{L}(c_1, \dots, c_9) = & \\ \left[\begin{array}{ccc|ccc} -(c_1 + c_2) & c_1 & c_2 & -\sqrt{2} (c_4 + c_5) & \sqrt{2} c_6 & \sqrt{2} c_8 \\ -(c_1 + c_3) & c_3 & c_2 & \sqrt{2} c_4 & -\sqrt{2} (c_6 + c_7) & \sqrt{2} c_9 \\ -(c_2 + c_3) & & \sqrt{2} c_5 & \sqrt{2} c_7 & & -\sqrt{2} (c_8 + c_9) \end{array} \right] & \\ \text{completely} & \text{symmetric} \\ \mathbf{B}_\xi^V \otimes \mathbf{B}_\zeta^V. & \end{aligned} \quad (5.67)$$

Starting from the triclinic case in Equations (5.66) and (5.67), material symmetries may be deployed to further reduce the number of indepen-

dent components of the Lagrange multipliers, as the fiber orientation tensors and the reconstructed FODF share their symmetry group, i.e., $\mathcal{S}^{\hat{\psi}} = \mathcal{S}^{\mathbb{N}}$ with

$$\hat{\psi}(\mathbf{Q} \star \mathbf{n}) = \hat{\psi}(\mathbf{n}) \quad \forall \mathbf{Q} \in \mathcal{S}^{\hat{\psi}}, \quad (5.68)$$

$$\mathbf{Q} \star \mathbb{N} = \mathbb{N} \quad \forall \mathbf{Q} \in \mathcal{S}^{\mathbb{N}} \quad (5.69)$$

which follows directly from the definition of \mathbb{N} in Equation (5.7). Similar to the FODF reconstruction by truncated Fourier series, the ansatz $\hat{\psi}^{\text{me}}$ in Equation (5.65) contains deviators from a central state, which in 3D is the isotropic state. In order to reconstruct planar FODF based on planar fiber orientation tensors, it is beneficial to deploy a two-dimensional framework with deviators deviating from the planar isotropic state. In the orientation coordinate system the Lagrange multipliers of order two and four read as

$$\underline{\mathbf{L}}(f_1, f_2) = \begin{bmatrix} f_1 & f_2 \\ \text{sym} & -f_1 \end{bmatrix} \underline{\mathbf{v}}_i \otimes \underline{\mathbf{v}}_j, \quad (5.70)$$

$$\underline{\mathbb{L}}(g_1, g_2) = \begin{bmatrix} -g_1 & g_1 & \sqrt{2} g_2 \\ -g_1 & -g_1 & -\sqrt{2} g_2 \\ \text{compl.} & & \text{sym.} \end{bmatrix} \underline{\mathbf{B}}_{\xi}^{\mathbf{v}} \otimes \underline{\mathbf{B}}_{\zeta}^{\mathbf{v}}. \quad (5.71)$$

In consequence, combination of Equations (5.70) and (5.71) leads to

$$\begin{aligned} \hat{\psi}^{\text{me}}(\varphi, L, f_1, f_2, g_1, g_2) = \exp \Big(& -1 - L - f_1 \cos(2\varphi) \\ & - f_2 \sin(2\varphi) + g_1 \cos(4\varphi) - g_2 \sin(4\varphi) \Big). \end{aligned} \quad (5.72)$$

For a given $\underline{\mathbf{N}}(\lambda_1, d_1, d_8)$ following Equation (5.50) and a specific selection of independent tensor components, the resulting five scalar

equations are

$$\int_{S^1} \hat{\psi}(\mathbf{n}, L, f_1, f_2, g_1, g_2) dS - 1 = 0, \quad (5.73)$$

$$\int_{S^1} \hat{\psi}(\mathbf{n}, L, f_1, f_2, g_1, g_2) \left(\frac{1}{2} \cos(2\varphi) \right) dS - \left(\lambda_1 - \frac{1}{2} \right) = 0, \quad (5.74)$$

$$\int_{S^1} \hat{\psi}(\mathbf{n}, L, f_1, f_2, g_1, g_2) \left(\frac{1}{2} \sin(2\varphi) \right) dS - 0 = 0, \quad (5.75)$$

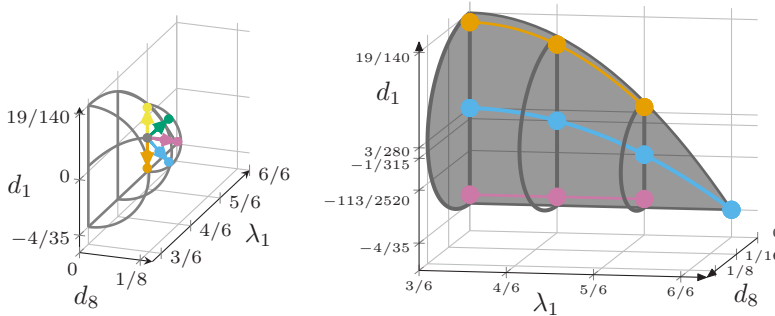
$$\int_{S^1} \hat{\psi}(\mathbf{n}, L, f_1, f_2, g_1, g_2) \left(-\frac{1}{8} \cos(4\varphi) \right) dS - \left(d_1 - \frac{3}{280} \right) = 0, \quad (5.76)$$

$$\int_{S^1} \hat{\psi}(\mathbf{n}, L, f_1, f_2, g_1, g_2) \left(\frac{\sqrt{2}}{8} \sin(4\varphi) \right) dS - \sqrt{2} d_8 = 0. \quad (5.77)$$

The equations are solved numerically for a given tripled (λ_1, d_1, d_8) . Numerical integration on the unit circle is done with nschloe (2021) based on Krylov and Stroud (2006).

5.4.4 Visualization of reconstructed planar fiber orientation distribution functions

Fiber orientation tensors represent averaged properties of an underlying FODF. In consequence, a complete reconstruction of the underlying FODF is not possible. It is of interest to visualize possible shapes of reconstructed FODFs based on admissible mean values. The admissible mean values are given by the set of distinct and admissible fiber orientation tensors of fourth order $\mathcal{N}^{\text{planar}}$ which can be combined with the developed reconstruction methods $\hat{\psi}$ and $\hat{\psi}^{\text{me}}$. The parameter space $\mathcal{N}^{\text{planar}}$ is discretized and for selected points in $\mathcal{N}^{\text{planar}}$, i.e., for selected $\underline{\mathbb{N}}$, reconstructed FODFs are visualized. The discretization is based on several slices through $\mathcal{N}^{\text{planar}}$ which are given in Figures 5.4 and 5.5. The arrangement of the visualizations of the reconstructed FODFs in figures 5.7, 5.8, 5.9 and 5.10 mimic the position of the points on the slices and reuse the color coding of the overview plots. In consequence, the



(a) Points in the plane
 $\lambda_1 = 5/6$ used in figure 5.10

(b) Ten points in the plane of planar orthotropic fiber orientation tensors of fourth order being a slice of N^{planar} . The points are used in figure 5.7

Figure 5.5: Definition of additional representative points, see also Figure 5.4

influence of the position inside N^{planar} on the shape of the reconstructed FODF is obtained. The developed visualizations directly show the variety of reconstructed FODFs and as a side effect act as an intuitive view on fiber orientation tensors of fourth order. As the truncated FODF reconstruction does not fulfill the non-negativity constraint, negative values of $\hat{\psi}$ are highlighted in red, as defined in the shared legend in Figure 5.6. Parameters of the utilized orientation tensors are listed in Table B.1. The scaling of all polar plots of FODFs in Figures 5.7, 5.8, 5.9 and 5.10 is homogeneous with the lower radial limit being zero and the upper radial limit 0.9.

A slice containing orthotropic (Bauer and Böhlke, 2022c) fiber orientation tensors is shown in Figure 5.5b and the corresponding FODFs are given in Figure 5.7. The transition from the planar isotropic state in Figure



Figure 5.6: Shared legend for figures 5.7, 5.9, 5.9 and 5.10. $\hat{\psi}(\varphi)$ and $\hat{\psi}^{\text{me}}(\varphi)$ are defined in Equations (5.54) and (5.72) respectively.

5.7(4) towards the unidirectional state in Figure 5.7(10) demonstrates the degeneration of the variety of fourth-order fiber orientation tensors towards the unidirectional state, which is defined completely by $\lambda_1 = 1$. Figures 5.7(1) to 5.7(3) correspond to orientation states represented by orange points in Figure 5.5b. These points keep a distance in the d_1 -direction from the boundary of the admissible body, as orientation states at the boundary itself, correspond to Dirac distributions into two directions each (see Bauer and Böhlke (2022c, Figure 9)). In analogy, Figures 5.7(7) to 5.7(9) correspond to points highlighted in magenta in Figure 5.5b and are also located off the boundary of the admissible region. Figure 9 in Bauer and Böhlke (2022c) contains FODF approximations based on a limited number of discrete fibers aligned along the axes of the orientation coordinate system which correspond to points on the

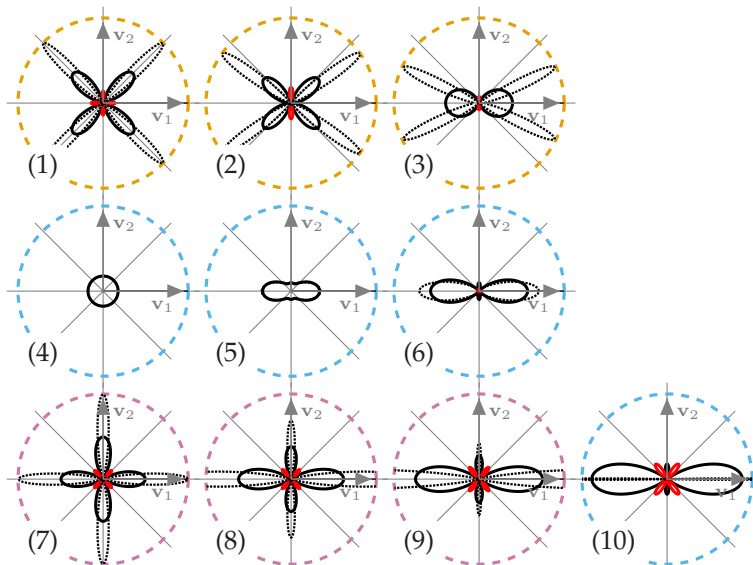


Figure 5.7: Reconstructed FODF at specific points which are defined in Figure 5.5b. A legend is given in Figure 5.6

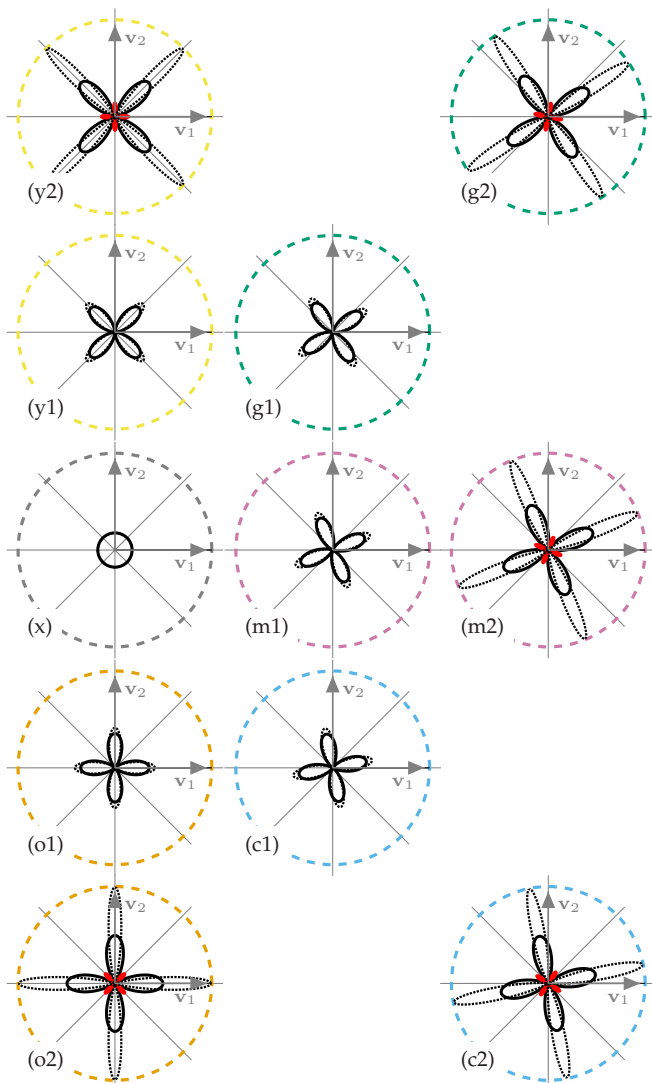


Figure 5.8: Reconstructed FODF at specific points along paths defined in Figure 5.4a. The radial spacing of the plots along the green and blue paths are not to true scale to allow for larger plots. A legend is given in Figure 5.6

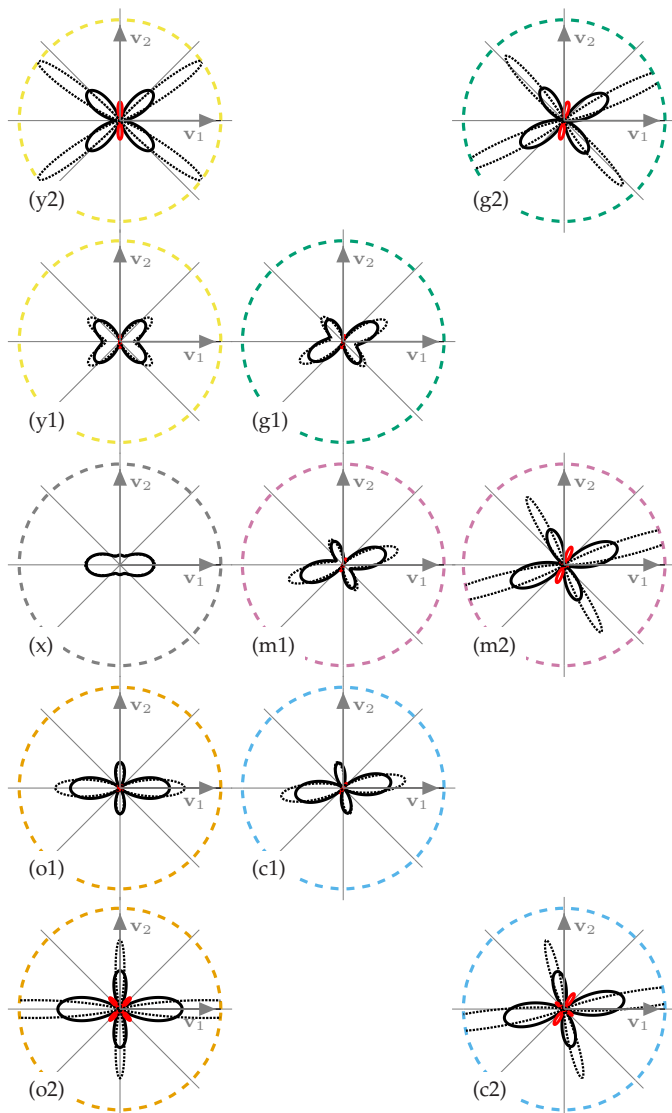


Figure 5.9: Reconstructed FODF along several paths. The radial spacing of the plots along the green and blue paths are not to true scale to allow for larger plots. A legend is given in Figure 5.6 and parameters of the points in $\mathcal{N}^{\text{planar}}$, i.e., $\mathbb{N}^{\text{planar}}$, are listed in Table B.1. Paths are defined in Figure 5.4b.

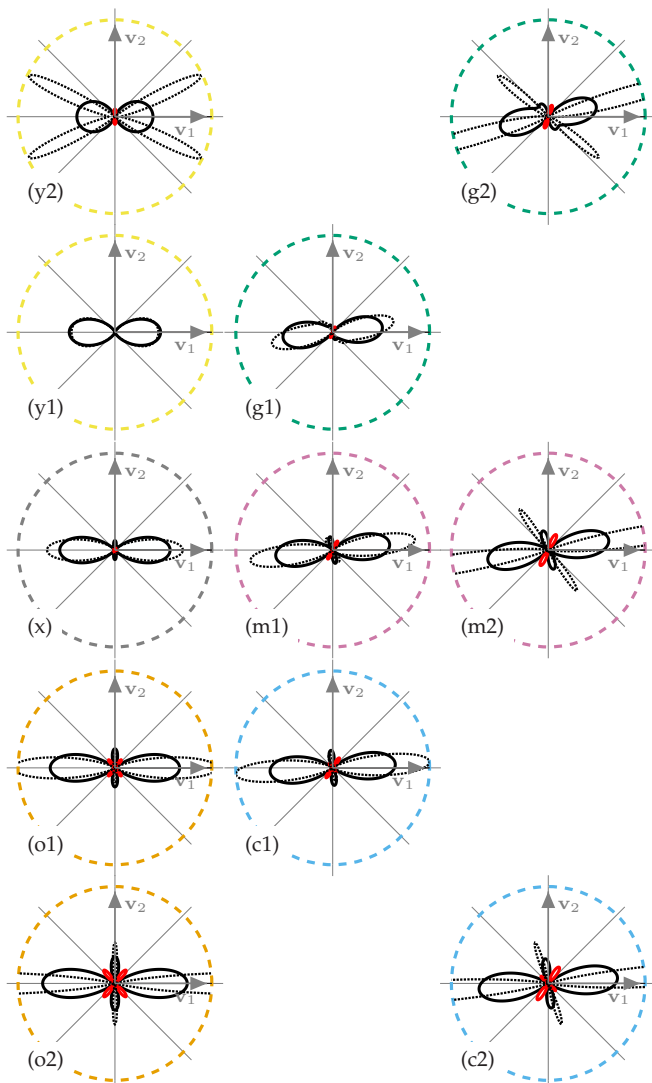


Figure 5.10: Reconstructed FODF along several paths. The radial spacing of the plots along the green and blue paths are not to true scale to allow for larger plots. A legend is given in Figure 5.6 and parameters of the points in $\mathcal{N}^{\text{planar}}$, i.e., $\mathbb{N}^{\text{planar}}$, are listed in Table B.1. Paths are defined in Figure 5.5a.

boundary of the admissible region specified by the line $d_1 = -4/35$ and $d_8 = 0$ in Figure 5.5b. Planar fiber orientation tensors at the boundary of the admissible region directly correspond to orientation states of a limited number of Dirac distributions. This observation explains why experimentally identified fiber orientation tensors obtained from comparably large fiber arrangements may not fill the complete admissible region but fill only a (equally shaped) subregion within the admissible region. In a comparably large fiber arrangement, Dirac distributions are unlikely. The entropy reconstruction scheme contains a basis function involving a direction depended exponential function. Although the slope of an exponential function is rather steep, extreme values of the Lagrange multipliers are necessary to approximate Dirac distributions. Therefore, the entropy reconstruction scheme, which includes numerical integration and a numerical solver, is not completely stable when operating on orientation states at the boundary of the admissible region. As the unidirectional case in Figure 5.7(10) lies on the radial boundary of the admissible orientation states, the corresponding entropy-based reconstruction FODF degenerates to a single Dirac distribution. The approximation $\hat{\psi}^{\text{me}}$ in this figure is localized, i.e., vanishes for all angles except those pointing along axes of the orientation coordinate system.

The slices defined in Figures 5.4, 5.5a and the corresponding FODF approximations in figures 5.8, 5.9 and 5.10 visualize the variety of reconstructed FODF among fourth-order fiber orientation tensors which contract to identical second-order fiber orientation tensors. Any FODF in Figure 5.8 leads to the planar isotropic second-order fiber orientation tensor $N(\lambda_1 = 1/2)$. In analogy, any FODF in Figure 5.9 has an identical second-order fiber orientation tensor being $N(\lambda_1 = 2/3)$. From this viewpoint, the figures in any of the figures 5.8, 5.9 or 5.10 visualize the variety of planar fourth-order fiber orientation tensors for a fixed second-order orientation tensor. Figure 5.8 shows the redundancy inside

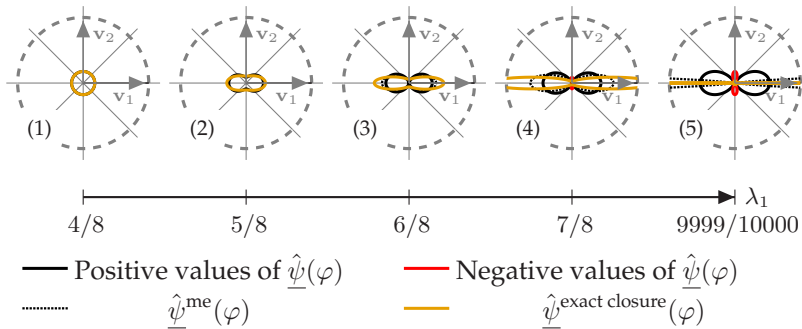


Figure 5.11: Influence of λ_1 on reconstructed FODF for selected reconstruction methods based on second-order fiber orientation tensors. For $\lambda_1 = 1/2$ all approximations coincide.

$\mathcal{N}^{\text{planar}}$ identified in Equation (5.27) as FODFs with identical radial distance to the centered Figure 5.8(x) only differ by a rotation. In contrast, interference of the non-vanishing second-order contribution with the fourth-order contribution in figures 5.9 and 5.10 leads to a variety of FODF approximations. The developed views on $\mathcal{N}^{\text{planar}}$ based on slices and selected points can be reused to analyse and visualize any quantity which depends on planar fourth-order fiber orientation tensors.

5.4.5 Reconstruction solely based on second-order fiber orientation tensors

If fourth-order fiber orientation information is not available, the parameter space of reconstructed FODFs degenerates to one parameter, e.g., $1/2 \leq \lambda_1 \leq 1$, which defines the second-order fiber orientation tensor. Missing fourth-order fiber orientation information implies vanishing fourth-order deviators and therefore leads to FODF reconstructions with $\hat{\psi}(\varphi, \lambda_1, p_1 = 0, p_2 = 0)$ in Equation (5.53) and $\hat{\psi}^{\text{me}}(\varphi, L, f_1, f_2, g_1 = 0, g_2 = 0)$ in Equation (5.72). Figure 5.11 shows the influence of λ_1 on reconstructed FODFs for the methods used in the previous section and in addition for the FODF approximation obtained by the exact

closure approximation (Montgomery-Smith et al., 2011a). The exact closure approximation is frequently used, e.g., in Goldberg et al. (2017); Schneider (2017); Hessman et al. (2021); Görthofer et al. (2020) and postulates a one-to-one correspondence between a given second-order fiber orientation tensor and an a priori unknown FODF $\hat{\psi}^{\text{exact closure}}$ of special shape. In the general three-dimensional case this FODF can be identified by solving elliptic integrals (Montgomery-Smith et al., 2011a). For the planar case, Görthofer et al. (2020) gives explicit formulas which, combined with Equation (5.14), lead to

$$\hat{\psi}^{\text{exact closure}}(\varphi, \lambda_1) = \frac{1}{2\pi} \frac{(1 - \lambda_1)\lambda_1}{\lambda_1^2 + (1 - 2\lambda_1)\cos(\varphi)^2}. \quad (5.78)$$

Visualization of Equation (5.78) for five values of λ_1 is given in Figure 5.11. If missing fourth-order orientation information is compensated by deploying closure approximations, the variety of resulting FODFs shown in Figures 5.7, 5.9 and 5.10 is not reachable. Instead, the parameter space of structurally differing resulting FODFs degenerates to the parameter space of the second-order orientation tensor within the orientation coordinate system. If closure approximations are used in the context of planar fiber orientations, the complete orientation information is contained within two scalar parameters. One scalar parameters specifies the orientation coordinate system and the other parameter specifies the structure of the second-order fiber orientation tensor. In contrast, if the discrete orientation of each single fiber is known, e.g., based on direct fiber simulation (Meyer et al., 2020b), the variety of resulting FODF is generic. However, averaged information of such a discrete set of fibers expressed by fiber orientation tensors is still limited.

5.5 Summary and conclusion

Planar fourth-order fiber orientation tensors describe the fiber orientation in many sheet-like fiber reinforced composites. The variety of these tensors is known (Bauer and Böhlke, 2022c). The variety of reconstructed fiber orientation distribution functions (FODFs) based on planar fourth-order fiber orientation tensors is studied in this work leading to the following insights:

1. Based on the set of admissible planar fiber orientation tensors in Bauer and Böhlke (2022c), a minimal set of admissible and distinct planar fiber orientation tensors of fourth order $\hat{\mathcal{N}}^{\text{planar}}$ is derived and given in Equation (5.28). This set is the basis for studies on the influence of planar fourth-order fiber orientation tensors on any physical quantity or material function which is formulated in this directional measure.
2. The variety of reconstructed FODF is visualized by an arrangement of polar plots which mimics the shape of the admissible and distinct parameter space. This arrangement or view is generic and may be applied to study the dependence of other quantities on planar fourth-order fiber orientation tensors.
3. Reconstructed FODF based on truncated series expansion within a three-dimensional framework are identified to be not planar as the central state in three dimensions is isotropic.
4. A two-dimensional formulation of planar fiber orientation tensors is introduced and linked to parameterizations of planar fiber orientation tensors in three dimensions. The central, i.e., “isotropic”, state in two dimensions is planar isotropic.
5. Within the two dimensional framework it is shown that interference of second and fourth-order contributions leads to the variety of reconstructed FODF based on truncated Fourier series.
6. Visualizations of truncated FODF reconstructions in Figures 5.7, 5.9

and 5.10 highlight their limitations and motivate more advanced reconstruction methods. The maximum entropy reconstruction of Müller and Böhlke (2016) is explicitly formulated for the general three-dimensional case and recast for the planar case in a two-dimensional framework which leads to a low-dimensional optimization problem. Resulting FODF approximations are normalized and non negative.

7. For given reconstruction methods, the structural variety of reconstructed FODF based on planar fourth-order fiber orientation tensors is limited. Throughout this work, separation of rigid-body rotations, and thus orientation in space, from structural properties of represented FODFs is accomplished by representations in the orientation coordinate system.
8. Visualization of reconstructed FODFs solely based on second-order fiber orientation tensors, including a reconstruction method based on the exact closure (Montgomery-Smith et al., 2011a; Görthofer et al., 2020), close this paper and motivate higher order directional measures.

Chapter 6

On the Dependence of Orientation Averaging Mean Field Homogenization on Planar Fourth-Order Fiber Orientation Tensors¹

6.1 Introduction

The effective mechanical properties of fiber reinforced composites highly depend on the microstructure. The microstructure descriptors fiber volume content and fiber orientation tensors are commonly used in homogenization techniques for two-phase composites (Buck et al., 2015; Brylka, 2017; Hessman et al., 2021; Schemmann et al., 2018b; Kehrer et al., 2020). Experimental or numerical identification and subsequent use of second-order fiber orientation tensors is well established in process chains (Görthofer et al., 2019) and commercial software. The use of higher-order fiber orientation tensors or the direct use of a fiber

¹ This chapter reproduces (Bauer and Böhlke, 2022b), i.e., Bauer, J. K., Böhlke, T., 2022. On the dependence of orientation-averaging mean field homogenization on planar fourth-order fiber orientation tensors. Mechanics of Materials 170, 104307, 10.1016/j.mechmat.2022.104307. Reproduced with permission. ©2022 The Authors. Published by Elsevier Ltd under CC BY 4.0

orientation distribution function, is progressing (Meyer et al., 2020b). Nevertheless, closure approximations, which identify higher-order orientation information based on assumptions instead of information, are still used in material modeling. For the special case of linear elasticity, mean field homogenization is popular due to its simplicity (Kehrer et al., 2020). A unified formulation of several mean field approximations is given in Hessman et al. (2021). The influence of model parameters, the fiber volume content or the aspect ratio of either the fiber's shape or the two-point correlation functions, on the predicted effective mechanical properties obtained by mean field homogenization, is studied extensively, e.g., in Kehrer et al. (2020); Buck et al. (2015); Brylka (2017); Hessman et al. (2021); Müller (2016); Trauth et al. (2021); Kehrer (2019). However, the influence of fiber orientation distributions on the effective properties has not been studied systematically. In this work, the influence of fiber orientation distributions on the effective properties of long-fiber-reinforced composites with large aspect ratios, such as sheet molding compound (SMC), is studied. Fiber distributions of SMC are identified to be in most cases approximately planar and therefore correspond to fiber orientation tensors which are planar as well. A set of all admissible and structurally differing planar fiber orientation tensors of fourth order is identified by Bauer and Böhlke (2022c;a) within a three-dimensional framework. This set is the basis for a complete study on the influence of the fiber orientation distribution on the effective mechanical properties for selected orientation-averaging mean field homogenizations within this work. This complete study is new and of high relevance as it visualizes all possible effective stiffness tensors which can be obtained for planar distributions and selected homogenizations. The methodology may be applied to any other homogenization or any effective quantity, which is a function of a planar fourth-order fiber orientation tensor. As a side effect, the limitations of the use of second-order orientation tensors only are visualized. The developed visualization method may be adopted to higher-dimensional

parameter spaces of fourth-order fiber orientation tensors with lower symmetry.

This paper starts with definitions of fiber orientation tensors before orientation states of SMC specimen obtained by computer tomography (Pinter et al., 2018; Schöttl et al., 2020) are identified to be approximately planar. In consequence, the microstructure of SMC can be parameterized in the three-dimensional space of admissible planar fourth-order fiber orientation tensors. A parameterization of this space is obtained in Bauer and Böhlke (2022c) and combined with a minimal parameter set of structurally distinct planar fourth-order fiber orientation tensors given in Bauer and Böhlke (2022a). As the Advani-Tucker orientation average (Advani and Tucker III, 1987) is an essential building block of various mean field schemes, but the implication of its linearity in both the orientation tensor and the averaged quantity is seldom addressed explicitly, a reformulation based on the harmonic decomposition (linear invariant decomposition) is given. A new numerical variant of the Advani-Tucker orientation average based on reconstructed FODF following the maximum entropy method, developed in Müller and Böhlke (2016); Bauer and Böhlke (2022a), is given and shown to have a good convergence for non-localized orientation states. In a next step, four mean field homogenization approximations (Kehrer et al., 2020; Walpole, 1966a;b; Benveniste, 1987) are reviewed, partially reformulated and investigated. Implementations are made available at Bauer (2022). The first approximations are orientation-averaging Mori-Tanaka following Benveniste (1987) and a two step Hashin-Shtrikman homogenization scheme (Kehrer et al., 2020) both in formulations based on the orientation average following Advani and Tucker III (1987). The remaining two approximations are direct Advani-Tucker orientation averages of either a unidirectional stiffness or compliance obtained by the Mori-Tanaka approximation (Mori and Tanaka, 1973). Views on the effective stiffnesses obtained by the selected schemes are given

based on Young's modulus and generalized bulk modulus following Böhlke and Brüggemann (2001). Observations on structural differences of the effective stiffnesses obtained by schemes averaging stiffness- or compliance-like quantities close this work.

6.2 Sheet molding compound and planar microstructures

Sheet molding compound (SMC) is a material class with a thermoset polymer matrix enforced by long glass fibers and is of special interest in this work. Due to the manufacturing process (Böhlke et al., 2019), components made from SMC are shell-shaped, i.e., at each point of the component, the thickness is significantly smaller than the remaining two dimensions of the component. As the fiber length exceeds the component thickness, alignment of fibers perpendicular to the local plane of the shell is limited to local fiber bending. In consequence, local directional measures which describe the orientation of fibers in SMC components are approximately planar. In order to elaborate the consequences of this planarity, directional measures are introduced, closely following a more comprehensive discussion in Bauer and Böhlke (2022c, sections 2.1 and 2.2).

A fiber orientation density function (FODF) is an established directional measure for the orientation of axisymmetric fibers contained inside a reference volume. Such a reference volume can be interpreted as a section of a structural component of specified size. The size of the reference volume influences the directional measurement and represents a scaling parameter in measurement algorithms, e.g., in Görthofer et al. (2019, Figure 4) or Schöttl et al. (2020). The FODF

$$\psi : \mathcal{S}^2 \rightarrow \mathbb{R}, \text{ with } \mathcal{S}^2 = \{\mathbf{n} \in \mathbb{R}^3 \mid \|\mathbf{n}\| = 1\} \quad (6.1)$$

at a given position inside a component maps any direction \mathbf{n} , being part of the two-dimensional surface of a unit sphere in three dimensions S^2 , onto a scalar value $\psi(\mathbf{n})$. The function $\psi(\mathbf{n})$ is non-negative, normalized and symmetric (see Advani and Tucker III (1987); Bauer and Böhlke (2022c); Görthofer et al. (2020); Bauer and Böhlke (2022a)). The FODF contains the complete directional information, which can be contained in a one-point correlation function, but is usually unknown. In contrast, orientation tensors only contain a limited amount of averaged information but can be obtained by computer tomography scans or flow simulations (Görthofer et al., 2019) and fit into the tensor framework of continuum mechanics. In this work, fiber orientation tensors of Kanatani first kind (Kanatani, 1984) of second \mathbf{N} and fourth order \mathbb{N} are used and defined by

$$\mathbf{N} = \int_{S^2} \psi(\mathbf{n}) \mathbf{n} \otimes \mathbf{n} d\mathbf{n}, \quad (6.2)$$

$$\mathbb{N} = \int_{S^2} \psi(\mathbf{n}) \mathbf{n} \otimes \mathbf{n} \otimes \mathbf{n} \otimes \mathbf{n} d\mathbf{n}. \quad (6.3)$$

The fiber orientation tensors represent averaged directional measures and are coefficients of a three-dimensional tensorial Fourier series representation of the FODF

$$\psi(\mathbf{n}) = \frac{1}{4\pi} \sum_{k=0}^{\infty} \frac{2k+1}{2^k} \binom{2k}{k} \text{dev}(\mathbb{N}_{(k)}) \cdot \mathbf{n}^{\otimes k} \quad (6.4)$$

called spherical harmonic expansion (Kanatani, 1984, page 154), with the operator $\text{dev}(\cdot)$ extracting the deviatoric part, see Spencer (1970). Higher order fiber orientation tensors contain all tensors of lower order which implies $\mathbf{N} = \mathbb{N}[\mathbf{I}]$ for the tensors orders two and four, with the identity on second-order tensors $\mathbf{I} = \delta_{ij} \mathbf{e}_i \otimes \mathbf{e}_j$.

In order to define planarity of the directional measures, the basic properties of the second-order orientation tensor \mathbf{N} are briefly summarized

following Bauer and Böhlke (2022c). As \mathbf{N} is symmetric and positive semi-definite, it can be diagonalized, i.e., pairs of eigenvalues λ_i with $\lambda_i \geq 0$ and orthonormal eigenvectors \mathbf{v}_i for $i \in [1, 2, 3]$ exist, such that

$$\begin{aligned}\mathbf{N} &= N_{ij}^{(2)} \mathbf{e}_i \otimes \mathbf{e}_j = \sum_{i=1}^3 \lambda_i \mathbf{v}_i \otimes \mathbf{v}_i \\ &= \begin{bmatrix} \lambda_1 & 0 & 0 \\ & \lambda_2 & 0 \\ \text{sym} & & \lambda_3 \end{bmatrix} \mathbf{v}_i \otimes \mathbf{v}_j\end{aligned}\quad (6.5)$$

holds with the ordering convention $\lambda_3 \leq \lambda_2 \leq \lambda_1$ and there exists a rotation defined by an orthogonal tensor

$$\mathbf{Q} = \mathbf{v}_i \otimes \mathbf{e}_i \quad (6.6)$$

mapping the arbitrary but fixed basis $\{\mathbf{e}_i\}$ onto the basis $\{\mathbf{v}_i\}$. A visual classification of structurally differing orientation tensors is given by the so called orientation triangle (Cintra Jr and Tucker III, 1995; Chung and Kwon, 2002; Goldberg et al., 2017; Köbler et al., 2018). As $\lambda_3 = 1 - \lambda_1 - \lambda_2$ holds due to the normalization of ψ , any second-order orientation tensor can be represented by a pair (λ_1, λ_2) , which is connected to a point inside the orientation triangle and by a mapping \mathbf{Q} which defines the orthonormal basis $\{\mathbf{v}_i\}$ spanned by the eigenvectors. This basis is called orientation coordinate system (Bauer and Böhlke, 2022c) and can be used to define the term planarity for FODF and fiber orientation tensors. A FODF is planar, if

$$\psi(\mathbf{n}(\varphi, \theta)) = 0 \quad \forall \varphi, \forall \theta \neq \frac{\pi}{2} \quad (6.7)$$

holds with a unit vector parameterized in two spherical angles in the

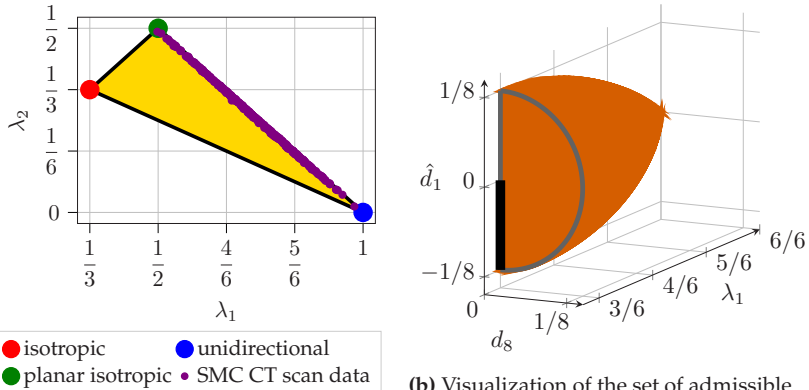


Figure 6.1

orientation coordinate system

$$\mathbf{n}(\varphi, \theta) = \sin(\theta) \cos(\varphi) \mathbf{v}_1 + \sin(\theta) \sin(\varphi) \mathbf{v}_2 + \cos(\theta) \mathbf{v}_3. \quad (6.8)$$

A fiber orientation tensor of arbitrary order is planar if its successive contraction yields a second-order fiber orientation tensor with vanishing third eigenvalue.

The assumption of the planarity of SMC microstructures is assessed by inspection of a biaxial tensile specimen made of SMC. Second-order fiber orientation tensors following equation (6.5) at several locations inside this specimen are obtained by computer tomography following (Schöttl et al., 2020) and are referenced as $\mathcal{N}_{\text{SMC}}^{\text{CT}}$. The obtained fiber orientation tensors are visualized as points inside an orientation triangle in Figure 6.1a. The orientation states along the upper right border of the triangle in Figure 6.1a represent perfectly planar orientations, as the third eigen-

value $\lambda_3 = 1 - \lambda_1 - \lambda_2$ vanishes. The measured fiber orientation tensors align well onto the planar border of the orientation triangle in Figure 6.1a and therefore confirm the planarity assumption. However, the spatial resolution of CT images as well as the choice of algorithm parameters for the processing of the CT images, influence the planarity of the resulting fiber orientation tensors. Not all fiber orientation tensors obtained for SMC in the literature are perfectly planar. As an example, Kehrer et al. (2020, Figure 5) contains non-planar fiber orientation states, obtained by CT scans, indicating a high spatial resolution of the corresponding CT images combined with small extraction cylinders (see Görthofer et al. (2019, Figure 4)) in the post-processing of the CT images. Visualizations of SMC microstructure data obtained by computer tomography (CT) are, e.g., given in Trauth et al. (2021, Figure 2). Artificially generated SMC microstructures can be found in Görthofer et al. (2020, Figure 3b and 5). The algorithm, which Görthofer et al. (2020) used to generate artificial microstructures, hints towards the planarity of the resulting directional measures. Throughout this work, fiber orientation tensors of SMC are assumed to be perfectly planar and hence, the dependence of the mechanical response of shell-like SMC structures on a varying microstructure can be investigated based on planar fiber orientation tensors. In this work, the SMC-specific bundle structure which is, e.g., considered in Schöttl et al. (2021); Görthofer et al. (2020), is not taken into account.

6.3 Planar fourth-order fiber orientation tensors

A parameterization of planar fiber orientation tensors of second-order $\mathbf{N}^{\text{planar}}$ is given by

$$\begin{aligned}\mathbf{N}^{\text{planar}}(\lambda_1) &= \lambda_1 \mathbf{v}_1 \otimes \mathbf{v}_1 + (1 - \lambda_1) \mathbf{v}_2 \otimes \mathbf{v}_2 \\ &= \begin{bmatrix} \lambda_1 & 0 & 0 \\ & 1 - \lambda_1 & 0 \\ \text{sym} & & 0 \end{bmatrix} \mathbf{v}_i \otimes \mathbf{v}_j\end{aligned}\quad (6.9)$$

in the orientation coordinate system $\{\mathbf{v}_i\}$ which is defined in Equation (6.6). Positive definiteness and normalization of the trace combined with the ordering convention of the eigenvalues demand the parameter range $1/2 \leq \lambda_1 \leq 1$. Bauer and Böhlke (2022c) discuss that planar fiber orientation tensors of fourth order only depend on three independent parameters and derive admissible ranges of these parameters demanding positive definiteness of the orientation tensors. Among the admissible parameters, Bauer and Böhlke (2022a) identify a subset of parameter combinations which represent all admissible and structurally distinct planar fourth-order fiber orientation tensors. Following Bauer and Böhlke (2022a), two tensors \mathbb{A} and \mathbb{B} are structurally distinct if

$$\nexists \mathbf{Q} \in \text{SO}(3) \text{ with } \mathbf{Q} \star \mathbb{A} = \mathbb{B} \quad (6.10)$$

with the special orthogonal group $\text{SO}(3)$, which contains all proper rotations. These results are summarized by the parameterization

$$\begin{aligned} \mathbb{N}^{\text{planar}}(\lambda_1, \hat{r}, \hat{\beta}) = & \\ \left[\begin{array}{c|c} \begin{matrix} -\hat{r} \sin(\hat{\beta}) - \hat{R}(\lambda_1) + \lambda_1 \hat{r} \sin(\hat{\beta}) + \hat{R}(\lambda_1) \\ -\hat{r} \sin(\hat{\beta}) - \hat{R}(\lambda_1) + (1 - \lambda_1) \end{matrix} & \begin{matrix} 0 & 0 & \sqrt{2} \hat{r} \cos(\hat{\beta}) \\ 0 & 0 & -\sqrt{2} \hat{r} \cos(\hat{\beta}) \\ 0 & 0 & 0 \end{matrix} \\ \hline \text{completely} & \text{symmetric} \end{array} \right] \\ \mathbf{B}_\xi^v \otimes \mathbf{B}_\zeta^v \end{aligned} \quad (6.11)$$

which follows from Bauer and Böhlke (2022a, Equation (22)) with

$$\hat{R}(\lambda_1) = (\lambda_1 - \lambda_1^2)/2 \quad (6.12)$$

and is represented in Kelvin-Mandel notation (Thomson, 1856; Mandel, 1965; Mehrabadi and Cowin, 1990). This notation is explained in detail in Appendix B.1 and the basis $\mathbf{B}_\xi^v \otimes \mathbf{B}_\zeta^v$ is spanned in the orientation coordinate system $\{\mathbf{v}_i\}$, i.e., for example the fifth basis vector in Equation (6.11) becomes $\mathbf{B}_5^v = \frac{\sqrt{2}}{2} (\mathbf{v}_1 \otimes \mathbf{v}_3 + \mathbf{v}_3 \otimes \mathbf{v}_1)$. The parameterization in Equation (6.11) can be combined with the set of parameter combinations which leads to admissible and distinct $\mathbb{N}^{\text{planar}}$. This set is

$$\begin{aligned} \hat{\mathcal{N}}^{\text{planar}} = & \left\{ \mathbb{N}^{\text{planar}}(\lambda_1, \hat{r}, \hat{\beta}) \mid \frac{1}{2} < \lambda_1 \leq 1, 0 \leq \hat{r} \leq \hat{R}(\lambda_1), \right. \\ & \left. -\frac{\pi}{2} \leq \hat{\beta} \leq \frac{\pi}{2} \right\} \\ \cup & \left\{ \mathbb{N}^{\text{planar}}(\lambda_1, \hat{r}, \hat{\beta}) \mid \lambda_1 = \frac{1}{2}, 0 \leq \hat{r} \leq \frac{1}{8}, \hat{\beta} = -\frac{\pi}{2} \right\} \end{aligned} \quad (6.13)$$

following Bauer and Böhlke (2022a, Equation (28)). A visualization of the body of admissible and distinct orientation tensors $\hat{\mathcal{N}}^{\text{planar}}$ in Cartesian

coordinates

$$\hat{d}_1 = \hat{r} \sin(\hat{\beta}), \quad d_8 = \hat{r} \cos(\hat{\beta}) \quad (6.14)$$

is given in Figure 6.1b. The data set $\mathcal{N}_{\text{SMC}}^{\text{CT}}$ of fiber orientation tensors obtained by CT, which second-order information is visualized in Figure 6.1a, is represented in the parameter space $\hat{\mathcal{N}}^{\text{planar}}$ in Figure 6.2. The data points are preferably concentrated around the axis of vanishing values of \hat{d}_1 and d_8 . This observation supports the statement of Hine et al. (2004), that real fiber orientations preferably scatter around orientation states with maximum entropy, i.e., those which are approximately isotropic. Analysis of additional data sets reveals, that the size of the reference volume associated with each discrete fiber orientation tensor significantly determines the resulting distribution inside the admissible region. However, quantitative investigations on the dependence of fiber orientation states on processing and CT settings is moved to a follow-up publication. Based on the parameterization $\mathbb{N}^{\text{planar}}(\lambda_1, \hat{r}, \hat{\beta})$ and the set $\hat{\mathcal{N}}^{\text{planar}}$, a visualization method, motivated by Bauer and Böhlke (2022a), can be used to study the influence of planar fourth-order fiber orientation tensors on the mechanical properties predicted by orientation-averaging mean field homogenization techniques.

Although the planar fiber orientation tensors given in Equations (6.9) and (6.11) fit into a two-dimensional framework, e.g., used in Bauer and Böhlke (2022a), a three-dimensional tensor framework is deployed within this work, as the mechanical behavior of real materials is defined by the laws of physics of the three-dimensional world. Boundary condition into the out-of-plane direction influence the mechanical response of planar structures, see Nordmann et al. (2020).

6.4 Orientation averages

Orientation-averaging mean field homogenization demands analytical or numerical schemes which yield averages of direction-dependent tensorial quantities over orientations. Advani and Tucker III (1987) define the orientation average of a tensorial quantity \mathbb{A} by

$$\langle \mathbb{A} \rangle_{\text{AT}} = \int_{S^2} \psi(\mathbf{n}) \mathbb{A}(\mathbf{n}) dS, \quad (6.15)$$

i.e., as a weighted summation with weights defined by the FODF. Several formulations and approximations of Equation (6.15) exist in the literature. An exact formulation given in the original paper Advani

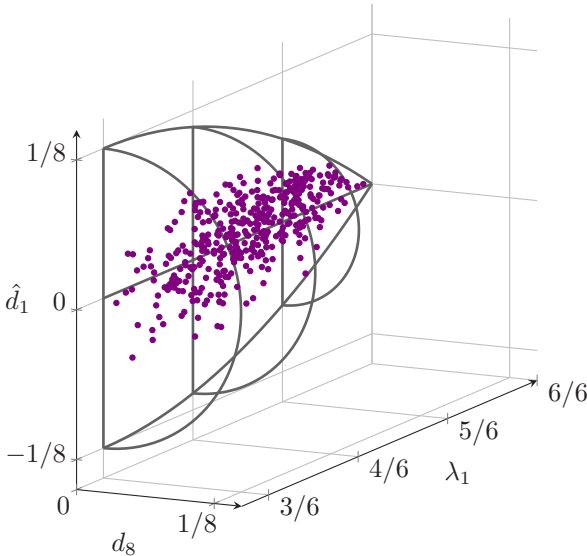


Figure 6.2: Fourth-order orientation tensors $N_{\text{SMC}}^{\text{CT}}$ obtained by computer tomography (CT) scans at several positions of a SMC specimen, represented by points inside the admissible and distinct planar parameter space $\mathcal{N}_{\text{planar}}$. The size of the reference volume associated with each discrete fiber orientation tensor significantly determines the resulting distribution inside the admissible region.

and Tucker III (1987, Equation (28)), frequently used in, e.g., Lielens et al. (1998); Jack and Smith (2008); Camacho et al. (1990); Brylka (2017); Kehrer et al. (2020); Hessman et al. (2021) is labeled $\langle \cdot \rangle_{\text{ATN}}$ in this work. This formulation is given directly in terms of fiber orientation tensors of second and fourth-order Kanatani first kind (Kanatani, 1984), and in its original formulation is restricted to transversely isotropic elasticity tensors $\mathbb{H} = H_{ijkl} \mathbf{e}_i \otimes \mathbf{e}_j \otimes \mathbf{e}_k \otimes \mathbf{e}_l$, i.e., stiffness or compliance-like quantities with major and both minor symmetries which may be specified in index notation by $H_{ijkl} = H_{jikl} = H_{ijlk}$. However, the original formulation in Advani and Tucker III (1987), which is repeated in slightly varying notation in, e.g., Kehrer et al. (2020); Brylka (2017); Heller et al. (2016), can be extended to transversely isotropic tensors which lack the major symmetry of an elasticity tensor. Such a generalization is given in Appendix C.4 based on the formulation introduced in the next section. The explicit formulation of $\langle \cdot \rangle_{\text{ATN}}$ in orientation tensors is simple and efficient, but complicates adaption of empirical fiber damage (Schemmann et al., 2018b) or incorporation of direction-dependent fiber length distributions (Brylka, 2017). A reformulation based on the harmonic decomposition Rychlewski (2000); Forte and Vianello (1996); Olive et al. (2018); Böhlke and Brüggemann (2001) explicitly revealing the structure of the scheme is given in the next section.

6.4.1 Reformulation of the explicit Advani-Tucker orientation average

A transversely isotropic elasticity tensor is completely defined by five independent parameters and a direction, i.e., a normal vector \mathbf{q} , and can be written as $\mathbb{C}^{\text{transv}}(h_1, h_2, h_3, h_4, h_5, \mathbf{q})$ following Equation (C.3) in C.2. The orientation average $\langle \cdot \rangle_{\text{ATN}}$ of a transversely isotropic elasticity

tensor is independent of \mathbf{q} and given by

$$\begin{aligned} & \langle \mathbb{C}^{\text{transv}}(h_1, h_2, h_3, h_4, h_5, \mathbf{q}) \rangle_{\text{ATN}}(\mathbb{N}) \\ &= h_1 \mathbb{P}_1 + h_2 \mathbb{P}_2 + h_3 \mathbb{J}_3 [\text{dev}(\mathbb{N})] + h_4 \mathbb{J}_4 [\text{dev}(\mathbb{N})] + h_5 \text{dev}(\mathbb{N}) \end{aligned} \quad (6.16)$$

with the irreducible parts of \mathbb{N}

$$\text{dev}(\mathbb{N}) = \mathbb{N} - \mathbb{N}^{\text{iso}} \quad (6.17)$$

$$\text{dev}(\mathbb{N}) = \mathbb{N} - \frac{6}{7} \text{sym}(\text{dev}(\mathbb{N}) \otimes \mathbf{I}) - \mathbb{N}^{\text{iso}} \quad (6.18)$$

and the isotropic parts of the second- and fourth-order fiber orientation tensors of Kanatani first kind (Kanatani, 1984)

$$\mathbb{N}^{\text{iso}} = \frac{1}{3} \mathbf{I}, \quad \mathbb{N}^{\text{iso}} = \frac{7}{35} \text{sym}(\mathbf{I} \otimes \mathbf{I}) \quad (6.19)$$

following Bauer and Böhlke (2022c). The isotropic sixth order tensors \mathbb{J}_3 and \mathbb{J}_4 are defined in Equations (C.6) and (C.7). The operator $\text{sym}(\cdot)$ extracts the totally symmetric part with respect to symmetry following Spencer (1970) and the operator $\text{dev}(\cdot)$ extracts the deviatoric part also discussed in Spencer (1970). Linearity of the harmonic decomposition in Equation (6.16) implies that the orientation average following Advani and Tucker III (1987) is linear in both $\mathbb{C}^{\text{transv}}$ and \mathbb{N} . This implication might be obvious to some authors, as the only source of orientation dependent structural information is \mathbb{N} . However, the original formulation in Advani and Tucker III (1987) does not directly reveal, that the isotropic part of the averaged elasticity tensor is unaffected, as one would expect from a physical point of view. In addition, the first and second deviatoric parts of the orientation average in Equation (6.16), i.e., $h_3 \text{dev}(\mathbb{N})$ and $h_4 \text{dev}(\mathbb{N})$, only differ by a scaling factor and share the tensor structure of $\text{dev}(\mathbb{N})$. As \mathbb{N} is completely symmetric, its first and second deviatoric parts coincide, see Bauer and Böhlke (2022c). As the manual derivation of Equation (6.16) is lengthy, listing C.1 combined

with code in Bauer (2022) is used to validate the representation of the orientation average. Any material model which contains the Advani-Tucker orientation average, implicitly contains a linearity assumption of at least an intermediate quantity in the fiber orientation or fabric tensor. For reference, some authors Schemmann et al. (2018a;b); Karl et al. (2021b) explicitly postulate linearity of an effective stiffness or viscosity in fiber orientation or fabric tensors. In contrast, a material model of a porous, anisotropic, linear elastic material being non-linear in a fabric tensor is given in Cowin (1985).

6.4.2 Direct numerical integration and the adaptive scheme based on angular central Gaussian distributions

Direct numerical integration of Equation (6.15) requires both a given FODF and a large number of integration points on the two-dimensional area of integration S^2 , but leads to insufficient accuracy despite high numerical effort, especially in the case of strongly localized FODF. This performance and accuracy issue motivates a recently developed numerical scheme (Goldberg et al., 2017) denoted by $\langle \cdot \rangle_{\text{ATGOS}}$ which is based on a special class of FODF basis functions called angular central Gaussian. Although this scheme is not used within this work, it is shortly introduced as a comparison. The scheme $\langle \cdot \rangle_{\text{ATGOS}}$ leads to an approximation resulting in a weighted summation of the quantity of interest pointing into a number of N^{GOS} discrete directions

$$\langle \mathbb{A} \rangle_{\text{AT}} \approx \langle \mathbb{A} \rangle_{\text{ATGOS}} (\mathbf{N}) = \sum_i^{N^{\text{GOS}}} w_i^{\text{GOS}} (\mathbf{N}) \mathbb{A}(\mathbf{n}_i) \quad (6.20)$$

with the weights being a function of the second-order fiber orientation tensor. The weights can be pre-calculated and stored in efficient look-up structures. Implementation details are given for the three-dimensional

case in Goldberg et al. (2017); Hessman et al. (2021) and for the two-dimensional case in Görthofer et al. (2020). This formulation yields reasonable accuracy even for localized FODF with a limited number of integration points (Goldberg et al., 2017), e.g., $N^{\text{GOS}} = 434$ in Hessman et al. (2021). Due to the structure in Equation (6.20), any direction-dependent quantity can be averaged and the weights may be modeled for empirical simulation of damage. However, the orientation average $\langle \cdot \rangle_{\text{ATGOS}}$ is solely based on the directional information contained within a second-order orientation tensor, which is limited to two scalars describing the half axes of an ellipsoid combined with the definition of a coordinate system.

6.4.3 Orientation average by reconstructed planar FODF based on a maximum entropy method

A maximum entropy FODF reconstruction for planar fiber orientations developed by Bauer and Böhlke (2022a) based on Müller and Böhlke (2016), can be combined with any numerical integration on S^1 leading to an approximation of the Advani-Tucker orientation average, which shares the simple structure of $\langle \mathbb{A} \rangle_{\text{ATGOS}}$, uses fourth-order fiber orientation tensor information and makes use of the reduced dimension of planar fiber orientation tensors. However, as this scheme uses direct numerical integration on S^1 , it leads to insufficient accuracy for localized fiber orientation states. Fortunately, the localized orientation states are known through analysis of the admissible region $\hat{\mathcal{N}}^{\text{planar}}$ in Bauer and Böhlke (2022a) and can be captured in implementations. Following Bauer and Böhlke (2022a), for any admissible non-localized fiber orientation tensor of fourth-order, a planar FODF, $\hat{\psi}^{\text{ME}}(\varphi, \mathbb{N}^{\text{planar}})$ parameterized in one spherical angle defined in Equation (6.8) with $0 \leq \varphi < 2\pi$ can be identified. This leads to an approximation of the Advani-Tucker average

in Equation (6.15) for the planar case by

$$\begin{aligned}
\langle \mathbb{A} \rangle_{\text{AT}}(\mathbb{N}^{\text{planar}}) &\approx \langle \mathbb{A} \rangle_{\text{ME}}(\mathbb{N}^{\text{planar}}) \\
&= \int_0^{2\pi} \hat{\psi}^{\text{ME}}(\varphi, \mathbb{N}^{\text{planar}}) \mathbf{Q}(\varphi) \star \mathbb{A} d\varphi \\
&\approx 2\pi \sum_{i=1}^{N^{\text{ME}}} w_i \hat{\psi}^{\text{ME}}(\varphi_i, \mathbb{N}^{\text{planar}}) \mathbf{Q}(\varphi_i) \star \mathbb{A} \\
&= 2\pi \sum_{i=1}^{N^{\text{ME}}} w_i^{\text{ME}}(\mathbb{N}^{\text{planar}}) \mathbf{Q}(\varphi_i) \star \mathbb{A}
\end{aligned} \tag{6.21}$$

with a rotation around the \mathbf{v}_3 axis \mathbf{Q} , evaluated at specified angles which are defined by any numerical integration scheme on S^1 with weights w_i . Within this work, numerical integration on S^1 with homogeneous weights $w_i = 1/N^{\text{ME}}$ and equidistant angles $w_i = 2\pi i/N^{\text{ME}}$ following Krylov and Stroud (2006) is used. The weights of the numerical integration scheme might be combined with the direction specific value of the FODF in Equation (6.21). The accuracy of the average $\langle \cdot \rangle_{\text{ME}}$ is assessed by averaging of moment tensors, as

$$\langle \mathbf{n}^{\otimes 4} \rangle_{\text{AT}}(\mathbb{N}^{\text{planar}}) = \mathbb{N}^{\text{planar}} \approx \langle \mathbf{n}^{\otimes 4} \rangle_{\text{ME}}(\mathbb{N}^{\text{planar}}) \tag{6.22}$$

has to hold. The assessment is done for all fourth-order fiber orientation tensors specified in Table C.1 except for the unidirectional case notated as $\mathcal{N}_{\text{selected}}^{\text{planar}}$, as this localized orientation state is insufficiently handled by the numerical integration. The deviation is quantified by

$$\Delta^{\max}(N^{\text{ME}}) = \max_{\mathbb{N}^{\text{planar}} \in \mathcal{N}_{\text{selected}}^{\text{planar}}} \frac{\| \langle \mathbf{n}^{\otimes 4} \rangle_{\text{ME}}(N^{\text{ME}}, \mathbb{N}^{\text{planar}}) - \mathbb{N}^{\text{planar}} \|}{\| \mathbb{N}^{\text{planar}} \|} \tag{6.23}$$

and given for varying order of the numerical integration N^{ME} in Figure 6.3. The target precision of 10^{-7} is reached. Studying the convergence of the numerical averaging scheme, by averaging a specific, randomly

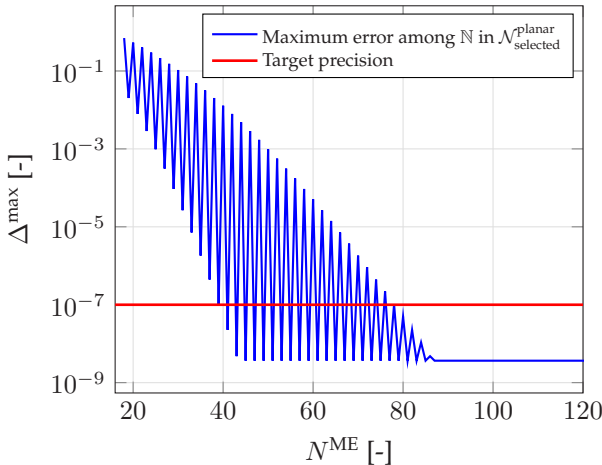


Figure 6.3: Influence of the number of integration points on the deviation of $\langle n^{\otimes 4} \rangle_{\text{ME}}$ from $\langle n^{\otimes 4} \rangle_{\text{ATN}}$ with Δ^{\max} defined in Equation (6.23)

chosen, elasticity tensor instead of the moment tensor in Equation (6.23), following Hessman et al. (2021), leads to similar convergence.

6.5 Orientation-averaging mean field homogenization

Sheet molding compound is a two-phase composite with glass fibers embedded irregularly in a thermoset polymer matrix. For isothermal applications, isotropic linear elasticity states a reasonable assumption for both the fiber and the matrix behavior, see Kehrer et al. (2020). In consequence, the local stress-strain relation inside the fiber and matrix phase at position \mathbf{x} is

$$\boldsymbol{\sigma}(\mathbf{x}) = \mathbb{C}_f [\varepsilon(\mathbf{x})] \quad \forall \mathbf{x} \in \mathcal{B}_f \quad (6.24)$$

$$\boldsymbol{\sigma}(\mathbf{x}) = \mathbb{C}_m [\varepsilon(\mathbf{x})] \quad \forall \mathbf{x} \in \mathcal{B}_m \quad (6.25)$$

	Young's mod.	Poissons ratio	Bulk mod.	Shear mod.
Fibers	73.0 GPa	0.22	43.45 GPa	29.92 GPa
Matrix	3.4 GPa	0.385	4.93 GPa	1.23 GPa

Table 6.1: Material parameters of the SMC constituents glass fiber and neat matrix (UPPH, i.e., unsaturated polyester-polyurethane hybrid) adopted from Kehrer et al. (2020, Table 2) citing additional references. Bulk and shear modulus are derived from Young's modulus and Poisson's ratio. The volume fractions of the fiber and matrix phases are $c_p = 0.256$ and $c_p = 0.744$.

with parts of the representative volume element (RVE) occupied by the fibers \mathcal{B}_f and the matrix \mathcal{B}_m , respectively. The stiffness of a fiber is denoted by C_f and C_m represents the stiffness of the matrix. Isotropy implies that C_f and C_m in Equations (6.24) and (6.25) do not depend on the spatial orientation and are given by

$$C_f = 3K_f \mathbb{P}_1 + 2G_f \mathbb{P}_2 \quad (6.26)$$

$$C_m = 3K_m \mathbb{P}_1 + 2G_m \mathbb{P}_2 \quad (6.27)$$

with the first and second isotropic projectors \mathbb{P}_1 and \mathbb{P}_2 respectively and bulk and shear modulus denoted by K and G . Throughout this work, material parameters are adopted from Kehrer et al. (2020, Table 2) and listed in Table 6.1. Two one-point characteristics describing the microstructure of a RVE at a material point inside a SMC-component are considered. The first characteristic is the volume fraction of the fibers c_f , which implies the volume fraction of the matrix $c_m = 1 - c_f$. The second characteristic is a fourth-order fiber orientation tensor N . In the absence of any non-linearities, such as cracks, the effective elastic stiffness \bar{C} of the RVE exists and is of interest. The effective stiffness maps effective strains $\bar{\varepsilon} = \langle \varepsilon(x) \rangle$ onto effective stresses $\bar{\sigma} = \langle \sigma(x) \rangle$ by

$$\bar{\sigma} = \bar{C}[\bar{\varepsilon}]. \quad (6.28)$$

The operator $\langle \cdot \rangle$ takes the volume average of a spatially varying field quantity, e.g., $\sigma(x)$, inside the RVE. Four mean field approximations

are briefly reviewed and examined for given material parameters and variable fiber orientation tensors.

6.5.1 Two-step Hashin-Shtrikman

A two-step Hashin-Shtrikman scheme for fiber reinforced composites following Kehrer et al. (2020), based on Walpole (1966a;b; 1969) and proposed by Fernández and Böhlke (2019) is used to study the influence of a fourth-order orientation tensor on the effective stiffness. Detailed derivations of the Hashin-Shtrikman bounds, based on a variational principle, are given in Walpole (1966a); Fernández and Böhlke (2019). In this work only the resulting equations are of interest. Under the assumption of phase-wise constant stress polarizations, the Green's function of a material without long-range order and ellipsoidal two-point statistics, is constant (Fernández and Böhlke, 2019, section 2.2). This constant Green's function is represented by the Hill's (Hill, 1965a) polarization tensor \mathbb{P} and reflects the ellipsoidal symmetry of the two-point statistics. Under these assumptions, the effective stiffness of a material made up of n phases with stiffnesses $\{\mathbb{C}_i\}$ for $i \in [1, \dots, n]$ is given as a function of a comparison stiffness \mathbb{C}_0 by

$$\bar{\mathbb{C}}^{\text{HSW}}(\mathbb{C}_0, \mathbb{P}(\mathbb{C}_0, a), \{\mathbb{C}_i\}, \langle \langle \cdot \rangle \rangle) = \mathbb{C}_0 - \mathbb{P}^{-1} + [\langle \langle \mathbb{W}(\mathbb{C}_0, \mathbb{P}, \mathbb{C}_i) \rangle \rangle]^{-1} \quad (6.29)$$

with

$$\mathbb{W}(\mathbb{C}_0, \mathbb{P}, \mathbb{C}_i) = [\mathbb{P}^{-1} + \mathbb{C}_i - \mathbb{C}_0]^{-1} \quad (6.30)$$

and with $\mathbb{P}(\mathbb{C}_0, a)$ depending on the symmetry of the two point statistics. For simplicity, the dependence of \mathbb{P} upon the two point statistic is represented by an aspect ratio a with $1/2 \leq a \leq \infty$ reaching from the isotropic case $\mathbb{P}^0(\mathbb{C}_0) = \mathbb{P}(\mathbb{C}_0, 1/2)$ to the limiting unidirectional case $\mathbb{P}^{\text{UD}}(\mathbb{C}_0) = \mathbb{P}(\mathbb{C}_0, \infty)$. This restriction of \mathbb{P} from generally ellipsoidal

shapes to spheroidal shapes is common in the context of fiber reinforced composites. The operator $\langle \langle \cdot \rangle \rangle$ takes the average over the RVE. Alternative formulations of the Hashin-Shtrikman scheme exist, e.g., in Willis (1977; 1981) and remarks on the different formulations are given in Fernández and Böhlke (2019). The formulation in Equation (6.29) is not directly applicable to singular, i.e., non-invertible, polarization tensors. However, Walpole (1969, page 238) proposes a dual scheme which can be used to evaluate Equation (6.29) for singular polarization tensors, e.g., \mathbb{P}^{UD} . If the comparison material with stiffness \mathbb{C}_0 is selected, such that the stiffnesses of all phases are smaller (larger) than \mathbb{C}_0 , e.g., using first order bounds, Equation (6.29) yields a lower (upper) Hashin-Shtrikman bound. As SMC is a two-phase composite, for any choice of the comparison stiffness \mathbb{C}_0 in between \mathbb{C}_m and \mathbb{C}_f , Equation (6.29) gives an admissible effective stiffness in between the Hashin-Shtrikman bounds. Following Kehrer et al. (2020, Equation (24)), a comparison stiffness as a function of an interpolation parameter k is introduced by

$$\hat{\mathbb{C}}_0(k) = [1 - k] \mathbb{C}_m + k \mathbb{C}_f \quad (6.31)$$

with $0 \leq k \leq 1$. With this notation, the scheme of Kehrer et al. (2020) is reformulated as a generic two-step Hashin-Shtrikman scheme. In a first step, the effective stiffness of an artificially pseudo grain $\bar{\mathbb{C}}^{\text{UD}}$ is calculated by

$$\begin{aligned} \bar{\mathbb{C}}^{\text{UD}}(k_1, c_f, \mathbb{C}_f, \mathbb{C}_m) &= \bar{\mathbb{C}}^{\text{HSW}}\left(\mathbb{C}_0 = \hat{\mathbb{C}}_0(k_1), \mathbb{P} = \mathbb{P}^{\text{UD}}(\mathbb{C}_0), \right. \\ &\quad \left. \{\mathbb{C}_i\} = \{\mathbb{C}_f, \mathbb{C}_m\}, \langle \langle \cdot \rangle \rangle = \langle \cdot \rangle(c_f) \right). \end{aligned} \quad (6.32)$$

This pseudo grain contains unidirectional fibers with a volume content which is equal to the volume content of the fibers in the overall two-phase composite c_f . To be explicit, the operator $\langle \cdot \rangle$ in Equation (6.32) applied to $\mathbb{W}(\mathbb{C}_0, \mathbb{P}, \mathbb{C}_i)$ with $i \in [m, f]$ reads as $\langle \mathbb{W}(\dots, \mathbb{C}_i) \rangle = c_m \mathbb{W}(\dots, \mathbb{C}_m) + c_f \mathbb{W}(\dots, \mathbb{C}_f)$, with the abbreviation “...” for additional

function arguments. The stiffness $\bar{\mathbb{C}}^{\text{UD}}$ obtained by Equation (6.32) is transversely isotropic. As the Hill polarization \mathbb{P} in Equations (6.30) and (6.32) reflects the shape of the two-point statistics, the specific choice of \mathbb{P}^{UD} for a single grain implies a laminate-like two-point statistic. It should be noted, that the inclusion shape is not specified. However, specification of the two-point statistic is not independent of the inclusion shape. In the second step, the stiffness obtained in step one is orientation averaged based on the Hashin-Shtrikman scheme in Equation (6.29), where the average over the RVE $\langle \langle \cdot \rangle \rangle$ is transferred into an average over orientations. The operator $\langle \cdot \rangle_{\text{ATN}}$ defined in Equation (6.16) represents a commonly used Lielens et al. (1998); Jack and Smith (2008); Camacho et al. (1990) average over orientations, based on a fourth-order fiber orientation tensor \mathbb{N} , following Advani and Tucker III (1987). As the pseudo grain is artificial, the two-point statistics in the second step are assumed to be isotropic and are therefore reflected by the Hill polarization tensor for spherical inclusions \mathbb{P}^0 . This leads to the approximation $\bar{\mathbb{C}}^{\text{HSW2}}$ of the effective overall stiffness with

$$\begin{aligned}\bar{\mathbb{C}}^{\text{HSW2}}(k_1, k_2, \mathbb{N}, c_f, \mathbb{C}_f, \mathbb{C}_m) = \\ \bar{\mathbb{C}}^{\text{HSW}} \left(\mathbb{C}_0 = \hat{\mathbb{C}}_0(k_2), \mathbb{P} = \mathbb{P}^0(\mathbb{C}_0), \{\mathbb{C}_i\} = \{\bar{\mathbb{C}}^{\text{UD}}(k_1, \dots)\}, \right. \\ \left. \langle \langle \cdot \rangle \rangle = \langle \cdot \rangle_{\text{ATN}}(\mathbb{N}) \right).\end{aligned}\quad (6.33)$$

The connection to the formulas in Kehrer et al. (2020) is given in C.5. The formulation of $\langle \cdot \rangle_{\text{ATN}}$ in Equation (6.16) shows the linearity of the orientation average in both arguments.

For the special case of planar fourth-order orientation information, i.e., $\mathbb{N}^{\text{planar}}$ and a given transversely isotropic pseudo grain stiffness $\bar{\mathbb{C}}^{\text{UD}}$, the structure of the effective stiffness is given analytically. Starting from a given transversely isotropic stiffness $\bar{\mathbb{C}}^{\text{UD}}$ obtained in a first homogenization step, e.g., following Equation (6.32), the second homogenization step in Equation (6.33) for the special case of a planar orientation tensor

$\mathbb{N}^{\text{planar}}$, is of interest. Omitting functional dependencies, the expansion of Equation (6.29) reads as

$$\bar{\mathbb{C}}^{\text{HSW}} = \mathbb{C}_0 - [\mathbb{P}^0]^{-1} + \mathbb{G} \quad (6.34)$$

with

$$\begin{aligned} \mathbb{G} &= \left[\langle \left[[\mathbb{P}^0]^{-1} + \bar{\mathbb{C}}^{\text{UD}} - \mathbb{C}_0 \right]^{-1} \rangle_{\text{ATN}} \right]^{-1} \\ &= [\langle \mathbb{A}^{-1} \rangle_{\text{ATN}}]^{-1} = [\langle \mathbb{B} \rangle_{\text{ATN}}]^{-1} = [\mathbb{E}]^{-1}. \end{aligned} \quad (6.35)$$

The Hill polarization \mathbb{P}^0 is isotropic and its inverse is given by

$$[\mathbb{P}^0]^{-1} = h_1^{\text{P0-}} \mathbb{P}_1 + h_2^{\text{P0-}} \mathbb{P}_2 \quad (6.36)$$

with

$$h_1^{\text{P0-}} = h_1^0 + 2h_2^0, \quad h_2^{\text{P0-}} = \frac{\frac{5}{2}h_2^0 [h_1^0 + 2h_2^0]}{h_1^0 + 3h_2^0} \quad (6.37)$$

and $h_1^0 = 3K^0$, $h_2^0 = 2G^0$ and the bulk and shear modulus of the isotropic comparison material K^0 and G^0 . As both the Hill polarization and the stiffness of the comparison material are isotropic, the intermediate quantity \mathbb{A} in Equation (6.35) inherits the transversely isotropic symmetry from the unidirectional stiffness \mathbb{C}^{UD} . With the short hand notation of a transversely isotropic elasticity tensor defined in Equation (C.13) the tensor \mathbb{A} is given by

$$\mathbb{A} = \left[h_1, h_2, h_3, h_4, h_5, \mathbf{q} = \mathbf{v}_1 \right] \quad (6.38)$$

with

$$h_1 = h_1^{\text{P}0\text{-}} - h_1^0 + h_1^{\text{UD}}, \quad h_2 = h_2^{\text{P}0\text{-}} - h_2^0 + h_2^{\text{UD}}, \quad (6.39)$$

$$h_3 = h_3^{\text{UD}}, \quad h_4 = h_4^{\text{UD}}, \quad (6.40)$$

$$h_5 = h_5^{\text{UD}} \quad (6.41)$$

based on

$$\bar{\mathbb{C}}^{\text{UD}} = \left[h_1^{\text{UD}}, h_2^{\text{UD}}, h_3^{\text{UD}}, h_4^{\text{UD}}, h_5^{\text{UD}}, \mathbf{q} = \mathbf{v}_1 \right]. \quad (6.42)$$

As the orientation of the pseudo grain stiffness is arbitrary, without loss of generality, $\mathbf{q} = \mathbf{v}_1$ holds in Equations (6.38) and (6.42). The inversion of a transversely isotropic stiffness is discussed in, e.g., Lubarda and Chen (2008, Equation (31)), and leads to a transversely isotropic compliance

$$\mathbb{B} = \mathbb{A}^{-1} = \left[h_1^{\text{B}}, h_2^{\text{B}}, h_3^{\text{B}}, h_4^{\text{B}}, h_5^{\text{B}}, \mathbf{q} = \mathbf{v}_1 \right] \quad (6.43)$$

$$= \begin{bmatrix} B_{11} & B_{12} & B_{12} & 0 & 0 & 0 \\ & B_{22} & B_{23} & 0 & 0 & 0 \\ & & B_{22} & 0 & 0 & 0 \\ & & & B_{22} - B_{23} & 0 & 0 \\ \text{sym} & & & & 2B_{55} & 0 \\ & & & & & 2B_{55} \end{bmatrix} \mathbf{B}_{\xi} \otimes \mathbf{B}_{\zeta}$$

with h_i^{B} for $i \in \{1, 2, 3, 4, 5\}$ given in C.6 in Equations (C.33) to (C.38). The general correspondence of stiffness and compliance is discussed in Rychlewski (1984). Simpler representations of a transversely isotropic compliance (Lubarda and Chen, 2008; Cowin and Van Buskirk, 1986; Vannucci, 2018), e.g., in tensor components or engineering notation, exist. However, Equations (C.33) to (C.38) show the interaction of the harmonic coefficients h_i with $i \in \{1, 2, 3, 4, 5\}$ during the tensor inversion. Each coefficient of \mathbb{B} is a function of all five coefficients of \mathbb{A} .

Taking the orientation average (Advani and Tucker III, 1987) of \mathbb{B} , e.g., using Equation (6.16), leads to

$$\mathbb{E} = \langle \mathbb{B} \rangle_{\text{ATN}} = \begin{bmatrix} E_{11} & E_{12} & E_{13} & 0 & 0 & E_{16} \\ E_{22} & E_{23} & 0 & 0 & -E_{16} & \\ E_{33} & 0 & 0 & 0 & & \\ & E_{44} & 0 & 0 & & \\ \text{sym} & & E_{55} & 0 & & \\ & & & E_{66} & & \end{bmatrix} \mathbf{B}_\xi \otimes \mathbf{B}_\zeta. \quad (6.44)$$

The tensor components in Equation (6.44) are specified in Equations (C.41) to (C.50) in C.6. The inversion of \mathbb{E} leads to

$$\mathbb{G} = [\mathbb{E}]^{-1} = \begin{bmatrix} G_{11} & G_{12} & G_{13} & 0 & 0 & G_{16} \\ G_{22} & G_{23} & 0 & 0 & G_{26} & \\ G_{33} & 0 & 0 & 0 & G_{36} & \\ & G_{44} & 0 & 0 & & \\ \text{sym} & & G_{55} & 0 & & \\ & & & G_{66} & & \end{bmatrix} \mathbf{B}_\xi \otimes \mathbf{B}_\zeta \quad (6.45)$$

with tensor components given in Equations (C.51) to (C.63) in C.6. Equations (C.51) to (C.63) combined with Equations (C.41) to (C.50) show that the effective stiffness $\bar{\mathbb{C}}^{\text{HSW}}$ is nonlinear in the parameters of the fiber orientation tensor λ_1, d_1, d_8 . In addition, the structure of $\bar{\mathbb{C}}^{\text{HSW}}$ and \mathbb{G} differs from that of the intermediate quantity \mathbb{E} , as the tensor component G_{36} in Equation (6.45) does not vanish, although E_{36} in Equation (6.44) does vanish. $\bar{\mathbb{C}}^{\text{HSW}}$ inherits the structure from \mathbb{G} .

6.5.2 Orientation-averaging Mori-Tanaka following Benveniste (1987)

Various aspects of the orientation-averaging Mori-Tanaka approximation are discussed in Brylka (2017); Weng (1990); Qiu and Weng (1990).

Nevertheless, a comprehensive summary of the basic equations for the special case of homogeneous fiber lengths, i.e., an isotropic fiber length distribution, is given hereafter. The RVE is denoted by \mathcal{B} and any point inside the RVE is identifiable by a position $\mathbf{x} \in \mathcal{B}$. Introducing a field of strain localization tensors $\mathbb{A}(\mathbf{x})$ mapping the effective strain of the RVE, $\bar{\varepsilon}$, onto the local strain $\varepsilon(\mathbf{x})$ with

$$\varepsilon(\mathbf{x}) = \mathbb{A}(\mathbf{x})[\bar{\varepsilon}] \quad (6.46)$$

yields an exact representation of the effective stiffness by

$$\bar{\mathbb{C}} = \langle \mathbb{C}(\mathbf{x})\mathbb{A}(\mathbf{x}) \rangle \quad (6.47)$$

due to

$$\begin{aligned} \bar{\sigma} &= \langle \sigma(\mathbf{x}) \rangle = \langle \mathbb{C}(\mathbf{x})[\varepsilon(\mathbf{x})] \rangle \\ &= \langle \mathbb{C}(\mathbf{x})\mathbb{A}(\mathbf{x})[\bar{\varepsilon}] \rangle = \langle \mathbb{C}(\mathbf{x})\mathbb{A}(\mathbf{x}) \rangle [\bar{\varepsilon}]. \end{aligned} \quad (6.48)$$

If the exact strain localization field $\mathbb{A}(\mathbf{x})$ for an RVE is known, the effective stiffness $\bar{\mathbb{C}}$ is given by Equation (6.47). The volume average of Equation (6.47) implies $\langle \mathbb{A}(\mathbf{x}) \rangle = \mathbb{I}^s$ with \mathbb{I}^s being the identity acting on the space of symmetric second-order tensors. An exact decomposition of the volume average over the RVE into volume averages over the different phases in the special case of a two phase composite yields

$$\langle \mathbb{A} \rangle = \mathbb{I}^s = c_m \langle \mathbb{A} \rangle_m + c_f \langle \mathbb{A} \rangle_f \quad (6.49)$$

with the volume fraction c_α of phase $\alpha \in [f, m]$ and therefore

$$\langle \mathbb{A} \rangle_m = \frac{1}{c_m} [\mathbb{I}^s - c_f \langle \mathbb{A} \rangle_f]. \quad (6.50)$$

For a two-phase material with piece-wise constant stiffnesses, Equation (6.47) combined with Equation (6.50) leads to

$$\bar{\mathbb{C}} = c_m \langle \mathbb{C}(\mathbf{x}) \mathbb{A}(\mathbf{x}) \rangle_m + c_f \langle \mathbb{C}(\mathbf{x}) \mathbb{A}(\mathbf{x}) \rangle_f \quad (6.51)$$

$$= c_m \mathbb{C}_m \langle \mathbb{A}(\mathbf{x}) \rangle_m + c_f \mathbb{C}_f \langle \mathbb{A}(\mathbf{x}) \rangle_f \quad (6.52)$$

$$= c_m \mathbb{C}_m \frac{1}{c_m} [\mathbb{I}^s - c_f \langle \mathbb{A} \rangle_f] + c_f \mathbb{C}_f \langle \mathbb{A}(\mathbf{x}) \rangle_f \quad (6.53)$$

$$= \mathbb{C}_m + c_f \Delta \mathbb{C} \langle \mathbb{A} \rangle_f \quad (6.54)$$

introducing the short hand notation for the material contrast $\Delta \mathbb{C} = \mathbb{C}_f - \mathbb{C}_m$. The strain localization tensor of the Mori-Tanaka approximation (Mori and Tanaka, 1973) for a two-phase composite reads as

$$\begin{aligned} \langle \mathbb{A} \rangle_f &\approx \langle \mathbb{A} \rangle_f^{MT} = \mathbb{A}_f^{SI} [c_m \mathbb{I}^s + c_f \mathbb{A}_f^{SI}]^{-1} \\ &= \left[c_m [\mathbb{A}_f^{SI}]^{-1} + c_f \mathbb{I}^s \right]^{-1} \end{aligned} \quad (6.55)$$

with the strain localization tensor of the inclusion (fiber) phase in the single inclusion problem \mathbb{A}_f^{SI} (Eshelby, 1957) given by

$$\mathbb{A}_f^{SI} = [\mathbb{P}(\mathbb{C}_m, a) [\mathbb{C}_f - \mathbb{C}_m] + \mathbb{I}^s]^{-1}. \quad (6.56)$$

The Hill polarization tensor $\mathbb{P}(\mathbb{C}_m, a)$ for spheroidal inclusion shapes is parameterized by an aspect ratio a . Inserting the approximated strain localization tensor of Equation (6.55) into Equation (6.54) leads to the effective stiffness of the Mori-Tanaka approximation for a two-phase composite

$$\bar{\mathbb{C}}^{MT}(c_f, \mathbb{C}_f, \mathbb{C}_m, \mathbb{P}) = \mathbb{C}_m + c_f \Delta \mathbb{C} \langle \mathbb{A} \rangle_f^{MT}. \quad (6.57)$$

The Hill polarization \mathbb{P} in the single inclusion problem reflects the shape of the inclusion. A study on the influence of the inclusion shape onto the effective stiffness is given in Müller (2016). The large aspect ratio of SMC

fibers motivates the use of \mathbb{P}^{UD} , e.g., in Kehrer et al. (2020). Orientation-averaging Mori-Tanaka for two-phase composites with anisotropic constituents and an inclusion phase consisting of aligned or randomly orientated ellipsoidal particles following Benveniste (1987) combined with an orientation-averaging scheme following Advani and Tucker III (1987), depicted by $\langle \cdot \rangle_{\text{ATN}}$, reads as

$$\begin{aligned}\langle \mathbb{A} \rangle_f &\approx \langle \mathbb{A} \rangle_f^{\text{MTOAB}} (\mathbb{N}, c_f, \mathbb{C}_f, \mathbb{C}_m) \\ &= \left[c_m \left[[\Delta \mathbb{C}]^{-1} \langle \Delta \mathbb{C} \mathbb{A}_f^{\text{SI}} \rangle_{\text{ATN}} (\mathbb{N}) \right]^{-1} + c_f \mathbb{I}^s \right]^{-1}\end{aligned}\quad (6.58)$$

leading to the Mori-Tanaka orientation averaged approximation following Benveniste (1987) with

$$\bar{\mathbb{C}}^{\text{MTOAB}} (\mathbb{N}, c_f, \mathbb{C}_f, \mathbb{C}_m) = \mathbb{C}_m + c_f \Delta \mathbb{C} \langle \mathbb{A} \rangle_f^{\text{MTOAB}} (\mathbb{N}, c_f, \mathbb{C}_f, \mathbb{C}_m). \quad (6.59)$$

Orientation-averaging Mori-Tanaka following Benveniste (1987) is used in Brylka (2017); Schemmann et al. (2018b) and limitations are discussed in, e.g., Benveniste et al. (1991). As the orientation-averaging scheme $\langle \cdot \rangle_{\text{ATN}}$ in its original formulation is limited to elasticity tensors, i.e., any tensor $\mathbb{C} = C_{ijkl} \mathbf{e}_i \otimes \mathbf{e}_j \otimes \mathbf{e}_k \otimes \mathbf{e}_l$ with both minor and the major symmetries $C_{ijkl} = C_{jikl} = C_{ijlk} = C_{klji}$, but strain localization tensors may lack the main symmetry, an intermediate elasticity tensor $\Delta \mathbb{C} \mathbb{A}_f^{\text{SI}} = [\mathbb{P} + \Delta \mathbb{C}^{-1}]^{-1}$ is averaged in Equation (6.58) before the effect of $\Delta \mathbb{C}$ is removed by $\Delta \mathbb{C}^{-1}$. This step could be avoided using the generalization of the orientation average $\langle \cdot \rangle_{\text{ATN}}$ in Appendix C.4. The unity of all fibers is treated as one phase.

6.5.3 Direct orientation average of a transversely isotropic stiffness

Some authors (Iorga et al., 2008; Schjødt-Thomsen and Pyrz, 2001) identify the linear orientation average of transversely isotropic stiffness (Advani and Tucker III, 1987) as an approximation for the effective stiffness with

$$\bar{\mathbb{C}}^{\text{MTlinearStiffness}} (\mathbb{N}, \dots) = \langle \bar{\mathbb{C}}^{\text{MT}} (\dots) \rangle_{\text{ATN}} (\mathbb{N}) \quad (6.60)$$

which is based on the Mori-Tanaka approximation in Equation (6.57) and is used in commercial software (Smith, 2019).

6.5.4 Direct orientation average of a transversely isotropic compliance

In analogy to the approximation defined in Equation (6.60), another approximation is given by the orientation average of an unidirectional compliance obtained by the Mori-Tanaka approximation

$$\bar{\mathbb{C}}^{\text{MTlinearCompliance}} (\mathbb{N}, \dots) = \left[\langle [\bar{\mathbb{C}}^{\text{MT}} (\dots)]^{-1} \rangle_{\text{ATN}} (\mathbb{N}) \right]^{-1}. \quad (6.61)$$

6.6 Graphical representation of elasticity tensors

The last building block for the systematic investigation of the dependence of linear elastic effective stiffness tensors on planar fiber orientation tensors, is a compact, preferably two-dimensional, visualization of effective stiffness tensors. Following Böhlke and Brüggemann (2001), two scalar functions $E(\mathbb{C}, \mathbf{n})$ and $K(\mathbb{C}, \mathbf{n})$, equivalently describe an anisotropic stiffness \mathbb{C} . The direction-dependent Young's modulus

$E(\mathbb{C}, \mathbf{n})$ defined by

$$\begin{aligned} E(\mathbb{C}, \mathbf{n}) &= \frac{\sigma(\mathbf{n})}{\varepsilon(\mathbf{n})} = \left[\frac{\varepsilon(\mathbf{n})}{\sigma(\mathbf{n})} \right]^{-1} = \left[\frac{\mathbf{n}^{\otimes 2} \cdot \varepsilon(\mathbf{n})}{\sigma(\mathbf{n})} \right]^{-1} \\ &= \left[\frac{\mathbf{n}^{\otimes 2} \cdot \mathbb{C}^{-1}[\sigma(\mathbf{n})]}{\sigma(\mathbf{n})} \right]^{-1} = [\mathbb{C}^{-1} \cdot \mathbf{n}^{\otimes 4}]^{-1} \end{aligned} \quad (6.62)$$

represents the ratio of the tensile stress $\sigma(\mathbf{n})$ and the tensile strain $\varepsilon(\mathbf{n})$ during a tensile test in direction \mathbf{n} . The tensile stress caused by a virtual unidirectional tensile test into direction \mathbf{n} , is related to the stress tensor $\sigma(\mathbf{n})$ by $\sigma(\mathbf{n}) = \sigma \mathbf{n}^{\otimes 2} = \sigma \mathbf{n} \otimes \mathbf{n}$. The tensile strain $\varepsilon(\mathbf{n})$ is obtained by a projection of the infinitesimal strain tensor ε onto the direction \mathbf{n} , i.e., $\varepsilon = \varepsilon \cdot \mathbf{n}^{\otimes 2}$. Following He and Curnier (1995); Böhlke and Brüggemann (2001), the generalized bulk modulus $K(\mathbb{C}, \mathbf{n})$ is defined by

$$\begin{aligned} 3K(\mathbb{C}, \mathbf{n}) &= \left[\frac{\mathbf{I} \cdot \varepsilon(\mathbf{n})}{\sigma(\mathbf{n})} \right]^{-1} = \left[\frac{\mathbf{I} \cdot \mathbb{C}^{-1}[\sigma(\mathbf{n})]}{\sigma(\mathbf{n})} \right]^{-1} \\ &= [\mathbf{I} \cdot \mathbb{C}^{-1}[\mathbf{n}^{\otimes 2}]]^{-1} \end{aligned} \quad (6.63)$$

and measures the relative change of volume $\mathbf{I} \cdot \varepsilon = [dV - dV_0]/dV_0$ caused by uniaxial tension in direction \mathbf{n} , i.e., $\sigma = \sigma \mathbf{n}^{\otimes 2}$. For a given stiffness \mathbb{C} , both $E(\mathbb{C}, \mathbf{n})$ and $K(\mathbb{C}, \mathbf{n})$ are functions on the unit sphere. The influence of $\mathbb{N}^{\text{planar}}$ on the mechanical properties in the \mathbf{v}_1 - \mathbf{v}_2 -plane is investigated by

$$E^{\text{planar}}(\mathbb{C}, \varphi) = E(\mathbb{C}, \mathbf{n}(\varphi, \theta = \pi/2)) \quad (6.64)$$

$$K^{\text{planar}}(\mathbb{C}, \varphi) = K(\mathbb{C}, \mathbf{n}(\varphi, \theta = \pi/2)) \quad (6.65)$$

with the unit vector $\mathbf{n}(\varphi, \theta)$ specified in Equation (6.8). The two quantities $E^{\text{planar}}(\mathbb{C}, \varphi)$ and $K^{\text{planar}}(\mathbb{C}, \varphi)$ uniquely define the mechanical response of the effective stiffness in the plane spanned by \mathbf{v}_1 and \mathbf{v}_2 . Alternative representations of three-dimensional fourth-order tensors

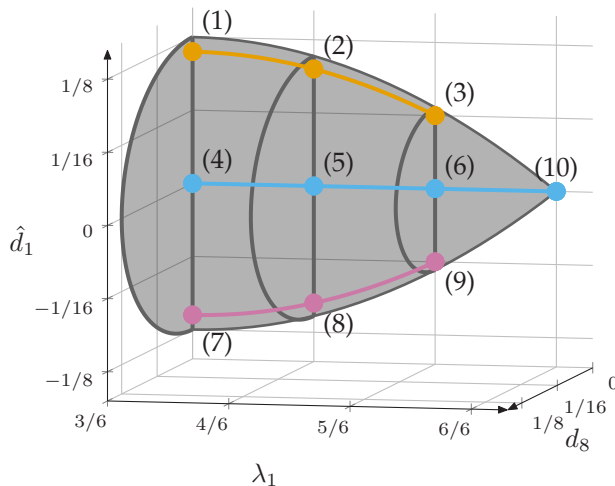
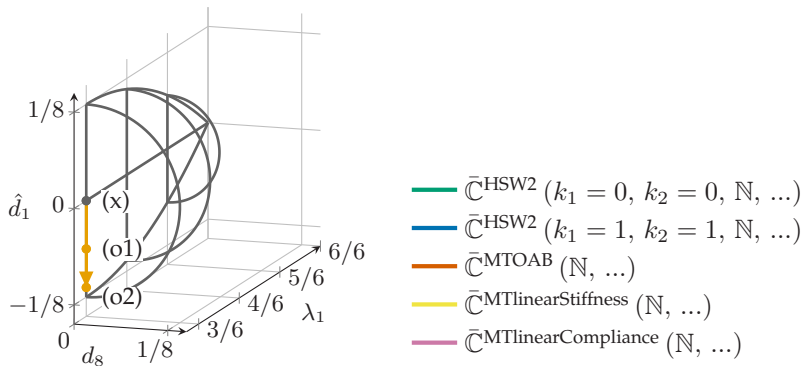


Figure 6.4: Ten points in the plane of planar orthotropic fiber orientation tensors of fourth-order used in Figures 6.7a and 6.7b

are, e.g., given in Vannucci (2018, p. 62).



(a) Points in the plane $\lambda_1 = 3/6$ used in Figures 6.8a, 6.8b

(b) Shared legend for Figures 6.7, 6.8, 6.9, 6.10, 6.11 and 6.12.

Figure 6.5: Definition of representative points in the parameter space $\hat{\mathcal{N}}^{\text{planar}}$ in the plane $\lambda_1 = 3/6$ and shared legend for mean field approximations.

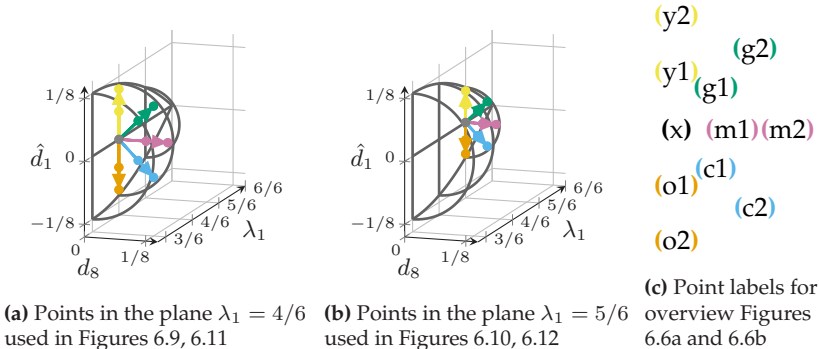


Figure 6.6: Definition of representative points in the parameter space $\mathcal{N}^{\text{planar}}$ of planar fourth-order fiber orientation tensors. Parameters of each point are listed in Table C.1.

6.7 Effective stiffnesses: Polar plots and the dependence on planar fourth-order fiber orientations

In this section, the building blocks developed in the previous sections are combined to study the dependence of linear elastic effective stiffnesses obtained by mean field homogenization on fourth-order fiber orientation tensors. As the dimensionality of the study is already high due to the flexible orientation, the material parameters of the constituents are fixed and specified in Table 6.1.

6.7.1 Visualization setup

The space of admissible and distinct planar fourth-order fiber orientations $\mathcal{N}^{\text{planar}}$ is discretized by a small number of representative fiber orientations. Slices through the three-dimensional body $\mathcal{N}^{\text{planar}}$ are defined in Figures 6.4 to 6.6b. On each slice, a small number of points, each representing a specific fourth-order fiber orientation tensor $\mathcal{N}^{\text{planar}}$, are selected. For each point, effective stiffnesses are calculated using the

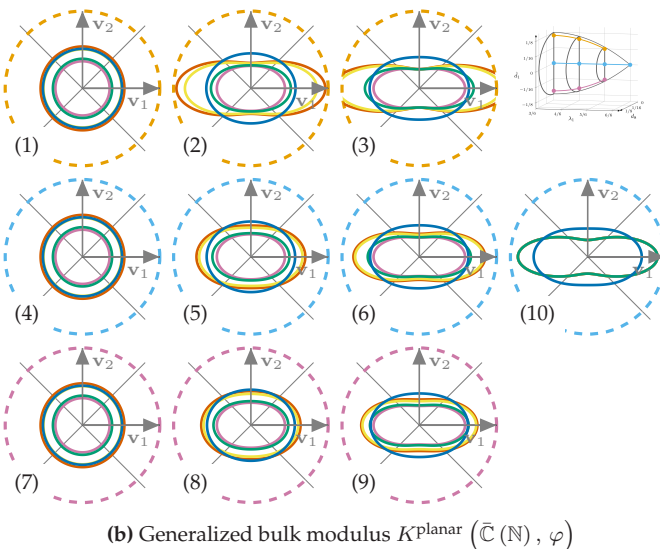
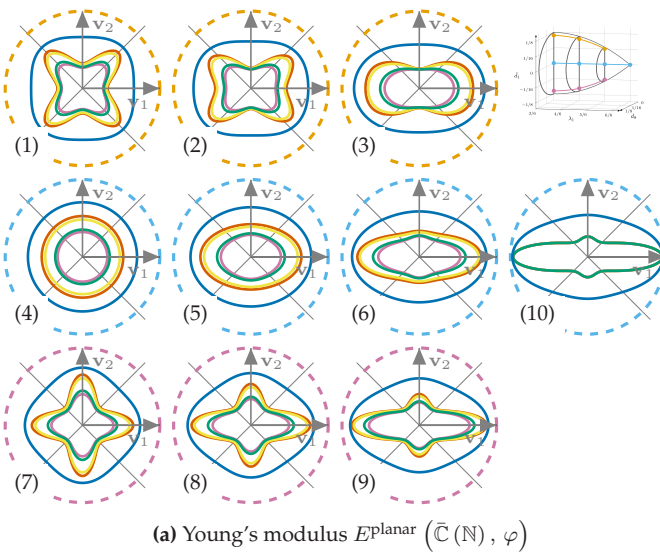


Figure 6.7: Polar plots for selected \mathbb{N} specified in Figure 6.4 and Table C.1 and mean field approximations specified in the legend in Figure 6.5b

orientation-averaging homogenization schemes listed in Figure 6.5b and described in Section 6.5. The planar properties of each effective stiffness can be visualized by the planar projection of the direction dependent Young's modulus and generalized bulk modulus, introduced in Section 6.6. In consequence, for each point, two sets of polar plots representing Young's modulus on the one hand and generalized bulk modulus on the other hand, are obtained for a selection of homogenization schemes. Each set of polar plots is combined into one sub-Figure which is arranged according to the position of the point inside the slice of $\mathcal{N}^{\text{planar}}$. This way, a graphical representation of the influence of the fiber orientation on effective stiffnesses is generated. The first slice, visualized in Figure 6.4, contains ten points, each representing one planar orthotropic (Bauer and Böhlke, 2022c, Equation (84)) fiber orientation tensor $\mathbb{N}^{\text{planar}}(\lambda_1, \hat{d}_1, d_8)$ with vanishing parameter d_8 defined in Equation (6.14). For each point,

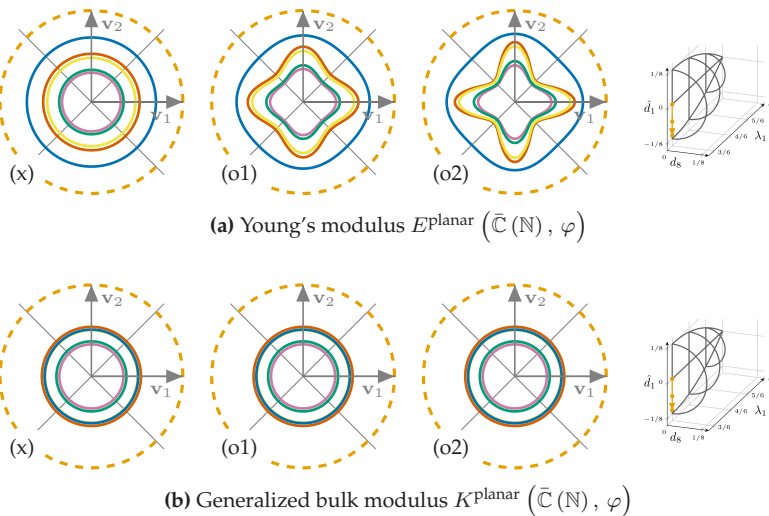


Figure 6.8: Polar plots for selected \mathbb{N} with $\lambda_1 = 3/6$ specified in Figure 6.5a and Table C.1 and mean field approximations specified in the legend in Figure 6.5b. The order along the path in Figure 6.5a is given from left to right.

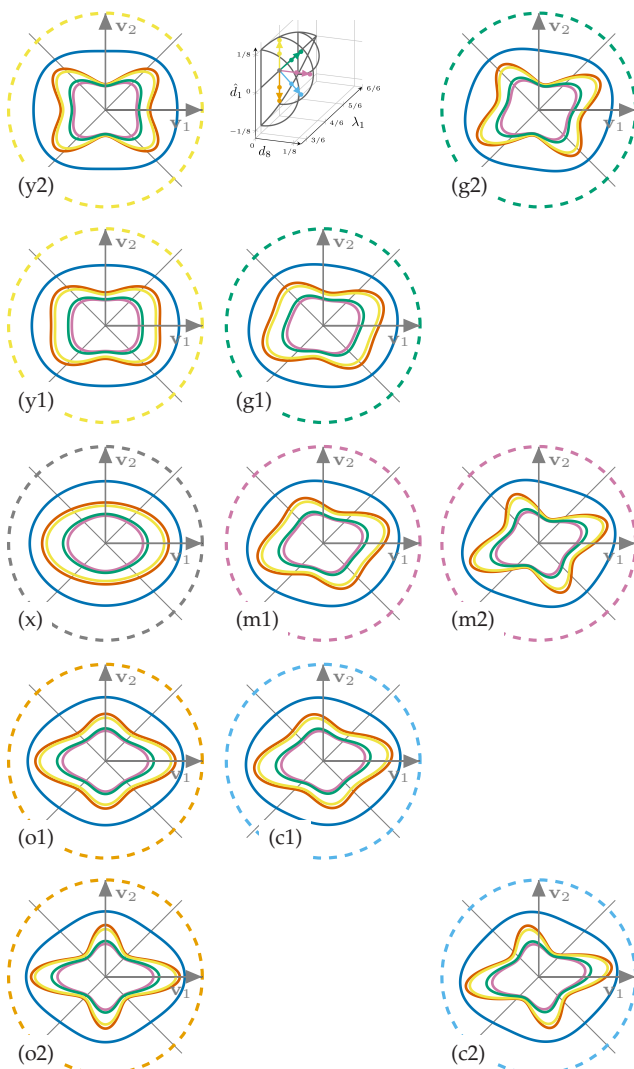


Figure 6.9: Young's modulus $E^{\text{planar}}(\bar{\mathbb{C}}(\mathbb{N}), \varphi)$ for mean field approximations specified in Figure 6.5b. The arrangement of the polar plots follows the arrangement of points in the parameter space of $\mathbb{N}^{\text{planar}}$ with $\lambda_1 = 4/6$ in Figure 6.6a listed in Table C.1.

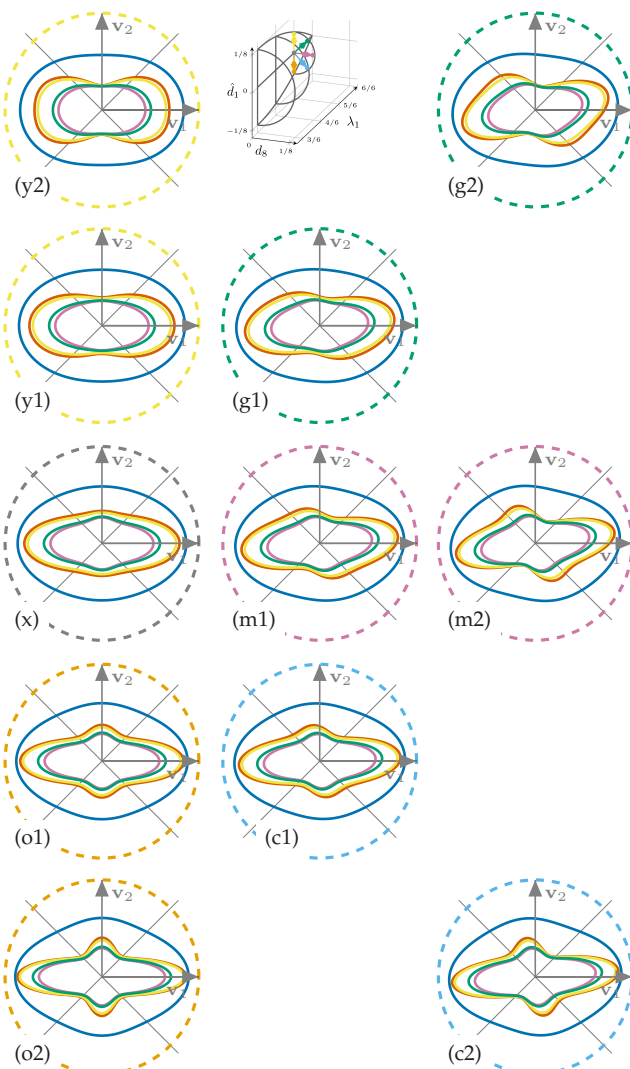


Figure 6.10: Young's modulus $E^{\text{planar}} (\bar{\mathbb{C}}(\mathbb{N}), \varphi)$ for mean field approximations specified in Figure 6.5b. The arrangement of the polar plots follows the arrangement of points in the parameter space of $\mathbb{N}^{\text{planar}}$ with $\lambda_1 = 5/6$ in Figure 6.6b listed in Table C.1.

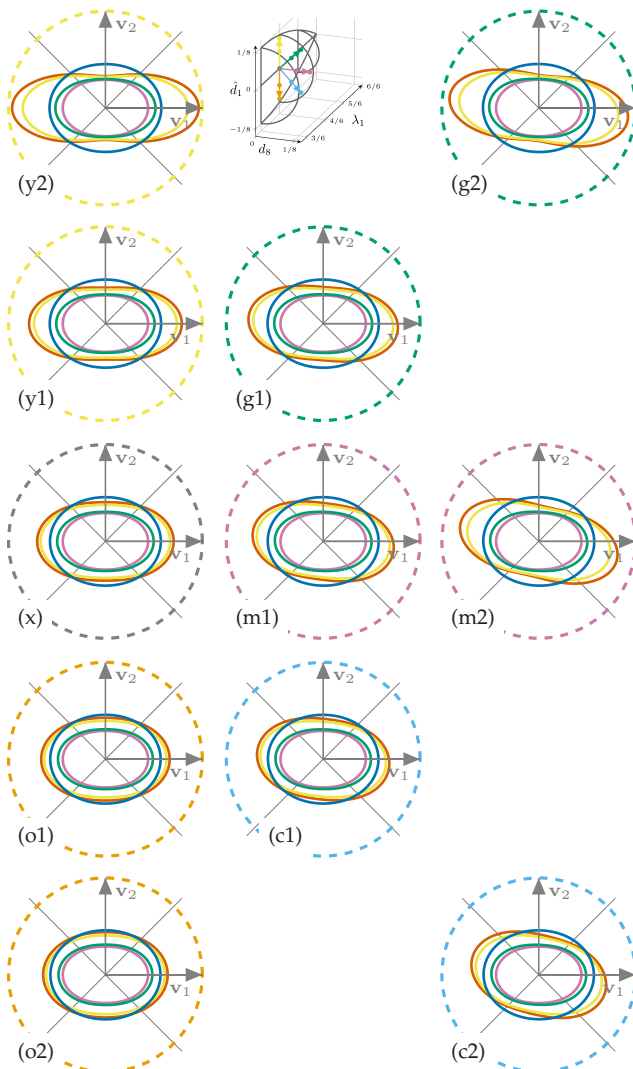


Figure 6.11: Generalized bulk modulus $K^{\text{planar}}(\bar{\mathbb{C}}(\mathbb{N}), \varphi)$ for mean field approximations specified in Figure 6.5b. The arrangement of the polar plots follows the arrangement of points in the parameter space of $\mathbb{N}^{\text{planar}}$ with $\lambda_1 = 4/6$ in Figure 6.6a listed in Table C.1.

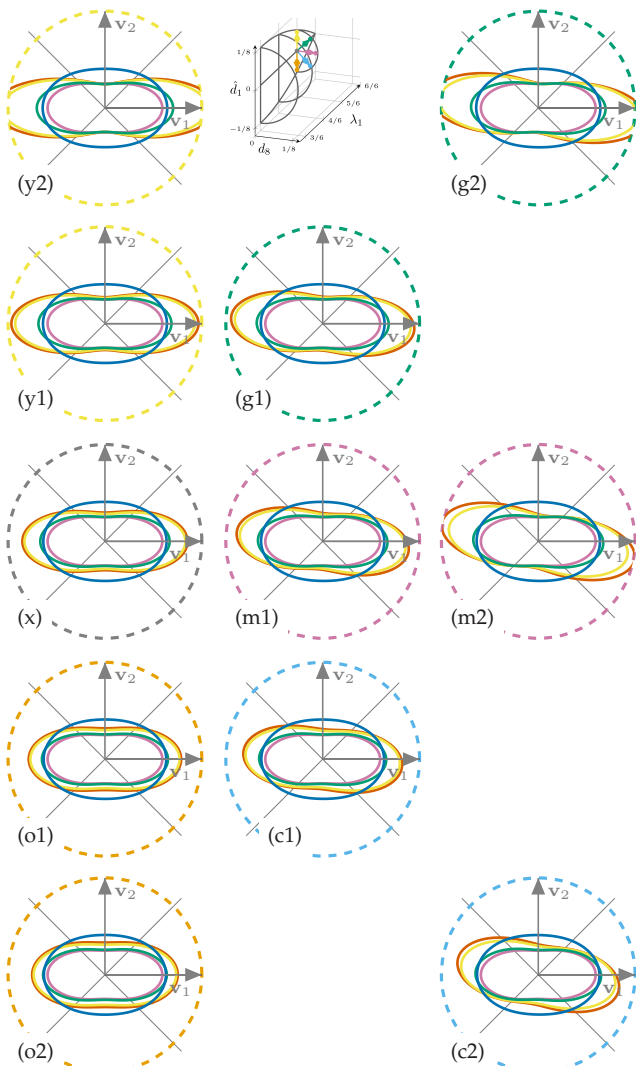


Figure 6.12: Generalized bulk modulus $K^{\text{planar}}(\bar{\mathbb{C}}(\mathbb{N}), \varphi)$ for mean field approximations specified in Figure 6.5b. The arrangement of the polar plots follows the arrangement of points in the parameter space of $\mathbb{N}^{\text{planar}}$ with $\lambda_1 = 5/6$ in Figure 6.6b listed in Table C.1.

a polar plot of $E^{\text{planar}}(\bar{\mathbb{C}}(\mathbb{N}), \varphi)$ is given in Figure 6.7a and a polar plot of $K^{\text{planar}}(\bar{\mathbb{C}}(\mathbb{N}), \varphi)$ is given in Figure 6.7b. The arrangements of the polar plots in Figures 6.7a and 6.7b mimic the position of the points in the overview Figure 6.4 and the correspondence is stressed by the color of the thick dashed circles around the polar plots. The line colors of the polar plots indicate the mean field approximation which are specified in the shared legend in Figure 6.5b. Parameters of each point are given in Table C.1 in C.7.

Similar visualizations based on slices in Figures 6.5a to 6.6b are given in Figures 6.8 to 6.12. Each of the slices in Figures 6.5a to 6.6b represents the variety of planar fourth-order fiber orientation tensors for a fixed second-order fiber orientation tensor, as the parameter λ_1 is constant.

The limits of all plots of E^{planar} are homogeneous and given by 0 GPa and 22 GPa. The limits of all plots of K^{planar} are also homogeneous and given by 0 GPa and 24 GPa.

6.7.2 Observations on bounds

In the unidirectional case, visualized in polar plot (10) in Figure 6.7a, all approximations except $\bar{\mathbb{C}}^{\text{HSW}2}(1, 1)$ coincide (Weng, 1990). Young's modulus $E^{\text{planar}}(\mathbb{C}, \varphi)$ obtained for the approximations $\bar{\mathbb{C}}^{\text{MTOAB}}$ and $\bar{\mathbb{C}}^{\text{MTlinearStiffness}}$ are between the values obtained for $\bar{\mathbb{C}}^{\text{HSW}2}(0, 0)$ and $\bar{\mathbb{C}}^{\text{HSW}2}(1, 1)$. This does not hold for the approximation $\bar{\mathbb{C}}^{\text{MTlinearCompliance}}$. The limiting two-step Hashin-Shtrikman homogenizations are bounds on the energy of the effective material. Both Youngs's modulus and the generalized bulk modulus are material characteristics related to uniaxial tensile tests. Motivated by Figure 6.7b(10), the complementary energy density (Bertram and Glüge, 2013) induced by a virtual direction-dependent unidirectional tensile test starting from a stress-free initial

configuration

$$w^*(\mathbb{C}, \sigma, \mathbf{n}) = \frac{1}{2} \boldsymbol{\sigma}(\sigma, \mathbf{n}) \cdot \mathbb{C}^{-1} [\boldsymbol{\sigma}(\sigma, \mathbf{n})] = \frac{1}{2} \sigma^2 \mathbb{C}^{-1} \cdot \mathbf{n}^{\otimes 4} \quad (6.66)$$

is plotted in Figure C.1, C.2 and C.3 in C.8 for a unit stress $\sigma = 1$ and for all views defined in Figures 6.4 to 6.6b. The energies of the approximations $\bar{\mathbb{C}}^{\text{MTOAB}}$ and $\bar{\mathbb{C}}^{\text{MTlinearStiffness}}$ are within the bounds for all inspected orientation tensors whereas the approximation $\bar{\mathbb{C}}^{\text{MTlinearCompliance}}$ violates the bounds and therefore is non-physical.

6.7.3 Observations on the shape of the Young's modulus

The maximum number of extrema of the Young's modulus E^{planar} within the $\mathbf{v}_1\text{-}\mathbf{v}_2$ -plane is four, as this quantity is obtained by contraction of the effective compliance with a fourth-order moment. The maximum values of the Young's modulus for all mean field approximations point into the directions of maximum fiber content, which are visualized in Bauer and Böhlke (2022a). For example, polar plots with $\hat{\beta} = -\pi/2$, i.e., $d_8 = 0$ and $d_1 \leq 0$, have their maxima aligned with the axes \mathbf{v}_1 or \mathbf{v}_2 , see Figures 6.9 and 6.10.

6.7.4 Observations on the shape of the generalized bulk modulus

In contrast to the Young's modulus, the number of maxima of the generalized bulk modulus K^{planar} and the resulting shapes are strongly limited, as the highest moment of \mathbf{n} which enters K^{planar} is of second order, see Böhlke and Brüggemann (2001). The changes in K^{planar} for fixed second-order fiber orientation tensor contribution, i.e., fixed values of λ_1 , but different fourth-order fiber orientation tensor contribution, i.e., values of \hat{d}_1 and d_8 defining $\text{dev}(\mathbb{N}^{\text{planar}})$, are marginal for the selected approximations $\bar{\mathbb{C}}^{\text{HSW2}}(k_1, k_2)$ and $\bar{\mathbb{C}}^{\text{MTlinearCompliance}}$. These

three approximations take the orientation average on compliance-like quantities. In contrast, the influence of both \hat{d}_1 and d_8 on the remaining approximations $\bar{\mathbb{C}}^{\text{MTOAB}}$ and $\bar{\mathbb{C}}^{\text{MTlinearStiffness}}$ is clearly visible. The latter two approximations take the orientation average on stiffness-like quantities. For these approximations, increase of d_8 induces a clock-wise rotation of the K^{planar} -body whereas increase of \hat{d}_1 leads to a stretch of this body. In Figure 6.8b, no stretch is induced by increase of \hat{d}_1 . It is noted, that E^{planar} and K^{planar} are obtained by contraction of the effective compliance. The strong influence of the fourth-order fiber orientation contribution $\text{dev}(\mathbb{N}^{\text{planar}})$ on the shape of the bulk modulus for the approximations $\bar{\mathbb{C}}^{\text{MTOAB}}$ and $\bar{\mathbb{C}}^{\text{MTlinearStiffness}}$ is subject of further research.

6.7.5 Implications of closure approximations based on second-order fiber orientation tensors

Closure approximations (Advani and Tucker III, 1990; Han and Im, 1999; Cintra Jr and Tucker III, 1995; Chung and Kwon, 2002; Montgomery-Smith et al., 2011a) identify a fourth-order fiber orientation tensor which corresponds to a given second-order fiber orientation tensor. As any second-order orientation tensor is orthotropic or has even stronger material symmetry, closure approximations based on a second-order orientation tensor lead to orthotropic fourth-order fiber orientation tensors. In consequence, any virtual process chain which involves a closure approximation is limited to orthotropic effective stiffnesses. The planar orthotropic subspace is discretized in Fig. 6.4 and discussed in Bauer and Böhlke (2022c). Among the discrete stiffnesses represented in Figures 6.9 to 6.12 only the left column, i.e., those stiffnesses labeled (y2), (y1), (x), (o1), (o2), are orthotropic.

6.8 Summary and conclusions

Computer tomography scans combined with knowledge on the variety of fiber orientation tensors and experience in process simulation, reveal that fiber architectures of sheet molding compound specimen are approximately planar. The planarity assumption significantly reduces the dimensionality of the space of fiber orientation tensors from eleven to three in the orientation coordinate system (Bauer and Böhlke, 2022c). An invariant and redundancy-free parameter set of structurally differing fiber orientation tensors following Bauer and Böhlke (2022a) states the main building block for investigations on the influence of fiber orientation tensors on effective mechanical properties.

The orientation average of transversely isotropic elasticity tensors following Advani and Tucker III (1987) formulated directly in fiber orientation tensors, is explicitly recast as linear invariant composition in the fiber orientation tensors of second- and fourth-order Kanatani third kind (Kanatani, 1984). To the best of the authors knowledge, this essential assumption of the popular orientation average is not mentioned explicitly in the literature. It should be noted, that, e.g., in the field of biomechanics, material models being non-linear in fabric tensors (Cowin, 1985; Turner and Cowin, 1987; Biegler and Mehrabadi, 1995; Cowin and Cardoso, 2011), are established. Such models are based on isotropic tensor functions, i.e., representation theory. A numerical orientation-averaging scheme restricted to the special class of planar fiber orientations based on a maximum entropy reconstruction of fiber orientation distribution functions following Bauer and Böhlke (2022a) is proposed. The new scheme shows fast converges against the exact formulation of Advani and Tucker III (1987) for non-localized fiber orientation tensors which are dominant in sufficient large fiber arrangements.

Four mean field homogenization approximations are reviewed and investigated. The first two approximations are orientation-averaging Mori-

Tanaka following Benveniste (1987) and a two step Hashin-Shtrikman homogenization scheme (Kehrer et al., 2020) both in formulations based on the Advani-Tucker orientation average (Advani and Tucker III, 1987). The remaining two approximations are direct Advani-Tucker orientation averages of either a unidirectional stiffness or compliance obtained by the Mori-Tanaka approximation (Mori and Tanaka, 1973). Effective stiffnesses obtained by the approximations, are visualized by two-dimensional polar plots of Young's and generalized bulk modulus (Böhlke and Brüggemann, 2001). Plots are generated for specific points in the three-dimensional body of structurally differing planar fiber orientation tensors. The developed views establish a new methodology for studies and visualizations of the dependence of material models on planar fourth-order fiber orientation tensors. Inspection of polar plots of the generalized bulk modulus reveals clear structural differences between effective stiffnesses obtained by mean field schemes taking the orientation average in the stiffness or compliance domain. Those stiffnesses averaged in the compliance domain, hardly show a dependence of the generalized bulk modulus on $\text{dev}(\mathbb{N}^{\text{planar}})$ whereas this dependence is pronounced for stiffnesses averaged in the stiffness domain. The reason for this observation and the physical interpretation of the pronounced dependence is subject of further research. Lack of fourth-order contribution to the generalized bulk modulus (Böhlke and Brüggemann, 2001) restricts the possible shapes of its contour plots. Bauer and Böhlke (2022a, Figure 7) visualize reconstructions of fiber orientation distribution functions based on leading fiber orientation tensors up to fourth order. The resulting plots visualize the direct connection between the causing orientation measure and the effected mechanical behavior, e.g., visualized by the effective Young's modulus in Figures 6.9 and 6.10.

The main conclusions of this work are

- Fiber orientations of sheet molding compound are approximately

planar, leading to a reduction of the independent components of fourth-order fiber orientation tensors from eleven to three in the orientation coordinate system.

- An invariant and redundancy-free set of structurally differing fiber orientation tensors of fourth order can be used to investigate the dependence of effective material properties on fiber orientation tensors.
- The orientation average of an elasticity tensor based on an fiber orientation tensor following Advani and Tucker III (1987) is linear in both the elasticity tensor and the fourth-order fiber orientation tensor.
- A new numerical formulation of the Advani-Tucker orientation average in fiber orientation tensors (Advani and Tucker III, 1987) for the special class of planar fiber orientations is proposed based on a maximum entropy reconstruction of fiber orientation distribution functions following Bauer and Böhlke (2022a).
- The orientation dependence of the generalized bulk modulus differs significantly for homogenizations which take the orientation average in the stiffness domain and those which take the average in the compliance domain. In contrast, the direction of maxima of the orientation-dependent Young's modulus is homogeneous for both groups of homogenizations and the difference on the size of the Young's modulus is barely influenced by the fiber orientation tensor.
- The orientation dependence of the effective anisotropic material response, e.g., described by orientation-dependent Young's and generalized bulk modulus, is restricted. Restrictions are caused by the limited averaged information given by fourth-order fiber orientation tensors and due to the constraints of linear elasticity. Possible directional dependencies of the elastic response for Advani-Tucker averaged two-phase materials of isotropic constituents and planar orientation measures are comprehensively presented. This presentation is complete and it's methodology states the main contribution of this work. The methodology can be used to express the orientation dependence

of any quantity which is a function of planar fiber orientation tensors up to fourth order.

- Orthotropy of closure approximations, which are based on second-order fiber orientation tensors, is shown to be a major restriction on the effective anisotropic material response.

The methodology developed for the low-dimensional subspace of planar fourth-order fiber orientation tensors may be applied to sub spaces of fiber orientation tensors with less symmetry.

Chapter 7

Conclusions and Outlook

7.1 Conclusions

Combination of the detailed summaries in Sections 4.8, 5.5 and 6.8, leads to the following insights and conclusions.

Significant progress has been made in the search for a complete description of the phase space of fourth-order fiber orientation tensors. A complete description is obtained for selected subspaces. A natural parameterization of generic fourth-order fiber orientation tensors is given by a linear invariant composition of the isotropic reference state and one second- and one fourth-order deviator in an eigensystem of the corresponding second-order FOT. The use of the eigensystem separates structural properties represented by deviators and superposed rotations. In addition, the parameterization naturally separates second- and fourth-order contributions and can be refined according to material symmetries, thereby reducing the number of independent components significantly. A similar parameterization of second-order FOTs based on an isotropic central state and deviators increases the knowledge, e.g., on transversely isotropic states inside the commonly used orientation triangle. Demanding positive semi-definiteness of fourth-order FOTs, defines admissible parameter ranges. These ranges are given in closed form for transversely isotropic as well as planar orientation states. For weaker constraints, admissible parameter ranges can be obtained numerically

and are visualized for the important orthotropic case. The use of material symmetries artificially reduces the complexity of problems and realizes solvability.

A compact and natural description of admissible fiber orientation tensors allows systematic investigations of processes and methods which use fiber orientation tensors either as input or result. The combination of simple and mathematically motivated parameterizations with the condition of positive semi-definiteness appears trivial, but holds great potential. For example, closure approximations which lead to fourth-order FOTs outside the admissible region, e.g., visualized in Fig. 4.3, can be easily discarded. Algebraic constraints on admissible parameter ranges are connected with intuitive limiting fiber arrangements by the following observation. Orientation states at the boundary of admissible parameter regions for transversely isotropic and planar states, can be represented by a minimal number of Dirac distributions in particular directions, which might be called localized. For measured data, depending on the resolution of the measurement and the size of the reference volume, associated with a single measured FOT, these localized states are not obtained. This observation is explained by the localized character of such orientation states, which is in contrast to the white noise induced by a large number of fibers within the particular reference volume. Furthermore, the structure of admissible regions demonstrates the pronounced role of the isotropic, unidirectional or planar-isotropic orientation states and shows links between these special states.

A deep understanding of the variety of FOTs is crucial for the assessment of closure approximations and demonstrates the ill-posed character of closure problems, postulating an artificial one-to-one mapping between second- and fourth-order FOTs.

The transition from analytical investigations on admissible FOTs to mechanical properties of SMC within this work is guided by a detailed inspection of planar FOTs and corresponding FODF. Therefore, the

connection between FODF and FOT for the planar subspace is investigated. Due to symmetry-induced ambiguities of the eigensystem, admissible parameter sets do not necessarily lead to distinct FOTs. This observation leads to a refinement of the admissible region into a set of admissible and distinct planar FOT of fourth order by removing redundancies. The observed redundancies are two-fold. On the one hand, full isotropy or partial isotropy in the case of transversely isotropic states, induce a continuous randomness of the eigensystem, which leads to a degeneration of the corresponding part of admissible ranges. On the other hand, indefiniteness or ambiguity of the eigensystem of positive definite second-order tensors (Bro et al., 2008), due to their inherent orthotropy, induces a discrete ambiguity which can be handled by a sign convention in a suitable parameterization. Three reconstruction methods of FODF by leading planar FOT lead to fundamentally different results. Deploying a generic truncated Fourier series in a 3D-framework leads to non-planar and non-positive semi-definite FODF. Truncated Fourier series in a 2D-framework ensure planarity, but not positive semi-definiteness. Maximum entropy reconstruction in a 2D-framework leads to reasonable reconstructions which fulfill algebraic constraints. The proposed explicit and minimal formulation of the maximum entropy method represents a valuable tool for non-linear applications which might require numerical integration of tensorial quantities weighted by FODF based on leading FOTs. The reconstruction methods associate a given FOT with the intuitive FODF which is directly associated with fiber distributions, and is more general than ensembles of discrete Dirac distributions.

In order to represent reconstructed FODFs based on distinct planar FOTs, an innovative visualization method is developed in this work. This method can be used to visualize any direction-dependent scalar quantity, which is a function of distinct planar FOT. The method deploys a discretization strategy and consists of overview plots as well as polar

plot ensembles. The overview plots slice the admissible and distinct parameter space and define points on these slices. For each slice, an polar plot ensemble consisting of one polar plot for each point on the slice is given. The views on reconstructed FODFs directly associate FOTs with fiber alignments.

In a subsequent step, the visualization method is applied to effective stiffnesses obtained by several mean field homogenizations which are popular in both academia and industry. The obtained views on the stiffnesses directly associate mechanical properties with FOTs, which are associated with fiber alignment through the views on reconstructed FODFs. In consequence, a complete study of the influence of fiber orientation tensors on effective stiffnesses of SMC, based on the selected homogenizations, is given.

Again, consequences of deploying closure approximations to gain seemingly fourth-order information can be presented. Any reasonable closure approximation is orthotropic and the left most columns in Figures 6.9 to 6.12 represent orthotropic orientation states. In consequence, only one third of the visualized stiffnesses can be obtained, if closure approximations are contained within a virtual process chain. Observations on the algebraic structure of the selected homogenizations complete these investigations.

In summary, the present work provides comprehensive contributions to the understanding of the variety of FOT, being a widely used directional measure. Interaction of this variety with fiber orientation density distributions as well as consequences for derived effective mechanical properties are presented. These findings are seminal to the understanding and design of fiber reinforced plastics in a wide variety of applications.

7.2 Outlook

Departing from this work's conclusions, the following statements provide starting points for future research questions.

- The parameterization of triclinic fourth-order FOTs implies a classification scheme, which can be applied to study fields of FOTs.
- Closure approximations can be systematically assessed by their ability to remain within the admissible parameter region and maintain symmetry.
- The parameterizations based on deviators from the isotropic state naturally induces an interpolation scheme for fourth-order FOTs.
- Advanced material models, e.g., including damage or failure surfaces, can be defined based on the developed parameterizations.
- The planarity assumption with respect to SMC combined with the derived variety of effective stiffnesses offers great potential for efficient clustering techniques for mechanical properties within a virtual process chain. Similar to Goldberg et al. (2017), the admissible parameter space could be discretized.
- The visualization method presenting the dependence of effective mechanical properties on planar FOTs offers the possibility to study and compare additional analytical as well as numerical homogenization schemes.
- The investigations on the dependence of material models on FOTs can be extended to thermo-mechanical models.

Appendix A

Appendices to Chapter 4¹

A.1 Material symmetries of second-order tensors

Following Cowin (1985), any symmetric tensor of second order \mathbf{A} is either isotropic, transversely isotropic or orthotropic. This means, for symmetric second-order tensors, three material symmetry classes exist and representations of \mathbf{A} in its material coordinate system $\{\mathbf{v}_i\}$ are given for the case of isotropy \mathbf{A}^{iso} , transversely isotropy $\mathbf{A}^{\text{transv}}$ and orthotropy

¹ This appendix reproduces the appendix of (Bauer and Böhlke, 2022c), i.e., Bauer, J. K., Böhlke, T., 2022. Variety of fiber orientation tensors. Mathematics and Mechanics of Solids 27 (7), 1185–1211, 10.1177/10812865211057602. Reproduced with permission. ©2021 The Authors. Published by SAGE Publications Ltd under CC BY-NC 4.0

$\mathbf{A}^{\text{ortho}}$ by

$$\mathbf{A}^{\text{iso}} = a_1 \begin{bmatrix} 1 & 0 & 0 \\ 0 & 1 & 0 \\ 0 & 0 & 1 \end{bmatrix} \mathbf{v}_i \otimes \mathbf{v}_j, \quad (\text{A.1})$$

$$\mathbf{A}^{\text{transv}} = \begin{bmatrix} a_1 & 0 & 0 \\ 0 & a_2 & 0 \\ 0 & 0 & a_2 \end{bmatrix} \mathbf{v}_i \otimes \mathbf{v}_j, \quad (\text{A.2})$$

$$\mathbf{A}^{\text{ortho}} = \begin{bmatrix} a_1 & 0 & 0 \\ 0 & a_2 & 0 \\ 0 & 0 & a_3 \end{bmatrix} \mathbf{v}_i \otimes \mathbf{v}_j. \quad (\text{A.3})$$

The principle direction of the transversely isotropic case is randomly chosen to be the first axis. The number of independent coefficients is one, two and three respectively and is indicated by the number of a_i .

A.2 Parameter sets of specific second-order orientation tensors

Table A.1 contains arguments of parameterizations given in Equations (4.25), (4.29) and (4.31) leading to special orientation states.

	$\mathbf{N}(\lambda_1, \lambda_2)$		$\mathbf{N}(\alpha_1, \alpha_3)$		$\mathbf{N}(\hat{a}, \hat{c})$		$\mathbf{N}(\hat{w}_1, \hat{w}_2, \hat{w}_3)$		
	λ_1	λ_2	α_1	α_3	\hat{a}	\hat{c}	\hat{w}_1	\hat{w}_2	\hat{w}_3
isotropic	1/3	1/3	0	0	0	0	a	a	a
unidirectional \mathbf{v}_1	1	0	2/3	0	2/3	-1/3	a	0	0
planar isotropic \mathbf{v}_1	0	1/2	-1/3	0	-1/3	1/6	0	a	a
planar isotropic \mathbf{v}_3	1/2	1/2	0	-1/3	1/6	-1/3	a	a	0

Table A.1: Arguments of parameterizations of \mathbf{N} for special orientation states with $a \in \mathcal{R}_*^+$, i.e., $a > 0$. Note: The orientation states labeled by planar isotropic \mathbf{v}_1 and planar isotropic \mathbf{v}_3 , differ only by ordering convention of the eigenvalues and describe the same physical state.

A.3 Coefficient-wise extrema of moment tensors

Given a triangulation which divides the unit sphere into m surfaces \mathcal{F}_γ with centered normal vectors \mathbf{n}_γ for $\gamma \in [1, \dots, m]$. The integration over S^2 in Equation (4.10) can be interpreted as a weighted summation with discrete weights w_γ derived by the FODF by

$$w_\gamma = \int_{\mathcal{F}_\gamma} \psi(\mathbf{n}) \, d\mathbf{n}. \quad (\text{A.4})$$

The properties of $\psi(\mathbf{n})$ imply non-negative and normalized weights, i.e., $0 \leq w_\gamma$ and $\sum_\gamma w_\gamma = 1$ holds. Definition of \mathbb{N} in Equation (4.10) is the limiting case

$$\mathbb{N} = \lim_{m \rightarrow \infty} \sum_\gamma^m w_\gamma \mathbf{n}_\gamma^{\otimes 4}. \quad (\text{A.5})$$

Defining coefficients of the γ -th moment tensor by $\mathbf{n}_\gamma^{\otimes 4} = (n_\gamma^{\otimes 4})_{\xi\xi} \mathbf{B}_\xi \otimes \mathbf{B}_\zeta$, Equation (A.5) reads

$$N_{\xi\xi}^{(4)} = \lim_{m \rightarrow \infty} \sum_\gamma^m w_\gamma (n_\gamma^{\otimes 4})_{\xi\xi}. \quad (\text{A.6})$$

The set of weights $\left\{ w_\gamma : 0 \leq w_\gamma, \sum_\gamma^m w_\gamma = 1 \right\}$ describes an m -dimensional region \mathcal{W} and \mathbb{N} is linear in these weights. Due to the linearity, the extreme values of \mathbb{N} arise at the boundary of \mathcal{W} , especially at points where only one weight equals one and the remaining weights are zero. Such points are corners of the boundary of \mathcal{W} . As

$$\sum_\gamma^m w_\gamma \left[(n_\gamma^{\otimes 4})_{\xi\xi} - (n_{\min}^{\otimes 4})_{\xi\xi} \right] \geq 0 \quad (\text{A.7})$$

is valid it follows from

$$\sum_{\gamma}^m w_{\gamma} (n_{\gamma}^{\otimes 4})_{\xi\xi} - (n_{\min}^{\otimes 4})_{\xi\xi} \geq 0 \quad (\text{A.8})$$

$$\sum_{\gamma}^m w_{\gamma} (n_{\gamma}^{\otimes 4})_{\xi\xi} \geq (n_{\min}^{\otimes 4})_{\xi\xi} \quad (\text{A.9})$$

that the minimum of a coefficient of a moment tensor $(n_{\min}^{\otimes 4})_{\xi\xi}$ is a lower bound for the corresponding coefficient of the fourth-order orientation tensor $N_{\xi\xi}^{(4)}$. Note, that for a fixed coordinate system, there exists a singular FODF $\psi^{\min}(\mathbf{n})$ of shape

$$\psi^{\min}(\mathbf{n}) = \frac{1}{2} (\delta(\mathbf{n} - \mathbf{n}^*) + \delta(\mathbf{n} + \mathbf{n}^*)) \quad (\text{A.10})$$

leading to $N_{\xi\xi}^{(4)} = (n_{\min}^{\otimes 4})_{\xi\xi}$. Similar reasoning leads to coefficient-wise upper limits of $N_{\xi\xi}^{(4)}$ defined by maximum coefficients of a moment tensor $(n_{\max}^{\otimes 4})_{\xi\xi}$ corresponding to a singular FODF. As a consequence, extreme values of tensor coefficients of \mathbb{N} can be derived from the moment tensor $\mathbf{n}^{\otimes 4}$. However, this coefficient-wise consideration neglects the interaction of the coefficients of \mathbb{N} and the procedure defining the orientation coordinate system $\{\mathbf{v}_i\}$. Tensor coefficients of a representation in a coordinate system, which depends, e.g., on the eigenvectors of \mathbb{N} , may not reach the extreme values reachable in a fixed coordinate system. Another consequence is that the norm of \mathbb{N} is bound by the value one, which is reached for a singular FODF. Parameterization of $\mathbf{n}^{\otimes 4}$ in two angles with

$$\mathbf{n}(\theta, \varphi) = \sin(\theta) \cos(\varphi) \mathbf{e}_1 + \sin(\theta) \sin(\varphi) \mathbf{e}_2 + \cos(\theta) \mathbf{e}_3 \quad (\text{A.11})$$

leads to a representation of the moment tensor by $\mathbf{n}^{\otimes 4} = n_{\xi\xi}^{\otimes 4} \mathbf{B}_\xi \otimes \mathbf{B}_\zeta$ with

$$n_{\xi\xi}^{\otimes 4} = \begin{bmatrix} s_\theta^4 c_\varphi^4 & s_\varphi^2 s_\theta^4 c_\varphi^2 & s_\theta^2 c_\varphi^2 c_\theta^2 & \sqrt{2}s_\varphi s_\theta^3 c_\varphi^2 c_\theta & \sqrt{2}s_\theta^3 c_\varphi^3 c_\theta & \sqrt{2}s_\varphi s_\theta^4 c_\varphi^3 \\ s_\varphi^4 s_\theta^4 & s_\varphi^2 s_\theta^2 c_\theta^2 & \sqrt{2}s_\varphi^3 s_\theta^3 c_\theta & \sqrt{2}s_\varphi^2 s_\theta^3 c_\varphi c_\theta & \sqrt{2}s_\varphi^3 s_\theta^4 c_\varphi & \\ c_\theta^4 & \sqrt{2}s_\varphi s_\theta c_\theta^3 & \sqrt{2}s_\theta c_\varphi c_\theta^3 & \sqrt{2}s_\varphi s_\theta^2 c_\varphi c_\theta^2 & & \end{bmatrix} \quad (\text{A.12})$$

completely	symmetric
------------	-----------

using the short hand notation

$$s_\theta = \sin(\theta), \quad c_\theta = \cos(\theta), \quad s_\varphi = \sin(\varphi), \quad c_\varphi = \cos(\varphi). \quad (\text{A.13})$$

The moment tensor has extreme coefficient-wise values

$$\begin{bmatrix} 0 & 0 & 0 & -b & -a & -a \\ 0 & 0 & & -a & -b & -a \\ 0 & & & -a & -a & -b \end{bmatrix} \leq n_{\xi\xi}^{\otimes 4} \leq \begin{bmatrix} 1 & 1/4 & 1/4 & b & a & a \\ 1 & 1/4 & & a & b & a \\ 1 & & & a & a & b \end{bmatrix} \quad (\text{A.14})$$

completely	symmetric
------------	-----------

$$= \min_{\phi, \theta} n_{\xi\xi}^{\otimes 4}$$

$$= \max_{\phi, \theta} n_{\xi\xi}^{\otimes 4}$$

with $a = \sqrt{2} \frac{3\sqrt{3}}{16}$ and $b = \frac{\sqrt{2}}{8}$. Exemplary application of the coefficient-wise limits on transversely isotropic fourth-order orientation tensors

defined in Equation (4.66), leads to the set

$$\begin{aligned} \mathcal{N}_{\text{linear}}^{\text{transv}} &= \left\{ \mathbb{N}^{\text{transv}} \mid \min_{\phi, \theta} n_{\xi\xi}^{\otimes 4} \leq N_{\xi\xi}^{(4)} \leq \max_{\phi, \theta} n_{\xi\xi}^{\otimes 4} \right\} \\ &= \left\{ \mathbb{N}^{\text{transv}}(\alpha, \rho) \mid -\frac{1}{3} \leq \alpha \leq \frac{2}{3}, \right. \\ &\quad \max \left(\frac{1}{280} (-30\alpha - 7), \frac{1}{105} (15\alpha - 7) \right) \\ &\quad \leq \rho \leq \\ &\quad \left. \frac{1}{840} (15\alpha + 14) \right\} \end{aligned} \quad (\text{A.15})$$

which is visualized in Figure 4.3.

A.4 Parameterization of admissible $\mathbb{N}^{\text{ortho}}$ with Isotropic \mathbf{N}

Explicit parameterization of those fourth-order orientation tensors which contract to the isotropic second-order orientation tensor is given by the set

$$\begin{aligned} \left\{ \mathbb{N}^{\text{ortho}}(\mathbf{N}^{\text{iso}}, d_1, d_2, d_3) \mid \right. & \quad (\text{A.16}) \\ & -\frac{1}{15} \leq d_1 \leq \frac{1}{10}, \\ & -\frac{1}{15} \leq d_2 \leq \frac{7}{45} + \frac{5}{9(45d_1 - 7)}, \\ & \left. -\frac{1}{15} \leq d_3 \leq \frac{4 - 60d_1 - 60d_2 + 675d_1d_2}{60 - 675d_1 - 675d_2} \right\} \subset \mathcal{N}^{\text{ortho}}. \end{aligned}$$

Appendix B

Appendices to Chapter 5¹

B.1 Kelvin-Mandel notation and completely symmetric tensors of fourth order

This appendix directly follows Bauer and Böhlke (2022c;a) for the current work to be self-contained. Kelvin-Mandel notation, explicitly introduced in Mandel (1965), originating from Thomson (1856), discussed in Mehrabadi and Cowin (1990); Cowin and Mehrabadi (1992); Böhlke (2001) and also known as normalized Voigt notation, enables compact two-dimensional representations of fourth-order tensors with at least minor symmetry. A fourth-order tensor $\mathbb{A} = A_{ijkl} \mathbf{e}_i \otimes \mathbf{e}_j \otimes \mathbf{e}_k \otimes \mathbf{e}_l$ is minor symmetric if it has both minor symmetries, i.e., $A_{ijkl} = A_{jikl} = A_{ijlk}$ holds. Introducing base tensors in an arbitrary Cartesian basis $\{\mathbf{e}_i\}$

¹ This appendix reproduces the appendix of (Bauer and Böhlke, 2022a), i.e., Bauer, J. K., Böhlke, T., 2022. Fiber orientation distributions based on planar fiber orientation tensors of fourth order. *Mathematics and Mechanics of Solids*, online first, 10.1177/10812865221093958. Reproduced with permission. ©2022 The Authors. Published by SAGE Publications Ltd under CC BY-NC 4.0

by

$$\begin{aligned} \mathbf{B}_1 &= \mathbf{e}_1 \otimes \mathbf{e}_1, & \mathbf{B}_4 &= \frac{\sqrt{2}}{2} [\mathbf{e}_2 \otimes \mathbf{e}_3 + \mathbf{e}_3 \otimes \mathbf{e}_2], \\ \mathbf{B}_2 &= \mathbf{e}_2 \otimes \mathbf{e}_2, & \mathbf{B}_5 &= \frac{\sqrt{2}}{2} [\mathbf{e}_1 \otimes \mathbf{e}_3 + \mathbf{e}_3 \otimes \mathbf{e}_1], \\ \mathbf{B}_3 &= \mathbf{e}_3 \otimes \mathbf{e}_3, & \mathbf{B}_6 &= \frac{\sqrt{2}}{2} [\mathbf{e}_2 \otimes \mathbf{e}_1 + \mathbf{e}_1 \otimes \mathbf{e}_2], \end{aligned} \quad (\text{B.1})$$

any minor symmetric tensor \mathbb{A} is represented by a six by six matrix of coefficients $A_{\xi\zeta}$

$$\mathbb{A} = A_{ijkl} \mathbf{e}_i \otimes \mathbf{e}_j \otimes \mathbf{e}_k \otimes \mathbf{e}_l = A_{\xi\zeta} \mathbf{B}_\xi \otimes \mathbf{B}_\zeta \quad (\text{B.2})$$

with ξ and ζ summing from 1 to 6. Complete index symmetry of a tensor \mathbb{N} implies the structure

$$\mathbb{N} = \quad (\text{B.3})$$

$$\left[\begin{array}{ccc|ccc} N_{11}^{(4)} & N_{12}^{(4)} & N_{13}^{(4)} & \sqrt{2}N_{14}^{(4)} & \sqrt{2}N_{15}^{(4)} & \sqrt{2}N_{16}^{(4)} \\ & N_{22}^{(4)} & N_{23}^{(4)} & \sqrt{2}N_{24}^{(4)} & \sqrt{2}N_{25}^{(4)} & \sqrt{2}N_{26}^{(4)} \\ & & N_{33}^{(4)} & \sqrt{2}N_{34}^{(4)} & \sqrt{2}N_{35}^{(4)} & \sqrt{2}N_{36}^{(4)} \\ \hline & \text{major symmetric} & & 2N_{23}^{(4)} & 2N_{36}^{(4)} & 2N_{25}^{(4)} \\ & & & & 2N_{13}^{(4)} & 2N_{14}^{(4)} \\ & & & & & 2N_{12}^{(4)} \end{array} \right] \mathbf{B}_\xi \otimes \mathbf{B}_\zeta.$$

As complete index symmetry implies major index symmetry, the coefficient matrix in Equation (B.3) is symmetric. In Equation (B.3) indices of redundant tensor coefficients are colored. The redundancy implies that six coefficients in the upper left quadrant and nine coefficients in the upper right quadrant of the coefficients in Kelvin-Mandel representation define a completely symmetric tensor. This motivates a short hand notation „completely symmetric“, see, e.g., Equation (5.15).

B.2 Parameter sets in polar plots

Table B.1 contains parameter combinations leading to selected fourth-order fiber orientation tensors, which are used to generate polar plots in figures 5.7, 5.8, 5.9 and 5.10. Numerical values of the Lagrange multipliers in Equation (5.72) are given with limited precision and absolute values smaller than $10^{-5} = 1E^{-5}$ set to zero.

Fig.	λ_1	$\hat{\beta}$	\hat{r}	d_1	d_8	L	f_1	f_2	g_1	g_2
5.7(1)	1/2	$\pi/2$	9/80	69/560	0	4.42E0	0	0	-5.30E0	0
5.7(2)	2/3	$\pi/2$	1/10	61/630	0	6.43E0	-7.69E0	0	-6.12E0	0
5.7(3)	5/6	$\pi/2$	1/16	89/5040	0	1.68E1	-2.46E1	0	-9.77E0	0
5.7(4)	1/2	0	0	3/280	0	8.38E-1	0	0	0	0
5.7(5)	2/3	0	0	-1/315	0	9.58E-1	-6.67E-1	0	1.20E-1	0
5.7(6)	5/6	0	0	-113/2520	0	1.45E0	-1.34E0	0	6.49E-1	0
5.7(7)	1/2	$-\pi/2$	9/80	-57/560	0	4.42E0	0	0	5.30E0	0
5.7(8)	2/3	$-\pi/2$	1/10	-13/126	0	5.01E0	-3.63E-1	0	5.89E0	0
5.7(9)	5/6	$-\pi/2$	1/16	-541/5040	0	8.20E0	-8.34E-1	0	9.13E0	0
5.7(10)	1	0	0	-4/35	0	1.84E3	-5.51E0	1.03E1	1.81E3	-5.18E0
5.8(0)	1/2	$-\pi/2$	1/16	-29/560	0	8.38E-1	0	0	0	0
5.8(01)	1/2	$-\pi/2$	9/80	-57/560	0	1.18E0	0	0	1.16E0	0
5.8(02)	1/2	$-\pi/2$	1/16	-1/180	0	4.42E0	0	0	5.30E0	0
5.8(1)	1/2	$-\pi/4$	1/16	$\sqrt{2}/32$	0	1.18E0	0	0	-8.20E-1	0
5.8(2)	1/2	$-\pi/4$	9/80	$3/280 - \sqrt{2}/160$	0	4.42E0	0	0	3.75E0	-3.75E0
5.8(3)	1/2	$-\pi/2$	1/16	9/160	0	1.18E0	0	0	-1.16E0	0
5.8(4)	1/2	$\pi/4$	1/16	$3/280 + \sqrt{2}/32$	0	1.18E0	0	0	-8.20E-1	-8.20E-1
5.8(5)	1/2	$\pi/4$	9/80	$3/280 + 9\sqrt{2}/160$	0	4.42E0	0	0	-3.75E0	-3.75E0
5.8(6)	1/2	$\pi/2$	1/16	41/560	0	1.18E0	0	0	-1.16E0	0
5.8(7)	1/2	$\pi/2$	9/80	69/560	0	4.42E0	0	0	-5.30E0	0
5.9(8)	2/3	0	0	-1/315	0	9.58E-1	-6.67E-1	0	1.20E-1	0
5.9(01)	2/3	$-\pi/2$	1/18	-37/630	0	1.30E0	-4.54E-1	0	1.30E0	0
5.9(02)	2/3	$-\pi/2$	1/10	-13/126	0	5.01E0	-3.63E-1	0	5.89E0	0
5.9(03)	2/3	$-\pi/4$	1/18	$-\sqrt{2}/36 - 1/315$	$\sqrt{2}/36$	1.31E0	-5.86E-1	3.36E-1	9.58E-1	-8.36E-1
5.9(04)	2/3	$-\pi/4$	1/10	$-\sqrt{2}/20 - 1/315$	$\sqrt{2}/20$	5.20E0	-1.39E0	2.51E0	4.22E0	-4.15E0
5.9(05)	2/3	0	1/18	-1/315	1/18	1.32E0	-1.08E-1	4.71E-1	1.20E-1	-1.19E0
5.9(06)	2/3	0	1/10	-1/315	1/10	5.68E0	-3.93E0	3.60E0	8.21E-2	-5.99E0
5.9(07)	2/3	$\pi/4$	1/18	$1/315 + \sqrt{2}/36$	$\sqrt{2}/36$	1.33E0	3.60E0	-7.18E-1	-8.40E-1	0
5.9(08)	2/3	$\pi/4$	1/10	$-1/315 + \sqrt{2}/20$	$\sqrt{2}/20$	6.21E0	-6.56E0	2.59E0	-4.26E0	-4.35E0
5.9(09)	2/3	$\pi/2$	1/18	11/1210	0	1.33E0	-1.33E0	0	-1.07E0	0
5.9(10)	2/3	$\pi/2$	1/10	61/630	0	6.43E0	-7.69E0	0	-6.12E0	0
5.10(01)	5/6	0	-113/2520	0	1.45E0	-1.34E0	0	6.49E-1	0	0
5.10(02)	5/6	$\pi/4$	5/144	-401/5040	0	2.00E0	-9.88E-1	0	1.96E0	0
5.10(03)	5/6	$-\pi/2$	1/16	-541/5040	0	8.20E0	-8.34E-1	0	9.13E0	0
5.10(04)	5/6	$-\pi/4$	5/144	-113/2520 + $5\sqrt{2}/288$	$5\sqrt{2}/288$	1.29E0	-9.33E-1	1.59E0	-9.71E-1	0
5.10(05)	5/6	$-\pi/4$	1/16	-113/2520 - $\sqrt{2}/32$	$\sqrt{2}/32$	9.37E0	-4.63E0	7.93E0	-6.27E0	0
5.10(06)	5/6	0	5/144	-113/2520	5/144	2.07E0	-1.93E0	1.25E0	6.77E-1	-1.36E0
5.10(07)	5/6	0	1/16	-113/2520	1/16	1.23E1	-1.20E1	1.17E1	5.68E-1	-9.41E0
5.10(08)	5/6	$\pi/4$	5/144	-113/2520 + $5\sqrt{2}/288$	$5\sqrt{2}/288$	1.95E0	-2.37E0	7.97E-1	-1.91E-1	-9.20E-1
5.10(09)	5/6	$\pi/4$	1/16	-113/2520 + $\sqrt{2}/32$	$\sqrt{2}/32$	1.55E1	-2.09E1	8.87E0	-6.48E0	-7.31E0
5.10(10)	5/6	$\pi/4$	1/144	-17/1680	0	1.68E1	-2.46E1	0	-5.16E-1	0
5.10(11)	5/6	$\pi/2$	1/16	89/5040	0	9.77E0	-9.77E0	0	0	0

Table B.1: See Appendix B.2

Appendix C

Appendices to Chapter 6¹

C.1 Kelvin-Mandel notation and completely symmetric tensors of fourth order

This appendix is shared with Chapter 5 and contained in Appendix B.1.

C.2 Harmonic decomposition of transversely isotropic elasticity tensors

Following Spencer (1982); Lubarda and Chen (2008); Walpole (1969), any transversely isotropic elasticity tensor can be parameterized by five scalars and a direction \mathbf{q} . For any choice of a non-unique orthonormal coordinate system \mathbf{m}_i with $\mathbf{m}_1 = \mathbf{q}$, there exists a mapping

$$\hat{\mathbf{Q}}(\mathbf{q}) = \mathbf{m}_i \otimes \mathbf{e}_i \quad (\text{C.1})$$

¹ This appendix reproduces the appendix of (Bauer and Böhlke, 2022b), i.e., Bauer, J. K., Böhlke, T., 2022. On the dependence of orientation-averaging mean field homogenization on planar fourth-order fiber orientation tensors. Mechanics of Materials 170, 104307, 10.1016/j.mechmat.2022.104307. Reproduced with permission. ©2022 The Authors. Published by Elsevier Ltd under CC BY 4.0

and enables the following representation of a transversely isotropic stiffness

$$\mathbb{C}^{\text{transv}}(h_1, h_2, h_3, h_4, h_5, \mathbf{q})$$

$$= \hat{\mathbf{Q}}(\mathbf{q}) \star \left(\begin{bmatrix} C_{11} & C_{12} & C_{12} & 0 & 0 & 0 \\ & C_{22} & C_{23} & 0 & 0 & 0 \\ & & C_{22} & 0 & 0 & 0 \\ & & & C_{22} - C_{23} & 0 & 0 \\ \text{sym} & & & & 2C_{55} & 0 \\ & & & & & 2C_{55} \end{bmatrix} \mathbf{B}_\xi \otimes \mathbf{B}_\zeta \right) \quad (\text{C.2})$$

$$\begin{aligned} &= h_1 \mathbb{P}_1 + h_2 \mathbb{P}_2 + \hat{\mathbf{Q}}(\mathbf{q}) \star \left[h_3 \mathbb{J}_3 [\mathbf{F}^{\text{transvx}}] \right. \\ &\quad \left. + h_4 \mathbb{J}_4 [\mathbf{F}^{\text{transvx}}] + h_5 \mathbb{F}^{\text{transvx}} \right] \end{aligned} \quad (\text{C.3})$$

with transversely isotropic structure tensors (Olive et al., 2018; Müller and Böhlke, 2016; Bauer and Böhlke, 2022c)

$$\mathbf{F}^{\text{transvx}} = \text{dev}(\mathbf{N}^{\text{UD}}) = \frac{2}{3} \begin{bmatrix} 1 & 0 & 0 \\ & -1/2 & 0 \\ \text{sym} & & -1/2 \end{bmatrix} \mathbf{e}_i \otimes \mathbf{e}_j \quad (\text{C.4})$$

$$\begin{aligned} \mathbb{F}^{\text{transvx}} &= \text{dev}(\mathbb{N}^{\text{UD}}) \\ &= \frac{1}{35} \begin{bmatrix} 8 & -4 & -4 & \left| \begin{array}{ccc} 0 & 0 & 0 \end{array} \right. \\ & 3 & 1 & \left| \begin{array}{ccc} 0 & 0 & 0 \end{array} \right. \\ & & 3 & \left| \begin{array}{ccc} 0 & 0 & 0 \end{array} \right. \\ \hline & \text{completely} & & \text{symmetric} \end{bmatrix} \mathbf{B}_\xi \otimes \mathbf{B}_\zeta \end{aligned} \quad (\text{C.5})$$

and isotropic sixth order tensors

$$\mathbb{J}_3 = [\delta_{ij}\delta_{km}\delta_{ln} + \delta_{kl}\delta_{im}\delta_{jn}] \mathbf{e}_i \otimes \mathbf{e}_j \otimes \mathbf{e}_k \otimes \mathbf{e}_l \otimes \mathbf{e}_m \otimes \mathbf{e}_n \quad (\text{C.6})$$

$$\begin{aligned} \mathbb{J}_4 = & \frac{1}{8} [\delta_{in}\delta_{jk}\delta_{lm} + \delta_{in}\delta_{jl}\delta_{km} + \delta_{im}\delta_{jk}\delta_{ln} \\ & + \delta_{im}\delta_{jl}\delta_{kn} + \delta_{ik}\delta_{jm}\delta_{ln} + \delta_{ik}\delta_{jn}\delta_{lm} \\ & + \delta_{il}\delta_{jm}\delta_{kn} + \delta_{il}\delta_{jn}\delta_{km}] \mathbf{e}_i \otimes \mathbf{e}_j \otimes \mathbf{e}_k \otimes \mathbf{e}_l \otimes \mathbf{e}_m \otimes \mathbf{e}_n. \end{aligned} \quad (\text{C.7})$$

The scaling factors $2/3$ and $1/35$ of the structure tensors in Equations (C.4) and (C.5) do not lead to a norm of value one. This is in contrast to formulations in, e.g., Fernández and Böhlke (2019, Equation (75)), but leads to a direct connection to unidirectional fiber orientation tensors $\mathbf{N}^{\text{UD}} = \mathbf{v}_1 \otimes \mathbf{v}_1$ and $\mathbb{N}^{\text{UD}} = \mathbf{B}_1^{\text{v}} \otimes \mathbf{B}_1^{\text{v}}$ and compact expressions for h_i with $i \in \{1, 2, 3, 4, 5\}$ in Equation (C.3) which are related to the tensor components in Equation (C.2) by

$$h_1 = 3K = \frac{1}{3} [C_{11} + 4C_{12} + 2C_{22} + 2C_{23}] \quad (\text{C.8})$$

$$h_2 = 2G = \frac{1}{15} [2C_{11} - 4C_{12} + 7C_{22} - 5C_{23} + 12C_{55}] \quad (\text{C.9})$$

$$h_3 = \frac{1}{7} [C_{11} + 5C_{12} + C_{22} - 7C_{23} - 4C_{55}] \quad (\text{C.10})$$

$$h_4 = \frac{1}{14} [2C_{11} - 4C_{12} - 5C_{22} + 7C_{23} + 6C_{55}] \quad (\text{C.11})$$

$$h_5 = \frac{1}{35} [C_{11} - 2C_{12} + C_{22} - 4C_{55}] \quad (\text{C.12})$$

with the bulk modulus K and the shear modulus G . Equations (C.1) to (C.3) motivate a short hand notation for a transversely isotropic elasticity tensor using $\lfloor \cdot \rfloor$ with

$$\mathbb{C}^{\text{transv}}(h_1, h_2, h_3, h_4, h_5, \mathbf{q}) = \left[h_1, h_2, h_3, h_4, h_5, \mathbf{q} \right]. \quad (\text{C.13})$$

Following Rychlewski (2000), Equation (C.3) represents the classical linear invariant decomposition of a transversely isotropic elasticity tensor into irreducible parts. The classical linear invariant decomposition is one out of an infinite number of possible linear invariant decompositions (Forte and Vianello, 1996; Rychlewski, 2000). Any non-classical linear

invariant decomposition leads to a representation of $\mathbb{C}^{\text{transv}}$ which differs from Equation (C.3) by the set of isotropic tensors J_3, J_4 and the values of the corresponding coefficients h_3 and h_4 .

C.3 Reformulation of the Advani-Tucker orientation average

Listing C.1 contains symbolic tensor manipulation code to validate the representation of the Advani-Tucker orientation average in the formulation given in Equation (6.16) and which is based on the classical linear invariant decomposition (Rychlewski, 2000).

Listing C.1: Validation of the orientation average following Advani and Tucker III (1987) given in Equation (6.16)

```
1 import sympy as sp
2 import symbolic as sb
3
4
5 D2 = sb.fabric_tensor.dev2_by_la0_la1()
6 D4 = sb.fabric_tensor.dev4_triclinic_by_d()
7 N4 = sb.special.combine_to_N4(D2=D2, D4=sb.tensorrr(D4))
8
9 # Equation (C.3) Transversely isotropic stiffness
10 stiffness = sb.material_symmetry.
11     transversely_isotropic_x_minimal_harmonic_normalized(
12         normalization="structure_tensor_multiplicity"
13     )
14 print("Orientation tensor fourth-order Kanatani first kind =\n", N4)
15 print("Transversely isotropic stiffness =\n", stiffness)
16
17 averager = sb.orientation_average.AdvaniTucker(N4=N4)
18 average = averager.average(stiffness)
19
20 decomposer_Rych = sb.elasticity.Rychlewski2000()
21 decomposition = decomposer_Rych.decompose_classical_harmonic(
22     stiffness=sb.tensorrr(average)
23 )["parts"]
```

```

26 def test_equality(A, B):
27     return sp.simplify(A) == sp.simplify(B)
28
29
30 assert test_equality(decomposition["h1"], sb.abc.h1)
31 assert test_equality(decomposition["h2"], sb.abc.h2)
32 assert test_equality(decomposition["H1"], D2 * sb.abc.h3)
33 assert test_equality(decomposition["H2"], D2 * sb.abc.h4)
34 assert test_equality(sb.mandel(decomposition["H"]), D4 * sb.abc.h5)

```

C.4 Advani-Tucker Orientation Average of Minor Symmetric Tensors

A generic transversely isotropic fourth-order tensor, which has both minor symmetries but lacks major symmetry, i.e., $H_{ijkl} = H_{ijlk} = H_{jikl}$ but $H_{ijkl} \neq H_{klji}$ with $\mathbb{H}^{\text{transv}} = H_{ijkl}\mathbf{e}_i \otimes \mathbf{e}_j \otimes \mathbf{e}_k \otimes \mathbf{e}_l$, depends on a direction \mathbf{q} and six scalars, see Schröder and Gross (2004); Brannon (2018). For any choice of a non-unique orthonormal coordinate system \mathbf{m}_i with $\mathbf{m}_1 = \mathbf{q}$, there exists a mapping

$$\hat{\hat{\mathbf{Q}}}(\mathbf{q}) = \mathbf{m}_i \otimes \mathbf{e}_i, \quad (\text{C.14})$$

which enables the following representation of a transversely isotropic minor symmetric fourth-order tensor lacking the major symmetry

$$\begin{aligned} \mathbb{H}^{\text{transv}}(H_{11}, H_{22}, H_{12}, H_{21}, H_{23}, H_{55}, \mathbf{q}) &= \\ \hat{\hat{\mathbf{Q}}}(\mathbf{q}) \star \left(\begin{bmatrix} H_{11} & H_{12} & H_{12} & 0 & 0 & 0 \\ H_{21} & H_{22} & H_{23} & 0 & 0 & 0 \\ H_{21} & H_{23} & H_{22} & 0 & 0 & 0 \\ 0 & 0 & 0 & H_{22} - H_{23} & 0 & 0 \\ 0 & 0 & 0 & 0 & 2H_{55} & 0 \\ 0 & 0 & 0 & 0 & 0 & 2H_{55} \end{bmatrix} \mathbf{B}_\xi \otimes \mathbf{B}_\zeta \right). \end{aligned} \quad (\text{C.15})$$

In other words, if the transversely isotropic axis is aligned with the e_1 -axis of the coordinate system underlying the Kelvin-Mandel basis $\mathbf{B}_\xi \otimes \mathbf{B}_\zeta$ in Equation (C.15), the matrix representation of Kelvin-Mandel components has the simplified structure shown in Equation (C.15). Compared to the representation of $\mathbb{C}^{\text{transv}}$ in Equation (C.2), lack of the major symmetry of $\mathbb{H}^{\text{transv}}$ results in one additional independent tensor component in Equation (C.15). In order to extend the reformulation of the Advani-Tucker orientation average in Equation (6.16) to tensors which lack the major symmetry, harmonic decomposition (Forte and Vianello, 1996; Rychlewski, 2000) of such tensors is investigated following Fernández and Böhlke (2019, Section 2.4) and Lobos et al. (2017, Appendix A). Lack of major symmetry of a minor symmetric fourth-order tensor, potentially adds three additional sub spaces of orders one, two and three, to the sub spaces of its harmonic decomposition. If the decomposed quantity is major symmetric, the contributions of these three additional sub spaces are zero (Lobos et al., 2017, Section 2.4). It is easy to show, that no non-vanishing first-order tensor \mathbf{a} fulfills

$$\mathbf{Q} \star \mathbf{a} = \mathbf{a} \quad \forall \quad \mathbf{Q} \in \mathcal{S}^{\text{transv}} \quad (\text{C.16})$$

with the transversely isotropic symmetry group $\mathcal{S}^{\text{transv}}$. Following Bran-non (2018), the same holds for harmonic tensors of third order. In consequence, the additional degree of freedom of $\mathbb{H}^{\text{transv}}$ in Equation (C.15) compared to $\mathbb{C}^{\text{transv}}$ in Equation (C.2) corresponds to the additional subspace of second order in the harmonic decomposition of minor symmetric fourth-order tensors which lack major symmetry. As the symmetry group of a tensor is the intersection of the symmetry groups of its harmonic parts (Forte and Vianello, 1996), transversely isotropy of $\mathbb{H}^{\text{transv}}$ demands that this subspace is also transversely isotropic, making it one-dimensional and being a multiple of a structure tensor $\mathbf{F}^{\text{transvx}}$ defined in Equation (C.4). Consequently, $\mathbb{H}^{\text{transv}}$ can be represented by

extending Equation (C.3) to

$$\begin{aligned} \mathbb{H}^{\text{transv}}(h_1, h_2, h_3, h_4, h_5, h_6, \mathbf{q}) \\ = h_1 \mathbb{P}_1 + h_2 \mathbb{P}_2 + \hat{\mathbf{Q}}(\mathbf{q}) \star \left[h_3 \mathbb{J}_3 [\mathbf{F}^{\text{transvx}}] + h_4 \mathbb{J}_4 [\mathbf{F}^{\text{transvx}}] \right. \\ \left. + h_5 \mathbb{F}^{\text{transvx}} + h_6 \mathbb{J}_6 [\mathbf{F}^{\text{transvx}}] \right] \end{aligned} \quad (\text{C.17})$$

with $\mathbf{F}^{\text{transvx}}$, $\mathbb{F}^{\text{transvx}}$, \mathbb{J}_3 and \mathbb{J}_4 defined in Equations (C.4) to (C.7) and with the isotropic sixth-order tensor

$$\mathbb{J}_6 = [-\delta_{ij}\delta_{kn}\delta_{lm} + \delta_{in}\delta_{jm}\delta_{kl}] \mathbf{e}_i \otimes \mathbf{e}_j \otimes \mathbf{e}_k \otimes \mathbf{e}_l \otimes \mathbf{e}_m \otimes \mathbf{e}_n \quad (\text{C.18})$$

following Fernández and Böhlke (2019), acting as

$$\mathbb{J}_6 [\mathbf{H}] = -\mathbf{I} \otimes \mathbf{H} + \mathbf{H} \otimes \mathbf{I}. \quad (\text{C.19})$$

The connection between h_i for $i \in [1, 2, 3, 4, 5]$ and components H_{ij} in Equation (C.15) follows the pattern in Equations (C.8) to (C.12) combined with

$$h_6 = \frac{1}{2} (H_{12} - H_{21}). \quad (\text{C.20})$$

Based on the representation of $\mathbb{H}^{\text{transv}}$ in Equation (C.17), the Advani-Tucker orientation average (Advani and Tucker III, 1987) given in equation (6.16) can be extended to minor symmetric fourth-order tensors which lack the major symmetry, leading to

$$\begin{aligned} \langle \mathbb{H}^{\text{transv}}(h_1, h_2, h_3, h_4, h_5, h_6, \mathbf{q}) \rangle_{\text{ATN}}(\mathbf{N}) = h_1 \mathbb{P}_1 + h_2 \mathbb{P}_2 \\ + h_3 \mathbb{J}_3 [\text{dev}(\mathbf{N})] + h_4 \mathbb{J}_4 [\text{dev}(\mathbf{N})] + h_5 \text{dev}(\mathbf{N}) + h_6 \mathbb{J}_6 [\text{dev}(\mathbf{N})] \end{aligned} \quad (\text{C.21})$$

with $\text{dev}(\mathbf{N})$, $\text{dev}(\mathbf{N})$ defined in Equations (6.17) and (6.18). An alternative representation closely following the original formulation of Advani

and Tucker III (1987) is given by

$$\begin{aligned} (\langle \mathbb{H}^{\text{transv}} \rangle_{\text{ATN}})_{ijkl} &= b_1 N_{ijkl}^{(4)} \\ &\quad + b_2 N_{ij} \delta_{kl} + b_6 N_{kl} \delta_{ij} \\ &\quad + b_3 (N_{ij} \delta_{jl} + N_{il} \delta_{jk} + N_{jl} \delta_{ik} + N_{jk} \delta_{il}) \\ &\quad + b_4 \delta_{ij} \delta_{kl} + b_5 (\delta_{ik} \delta_{jl} + \delta_{il} \delta_{jk}) \end{aligned} \quad (\text{C.22})$$

with component representations in an arbitrary coordinate system

$$\mathbb{N} = N_{ijkl}^{(4)} \mathbf{e}_i \otimes \mathbf{e}_j \otimes \mathbf{e}_k \otimes \mathbf{e}_l \quad (\text{C.23})$$

$$\mathbf{N} = N_{ij} \mathbf{e}_i \otimes \mathbf{e}_j. \quad (\text{C.24})$$

The coefficients b_i for $i \in [1, 2, 3, 4, 5, 6]$ are defined by

$$b_1 = H_{1111} + H_{2222} - H_{1122} - H_{2211} - 4 H_{1212} \quad (\text{C.25})$$

$$b_2 = H_{1122} - H_{2233} \quad (\text{C.26})$$

$$b_3 = H_{1212} + \frac{1}{2} (H_{2233} - H_{2222}) \quad (\text{C.27})$$

$$b_4 = H_{2233} \quad (\text{C.28})$$

$$b_5 = H_{2222} - H_{2233} \quad (\text{C.29})$$

$$b_6 = H_{2211} - H_{2233} \quad (\text{C.30})$$

based on tensor components of $\mathbb{H}^{\text{transv}} = H_{ijkl} \mathbf{e}_i \otimes \mathbf{e}_j \otimes \mathbf{e}_k \otimes \mathbf{e}_l$ in a coordinate system with \mathbf{e}_1 aligned along the transversely isotropic axis of $\mathbb{H}^{\text{transv}}$, i.e., the tensor components H_{ijkl} are directly related to the Kelvin-Mandel components H_{ij} in Equation (C.15). If the quantity to be averaged is major symmetric, the coefficients in Equations (C.25) to (C.30) coincide with those for the original formulation Advani and Tucker III (1987), e.g., given in Brylka (2017, Equation (2.89)) or Kehrer et al. (2020, Equation (27)).

C.5 Connection to Notation in Kehrer et al. (2020)

The two-step scheme in Equations (6.32) and (6.33) simplifies to the one proposed in Kehrer et al. (2020), if $k_1 = 0$ or $k_1 = 1$ and $k = k_2$. Equations (C.31) and (C.32) connect the notation of this work on the left hand side and the notation of Kehrer et al. (2020) on the right hand by

$$\bar{\mathbb{C}}^{\text{HSW}2}(k_1 = 0, k_2 = k, \dots) \hat{=} \bar{\mathbb{C}}^{\text{HS}^-}(k), \quad (\text{C.31})$$

$$\bar{\mathbb{C}}^{\text{HSW}2}(k_1 = 1, k_2 = k, \dots) \hat{=} \bar{\mathbb{C}}^{\text{HS}^+}(k). \quad (\text{C.32})$$

C.6 Component representations of tensor inversions

Explicit representations of components after matrix inversion in Equation (6.43) are given by

$$h_1^B = 3(105h_2 + 140h_4 + 36h_5)/b_1 \quad (\text{C.33})$$

$$h_2^B = 105(33075h_1h_2^2 + 22050h_1h_2h_4 + 5670h_1h_2h_5 \quad (\text{C.34})$$

$$\begin{aligned} & - 17640h_1h_4^2 - 3780h_1h_4h_5 - 864h_1h_5^2 - 52920h_2h_3^2 \\ & - 141120h_2h_3h_4 - 94080h_2h_4^2 + 17640h_3^2h_4 + 4536h_3^2h_5 \\ & + 47040h_3h_4^2 + 12096h_3h_4h_5 + 31360h_4^3 + 8064h_4^2h_5)/(b_1b_2) \end{aligned}$$

$$\begin{aligned} h_3^B = 45(102900h_1h_2h_4 + 98000h_1h_4^2 - 2520h_1h_4h_5 - 3600h_1h_5^2 \quad (\text{C.35}) \\ & - 77175h_2h_3^2 - 102900h_2^2h_4 - 44100h_2h_3^2 - 66150h_2h_3h_4 \\ & + 13230h_2h_3h_5 - 9800h_2h_4^2 + 17640h_2h_4h_5 - 117600h_3h_4^2 \\ & + 22680h_3^2h_5 - 245000h_3h_4^2 + 34020h_3h_4h_5 + 1008h_3h_5^2 \\ & - 117600h_4^3 + 5040h_4^2h_5 + 1344h_4h_5^2)/(b_1b_2), \end{aligned}$$

$$\begin{aligned} h_4^B = & -225(15435h_1h_2h_4 + 14700h_1h_4^2 - 378h_1h_4h_5 - 540h_1h_5^2) \quad (\text{C.36}) \\ & - 6615h_2h_3^2 - 17640h_2h_3h_4 - 11760h_2h_4^2 - 17640h_3^2h_4 \\ & + 3402h_3^2h_5 - 47040h_3h_4^2 + 9072h_3h_4h_5 \\ & - 31360h_4^3 + 6048h_4^2h_5)/(b_1b_2) \end{aligned}$$

$$\begin{aligned} h_5^B = & -1575(2205h_1h_2h_5 - 5880h_1h_4^2 - 2730h_1h_4h_5 + 216h_1h_5^2) \quad (\text{C.37}) \\ & - 6615h_2h_3^2 - 17640h_2h_3h_4 - 11760h_2h_4^2 + 13230h_3^2h_4 \\ & - 1008h_3^2h_5 + 35280h_3h_4^2 - 2688h_3h_4h_5 + 23520h_4^3 \\ & - 1792h_4^2h_5)/(b_1b_2), \quad (\text{C.38}) \end{aligned}$$

with

$$\begin{aligned} b_1 = & 315h_1h_2 + 420h_1h_4 + 108h_1h_5 - 630h_3^2 - 1680h_3h_4 \\ & - 1120h_4^2 \quad (\text{C.39}) \end{aligned}$$

$$b_2 = (105h_2 - 140h_4 + 6h_5)(105h_2 + 70h_4 - 24h_5), \quad (\text{C.40})$$

after orientation-averaging in Equation (6.44) by

$$\begin{aligned} E_{11} = & -\frac{1}{35} \left[35B_{11}d_1 - 35B_{11}\lambda_1 + 4B_{11} - 70B_{12}d_1 - 8B_{12} \right. \\ & \left. + 35B_{22}d_1 + 35B_{22}\lambda_1 - 31B_{22} - 140B_{55}d_1 - 16B_{55} \right] \quad (\text{C.41}) \end{aligned}$$

$$\begin{aligned} E_{12} = & \frac{1}{35} \left[35B_{11}d_1 + 4B_{11} - 70B_{12}d_1 + 27B_{12} + 35B_{22}d_1 \right. \\ & \left. + 4B_{22} - 140B_{55}d_1 - 16B_{55} \right] \quad (\text{C.42}) \end{aligned}$$

$$E_{13} = B_{12}\lambda_1 - B_{23}\lambda_1 + B_{23} \quad (\text{C.43})$$

$$E_{16} = \sqrt{2}d_8(B_{11} - 2B_{12} + B_{22} - 4B_{55}) \quad (\text{C.44})$$

$$\begin{aligned} E_{22} = & -\frac{1}{35} \left[35B_{11}d_1 + 35B_{11}\lambda_1 - 31B_{11} - 70B_{12}d_1 - 8B_{12} \right. \\ & \left. + 35B_{22}d_1 - 35B_{22}\lambda_1 + 4B_{22} - 140B_{55}d_1 - 16B_{55} \right] \quad (\text{C.45}) \end{aligned}$$

$$E_{23} = -B_{12}\lambda_1 + B_{12} + B_{23}\lambda_1 \quad (\text{C.46})$$

$$E_{33} = B_{22} \quad (\text{C.47})$$

$$E_{44} = B_{22}\lambda_1 - B_{23}\lambda_1 - 2B_{55}\lambda_1 + 2B_{55} \quad (\text{C.48})$$

$$E_{55} = -B_{22}\lambda_1 + B_{22} + B_{23}\lambda_1 - B_{23} + 2B_{55}\lambda_1 \quad (\text{C.49})$$

$$\begin{aligned} E_{66} = & \frac{2}{35} \left[35B_{11}d_1 + 4B_{11} - 70B_{12}d_1 - 8B_{12} + 35B_{22}d_1 \right. \\ & \left. + 4B_{22} - 140B_{55}d_1 + 19B_{55} \right] \end{aligned} \quad (\text{C.50})$$

with $d_1 = \hat{d}_1 + R(\hat{\lambda}_1) - \frac{4}{35}$ (see Bauer and Böhlke (2022a)) and after matrix inversion in Equation (6.45) by

$$G_{11} = \frac{E_{16}^2 E_{33} - E_{22} E_{33} E_{66} + E_{23}^2 E_{66}}{b} \quad (\text{C.51})$$

$$G_{12} = \frac{E_{12} E_{33} E_{66} - E_{13} E_{23} E_{66} + E_{16}^2 E_{33}}{b} \quad (\text{C.52})$$

$$G_{13} = -\frac{E_{12} E_{23} E_{66} + E_{13} E_{16}^2 - E_{13} E_{22} E_{66} + E_{16}^2 E_{23}}{b} \quad (\text{C.53})$$

$$G_{16} = \frac{E_{16} (E_{12} E_{33} - E_{13} E_{23} + E_{22} E_{33} - E_{23}^2)}{b} \quad (\text{C.54})$$

$$G_{22} = -\frac{E_{11} E_{33} E_{66} - E_{13}^2 E_{66} - E_{16}^2 E_{33}}{b} \quad (\text{C.55})$$

$$G_{23} = \frac{E_{11} E_{23} E_{66} - E_{12} E_{13} E_{66} - E_{13} E_{16}^2 - E_{16}^2 E_{23}}{b} \quad (\text{C.56})$$

$$G_{26} = -\frac{E_{16} (E_{11} E_{33} + E_{12} E_{33} - E_{13}^2 - E_{13} E_{23})}{b} \quad (\text{C.57})$$

$$G_{33} = \frac{E_{11} E_{16}^2 - E_{11} E_{22} E_{66} + E_{12}^2 E_{66} + 2E_{12} E_{16}^2 + E_{16}^2 E_{22}}{b} \quad (\text{C.58})$$

$$G_{36} = \frac{E_{16} (E_{11} E_{23} - E_{12} E_{13} + E_{12} E_{23} - E_{13} E_{22})}{b} \quad (\text{C.59})$$

$$G_{44} = \frac{1}{E_{44}}. \quad (\text{C.60})$$

$$G_{55} = \frac{1}{E_{55}} \quad (C.61)$$

$$G_{66} = - \left[E_{11}E_{22}E_{33} - E_{11}E_{23}^2 - E_{12}^2E_{33} + 2E_{12}E_{13}E_{23} - E_{13}^2E_{22} \right] / b \quad (C.62)$$

$$\begin{aligned} b = & E_{11}E_{16}^2E_{33} - E_{11}E_{22}E_{33}E_{66} + E_{11}E_{23}^2E_{66} + E_{12}^2E_{33}E_{66} \quad (C.63) \\ & - 2E_{12}E_{13}E_{23}E_{66} + 2E_{12}E_{16}^2E_{33} - E_{13}^2E_{16}^2 + E_{13}^2E_{22}E_{66} \\ & - 2E_{13}E_{16}^2E_{23} + E_{16}^2E_{22}E_{33} - E_{16}^2E_{23}^2. \end{aligned}$$

C.7 Parameter sets in polar plots

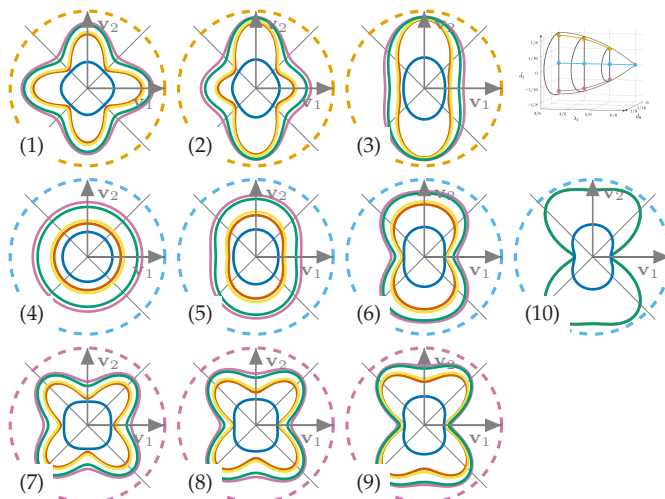
Table C.1 contains parameter combinations leading to selected fourth-order fiber orientation tensors, which are used to generate polar plots in Figures 6.7, 6.8, 6.9, 6.10, 6.11 and 6.12. The corresponding parameterization $\mathbb{N}^{\text{planar}}(\lambda_1, \hat{r}, \hat{\beta})$ is defined in Equation (6.11). Numerical values of the Lagrange multipliers (L, f_1, f_2, g_1, g_2) specifying $\hat{\psi}^{\text{ME}}(\varphi_i, \mathbb{N}^{\text{planar}})$ following Bauer and Böhlke (2022a, Equation (71)) are given with absolute values smaller than $10^{-5} = 1\text{E}^{-5}$ set to zero.

Figures	λ_1	$\hat{\beta}$	\hat{r}	L	f_1	f_2	g_1	g_2
6.7a(1), 6.7b(1)	1/2	$\pi/2$	9/80	4.42E^0	0	0	-5.30E^0	0
6.7a(2), 6.7b(2)	2/3	$\pi/2$	1/10	6.43E^0	-7.69E^0	0	-6.12E^0	0
6.7a(3), 6.7b(3)	5/6	$\pi/2$	1/16	1.66E^1	-2.46E^1	0	-9.77E^0	0
6.7a(4), 6.7b(4)	1/2	0	0	8.38E^{-1}	0	0	0	0
6.7a(5), 6.7b(5)	2/3	0	0	9.56E^{-1}	-6.67E^{-1}	0	1.20E^{-1}	0
6.7a(6), 6.7b(6)	5/6	0	0	1.45E^0	-1.34E^0	0	6.49E^{-1}	0
6.7a(7), 6.7b(7)	1/2	$-\pi/2$	9/80	4.42E^0	0	0	5.30E^0	0
6.7a(8), 6.7b(8)	2/3	$-\pi/2$	1/10	5.01E^0	-3.63E^{-1}	0	5.89E^0	0
6.7a(9), 6.7b(9)	5/6	$-\pi/2$	1/16	8.26E^0	-8.34E^{-1}	0	9.13E^0	0
6.7a(10), 6.7b(10)	1	0	0	1.81E^3	-5.51E^0	1.03E^1	1.81E^3	-5.18E^0
6.8a(x), 6.8b(x), 6.8a(y), 6.8b(y), 6.8a(o1), 6.8b(o2), 6.8a(o2), 6.8b(o2),	1/2	0	0	8.38E^{-1}	0	0	0	0
6.9(x), 6.11(x)	2/3	0	0	1.15E^0	0	0	1.16E^0	0
6.9(o1), 6.11(o1)	2/3	$-\pi/2$	9/80	4.42E^0	0	0	5.30E^0	0
6.9(o2), 6.11(o2)	2/3	$-\pi/2$	1/10	1.30E^0	-6.67E^{-1}	0	1.20E^{-1}	0
6.9(c1), 6.11(c1)	2/3	$-\pi/4$	1/10	5.01E^0	-4.54E^{-1}	0	1.30E^0	0
6.9(c2), 6.11(c2)	2/3	$-\pi/4$	1/18	1.31E^0	-3.63E^{-1}	0	5.89E^0	0
6.9(m1), 6.11(m1)	2/3	0	0	5.69E^0	-5.86E^{-1}	3.36E^{-1}	9.53E^{-1}	-8.36E^{-1}
6.9(m2), 6.11(m2)	2/3	$\pi/4$	1/10	5.20E^0	-1.39E^0	2.51E^0	4.22E^0	-4.15E^0
6.9(g1), 6.11(g1)	2/3	$\pi/4$	1/18	1.32E^0	-9.01E^{-1}	4.71E^{-1}	1.20E^{-1}	-1.19E^0
6.9(g2), 6.11(g2)	2/3	$\pi/4$	1/10	1.33E^0	-1.21E^0	3.30E^{-1}	8.21E^{-2}	-5.99E^0
6.9(y1), 6.11(y1)	2/3	$\pi/2$	1/18	6.21E^0	-6.56E^0	2.59E^0	-7.18E^{-1}	-8.40E^{-1}
6.9(y2), 6.11(y2)	2/3	$\pi/2$	1/10	6.43E^0	-1.33E^0	0	-4.26E^0	-4.35E^0
6.10(x), 6.12(x)	5/6	0	0	1.45E^0	-1.34E^0	0	-1.07E^0	0
6.10(o1), 6.12(o1)	5/6	$-\pi/2$	5/144	2.00E^0	-9.88E^{-1}	0	6.49E^{-1}	0
6.10(o2), 6.12(o2)	5/6	$-\pi/2$	1/16	8.26E^0	-8.34E^{-1}	0	1.96E^0	9.13E^0
6.10(c1), 6.12(c1)	5/6	$-\pi/4$	5/144	2.04E^0	-1.29E^0	9.33E^{-1}	1.59E^0	-9.71E^{-1}
6.10(c2), 6.12(c2)	5/6	$-\pi/4$	1/16	9.37E^0	-4.00E^0	7.92E^0	6.69E^0	-6.27E^0
6.10(m1), 6.12(m1)	5/6	0	5/144	2.07E^0	-1.93E^0	1.25E^0	6.77E^{-1}	-1.36E^0
6.10(m2), 6.12(m2)	5/6	0	1/16	1.23E^1	-1.20E^1	1.17E^1	5.68E^{-1}	-9.41E^0
6.10(g1), 6.12(g1)	5/6	$\pi/4$	5/144	1.95E^0	-2.37E^0	7.97E^{-1}	-1.91E^{-1}	-9.20E^{-1}
6.10(g2), 6.12(g2)	5/6	$\pi/4$	1/16	1.55E^1	-2.09E^1	8.87E^0	-6.48E^0	-7.31E^0
6.10(y1), 6.12(y1)	5/6	$\pi/2$	5/144	1.86E^0	-2.47E^0	0	-5.16E^{-1}	0
6.10(y2), 6.12(y2)	5/6	$\pi/2$	1/16	1.66E^1	-2.46E^1	-9.77E^0	0	0

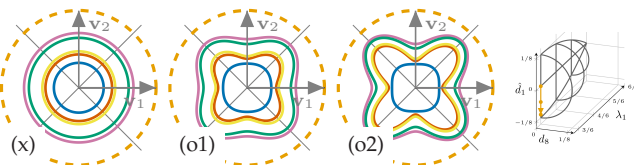
Table C.d: Parameter combinations and Lagrange multipliers of the reconstructed fiber orientation distributions. See Appendix C.7.

C.8 Effective complementary elastic energy density

Effective complementary elastic energy density due to uniaxial tension with unit stress $\sigma = 1 \text{ MPa}$ defined in Equation (6.66) for mean field homogenizations listed in Figure 6.5b are given in Figures C.1a to C.3. The bounds of the contour plots in Figures C.1a to C.3 are homogeneous and given by 0 MJ/m^3 and 0.1 MJ/m^3 .



(a) Polar plots for selected N specified in Figure 6.4 and Table C.1.



(b) Polar plots for selected N specified in Figure 6.5a and Table C.1. The order along the path in Figure 6.5a is given from left to right.

Figure C.1: Effective complementary elastic energy $w^*(\mathbb{C}, \sigma = 1 \text{ MPa}, \mathbf{n})$ due to uniaxial tension in varying direction defined in Equation (6.66) for mean field approximations specified in Figure 6.5b.

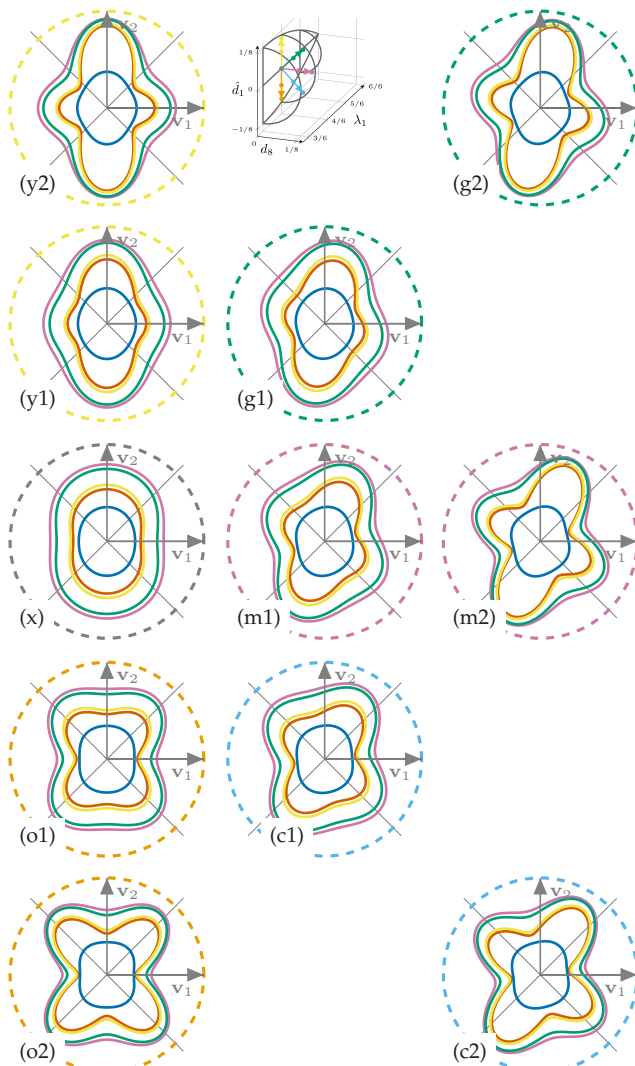


Figure C.2: Effective complementary elastic energy $w^*(C, \sigma = 1 \text{ MPa}, n)$ due to uniaxial tension in varying direction defined in Equation (6.66) for mean field approximations specified in Figure 6.5b. Polar plots for selected N specified in Figure 6.6a and Table C.1

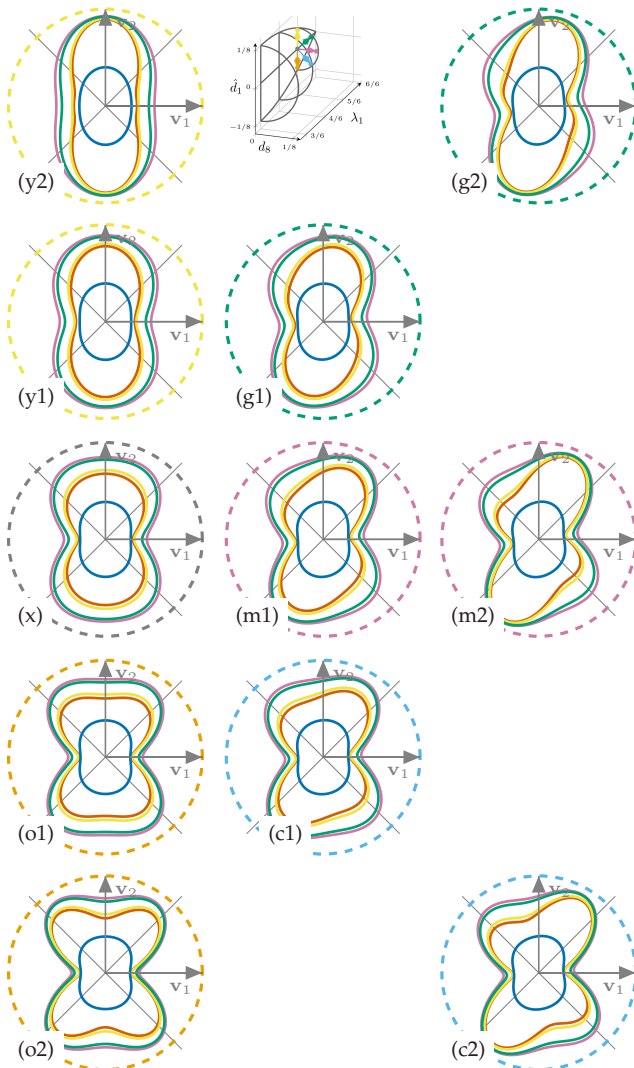


Figure C.3: Effective complementary elastic energy $w^*(\mathbb{C}, \sigma = 1 \text{ MPa}, \mathbf{n})$ due to uniaxial tension in varying direction defined in Equation (6.66) for mean field approximations specified in Figure 6.5b. Polar plots for selected N specified in Figure 6.6b and Table C.1

Bibliography

- Abramian, S., Desmorat, B., Desmorat, R., Kolev, B., Olive, M., 2020. Recovering the normal form and symmetry class of an elasticity tensor. *Journal of Elasticity* 142 (1), 1–33.
- Adams, B., Boehler, J., Guidi, M., Onat, E., 1992. Group theory and representation of microstructure and mechanical behavior of polycrystals. *Journal of the Mechanics and Physics of Solids* 40 (4), 723–737.
- Advani, S. G., Tucker III, C. L., 1987. The use of tensors to describe and predict fiber orientation in short fiber composites. *Journal of Rheology* 31 (8), 751–784.
- Advani, S. G., Tucker III, C. L., 1990. Closure approximations for three-dimensional structure tensors. *Journal of Rheology* 34 (3), 367–386.
- Aßmus, M., Eisenträger, J., Altenbach, H., 2017. Projector representation of isotropic linear elastic material laws for directed surfaces. *ZAMM-Journal of Applied Mathematics and Mechanics* 97 (12), 1625–1634.
- Backus, G., 1970. A geometrical picture of anisotropic elastic tensors. *Reviews of Geophysics* 8 (3), 633–671.
- Baerheim, R., 1993. Harmonic decomposition of the anisotropic elasticity tensor. *The Quarterly Journal of Mechanics and Applied Mathematics* 46 (3), 391–418.

- Bauer, J. K., 2022. Code accompanying the paper: On the dependence of orientation averaging mean field homogenization on planar fourth-order fiber orientation tensors. https://github.com/J JulianKarlBauer/orientation_averaging_mean_field.
- Bauer, J. K., Böhlke, T., 2022a. Fiber orientation distributions based on planar fiber orientation tensors of fourth order. *Mathematics and Mechanics of Solids* .
- Bauer, J. K., Böhlke, T., 2022b. On the dependence of orientation-averaging mean field homogenization on planar fourth-order fiber orientation tensors. *Mechanics of Materials* 170, 104307.
- Bauer, J. K., Böhlke, T., 2022c. Variety of fiber orientation tensors. *Mathematics and Mechanics of Solids* 27 (7), 1185–1211.
- Benveniste, Y., 1987. A new approach to the application of Mori-Tanaka's theory in composite materials. *Mechanics of Materials* 6 (2), 147 – 157.
- Benveniste, Y., Dvorak, G., Chen, T., 1991. On diagonal and elastic symmetry of the approximate effective stiffness tensor of heterogeneous media. *Journal of the Mechanics and Physics of Solids* 39 (7), 927–946.
- Bertram, A., 2012. *Elasticity and Plasticity of Large Deformations*. Springer.
- Bertram, A., Glüge, R., 2013. *Solid Mechanics*. Springer.
- Biegler, M., Mehrabadi, M., 1995. An energy-based constitutive model for anisotropic solids subject to damage. *Mechanics of Materials* 19 (2-3), 151–164.
- Blinowski, A., Ostrowska-Maciejewska, J., Rychlewski, J., 1996. Two-dimensional Hooke's tensors-isotropic decomposition, effective symmetry criteria. *Archives of Mechanics* 48 (2), 325–345.

- Boehler, J.-P., Kirillov, A., Onat, E. T., 1994. On the polynomial invariants of the elasticity tensor. *Journal of Elasticity* 34 (2), 97–110.
- Böhlke, T., 2001. Crystallographic texture evolution and elastic anisotropy: Simulation, modeling, and applications. Doctoral thesis, Shaker.
- Böhlke, T., 2005. Application of the maximum entropy method in texture analysis. *Computational Materials Science* 32 (3-4), 276–283.
- Böhlke, T., 2006. Texture simulation based on tensorial fourier coefficients. *Computers & structures* 84 (17-18), 1086–1094.
- Böhlke, T., 2014. Lecture notes in Plastizitätstheorie.
- Böhlke, T., 2021. Symmetries of irreducible tensors. Personal communication.
- Böhlke, T., Brüggemann, C., 2001. Graphical representation of the generalized Hooke's law. *Technische Mechanik* 21 (2), 145–158.
- Böhlke, T., Frohnäpfel, B., 2019. Lecture notes in Kontinuumsmechanik der Festkörper und Fluide.
- Böhlke, T., Henning, F., Hrymak, A., Kärger, L., Weidenmann, K., Wood, J. T., 2019. Continuous-Discontinuous Fiber-Reinforced Polymers: An Integrated Engineering Approach. Carl Hanser Verlag GmbH Co KG.
- Bóna, A., Bucataru, I., Slawinski, M. A., 2007. Coordinate-free characterization of the symmetry classes of elasticity tensors. *Journal of Elasticity* 87 (2), 109–132.
- Brannon, R. M., 2018. Tensor symmetry (not material symmetry). In: Rotation, Reflection, and Frame Changes. 2053-2563. IOP Publishing, pp. 20–1 to 20–42.

- Breuer, K., Stommel, M., Korte, W., 2019. Analysis and evaluation of fiber orientation reconstruction methods. *Journal of Composites Science* 3 (3), 67.
- Bro, R., Acar, E., Kolda, T. G., 2008. Resolving the sign ambiguity in the singular value decomposition. *Journal of Chemometrics: A Journal of the Chemometrics Society* 22 (2), 135–140.
- Brylka, B., 2017. Charakterisierung und modellierung der steifigkeit von langfaserverstärktem polypropylen. Doctoral thesis, KIT Scientific Publishing.
- Buck, F., Brylka, B., Müller, V., Müller, T., Weidenmann, K. A., Hrymak, A. N., Henning, F., Böhlke, T., 2015. Two-scale structural mechanical modeling of long fiber reinforced thermoplastics. *Composites Science and Technology* 117, 159–167.
- Budiansky, B., 1965. On the elastic moduli of some heterogeneous materials. *Journal of the Mechanics and Physics of Solids* 13 (4), 223–227.
- Camacho, C. W., Tucker III, C. L., Yalvaç, S., McGee, R. L., 1990. Stiffness and thermal expansion predictions for hybrid short fiber composites. *Polymer Composites* 11 (4), 229–239.
- Castañeda, P. P., Willis, J., 1995. The effect of spatial distribution on the effective behavior of composite materials and cracked media. *Journal of the Mechanics and Physics of Solids* 43 (12), 1919–1951.
- Cermelli, P., Fried, E., Gurtin, M. E., 2005. Transport relations for surface integrals arising in the formulation of balance laws for evolving fluid interfaces. *Journal of Fluid Mechanics* 544, 339–351.
- Chung, D. H., Kwon, T. H., 2001. Improved model of orthotropic closure approximation for flow induced fiber orientation. *Polymer Composites* 22 (5), 636–649.

- Chung, D. H., Kwon, T. H., 2002. Invariant-based optimal fitting closure approximation for the numerical prediction of flow-induced fiber orientation. *Journal of Rheology* 46 (1), 169–194.
- Cintra Jr, J. S., Tucker III, C. L., 1995. Orthotropic closure approximations for flow-induced fiber orientation. *Journal of Rheology* 39 (6), 1095–1122.
- Cowin, S., Mehrabadi, M., 1992. The structure of the linear anisotropic elastic symmetries. *Journal of the Mechanics and Physics of Solids* 40 (7), 1459–1471.
- Cowin, S. C., 1985. The relationship between the elasticity tensor and the fabric tensor. *Mechanics of materials* 4 (2), 137–147.
- Cowin, S. C., 1989. Properties of the anisotropic elasticity tensor. *The Quarterly Journal of Mechanics and Applied Mathematics* 42 (2), 249–266.
- Cowin, S. C., Cardoso, L., 2011. Fabric dependence of wave propagation in anisotropic porous media. *Biomechanics and Modeling in Mechanobiology* 10 (1), 39–65.
- Cowin, S. C., Mehrabadi, M. M., 05 1995. Anisotropic symmetries of linear elasticity. *Applied Mechanics Reviews* 48 (5), 247–285.
- Cowin, S. C., Van Buskirk, W. C., 1986. Thermodynamic restrictions on the elastic constants of bone. *Journal of Biomechanics* 19 (1), 85–87.
- Desmorat, B., Desmorat, R., 2015. Tensorial polar decomposition of 2d fourth-order tensors. *Comptes Rendus Mécanique* 343 (9), 471–475.
- Dray, D., Gilormini, P., Régnier, G., 2007. Comparison of several closure approximations for evaluating the thermoelastic properties of an injection molded short-fiber composite. *Composites Science and Technology* 67 (7-8), 1601–1610.

- Duschlbauer, D., Böhm, H. J., Pettermann, H. E., 2006. Computational simulation of composites reinforced by planar random fibers: homogenization and localization by unit cell and mean field approaches. *Journal of Composite Materials* 40 (24), 2217–2234.
- Eik, M., Puttonen, J., Herrmann, H., 2016. The effect of approximation accuracy of the orientation distribution function on the elastic properties of short fibre reinforced composites. *Composite Structures* 148, 12–18.
- Eshelby, J. D., 1957. The determination of the elastic field of an ellipsoidal inclusion, and related problems. *Proceedings of the Royal Society of London. Series A. Mathematical and Physical Sciences* 241 (1226), 376–396.
- Fernández, M. L., Böhlke, T., 2019. Representation of Hashin–Shtrikman bounds in terms of texture coefficients for arbitrarily anisotropic polycrystalline materials. *Journal of Elasticity* 134 (1), 1–38.
- Forte, S., Vianello, M., 1996. Symmetry classes for elasticity tensors. *Journal of Elasticity* 43 (2), 81–108.
- Forte, S., Vianello, M., 2014. A unified approach to invariants of plane elasticity tensors. *Mecanica* 49 (9), 2001–2012.
- Francois, M., Geymonat, G., Berthaud, Y., 1998. Determination of the symmetries of an experimentally determined stiffness tensor: application to acoustic measurements. *International Journal of Solids and Structures* 35 (31-32), 4091–4106.
- Goldberg, N., Ospald, F., Schneider, M., 2017. A fiber orientation-adapted integration scheme for computing the hyperelastic tucker average for short fiber reinforced composites. *Computational Mechanics* 60 (4), 595–611.

- Görthofer, J., Meyer, N., Pallicity, T. D., Schöttl, L., Trauth, A., Schemmann, M., Hohberg, M., Pinter, P., Elsner, P., Henning, F., Hrymak, A., Seelig, T., Weidenmann, K., Kärger, L., Böhlke, T., 2019. Virtual process chain of sheet molding compound: Development, validation and perspectives. Composites Part B: Engineering 169, 133–147.
- Görthofer, J., Schneider, M., Ospald, F., Hrymak, A., Böhlke, T., 2020. Computational homogenization of sheet molding compound composites based on high fidelity representative volume elements. Computational Materials Science 174, 109456.
- Han, K.-H., Im, Y.-T., 1999. Modified hybrid closure approximation for prediction of flow-induced fiber orientation. Journal of Rheology 43 (3), 569–589.
- Harris, C. R., Millman, K. J., van der Walt, S. J., Gommers, R., Virtanen, P., Cournapeau, D., Wieser, E., Taylor, J., Berg, S., Smith, N. J., Kern, R., Picus, M., Hoyer, S., van Kerkwijk, M. H., Brett, M., Haldane, A., del Río, J. F., Wiebe, M., Peterson, P., Gérard-Marchant, P., Sheppard, K., Reddy, T., Weckesser, W., Abbasi, H., Gohlke, C., Oliphant, T. E., Sep. 2020. Array programming with NumPy. Nature 585 (7825), 357–362.
- Hasan, K. M., Basser, P. J., Parker, D. L., Alexander, A. L., 2001. Analytical computation of the eigenvalues and eigenvectors in dt-mri. Journal of Magnetic Resonance 152 (1), 41–47.
- Hashin, Z., Shtrikman, S., 1962. A variational approach to the theory of the elastic behaviour of polycrystals. Journal of the Mechanics and Physics of Solids 10 (4), 343–352.
- He, Q.-C., Curnier, A., 1995. A more fundamental approach to damaged elastic stress-strain relations. International Journal of Solids and Structures 32 (10), 1433–1457.

- Heller, B. P., Smith, D. E., Jack, D. A., 2016. Computing mechanical properties from orientation tensor for fiber filled polymers in axisymmetric flow and planar deposition flow. In: SPE ACCE Conference.
- Hessman, P. A., Welschinger, F., Hornberger, K., Böhlke, T., 2021. On mean field homogenization schemes for short fiber reinforced composites: unified formulation, application and benchmark. International Journal of Solids and Structures , 111141.
- Hill, R., 1952. The elastic behaviour of a crystalline aggregate. Proceedings of the Physical Society. Section A 65 (5), 349.
- Hill, R., 1965a. Continuum micro-mechanics of elastoplastic polycrystals. Journal of the Mechanics and Physics of Solids 13 (2), 89–101.
- Hill, R., 1965b. A self-consistent mechanics of composite materials. Journal of the Mechanics and Physics of Solids 13 (4), 213–222.
- Hine, P. J., Lusti, H. R., Gusev, A. A., 2004. On the possibility of reduced variable predictions for the thermoelastic properties of short fibre composites. Composites science and technology 64 (7-8), 1081–1088.
- Iorga, L., Pan, Y., Pelegri, A., 2008. Numerical characterization of material elastic properties for random fiber composites. Journal of Mechanics of Materials and Structures 3 (7), 1279–1298.
- Jack, D., Smith, D., 2007. The effect of fibre orientation closure approximations on mechanical property predictions. Composites Part A: Applied Science and Manufacturing 38 (3), 975–982.
- Jack, D. A., Schache, B., Smith, D. E., 2010. Neural network-based closure for modeling short-fiber suspensions. Polymer Composites 31 (7), 1125–1141.
- Jack, D. A., Smith, D. E., 2004. Assessing the use of tensor closure methods with orientation distribution reconstruction functions. Journal of composite materials 38 (21), 1851–1871.

- Jack, D. A., Smith, D. E., 2008. Elastic properties of short-fiber polymer composites, derivation and demonstration of analytical forms for expectation and variance from orientation tensors. *Journal of Composite Materials* 42 (3), 277–308.
- Jerphagnon, J., Chemla, D., Bonneville, R., 1978. The description of the physical properties of condensed matter using irreducible tensors. *Advances in Physics* 27 (4), 609–650.
- Kanatani, K.-I., 1984. Distribution of directional data and fabric tensors. *International Journal of Engineering Science* 22 (2), 149–164.
- Karl, T., Gatti, D., Böhlke, T., Frohnäpfel, B., 2021a. Coupled simulation of flow-induced viscous and elastic anisotropy of short-fiber reinforced composites. *Acta Mechanica* 232 (6), 2249–2268.
- Karl, T., Gatti, D., Böhlke, T., Frohnäpfel, B., 2021b. Coupled simulation of flow-induced viscous and elastic anisotropy of short-fiber reinforced composites. *Acta Mechanica* 232 (6), 2249–2268.
- Karl, T., Gatti, D., Frohnäpfel, B., Böhlke, T., 2021c. Asymptotic fiber orientation states of the quadratically closed folgar-tucker equation and a subsequent closure improvement. *Journal of Rheology* 65 (5), 999–1022.
- Kehrer, L., Wood, J. T., Böhlke, T., 2020. Mean-field homogenization of thermoelastic material properties of a long fiber-reinforced thermoset and experimental investigation. *Journal of Composite Materials*, 0021998320920695.
- Kehrer, M. L., 2019. Thermomechanical mean-field modeling and experimental characterization of long fiber-reinforced sheet molding compound composites. Doctoral thesis, KIT Scientific Publishing.

- Köbler, J., Magino, N., Andrä, H., Welschinger, F., Müller, R., Schneider, M., 2021. A computational multi-scale model for the stiffness degradation of short-fiber reinforced plastics subjected to fatigue loading. *Computer Methods in Applied Mechanics and Engineering* 373, 113522.
- Köbler, J., Schneider, M., Ospald, F., Andrä, H., Müller, R., 2018. Fiber orientation interpolation for the multiscale analysis of short fiber reinforced composite parts. *Computational Mechanics* 61 (6), 729–750.
- Krylov, V. I., Stroud, A. H., 2006. Approximate Calculation of Integrals. Courier Corporation.
- Kuzmin, D., 2018. Planar and orthotropic closures for orientation tensors in fiber suspension flow models. *SIAM Journal on Applied Mathematics* 78 (6), 3040–3059.
- Lielens, G., Pirotte, P., Couniot, A., Dupret, F., Keunings, R., 1998. Prediction of thermo-mechanical properties for compression moulded composites. *Composites Part A: Applied Science and Manufacturing* 29 (1-2), 63–70.
- Lobos, M., Yuzbasioglu, T., Böhlke, T., 2017. Homogenization and materials design of anisotropic multiphase linear elastic materials using central model functions. *Journal of Elasticity* 128 (1), 17–60.
- Lobos Fernández, M., 2018. Homogenization and materials design of mechanical properties of textured materials based on zeroth-, first-and second-order bounds of linear behavior. Doctoral thesis, KIT Scientific Publishing.
- Lubarda, V., Chen, M., 2008. On the elastic moduli and compliances of transversely isotropic and orthotropic materials. *Journal of Mechanics of Materials and Structures* 3 (1), 153–171.
- Mandel, J., 1965. Généralisation de la théorie de plasticité de WT Koiter. *International Journal of Solids and Structures* 1 (3), 273–295.

- Mehrabadi, M. M., Cowin, S. C., 1990. Eigentensors of linear anisotropic elastic materials. *The Quarterly Journal of Mechanics and Applied Mathematics* 43 (1), 15–41.
- Mentges, N., Dashtbozorg, B., Mirkhalaf, S., 2021. A micromechanics-based artificial neural networks model for elastic properties of short fiber composites. *Composites Part B: Engineering*, 108736.
- Meurer, A., Smith, C. P., Paprocki, M., Certik, O., Kirpichev, S. B., Rocklin, M., Kumar, A., Ivanov, S., Moore, J. K., Singh, S., et al., 2017. Sympy: symbolic computing in Python. *PeerJ Computer Science* 3, e103.
- Meyer, N., Saburow, O., Hohberg, M., Hrymak, A. N., Henning, F., Kärger, L., 2020a. Parameter identification of fiber orientation models based on direct fiber simulation with smoothed particle hydrodynamics. *Journal of Composites Science* 4 (2), 77.
- Meyer, N., Schöttl, L., Bretz, L., Hrymak, A., Kärger, L., 2020b. Direct bundle simulation approach for the compression molding process of sheet molding compound. *Composites Part A: Applied Science and Manufacturing* 132, 105809.
- Mochizuki, E., 1988. Spherical harmonic decomposition of an elastic tensor. *Geophysical Journal International* 93 (3), 521–526.
- Montgomery-Smith, S., He, W., Jack, D. A., Smith, D. E., 2011a. Exact tensor closures for the three-dimensional jeffery's equation. *Journal of Fluid Mechanics* 680, 321–335.
- Montgomery-Smith, S., Jack, D., Smith, D. E., 2011b. The fast exact closure for Jeffery's equation with diffusion. *Journal of Non-Newtonian Fluid Mechanics* 166 (7-8), 343–353.
- Mori, T., Tanaka, K., 1973. Average stress in matrix and average elastic energy of materials with misfitting inclusions. *Acta Metallurgica* 21 (5), 571–574.

Moulinec, H., Suquet, P., 1994. A fast numerical method for computing the linear and nonlinear mechanical properties of composites. *Comptes Rendus de l'Académie des sciences. Série II. Mécanique, physique, chimie, astronomie* .

Moulinec, H., Suquet, P., 1998. A numerical method for computing the overall response of nonlinear composites with complex microstructure. *Computer methods in applied mechanics and engineering* 157 (1-2), 69–94.

Müller, V., 2016. Micromechanical modeling of short-fiber reinforced composites. Doctoral thesis, KIT Scientific Publishing.

Müller, V., Böhlke, T., 2016. Prediction of effective elastic properties of fiber reinforced composites using fiber orientation tensors. *Composites Science and Technology* 130, 36–45.

Musgrave, M., 1970. Crystal Acoustics. Holden-Day.

nilsmeyerkit, JulianKarlBauer, Apr. 2021. nilsmeyerkit/fiberoripy: v1.0.12.

URL <https://doi.org/10.5281/zenodo.4679756>

Nomura, S., Kawai, H., Kimura, I., Kagiyama, M., 1970. General description of orientation factors in terms of expansion of orientation distribution function in a series of spherical harmonics. *Journal of Polymer Science Part A-2: Polymer Physics* 8 (3), 383–400.

Nordmann, J., Aßmus, M., Glüge, R., Altenbach, H., 2020. On the derivation of Hooke's law for plane state conditions. *Technische Mechanik-European Journal of Engineering Mechanics* 40 (2), 160–174.

nschloe, Aug. 2021. nschloe/fiberoripy: v0.16.10.

URL <https://github.com/nschloe/quadpy>

- Olive, M., Kolev, B., Auffray, N., 2017. A minimal integrity basis for the elasticity tensor. *Archive for Rational Mechanics and Analysis* 226 (1), 1–31.
- Olive, M., Kolev, B., Desmorat, B., Desmorat, R., 2018. Harmonic factorization and reconstruction of the elasticity tensor. *Journal of Elasticity* 132 (1), 67–101.
- Olive, M., Kolev, B., Desmorat, R., Desmorat, B., 2022. Characterization of the symmetry class of an elasticity tensor using polynomial covariants. *Mathematics and Mechanics of Solids* 27 (1), 144–190.
- Onat, E., Leckie, F., 1988. Representation of mechanical behavior in the presence of changing internal structure .
- Pettermann, H., Böhm, H. J., Rammerstorfer, F. G., 1997. Some direction-dependent properties of matrix-inclusion type composites with given reinforcement orientation distributions. *Composites Part B: Engineering* 28 (3), 253–265.
- Pierard, O., Friebel, C., Doghri, I., 2004. Mean-field homogenization of multi-phase thermo-elastic composites: a general framework and its validation. *Composites Science and Technology* 64 (10-11), 1587–1603.
- Pinter, P., Dietrich, S., Bertram, B., Kehrer, L., Elsner, P., Weidenmann, K. A., 2018. Comparison and error estimation of 3D fibre orientation analysis of computed tomography image data for fibre reinforced composites. *NDT & E International* 95, 26–35.
- Prahs, A., 2020. A gradient crystal plasticity theory based on an extended energy balance. Doctoral thesis, KIT Scientific Publishing.
- Qiu, Y., Weng, G., 1990. On the application of Mori-Tanaka's theory involving transversely isotropic spheroidal inclusions. *International Journal of Engineering Science* 28 (11), 1121–1137.

- Reuß, A., 1929. Berechnung der fließgrenze von mischkristallen auf grund der plastizitätsbedingung für einkristalle. ZAMM-Journal of Applied Mathematics and Mechanics/Zeitschrift für Angewandte Mathematik und Mechanik 9 (1), 49–58.
- Rychlewski, J., 1984. On Hooke's law. Journal of Applied Mathematics and Mechanics 48 (3), 303–314.
- Rychlewski, J., 2000. A qualitative approach to Hooke's tensors. part I. Archives of Mechanics 52 (4-5), 737–759.
- Rychlewski, J., 2001. A qualitative approach to Hooke's tensors. part II. Archives of Mechanics 53 (1), 45–63.
- Schemmann, M., Brylka, B., Gajek, S., Böhlke, T., 2015. Parameter identification by inverse modelling of biaxial tensile tests for discontinuous fiber reinforced polymers. PAMM 15 (1), 355–356.
- Schemmann, M., Gajek, S., Böhlke, T., 2018a. Biaxial tensile tests and microstructure-based inverse parameter identification of inhomogeneous SMC composites. In: Advances in Mechanics of Materials and Structural Analysis. Springer, pp. 329–342.
- Schemmann, M., Görthofer, J., Seelig, T., Hrymak, A., Böhlke, T., 2018b. Anisotropic meanfield modeling of debonding and matrix damage in SMC composites. Composites Science and Technology 161, 143–158.
- Schjødt-Thomsen, J., Pyrz, R., 2001. The Mori–Tanaka stiffness tensor: diagonal symmetry, complex fibre orientations and non-dilute volume fractions. Mechanics of Materials 33 (10), 531–544.
- Schneider, M., 2017. The sequential addition and migration method to generate representative volume elements for the homogenization of short fiber reinforced plastics. Computational Mechanics 59 (2), 247–263.
- Schneider, M., 2021. A review of nonlinear fft-based computational homogenization methods. Acta Mechanica 232 (6), 2051–2100.

- Schöttl, L., Dörr, D., Pinter, P., Weidenmann, K. A., Elsner, P., Kärger, L., 2020. A novel approach for segmenting and mapping of local fiber orientation of continuous fiber-reinforced composite laminates based on volumetric images. *NDT & E International* 110, 102194.
- Schöttl, L., Weidenmann, K. A., Sabiston, T., Inal, K., Elsner, P., 2021. Fiber bundle tracking method to analyze sheet molding compound microstructure based on computed tomography images. *NDT & E International* 117, 102370.
- Schröder, J., Gross, D., 2004. Invariant formulation of the electromechanical enthalpy function of transversely isotropic piezoelectric materials. *Archive of Applied Mechanics* 73 (8), 533–552.
- Smith, M., 2019. ABAQUS/Standard User's Manual, Version 2019. Dassault Systèmes Simulia Corp, United States.
- Spencer, A., 1970. A note on the decomposition of tensors into traceless symmetric tensors. *International Journal of Engineering Science* 8 (6), 475–481.
- Spencer, A., 1982. The formulation of constitutive equation for anisotropic solids. In: Mechanical Behavior of Anisotropic Solids/Comportement Méchanique des Solides Anisotropes. Springer, pp. 3–26.
- Thomson, W., 1856. Elements of a mathematical theory of elasticity. *Philosophical Transactions of the Royal Society of London* (146), 481–498.
- Trauth, A., Kehrer, L., Pinter, P., Weidenmann, K., Böhlke, T., 2021. On the effective elastic properties based on mean-field homogenization of sheet molding compound composites. *Composites Part C: Open Access* 4, 100089.

- Turner, C. H., Cowin, S. C., 1987. Dependence of elastic constants of an anisotropic porous material upon porosity and fabric. *Journal of Materials Science* 22 (9), 3178–3184.
- Vannucci, P., 2018. Anisotropic Elasticity. Springer Singapore.
- VerWeyst, B. E., Tucker, C., Foss, P. H., O'Gara, J. F., 1999. Fiber orientation in 3-d injection molded features. *International Polymer Processing* 14 (4), 409–420.
- Vianello, M., 1997. An integrity basis for plane elasticity tensors. *Archives of Mechanics* 49 (1), 197–208.
- Voigt, W., 1889. Ueber die beziehung zwischen den beiden elasticitätsconstanten isotroper körper. *Annalen der Physik* 274 (12), 573–587.
- Walpole, L., 1966a. On bounds for the overall elastic moduli of inhomogeneous systems—I. *Journal of the Mechanics and Physics of Solids* 14 (3), 151–162.
- Walpole, L., 1966b. On bounds for the overall elastic moduli of inhomogeneous systems—II. *Journal of the Mechanics and Physics of Solids* 14 (5), 289–301.
- Walpole, L., 1969. On the overall elastic moduli of composite materials. *Journal of the Mechanics and Physics of Solids* 17 (4), 235–251.
- Weber, M., Glüge, R., Bertram, A., 2019. Distance of a stiffness tetrad to the symmetry classes of linear elasticity. *International Journal of Solids and Structures* 156, 281–293.
- Weng, G., 1990. The theoretical connection between Mori-Tanaka's theory and the Hashin-Shtrikman-Walpole bounds. *International Journal of Engineering Science* 28 (11), 1111–1120.

- Willis, J. R., 1977. Bounds and self-consistent estimates for the overall properties of anisotropic composites. *Journal of the Mechanics and Physics of Solids* 25 (3), 185–202.
- Willis, J. R., 1981. Variational and related methods for the overall properties of composites. In: *Advances in Applied Mechanics*. Vol. 21. Elsevier, pp. 1–78.
- Zheng, Q.-S., Boehler, J.-P., 1994. The description, classification, and reality of material and physical symmetries. *Acta Mechanica* 102 (1), 73–89.
- Zheng, Q.-S., Du, D.-X., 2001. An explicit and universally applicable estimate for the effective properties of multiphase composites which accounts for inclusion distribution. *Journal of the Mechanics and Physics of Solids* 49 (11), 2765–2788.

Schriftenreihe Kontinuumsmechanik im Maschinenbau
Karlsruher Institut für Technologie (KIT)
(ISSN 2192-693X)

- Band 1** Felix Fritzen
Microstructural modeling and computational homogenization of the physically linear and nonlinear constitutive behavior of micro-heterogeneous materials.
ISBN 978-3-86644-699-1
- Band 2** Rumena Tsotsova
Texturbasierte Modellierung anisotroper Fließpotentiale.
ISBN 978-3-86644-764-6
- Band 3** Johannes Wippler
Micromechanical finite element simulations of crack propagation in silicon nitride.
ISBN 978-3-86644-818-6
- Band 4** Katja Jöchen
Homogenization of the linear and non-linear mechanical behavior of polycrystals.
ISBN 978-3-86644-971-8
- Band 5** Stephan Wulffinghoff
Numerically Efficient Gradient Crystal Plasticity with a Grain Boundary Yield Criterion and Dislocation-based Work-Hardening.
ISBN 978-3-7315-0245-6
- Band 6** Viktor Müller
Micromechanical modeling of short-fiber reinforced composites.
ISBN 978-3-7315-0454-2

- Band 7** Florian Rieger
Work-hardening of dual-phase steel.
ISBN 978-3-7315-0513-6
- Band 8** Vedran Glavas
Micromechanical Modeling and Simulation of Forming Processes.
ISBN 978-3-7315-0602-7
- Band 9** Eric Bayerschen
Single-crystal gradient plasticity with an accumulated plastic slip: Theory and applications.
ISBN 978-3-7315-0606-5
- Band 10** Bartholomäus Brylka
Charakterisierung und Modellierung der Steifigkeit von langfaserverstärktem Polypropylen.
ISBN 978-3-7315-0680-5
- Band 11** Rudolf Neumann
Two-Scale Thermomechanical Simulation of Hot Stamping.
ISBN 978-3-7315-0714-7
- Band 12** Mauricio Lobos Fernández
Homogenization and materials design of mechanical properties of textured materials based on zeroth-, first- and second-order bounds of linear behavior.
ISBN 978-3-7315-0770-3
- Band 13** Malte Schemmann
Biaxial Characterization and Mean-field Based Damage Modeling of Sheet Molding Compound Composites.
ISBN 978-3-7315-0818-2
- Band 14** Jürgen Albiez
Finite element simulation of dislocation based plasticity and diffusion in multiphase materials at high temperature.
ISBN 978-3-7315-0918-9

- Band 15** Maria Loredana Kehrer
Thermomechanical Mean-Field Modeling and Experimental Characterization of Long Fiber-Reinforced Sheet Molding Compound Composites.
ISBN 978-3-7315-0924-0
- Band 16** Peter Hölz
A dynamic and statistical analysis of the temperature- and fatigue behavior of a race power unit – The effect of different thermodynamic states.
ISBN 978-3-7315-0988-2
- Band 17** Andreas Prahs
A Gradient Crystal Plasticity Theory Based on an Extended Energy Balance.
ISBN 978-3-7315-1025-3
- Band 18** Johannes Ruck
Modeling martensitic phase transformation in dual phase steels based on a sharp interface theory.
ISBN 978-3-7315-1072-7
- Band 19** Hannes Erdle
Modeling of Dislocation - Grain Boundary Interactions in Gradient Crystal Plasticity Theories.
ISBN 978-3-7315-1196-0
- Band 20** Johannes Görthofer
Microstructure generation and micromechanical modeling of sheet molding compound composites.
ISBN 978-3-7315-1205-9
- Band 21** Daniel Wicht
Efficient fast Fourier transform-based solvers for computing the thermomechanical behavior of applied materials.
ISBN 978-3-7315-1220-2
- Band 22** Juliane Lang
Thermomechanical Modeling and Experimental Characterization of Sheet Molding Compound Composites.
ISBN 978-3-7315-1232-5

Band 23 Julian Karl Bauer

**Fiber Orientation Tensors and Mean Field Homogenization:
Application to Sheet Molding Compound.**

ISBN 978-3-7315-1262-2

Effective mechanical properties of fiber-reinforced composites strongly depend on the microstructure, i.e., the fibers' alignment within the composite. In this work, we study the influence of a fiber orientation distribution on the effective properties of long-fiber-reinforced composites such as sheet molding compound (SMC). Averaged information of a fiber orientation distribution can be quantified by fiber orientation tensors. We identify the variety of fiber orientation tensors up to fourth-order, based on a simple and flexible parameterization based on irreducible tensors incorporating material symmetry. Admissible parameter ranges are identified by demanding positive semi-definiteness. Throughout this work, closure approximations are contrasted by the variety of fourth-order fiber orientation tensors. The correspondence of planar fiber distributions and planar fiber orientation tensors are presented in detail, deploying tensorial Fourier series in 2D- and 3D-frameworks as well as maximum entropy reconstruction of fiber orientation distributions by leading fiber orientation tensors. An innovative visualization method, combining overview plots and polar plot ensembles, shows the directional dependence of effective linear elastic stiffnesses predicted by mean field homogenization.

ISSN 2192-693X

ISBN 978-3-7315-1262-2

Gedruckt auf FSC-zertifiziertem Papier

ISBN 978-3-7315-1262-2



9 783731 512622